Université de Montréal
Département de chimie, Faculté des arts et des sciences

Cette thèse intitulée

Associations concave-convexe entre le C_{60} et les dérivés du phosphangulène, une triarylphosphine de forme conique

Présentée par
Alice Heskia

A été évalué par un jury composé des personnes suivantes

Gary Hanan
Président-rapporteur

James. D. Wuest
Directeur de recherche

Andreea-Ruxandra Schmitzer
Membre du jury

Derek Schipper
Examinateur externe

Université de Montréal

Associations concave-convexe entre le C_{60} et les dérivés du phosphangulène, une triarylphosphine de forme conique

par
Alice Heskia

Département de chimie
Faculté des arts et des sciences

Thèse présentée à la Faculté des études supérieures
en vue de l'obtention du grade de
Philosophiae Doctor (Ph. D.)
en chimie

Décembre 2019

Résumé

La performance des dispositifs moléculaires, tels que les cellules solaires ou des diodes électroluminescentes, peut être optimisée en contrôlant l'organisation des composantes des couches actives. Les fullerènes et leurs dérivés sont souvant utilisés dans des dispositifs photovoltaïques pour leurs propriétés électro-acceptrices et conductrices. Il est donc important de concevoir des structures moléculaires pouvant interagir avec les unités fullerène et ainsi de diriger leur organisation. Le caractère électro-accepteur et la forme convexe des fullerènes favorisent le choix d'un partenaire de surface complémentaire : électro-donneuse et concave. Le phosphangulène, une triarylphosphine hexacyclique qui répond à ces critères et est aisément fonctionnalisable, a été choisi comme structure de base pour la synthèse des cibles.

La présente thèse décrit la synthèse et la structure des dérivés du phosphangulène et des cocristaux obtenus avec les fullerènes au travers de quatre articles soumis au courant de ce doctorat. Le premier article décrit la synthèse des dérivés chalcogénures du phosphangulène. Ces dérivés-ci présentent de nombreux polymorphes, résultant en de bons candidats pour la cocristallisation. Le second article se concentre sur les cocristaux de ces dérivés chalcogénures avec le C_{60} et le C_{70}. Dans le troisième article, nous décrivons les complexes obtenus par la coordination du phosphangulène sur des métaux de transition. Enfin, dans le quatrième article, nous parlons des sels du μ-nitrido-bis(phosphangulène), un cation organique où deux unités phosphangulène sont pontées par un atome d'azote, ainsi que des cocristaux résultant de la combinaison de ce ligand pontant et du C_{60}.

Mots-clés : fullerènes, interactions concave-convexe, phosphine, phosphangulène, polymorphisme, cocristaux, complexes de coordination, sels organiques.

Abstract

The performance of molecular devices such as solar cells or light-emitting diodes can be optimized by controlling how the active-layer components are organized. Fullerenes and their derivatives are often used in photovoltaic devices for their electron-accepting and conductive properties. It is therefore important to design molecular structures that can interact with fullerene units and thus direct their organization. The electron-accepting character and convex shape of fullerenes favor the choice of a partner with a complementary surface that is electron-donating and concave. Phosphangulene, a hexacyclic triarylphosphine that meets these criteria and is easily functionalizable, was chosen as the basic structure for synthesizing targets.

This thesis describes the synthesis and structure of phosphangulene derivatives and their cocrystals obtained with fullerenes through four articles submitted during this doctorate. The first article describes the synthesis of chalcogenide derivatives of phosphangulene. These derivatives have many polymorphs, resulting in good candidates for cocrystallization. The second article focuses on cocrystals of these chalcogenide derivatives with C_{60} and C_{70}. In the third article, we describe the complexes obtained by the coordination of phosphangulene with transition metals. Finally, in the fourth article, we talk about the salts of μ-nitrido-bis (phosphangulene), an organic cation where two phosphangulene units are bridged by a nitrogen atom, as well as the crystals resulting from the combination of this bridging ligand and C_{60}.

Keywords: fullerenes, concave-convex interactions, phosphine, phosphangulene, polymorphism, cocrystals, coordination complexes, organic salts.

Table des matières

Table des tableaux

Table des schémas

Table des équations

Table des figures

Index des abréviations

Å	: Ångström
°C	: degré Celsius
μ	: coefficient d'absorption
μm	: micromètre
μmol	: micromole
calcd	: calculated
cm	: centimètre
d	: doublet (en RMN)
d_e	: distance séparant la surface d'Hirshfeld et le noyau atomique le plus près situé à **l'extérieur** de cette surface
d_i	: distance séparant la surface d'Hirshfeld et le noyau atomique le plus près situé à **l'intérieur** de cette surface
DMF	: *N,N*-diméthylformamide
DMSO	: diméthyl sulfoxyde
d_{norm}	: contribution normalisée des d_e et d_i en rapport aux rayons de van der Waals des atomes impliqués
equiv.	: équivalent
ESI	: electrospray ionisation
Et	: éthyle
FTIR	: Fourier transform infrared
g	: gramme

GoF : goodness-of-fit

h : heure

HOMO : highest occupied molecular orbital

HRMS : high-resolution mass spectrometry

Hz : hertz

hν : sous irradiation

IR : infrarouge

J : constante de couplage

K : Kelvin

LUMO : lowest unoccupied molecular orbital

M : molaire

m : masse ou multiplet (en RMN)

m/z : ratio masse / charge

Me : méthyle

Mes : mesitylène

mg : milligramme

MHz : mégahertz

min : minute

mL : millilitre

mm : millimètre

mM : millimolaire

mmol : millimole

mol : mole

mp : melting point

MS : mass spectrometry

nm : nanomètre

NMR : nuclear magnetic resonance

ORTEP : Oak Ridge Thermal Ellipsoid Program

$PC_{61}BM$: méthyl ester de l'acide [6,6]-phényl-C_{61}-butyrique

Ph : phényle

Phang : phosphangulène

PhCl : chlorobenzène

PhMe : toluène

ppm : partie par millions

q : quadruplet (en RMN)

quint : quintuplet (en RMN)

R_1 : facteur d'accord sur les réflexions observées

RMN : résonance magnétique nucléaire

rt : room temperature

s : singulet (en RMN)

T : température

t : triplet (en RMN)

THF : tétrahydrofuranne

UV : ultraviolet

V : volume

r^{vdW} : rayon de van der Waals

wR_2 : facteur d'accord pondéré

Z : nombre de molécules dans la maille élémentaire

Z' : nombre de molécules dans l'unité asymétrique

α : angle de déviation à la tangente

Δ : reflux

δ : déplacement chimique

λ : longueur d'onde

ρ : densité électronique

ρ_{calc} : calculated density (masse volumique)

χ : fraction molaire

Remerciements

La première personne que je dois remercier est bien évidemment mon directeur de recherche James D. Wuest. La rigueur scientifique, le souci du détail et la créativité ont fait de Jim un brillant chercheur. Je le remercie d'avoir partagé sa longue et solide expérience dans le domaine avec moi et de m'avoir dirigée et conseillée durant ce doctorat. La recherche scientifique est un océan tempétueux. En plus de m'avoir fourni bateau, cartes et boussoles, Jim a été un capitaine présent dans le bateau. Son implication dans le projet fût importante et sans lui, jamais je n'aurais été capable de faire la traversée de cet océan et de produire des résultats avec la même valeur. Il y a cependant autre chose mis à part son encadrement pour laquelle je voudrais le remercier.

Pendant les trois premières années de doctorat, je travaillais sur un projet qui ne fonctionnait pas. Je n'ai jamais réussi à synthétiser cette cible finale. Après trois ans, sans l'ombre d'un article en vue, et avec l'impression d'échec, il ne m'a pas demandé de commencer à rédiger ma thèse par résultats. J'imagine que j'aurais pu finir mon doctorat en quatre ans, en soumettant une thèse décrivant toutes les tentatives entreprises qui ont toutes échoué dans la synthèse de cette cible. J'aurais fini dans les temps, mais ça n'aurait pas été glorieux. Je n'en ai jamais discuté avec lui, mais je crois que pour Jim, il est préférable de finir une thèse en deux fois plus de temps et d'y présenter des résultats publiables où les objectifs ont été atteints, que de soumettre une thèse décrivant des travaux qui n'ont pas mené à rien, mais qui est dans «les temps». Pour ceux qui connaissent Jim, les délais ne sont pas toujours une priorité pour lui. Il lui arrive d'arriver en retard aux réunions de groupe ou de soumettre un formulaire à la dernière minute au département. Par contre, tout ce qui passe par lui est de

grande qualité. Il a un sens du perfectionnisme développé. Ses standards sont très hauts. Avec lui, j'ai appris que bien qu'il est important de respecter les délais, il est encore plus important de fournir un travail de qualité et que l'investissement du temps supplémentaire en vaut la peine. Je le remercie de m'avoir gardée plus longtemps, car finalement ma thèse en aura valu la peine. Ça m'aura pris plus de temps, mais au moins, j'ai quatre articles à vous présenter. Finalement, c'est un peu comme si j'avais fait deux doctorats. Un premier durant lequel je me suis acharchée sur un projet qui n'a mené qu'à des échecs pendant 2-3 ans, et un deuxième sur un autre projet qui a mené à quatre articles durant 4 ans. Il n'y aura pas une seule ligne dans la présente thèse concernant le premier projet. Alors je remercie Jim de m'avoir fait faire «un deuxième doctorat» plutôt que de m'arrêter à un seul, ce qui m'aurait laissée un goût très amer de la recherche.

La deuxième personne que je tiens absolument à remercier est Thierry Maris, notre cristallographe. C'est Thierry qui a fait toute la cristallographie présentée dans les travaux de cette thèse, et les études cristallographiques en sont un aspect important comme vous le verrez bientôt. Voulant maximiser mes chances d'obtenir des résultats, j'ai fait beaucoup de chimie combinatoire dans le but d'être sûre d'obtenir des cristaux. J'avais peut-être un total de 600 échantillons de cristallisation. Le moindrement que je pensais que l'échantillon avait le potentiel de produire une structure intéressante je le lui soumettais, même si j'avais des fois l'impression que les cristaux n'étaient pas de bonne qualité… Thierry ne s'en est jamais plaint et il m'a même miraculeusement produit des structures de cristaux difformes. Pour moi, c'est un magicien. Je lui ai soumis tellement d'échantillons et il a tellement travaillé sur ce projet.

S'il n'avait pas été là, je n'aurais pas cette thèse à vous présenter, ou du moins, pas de cette qualité du point de vue cristallographique.

Une autre personne importante qui mérite mes remerciements est Nino Gueorguiev, membre du groupe Wuest. Nino, qui aura fait sa maîtrise dans le groupe, est un garçon très brillant. Très passionné par la chimie, il connait des réactions apprises sur ses temps libres. En réunion de groupe, il est capable de proposer des solutions à des problèmes rencontrés par les doctorants du groupe et faire des suggestions de sous-projets ou de réactions alors qu'il n'est qu'à la maîtrise et est «moins expérimenté». Je le trouve exceptionnel. Il m'a aidée à comprendre certains mécanismes et principes de la chimie du phosphore. Je suis contente d'avoir pu, et que le groupe Wuest en général, ait pu profiter de sa curiosité et de ses connaissances.

Nino a commencé sa maîtrise vers la fin «de mon premier doctorat», alors que j'étais en pleine dépression majeure, causée entre autres, par les échecs répétés «du premier doctorat». C'est une personne qui s'intéresse à beaucoup de choses et parle avec beaucoup de passion. J'ai vite développé une amitié avec lui et c'est aujourd'hui un de mes meilleurs amis. Il m'a offert énormément de support moral. J'ai eu beaucoup de frustrations durant ce doctorat et il a été là pour m'écouter. Ça m'a fait du bien de l'avoir comme ami durant cette période difficile.

Enfin, je voudrais remercier mes parents. Ma mère a toujours beaucoup valorisé l'éducation, ayant elle-même deux maîtrises. Mes parents ne m'ont jamais demandé d'aller travailler pendant mon baccalauréat et j'ai pu continuer à vivre chez eux. J'ai pu ainsi me concentrer sur mes études pour avoir de bonnes notes. C'est ces bonnes notes qui m'ont permis d'obtenir des

bourses et de poursuivre au doctorat. Beaucoup d'étudiants doivent travailler durant leurs études, et de ce que j'ai vu, ils auraient pu avoir plus de succès et aller beaucoup plus loin dans leurs études si ce n'avait été de ces contraintes. Mes parents m'ont fourni le luxe de pouvoir me concentrer sur mes études. Ils ont toujours été là pour moi, même quand je ne pensais pas en avoir besoin. On prend toujours les choses que nous avons depuis notre naissance pour acquis et comme étant la base de tout être… La vérité est que tous les êtres humains ne grandissent pas dans les mêmes conditions. Je remercie mes parents de m'avoir fourni les conditions qui m'ont permise de me rendre jusqu'à un doctorat et qui ont fait de moi ce que je suis aujourd'hui.

Chapitre 1 :
Introduction

1.1 Introduction

Le XXI^{ème} s'annonce comme le siècle des appareils électroniques. Les ordinateurs, téléphones intelligents et tablettes se sont multipliés. L'avancée des technologies connait une croissance exponentielle. Les ordinateurs et autres appareils électroniques sont de plus en plus puissants, compactes et abordables. Le téléphone portable moyen d'aujourd'hui est plus puissant que les volumineux ordinateurs des années 1980 et 1990, et même ceux des années 2000. Cette avancé technologique fût permise par l'introduction de nouveaux dispositifs électroniques de plus en plus performants. Les diodes électroluminescentes, les transistors et les cellules photovoltaïques sont des exemples de nouvelles technologies permettant la production d'appareils électroniques innovateurs aux fonctions variées. Le monde de la recherche s'intéresse de plus en plus au développement de ces dispositifs.

Autrefois dominée par les matériaux inorganiques, cette industrie a connu la naissance et le développement de leurs homologues organiques. Ceux-ci promettent le développement d'une nouvelle génération de dispositifs plus légers, minces, flexibles et non-toxiques.[1-7] Parmi les matériaux organiques pouvant être exploités dans ces nouveaux dispositifs, on compte certains allotropes du carbone et leurs analogues, tels que le graphène, les nanotubes de carbone et les fullerènes. Les propriétés optoélectroniques et/ou semiconductrices intéressantes de ces composés sont ajustables par le biais de diverses stratégies telles que la fonctionnalisation et le contrôle morphologique. Dans le cas des cellules solaires organiques, où les fullerènes sont souvent employés en tant qu'électron-accepteurs, la morphologie au sein du matériau peut être critique. La modulation de celle-ci à l'échelle moléculaire peut être faite au moyen des

principes de la chimie supramoléculaire en faisant intervenir des associations intermoléculaires à l'état solide.

Le projet présenté dans cette thèse consiste au développement de nouveaux composés pouvant co-cristalliser avec fullerènes dans l'optique d'éventuelles applications dans le contrôle morphologique de dispositifs électroniques incorporant des fullerènes. Dans ce chapitre d'introduction, nous présenterons l'enjeu des technologies solaires, leur fonctionnement et leurs aspects morphologiques plus en détails. Une courte revue de la littérature sur les associations avec les fullerènes sera par la suite entreprise afin de situer nos travaux dans le domaine. Nous enchaînerons par la suite sur la présentation du motif de base de nos composés : le phosphangulène, une phosphine conjuguée aux propriétés remplissant les critères pour le mandat d'association avec fullerène à l'état solide. Enfin, les objectifs de cette thèse seront détaillés dans la dernière section de ce chapitre.

1.2 Cellules photovoltaïques organiques (OPV)

Il existe diverses technologies solaires développées depuis les années 1970. Les panneaux de silicium cristallin sont parmi les premiers employés dans le domaine et sont encore aujourd'hui les plus répandus pour l'utilisation à grande échelle. Néanmoins, la fabrication des panneaux de silicium était et reste encore aujourd'hui, onéreuse. En 1990, l'énergie générée par la technologie au silicium était estimée à 10 fois plus chère que celle produite par les méthodes traditionnelles.[8-9]

Les cellules à pigments photosensibilisateurs (« dye-sensitized solar cells » ou DSSC) ont ouvert le bal pour de nouvelles technologies au XXI^{ème} siècle. Un graphique montrant

l'évolution de ces technologies est présenté à la Figure 1.1. L'introduction de ligands organiques dans les DSSC a offert des composantes solubles et a ouvert ainsi la possibilité d'utiliser l'impression comme méthode de déposition. Cette évolution a été poussée plus loin par le développement des cellules photovoltaïques organiques (OPV). Ces dispositifs se basent sur une couche active constituée exclusivement de composés organiques, qui peuvent être des polymères ou des petites molécules. L'absence de métaux rares comme l'iridium ou le ruthénium dans le produit final ne permet pas nécessairement de réduire les coûts de production par rapport à ceux pour créer les DSSC, étant donné qu'il faut passer en contrepartie par des synthéses multi-étapes. Cependant, la présence uniquement de substances organiques permet d'envisager l'emploi de cellules solaires dans des objets ayant des contacts fréquents avec les êtres vivants. Par ailleurs, les cellules du type OPV et DSSC ont le potentiel d'être flexibles, promouvant ainsi l'application innovative dans des dispositifs électroniques portables. Cette technologie a un avenir prometteur.

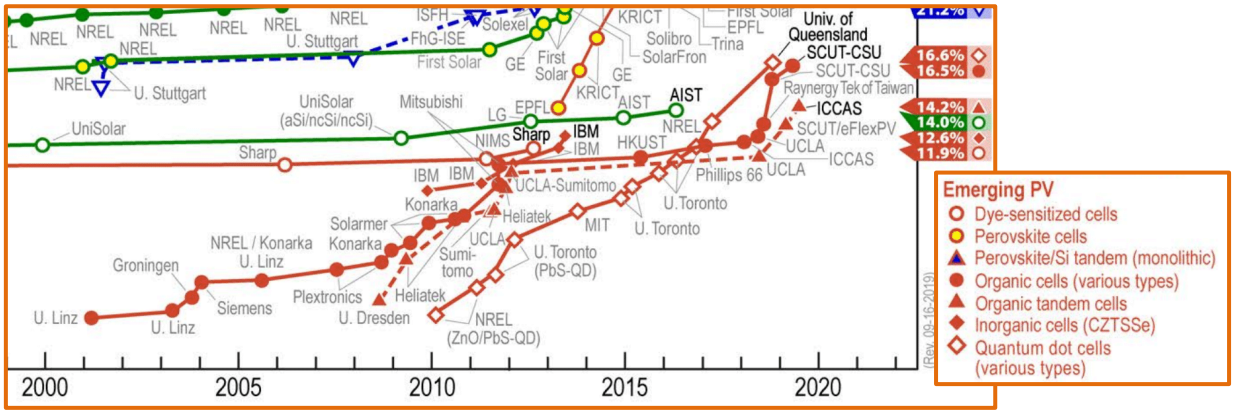

Figure 1.1 : Évolution des technologies émergentes en énergie solaire. Image tirée de la référence 10.

1.2.1 Fonctionnement

Dans l'optique d'optimiser les cellules OPV, il nous faut comprendre leur fonctionnement et ainsi leurs points faibles. La Figure 1.2 illustre le fonctionnement d'une cellule solaire organique bicouche simple. Deux composantes s'y retrouvent : le donneur et l'accepteur d'électrons. Les niveaux énergétiques des orbitales frontières de ces deux parties relativement de l'une à l'autre sont la clé du fonctionnement du dispositif photovoltaïque. Par définition, dans une cellule solaire, on veut promouvoir une circulation d'électrons suite à une excitation par un photon absorbé. On veut donc des électrons qui sont facilement excitables et qui diffusent aisément dans le matériel. Le donneur d'électron est un composé électron-riche dont la HOMO est plus haute en énergie que celle de l'accepteur. Ses électrons sont donc plus susceptibles à une photoexcitation. L'accepteur, comme son titre l'indique, est plus apte à accommoder des électrons de par son orbitale vacante plus basse énergétiquement (LUMO). L'électron excité du donneur peut alors relaxer vers la LUMO de l'accepteur, créant une séparation de charges et, par diffusion des charges, un courant électrique.

Le fonctionnement se résume ainsi par les étapes suivantes en se référant à la Figure 1.2 :

1) absorption des photons par la composante donneur générant ainsi des excitons (électron excité pairé avec la charge positive générée par son absence ou « trou »),

2) diffusion des excitons dans le matériel jusqu'à l'interface donneur-accepteur,

3) dissociation des charges, l'électron excité se rendant dans la LUMO de l'accepteur, et enfin,

4) transport des charges jusqu'aux électrodes, générant ainsi un courant électrique.

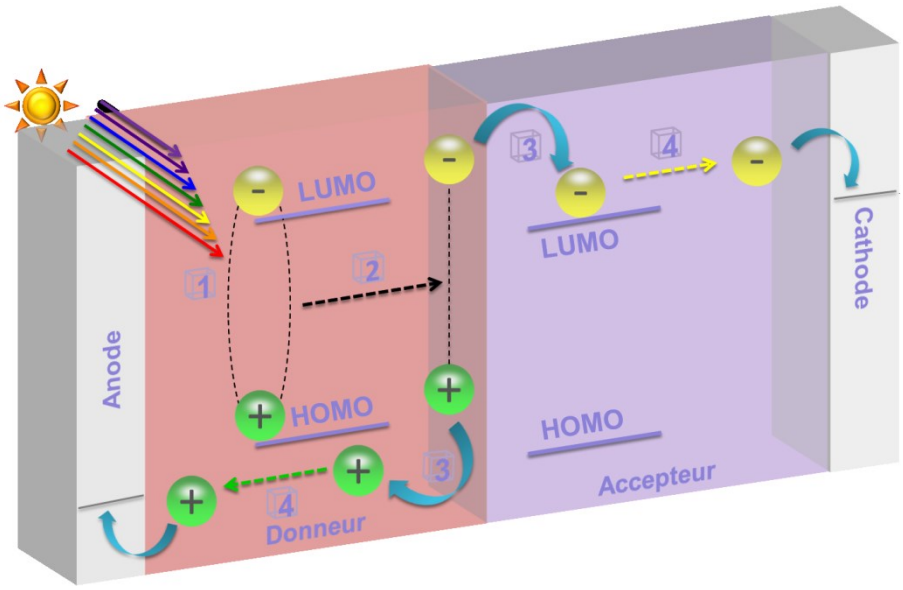

Figure 1.2 : Fonctionnement d'une cellule solaire organique de morphologie de type bicouche. Les niveaux énergétiques relatifs des orbitales frontières y sont schématisés. Il y a 1) absorption des photons par la composante donneur générant ainsi des excitons (électron excité pairé avec la charge positive générée par son absence), 2) diffusion des excitons dans le matériel jusqu'à l'interface donneur-accepteur, 3) dissociation des charges, l'électron excité se rendant dans la LUMO de l'accepteur et 4) transport des charges jusqu'aux électrodes. Le schéma est une gracieuseté de Dr. Minh-Trung Dang, ancien stagiaire postdoctoral dans le groupe Wuest.

1.2.2 Problèmes de morphologie

Afin d'améliorer les performances des cellules solaires ayant cette architecture, il va de soi d'optimiser les différentes étapes constituant le processus photovoltaïque. En faveur de la dissociation des charges (étape 3), on peut conclure qu'il est avantageux d'accroître le nombre

d'hétérojonctions entre l'accepteur et le donneur. En ce sens, une couche active composée d'un mélange uniforme des deux composantes (Figure 1.3a) semble indiquée à priori.

Néanmoins, une complication de la morphologie de la Figure 1.3a entre en jeu en ce qui concerne l'étape du transport des charges aux électrodes correspondantes (étape 4). Les charges ne peuvent diffuser à travers le matériel sans risquer de se recombiner. De plus grands domaines sont donc indiqués au détriment de l'interface telle que représentée à la Figure 1.3 b.

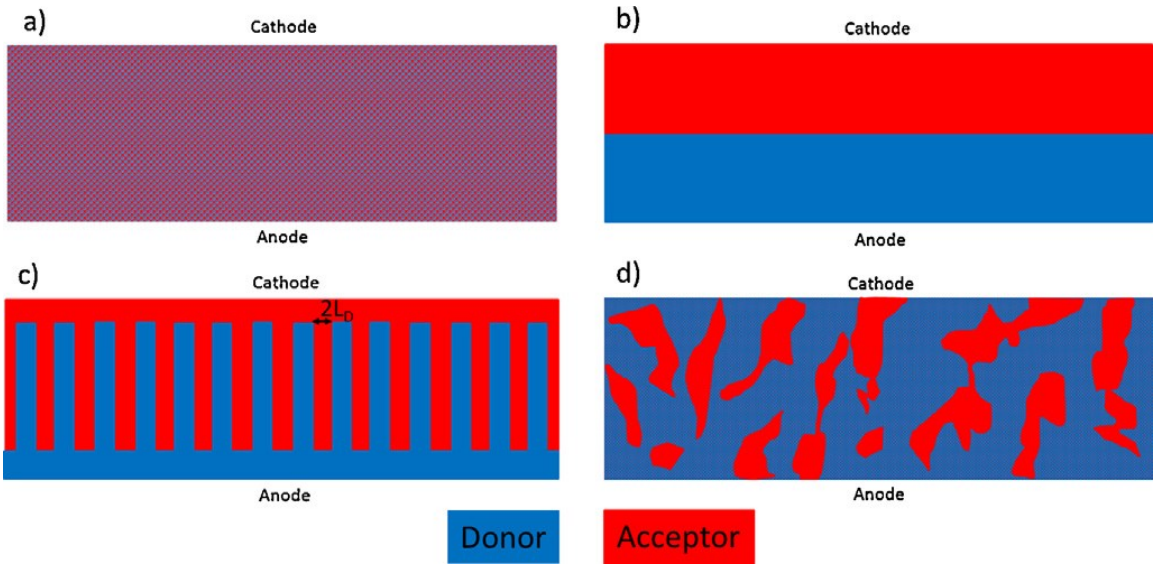

Figure 1.3 : Représentations des différents types de morphologies d'hétérojonction dans les cellules solaires. a) Mélange « homogène » ou avec de très petits domaines de donneurs et d'accepteurs. b) Hétérojonction en bicouche. c) Morphologie idéale de peignes imbriqués, où L_D est la distance de diffusion. d) Morphologie communément employée d'hétérojonction de masse. Image tirée de la référence 11.

Ainsi, un grand nombre de domaines de donneurs et d'accepteurs promeut la dissociation des excitons, mais de trop petits domaines diminuent l'efficacité du transport de charges vers les

électrodes correspondantes. Il y a alors un compromis à faire en vue de satisfaire les préférences de ces deux étapes. La morphologie idéale serait donc celle représentée à la Figure 1.3c, où les deux composantes sont interpénétrées l'une dans l'autre. La largeur idéale des domaines est égale à deux fois la distance de diffusion des excitons $L_{D,}$ ce qui correspond à environ 10 nm (donc 20 nm de largeur). Il est toutefois difficile d'obtenir une telle morphologie en pratique. La morphologie la plus commode est celle de l'hétérojonction de masse (*bulk heterojunction;* Figure 1.3d). La stratégie consiste à faire une solution du donneur et de l'accepteur, de la déposer sur le substrat, d'en évaporer le solvant et de procéder à un recuit qui résultera en la formation de domaines de taille variable selon les conditions de recuit.[11]

Par ailleurs, mises à part les performances initiales des cellules solaires organiques, il y a aussi un aspect de stabilité dans le temps à prendre en compte. Par définition, une cellule solaire doit être exposée au soleil pour remplir ses fonctions. Cette exposition cause une exposition à la chaleur qui à la longue aura les mêmes effets qu'un recuit. La taille des domaines risque alors de varier au fil de l'utilisation de la cellule, changeant alors la morphologie initiale et optimale, et donc diminuant significativement les performances du dispositif et sa durée de vie. Le contrôle morphologique est un aspect majeur dans la performance des cellules solaires organiques et suscite nombreuses recherches.[12-17]

Plusieurs des dispositifs photoélectroniques nécessitent une attention particulière à la morphologie à l'échelle nanoscopique de leurs composantes actives afin de fonctionner de façon optimale, voire de fonctionner tout court. Il n'est pas toujours évident de contrôler la morphologie au niveau du nanomètre à l'aide de méthodes physiques industrielles. De plus,

même lorsque ce contrôle est réussi, la stabilité dans le temps, et sous les conditions d'utilisations du dispositif, de la morphologie idéale n'est pas garantie. En effet, sous l'effet de la chaleur dû à l'exposition solaire ou à un courant électrique, un recuit peut survenir, entraînant un changement de morphologie. Ce problème touche particulièrement les cellules solaires organiques OPV.[13, 15]

Les principes de la chimie supramoléculaire inspirent des solutions en matière de contrôle morphologique en travaillant à l'échelle moléculaire. En exploitant les propriétés supramoléculaires des composantes actives, il est possible de contrôler leur auto-assemblage et donc leur morphologie et ainsi la stabilité de la couche active.[18] Une stratégie classique en sciences consiste à tirer parti des propriétés physico-chimiques des composantes moléculaires du système, particulièrement lorsque les problèmes sont originaires de ces composantes. Ici, nous ciblerons les fullerènes qui sont souvent employés en tant qu'électron-accepteurs dans les cellules photovoltaïques organiques.

1.3 Les fullerènes et leurs propriétés

En 1996, le prix Nobel de chimie fût décerné à Robert F. Curl Jr., Sir Harold W. Kroto et Richard E. Smalley pour la découverte dans les années 1980 du buckminsterfullerène, communément appelé C_{60}.[19] Depuis cette découverte, une nouvelle classe d'allotropes du carbone a vu le jour : les fullerènes, définis comme étant les composés présentant une surface courbe d'atomes de carbone π-conjugués. Dans cette famille, on retrouve le C_{60} et son cousin le C_{70}. Cette nouvelle classe des formes allotropiques du carbone s'est vue être le sujet de nombreuses études tant pour la curiosité scientifique que constituent de telles molécules que pour leurs applications dans le domaine des sciences des matériaux, de la nanotechnologie et de l'électronique.

Souvent incorporé dans les dispositifs photovoltaïques, le buckminsterfullerène, ou C_{60}, sert d'accepteur d'électrons. Grâce à la taille du système conjugué et aux niveaux énergétiques de leurs orbitales frontières, le C_{60} et d'autres fullerènes sont d'excellents accepteurs d'électrons et forment des anions stables. On ajoute à ça leurs propriétés photochimiques exceptionnelles : une photoexcitation permet de générer un état excité triplet de longue durée de vie avec un rendement quantique de près de 100 %.[20]

1.3.1 Découverte

Le C_{60} fut généré et observé au laboratoire pour la première fois en 1984 par Rohling, Cox et Kaldor alors qu'ils vaporisaient du carbone à l'aide d'un laser (Figure 1.4).[21] Ils reportèrent la production d'agrégats d'atomes de carbone C_n où n = 1 – 190. L'année suivante, Kroto, Smalley et Curl répétèrent l'expérience. Ils obtinrent des molécules constituées de soixante

atomes de carbone dont l'analyse indiquait une structure comportant des cycles à 5 et à 6 semblables à ceux retrouvés dans le produit de départ, le graphite. En se basant sur les études de Buckminster Fuller, ils proposèrent alors la structure d'icosahèdre tronqué que nous connaissons.[19 22-24]

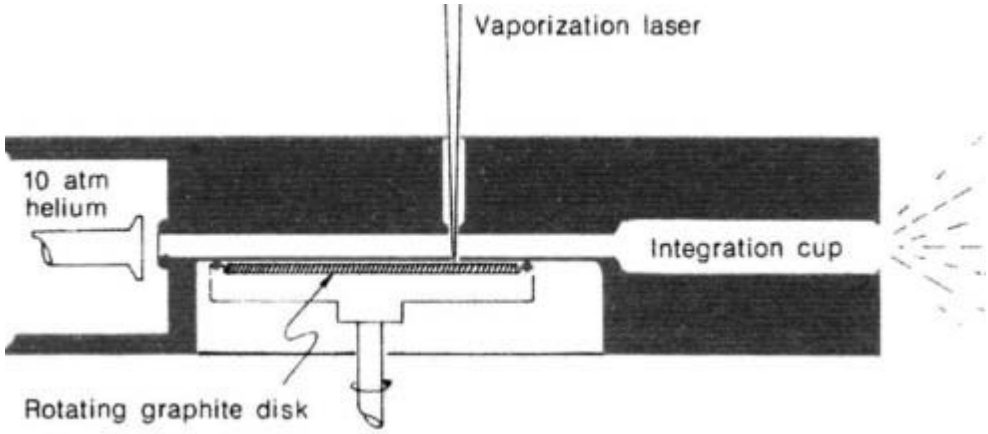

Figure 1.4 : Schéma de l'appareil employé pour la formation et l'analyse des agrégats de carbone résultant en la découverte des fullerènes. Image originale tirée de la référence 23.

La spectrométrie de masse a donné la preuve péremptoire de l'existence des buckyballes C_{60} et C_{70}. En effet, dans tous les spectres de masse des produits résultant de la sublimation induite au laser de graphite, un pic à 720 u.m.a était systématiquement présent, masse qu'aurait une molécule constituée de 60 atomes de carbone.

1.3.2 Structure

Le C_{60} et le C_{70} sont des cages fermées possédant une symétrie de rotation d'ordre 5; le C_{70} comporte un axe de symétrie C_5 et le C_{60} en présente 6 tel que le représente la Figure 1.5. Le C_{60} est considéré comme une molécule à haute symétrie, du groupe I_h, pour icosahèdre,

polyèdre dont les sommets tronqués résultent à la forme de la molécule. La forme géodésique des fullerènes a inspiré leur nom, en l'honneur de l'architecte américain Buckminster Fuller, connu pour le design du dôme géodésique. Un exemple célèbre de ce design est la Biosphère de Montréal (Figure 1.6).

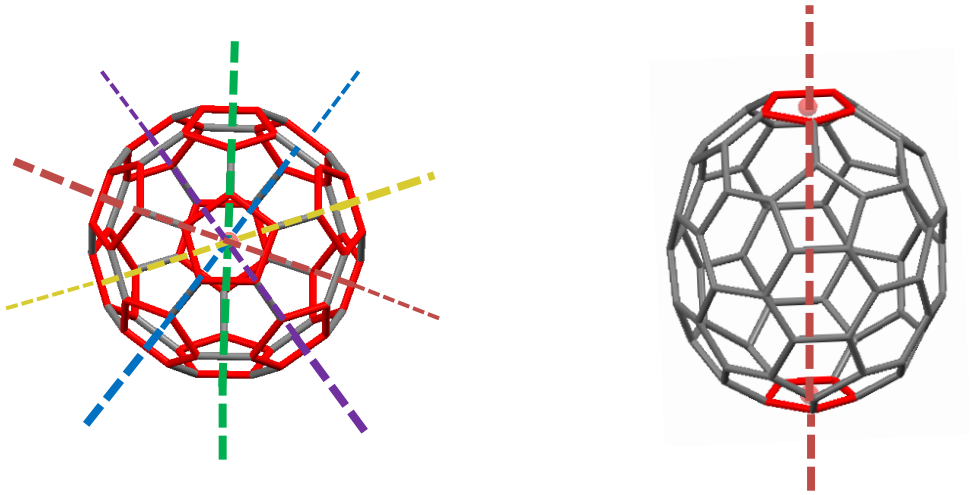

a b

Figure 1.5 : a) Structure du C_{60} montrant les 12 cycles à 5 en rouge. Chaque cycle à 5 est traversé en son centre par un axe de symétrie C_5 passant par le centroïde de la molécule. b) Structure du C_{70} montrant les deux cycles à 5 par où l'axe de symétrie C_5 passe.

Figure 1.6 : Biosphère de Montréal, conçue par l'architecte Buckminster Fuller. Image tirée de la référence 25.

Chaque atome de carbone dans le buckminsterfullerène est lié de façon covalente à trois autres en partageant trois de ses quatre électrons de valence. À priori, on pourrait penser que les atomes ont une hybridation sp^2 classique. Pourtant, la longueur des liens mesurée expérimentalement porte à croire que l'hybridation sp^2 n'est pas tout à fait la plus cohérente. D'abord, les liens les plus courts ne sont pas purement des liens doubles et les liens les plus longs n'ont pas non plus un caractère purement simple. Normalement, la longueur des liaisons dans le benzène est de 1,39 Å et celle du lien double dans le cyclopentène est de 1,337 Å. Or, pour le C_{60}, dans les structures obtenues par diffraction des rayons X, on observe que le lien 6,6 (le lien partagé par deux cycles à six) est de 1,355 Å et de 1,467 Å pour le lien 5,6 (lien partagé entre un cycle à cinq et un cycle à six). Ceci est expliqué par la pyramidalisation dans la molécule.

Étant donné que la molécule est sphérique, il y a une distorsion de la géométrie trigonale des carbones normalement sp^2 vers une géométrie tétraédrique plus propice à l'hybridation sp^3.

L'angle de pyramidalisation θ_p est défini par l'Équation 1.1 et quelques exemples sont présentés dans la Figure 1.7. Plusieurs exemples sont placés sur la courbe d'hybridation de l'orbitale π en fonction de l'angle de pyramidalisation sur le graphique de la Figure 1.8. Sur ce graphique, on remarque que l'orbitale π du C_{60} a un caractère s élevé. On comprend alors que les orbitales σ n'ont plus un caractère s normal et que l'hybridation se situe entre sp^2 (comme le graphite) et sp^3 (comme le diamant). Le fait que l'orbitale 2s du carbone s'est à présent invitée dans l'orbitale π, et qu'elle est beaucoup plus basse en énergie qu'une orbitale 2p, fait en sorte que les orbitales moléculaires résultantes de cette réhybridation auront une affinité électronique élevée comparativement aux orbitales moléculaires π standards découlant uniquement d'orbitales atomiques 2p du carbone.[26]

$$\theta_p = (\theta_{\sigma\pi} - 90)$$

Équation 1.1 : Angle de pyramidalisation θ_p défini comme la différence entre l'angle $\theta_{\sigma\pi}$ (entre le vecteur d'axe de l'orbitale π (*π-orbital axis vector*; POAV) et l'orbitale σ d'un des liens carbone-carbone) et 90°.

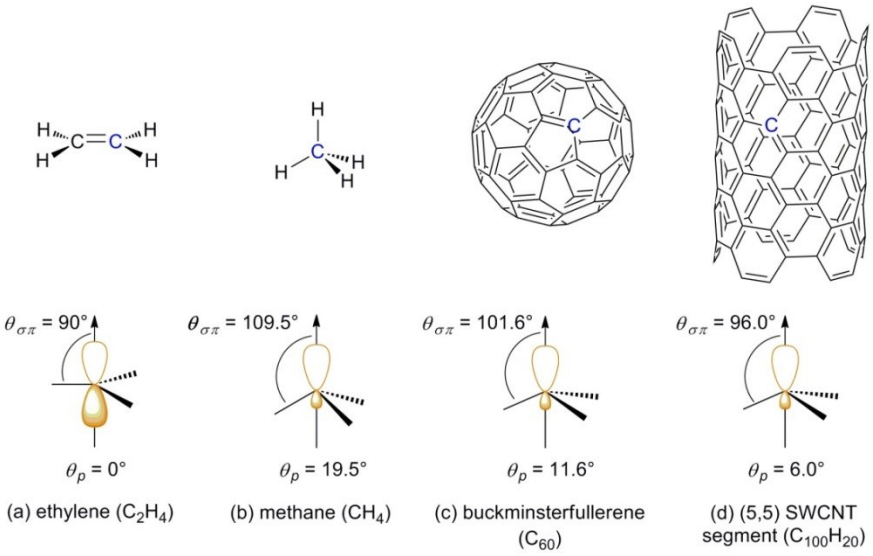

Figure 1.7 : Exemple d'angles de pyramidalisation. Image tirée de la référence 27.

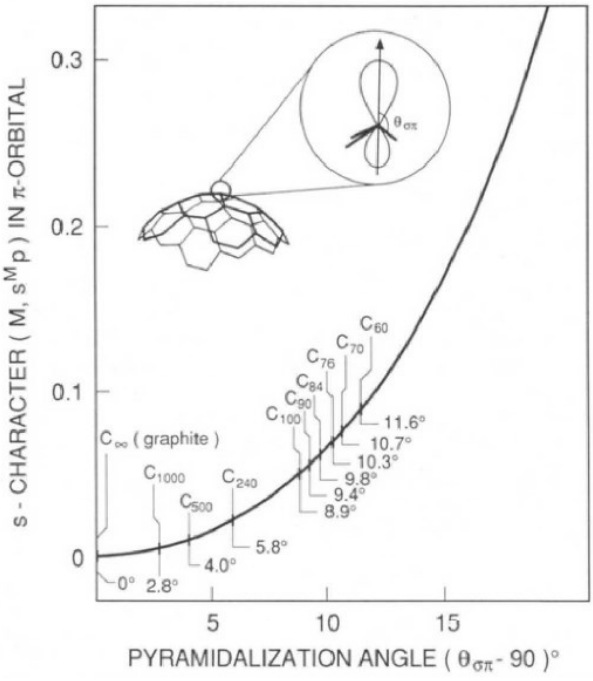

Figure 1.8 : Courbe de réhybridation selon l'angle de pyramidalisation. Graphique tiré de la référence 26.

1.3.3 Aromaticité

Pour déterminer si un composé est aromatique ou non, la règle de Hückel, où 4n+2 électrons π correspondent à un composé aromatique et 4n à un composé anti-aromatique, est une généralité permettant de rapidement répondre à la question. Si les annulènes et hétéroannulènes bidimensionnels obéissent à cette règle empirique, il en va autrement lorsqu'on adresse l'aromaticité de structures tridimensionnelles telles que les fullerènes. [24, 28-29] Une analyse plus poussée du système en question est nécessaire.

L'aromaticité est caractérisée par une stabilité et réactivité particulières d'un composé, et par certaines propriétés magnétiques. La stabilité de résonance des fullerènes n'est pas mesurable expérimentalement, puisqu'une comparaison d'énergie d'hydrogénation avec un fullerane mono-insaturé serait requise. De plus, le critère de réactivité est invalide dans le cas des fullerènes puisqu'il n'y a pas d'hydrogène pouvant être substitué.[28] Au niveau des propriétés magnétiques, le déplacement chimique indépendant du noyau (*nucleus-independent chemical shift*) NICS proposé par Schleyer et ses associés[30] s'est avéré à être un outil efficace dans la détermination de l'aromaticité. Il s'agit d'une méthode computationnelle calculant la valeur du blindage magnétique au centre d'un cycle. Lorsqu'un composé est aromatique, il y a un courant de cycle provoquant un champ magnétique. Au centre du cycle, le champ magnétique du cycle blinde et en RMN, on observe des valeurs vers le haut-champs. Les indices de NICS seront négatifs pour des composés aromatiques et positifs pour des anti-aromatiques. Pour les fullerènes, mises à part les méthodes computationnelles basées sur la mécanique quantique moderne,[31-32] les valeurs NICS peuvent être obtenues expérimentalement par mesure du déplacement chimique du ^{3}He situé dans un endofullerène.[33-36] Dans des travaux rapportés

dans le journal *Nature*, Saunders et ses associés[33] rapportent le spectre RMN du ^{3}He (Figure 1.9). On voit clairement que les fullerènes blindent le noyau d'hélium situé dans leurs cages : -6,3 ppm dans le C_{60} et -28,8 ppm dans le C_{70}. Ces valeurs observées sont comparables à celles prédites par Haddon[37] selon lesquelles le C_{60} devrait avoir un faible courant de cycle probablement paramagnétique. Le blindage devrait être moindre que dans le C_{70} qui devrait, selon les calculs, avoir un courant de cycle diamagnétique significatif.

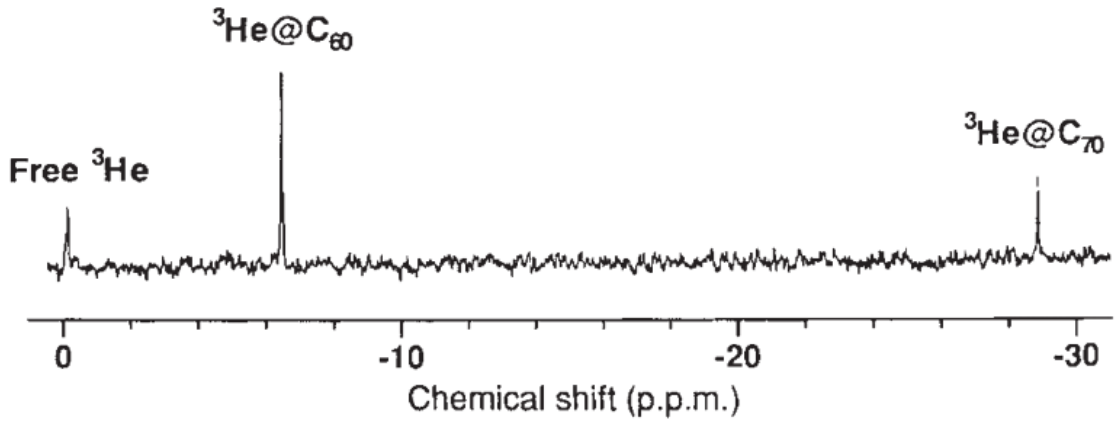

Figure 1.9 : Spectre RMN du ^{3}He (381 MHz) de composés de fullerène endohèdraux en solution dans le 1-méthylnaphtalène, obtenus en soumettant un mélange de C_{60} et de C_{70} à une pression de 2500 atm de ^{3}He à 600 °C pendant 5 h. Image tirée de la référence 33.

La différence notable de blindage entre le C_{60} et son analogue C_{70} s'expliquerait par la proportion de cycles à cinq et de cycles à six. Le déplacement chimique des protons des adduits de carbène avec le fullerène se trouve à haut-champs lorsqu'au-dessus d'un cycle à six et à bas-champs lorsque situé au-dessus d'un cycle à cinq.[38-39] Ainsi, le courant de cycle est diamagnétique pour l'anneau à six membres et paramagnétique pour celui à cinq. Ces courants

s'opposent et s'annulent; il est d'environ -4,5 ppm pour un cycle à six et de +7 ppm pour un cycle à cinq.[40] Ces valeurs sont concordantes avec les résultats obtenus par Saunders : C_{60} (12 cycles à cinq et 20 cycles à six), 12 x 7 + 20 x -4,5 = - 6 ppm; et C_{70} (12 cycles à cinq et 25 cycles à six), 12 x 7 + 25 x -4,5 = -28,5 ppm. Il semble alors que le C_{70} devrait être catégorisé comme aromatique dû à son courant de cycle diamagnétique significativement important, alors que le cas du C_{60} est plus ambigu. Néanmoins, l'ambigüité est levée lorsque le C_{60} est réduit.

1.3.4 Propriétés rédox

Ceci nous mène à nous intéresser aux propriétés d'oxydo-réduction des fullerènes. Le C_{60} et le C_{70} peuvent tout deux accommoder l'ajout de jusqu'à six électrons de façon réversible.[41-42] Rabinovitz *et al.*[43] ont mené une expérience de sonde endohèdrale en RMN du ^{3}He dans laquelle les fullerènes C_{60} et C_{70} sont réduits par traitement au lithium métallique jusqu'à l'obtention des hexaanions. Le Tableau 1.1 résume les résultats rapportés. Le déplacement chimique du noyau d'hélium dans le C_{60} se voit être blindé massivement jusqu'à -49,3 ppm après six réductions, alors que celui dans le C_{70} est massivement déblindé jusqu'à +8,2 ppm. Le faiblement aromatique C_{60} devient très aromatique lorsque réduit : de -6,4 ppm la valeur de δ ^{3}He passe à -49,3 ppm. L'effet est opposé pour le C_{70} qui semble devenir légèrement anti-aromatique sous sa forme d'hexaanion et le déplacement chimique du noyau ^{3}He va vers les bas-champs (de -28,8 à +8,2 ppm).

Tableau 1.1 : Déplacement chimique de l'hélium endohèdral en RMN du ^{3}He pour différentes espèces de fullerènes neutres et hexaanioniques.

Espèce	δ ^{3}He@C_n (ppm)
C_{60}	-6,403
C_{60}^{6-}	-49,266
C_{70}	-28,821
C_{70}^{6-}	+8,198

On peut rationnaliser ces résultats en prenant en compte que la délocalisation des électrons est faible dans les fullerènes, et donc en se concentrant sur les structures ou sous-unités locales

obtenues suite à ces additions d'électrons. On peut voir les molécules de C_{60} comme étant composées de six unités pyracyclène tel que montré dans la Figure 1.10. Dans la structure du pyracyclène, les deux cycles à cinq ne sont pas aromatiques : ils ont cinq électrons π par unité. Lorsqu'on injecte un électron dans le fullerène, un de ces cycles a la possibilité de devenir aromatique (Figure 1.11). On peut donc relier ces faits entre eux; on peut réduire jusqu'à six fois le fullerène C_{60} car il possède six unités pyracyclène dont l'addition d'un électron permet la formation d'un anneau aromatique. Cet argument explique pourquoi le C_{60} devient plus aromatique lorsque réduit.

a b

Figure 1.10 : a) Structure du pyracyclène. b) Unité pyracyclène dans le C_{60} accentuée en rouge.

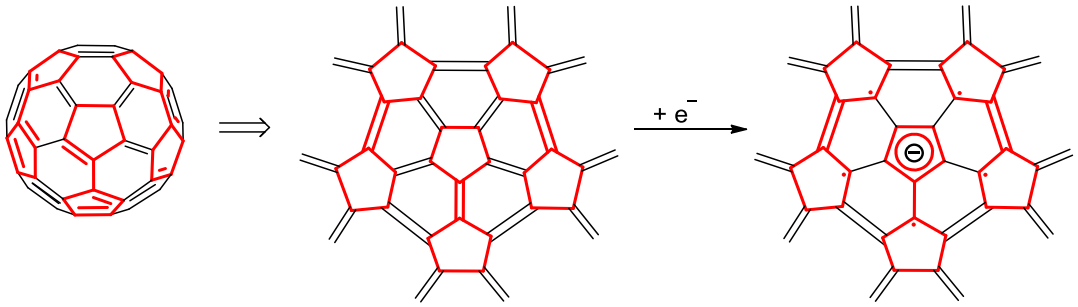

Figure 1.11 : Fragment d'une molécule de C_{60} centré sur un cycle à cinq qui devient aromatique suite à une réduction. Trois paires de cycles à cinq constituant un pyracyclène ont

été accentuées en rouge. On retrouve deux fois ce fragment dans le C_{60}. Il y a donc six unités pyracyclène.

Le C_{70} comporte également six sous-unités pyracyclène, ce qui explique la possibilité de le réduire lui aussi jusqu'à six fois. Echegoyen et ses collaborateurs[42] ont mesuré les potentiels de réduction des deux fullerènes jusqu'à l'hexaanion par voltampérométrie cyclique et différentielle (Figure 1.12). Ces potentiels sont rapportés dans le Tableau 1.2. Selon ces données, l'addition d'électrons sur le C_{70} serait plus facile que sur son homologue à 60 atomes, particulièrement dans le cas de la formation de l'hexaanion qui serait plus stable pour le fullerène ellipsoïde que pour le sphérique (-3,07 et -3,26 V respectivement). Il est à noter que la réduction plus aisée du C_{70} par rapport au C_{60} est très probablement le résultat de la délocalisation des électrons sur un plus grand réseau conjugué plutôt qu'une plus importante aromaticité résultante.

Tableau 1.2 : Potentiels de réduction versus le ferrocène ($E_{½}$ vs Fc/Fc^{+}) pour le C_{60} et le C_{70} tels qu'obtenus par Echegoyen et ses collaborateurs.[42]

	Potentiel de réduction (V)					
Réduction	1	2	3	4	5	6
C_{60}	-0,98	-1,37	-1,87	-2,35	-2,85	-3,26
C_{70}	-0,97	-1,34	-1,78	-2,21	-2,70	-3,07

On peut en conclure que ces deux fullerènes sont des agents d'oxydation et peuvent être réduits aisément par application de potentiel électrique ou par réaction chimique, par exemple, par traitement de métaux alcalins à l'état d'oxydation de zéro comme pour la réduction de Birch.[44]

a)

b)

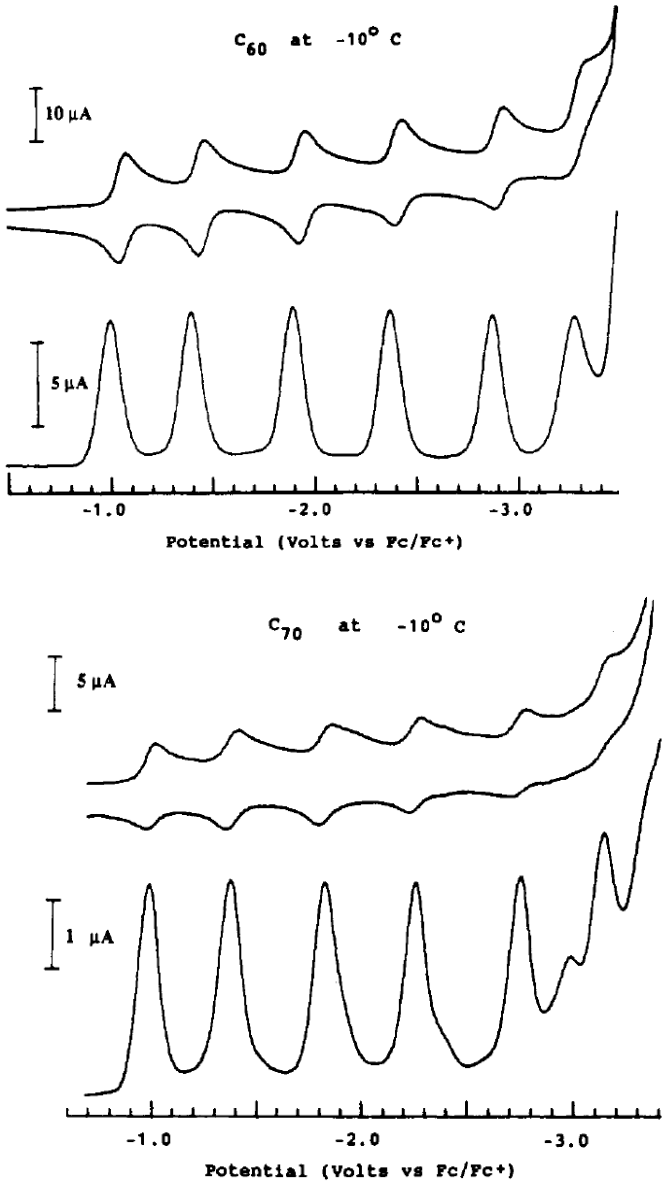

Figure 1.12 : Réduction du C_{60} (a) et du C_{70} (b) dans l'acétonitrile/toluène à -10 °C. Cyclovoltampérogrammes (courbes supérieures dans chaque graphique) à une vitesse de balayage de 100 mV/s; et voltampérogrammes différentiels (*differential pulse voltammetry*) (courbes inférieures dans chaque graphique) à impulsion de 50 mV, de durée d'impulsion de 50 ms, sur une période de 300 ms et à une vitesse de balayage de 25 mV/s. Image tirée de la référence 42.

1.3.5 Conductivité

Ainsi, les fullerènes sont des « éponges à radicaux » grâce à leur forte affinité électronique tel que démontré dans la section précédente sur leurs propriétés redox. Cette propriété, combinée à leur organisation à l'état solide, en fait un excellent candidat dans la chimie d'intercalation réductive à l'état solide. Malgré que le C_{60} à l'état fondamental et neutre soit un mauvais conducteur avec une bande interdite de 1,9 eV, lorsque mis en présence de bons électron-donneurs comme des métaux alcalins, sa conductivité électrique augmente de plusieurs ordres de magnitude.[45] Ceci a mené à un intérêt considérable dans l'étude de sels alcalins de fullerides intercalés.[46] Ces sels ont une stœchiométrie de M_xC_{60} où M est un élément de la famille des alcalins et x peut aller de 1 à 12 (RbC_{60} à $Li_{12}C_{60}$) dépendamment de la taille du cation et de l'état d'oxydation du fullerène pouvant aller de -1 à -12. Parmi eux, les sels de type M_3C_{60} se sont avérés à devenir des matériaux supraconducteurs en-dessous d'une température critique T_c, variant selon la nature et la taille du cation (Figure 1.13 a).[26, 47-51] Cette propriété est originaire de la nouvelle distribution des électrons dans les orbitales du trianion de C_{60}. Les trois électrons incorporés au fullerène peuplent l'orbital LUMO t_{1u} (Figure 1.13 b). La bande de conduction devient alors plus accessible en ayant une énergie de 1,2 eV.[46]

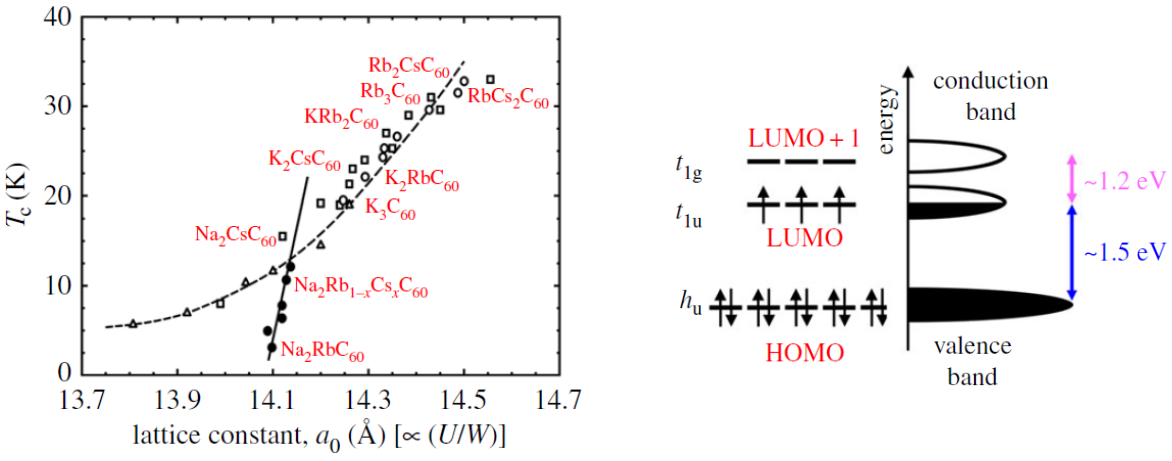

a b

Figure 1.13 : a) Température critique (T_c) de supraconductivité pour divers composés M_3C_{60} selon la constante cubique de maille a_0 pour les groupes d'espace face centrée cubique (M_3C_{60}) et cubique primitif (Na_2RbC_{60} ou Na_2CsC_{60}). Image tirée de la référence 46. b) Diagramme d'énergie des orbitales du C_{60}^{3-} dans un sel de type M_3C_{60} montrant la bande de valence et la bande de conduction.

Ainsi, les interstices entre les fullerènes créées par les cations influent sur la bande de conduction. Plus le cation dopant est volumineux, plus l'espacement entre les molécules de C_{60} augmente, et plus le recouvrement entre les molécules diminue. Cela mène alors à une largeur de bande de conduction réduite.[46] Deux différentes mailles élémentaires pour les sels alcalins du trianion de C_{60} sont présentées à la Figure 1.14.

a b

Figure 1.14 : Mailles élémentaires pour un sel de type M_3C_{60}. a) Cubique face centrée. b) Cubique centré. Image tirée de la référence 46.

1.3.6 Organisation à l'état solide

Ainsi, tel qu'abordé dans la section précédente sur la conductivité, l'organisation des fullerènes à l'état solide est un facteur primordial dans l'expression des propriétés du matériel. Les fullerènes forment des agrégats très facilement. Pour le C_{60} pur, ces amoncellements ont une structure cubique à face centrée (*fcc*) comme montré dans la Figure 1.17a. L'agrégation rend les fullerènes peu solubles dans les solvants organiques courants. Cet obstacle du point de vue pratique peut être contourné par la fonctionnalisation du composé.[52-54] En photovoltaïque organique, on emploie parfois, plutôt que le C_{60}, un dérivé soluble comme électron-accepteur : le méthyl ester de l'acide [6,6]-phényl-C_{61}-butyrique ($PC_{61}BM$). Les fullerènes sont peu solubles dans les solvants usuels, mais les meilleurs solvants sont aromatiques. Le $PC_{61}BM$ tend à cristalliser, bien que moins prône que le simple C_{60}, et forme ainsi de larges domaines cristallins, causant un changement morphologique dans le temps et diminuant la performance des dispositifs.[16-17]

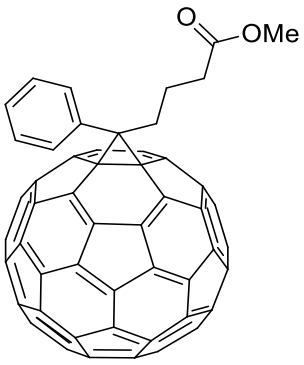

$PC_{61}BM$

Il est également possible d'altérer l'empaquetage des molécules de C_{60} dans la phase solide en y introduisant des partenaires de cocristallisation. On peut catégoriser les arrangements possibles du C_{60} en trois types selon le nombre d'axes dans lequel la formation se propage : en 1D où les fullerènes s'enchaînent dans une seule direction (Figure 1.15); en 2D où l'on voit la formation de couches (Figure 1.16); et en 3D où les molécules forment un réseau tridimensionnel (Figure 1.17).[55] Nous présenterons brièvement des exemples de chacune de ces catégories d'organisation à l'état solide dans cette section.

Parmi les formations unidimensionnelles les plus classiques du buckminsterfullerène dans les structures cocristallines, on compte (1) l'arrangement en mono-colonnes (Figure 1.15 a) qu'on peut obtenir dans le clathrate 1,3,5-triphénylbenzène · C_{60} · PhCl;[56] (2) les chaînes en zigzag (Figure 1.15 b) telles qu'observées pour le complexe de C_{60} · calix[5]arène;[57] et (3) une version plus compactée de ce dernier qu'est l'arrangement en double colonnes (Figure 1.15 c) qu'on retrouve dans la structure du complexe siloxane/C_{60}.[58]

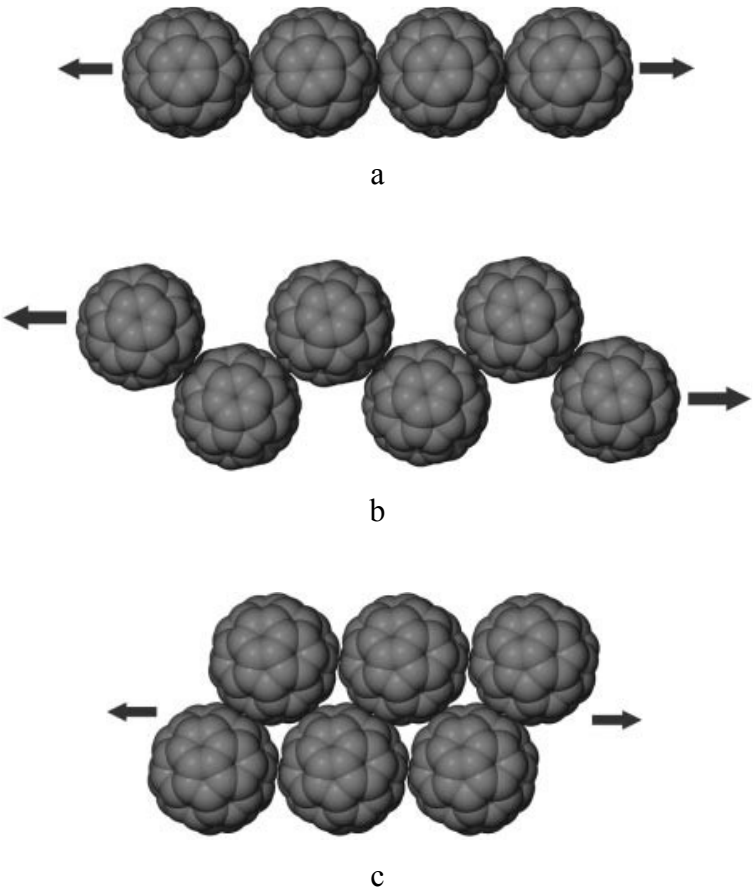

Figure 1.15 : Types d'organisations en 1D à l'état solide pour le C_{60}. a) Mono-colonne obtenue pour le clathrate 1,3,5-triphénylbenzène · C_{60} · PhCl (distance centroïde-centroïde : 10,10 Å).[56] b) Chaînes en zigzag obtenues pour le C_{60} · calix[5]arène (distance centroïde-centroïde : 10,03 Å).[57] c) Arrangement en double-colonnes dans un complexe de siloxane/C_{60} (distance centroïde-centroïde : 9,85–10,1 Å).[58] Images tirées de la référence 55.

En deux dimensions, comme beaucoup de molécules sphéroïdes, le C_{60} peut s'organiser en couche hexagonale comme dans un complexe avec le cyclotrivératrylène (Figure 1.16 a).[59] Les feuillets ondulés sont également un arrangement observable pour les molécules de C_{60} tel que montré à la Figure 1.16 b pour un complexe de tétraazacyclo-tétradécènenickel/C_{60}.[60] Moins

couramment, l'arrangement en ruche d'abeille du C_{60} peut être obtenu lorsque le composé est cocristallisé avec le tétraphénylporphyrine (Figure 1.16 c).[61]

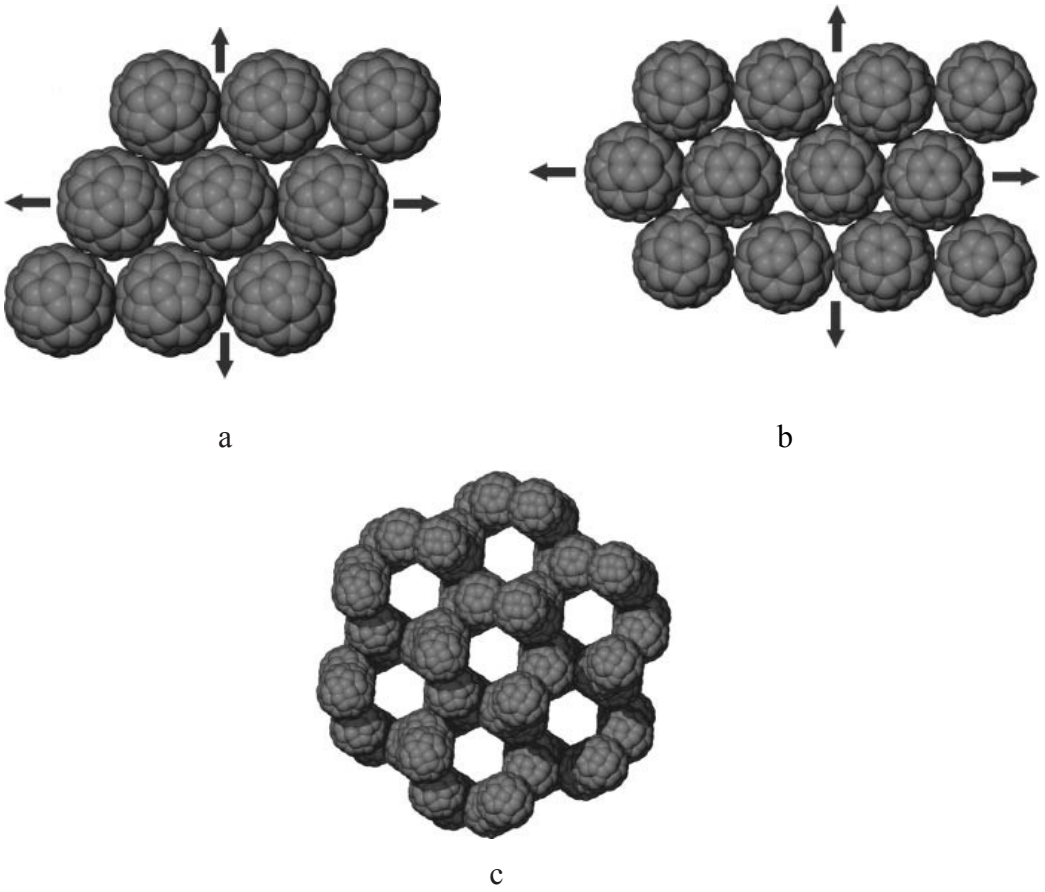

Figure 1.16 : Types d'organisations en 2D à l'état solide pour le C_{60}. a) Formation hexagonale comme dans le $(C_{60})_{1.5}$(cyclotrivératrylène) (distance centroïde-centroïde : 10,00-10,2 Å).[59] b) Arrangement en feuillets ondulés comme dans un complexe tétraazacyclotétradécènenickel/C_{60} (distance centroïde-centroïde : 9,99-10,07 Å).[60] c) Arrangement en ruche d'abeille du C_{60} lorsque cocristallisé avec le tétraphénylporphyrine (distance centroïde-centroïde : 9,98 Å).[61] Images tirées de la référence 55.

Enfin, parmi les réseaux tridimensionnels, on retrouve des structures cubiques des sels alcalins telles que présentées à la Figure 1.14, la structure *fcc* du C_{60} pur (Figure 1.17a) et de nombreux solvates du buckminsterfullerène. Comme on peut le voir dans l'empaquetement *fcc* de la molécule pure, il y a des interstices entre les unités sphéroïdes. La nature ayant horreur du vide, le C_{60} a tendance à former des solvates aisément afin de combler ces interstices. Un exemple classique est le solvate de disulfure de carbone tel que montré à la Figure 1.17b.

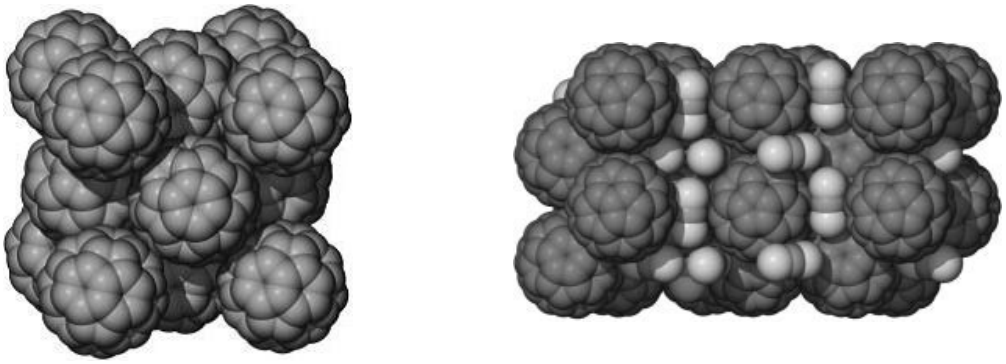

a b

Figure 1.17 : Types d'organisations en 3D à l'état solide pour le C_{60}. a) C_{60} à l'état pur (structure *fcc*). b) $(C_{60})_{1,5} \cdot CS_2$ (distance centroïde-centroïde la plus courte : 9,96 Å).[62] Images tirées de la référence 55.

On comprend ici que dépendamment du partenaire de cocristallisation, l'arrangement des fullerènes peut grandement varier. Encore une fois, l'organisation et la morphologie d'un matériel affectent ses propriétés. L'étude de l'association supramoléculaire des fullerènes avec divers additifs est de mise dans le but d'optimiser et de régler l'organisation à l'état solide pour les différentes applications électroniques.

1.4 Associations supramoléculaires de fullerènes

La forme sphérique des buckyballes a également inspiré des chercheurs à étudier la chimie supramoléculaire des fullerènes, surtout la conception des molécules pouvant les reconnaître et complexer. En effet, plusieurs tentatives furent entreprises dans le but d'obtenir un assemblage dans lequel le C_{60} ou le C_{70} serait contenu dans une cavité.[63-64] Les premiers assemblages rapportés dans la littérature furent ceux obtenus avec les hôtes traditionnels supramoléculaires (Figure 1.18), dont les aza-éther-couronnes,[65] les calix[n]arènes,[66-67] les calix[4]résorcinarènes,[68] les cyclotrivératrylènes,[69-70] et les cyclodextrines.[71-75] Mis à part ces classiques de la supramoléculaire, des cibles aux designs spécialement conçus pour s'associer avec les fullerènes ont été étudiées.

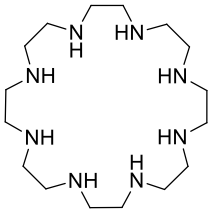

a

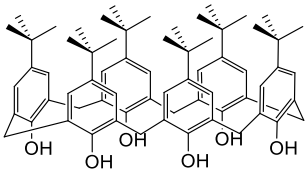

b

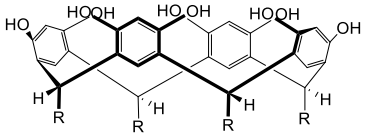

c

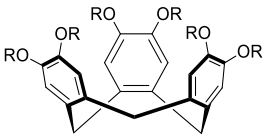

d

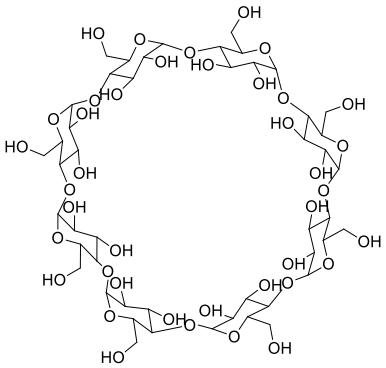

e

Figure 1.18 : Exemples d'hôtes classiques en chimie supramoléculaire. a) Aza-éther couronnes. b) Calixarènes. c) Résorcinarènes. d) Cyclotrivératrylènes. e) Cyclodextrines.

En exploitant la forme sphérique ou ellipsoïde des buckyballes et en les assemblant avec des molécules à surface concave, les chercheurs se sont aperçus qu'il existe une forme d'interactions particulières entre les surfaces moléculaires concaves et convexes. De nombreuses revues dans la littérature ainsi que des chapitres de livres résument bien les travaux des 30 dernières années sur le sujet des interactions concaves-convexes et des assemblages supramoléculaires de fullerènes.[18, 63-64, 76-85]

1.4.1 Interactions concaves-convexes

Mis à part la complémentarité géométrique des formes concaves et convexes, les interactions intermoléculaires constituent un facteur majeur dans la complexation des buckyballes comme dans tous les assemblages supramoléculaires. Il y a deux forces intermoléculaires principales :

1) **Les forces de van der Waals**. Elles désignent les interactions électrostatiques faibles. Il s'agit de forces attractives entre les dipôles permanents ou induits. Les fullerènes possèdent une grande surface prône à interagir avec les molécules environnantes.
2) **Les interactions électrostatiques.** Il s'agit d'interactions entre des espèces chargées opposées. Mis à part le résultat d'une ionisation, les fullerènes sont en général des espèces neutres. Néanmoins, étant donné que la surface π est courbée, il y a une polarisation asymétrique du nuage électronique de part et d'autre de cette surface. Le côté convexe est relativement plus pauvre en densité électronique par rapport au côté

concave. Kawase[86] introduit cet effet sous le nom **d'interactions π-π concaves-convexes**.

Ce cas particulier des interactions électrostatiques est de plus en plus mentionné et reconnu dans la littérature car on l'observe particulièrement chez les fullerènes. En effet, lors de la production de ceux-ci, il n'est pas rare d'observer des structures à couches multiples, imbriquées telles des poupées russes (

Figure 1.**19**).

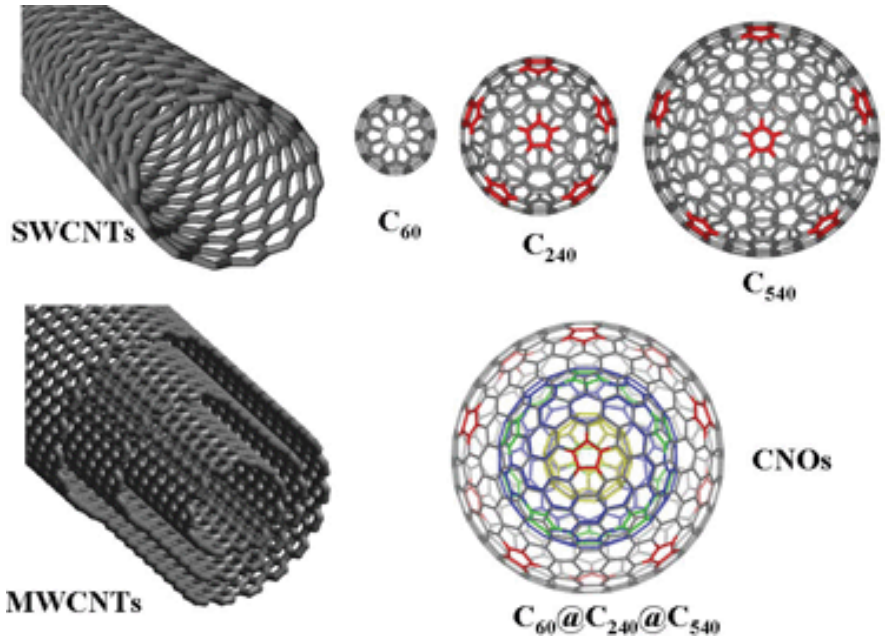

Figure 1.19 : Représentation des fullerènes imbriqués tels des poupées russes. Image tirée de la référence 87.

Ainsi, cela signifie que les interactions entre les couches courbées de graphène sont différentes de celles retrouvées dans les couches plates. Dû à la courbure de la surface, les orbitales π sont

polarisées et les interactions observées sont du type électrostatique plutôt que de van der Waals comme attendu pour des empilements π traditionnels plats (Figure 1.20 et Figure 1.21).[26, 88-90] On entend donc par interactions concaves-convexes la complémentarité de forme et la force électrostatique résultante de la courbure du système des orbitales π.

a b

Figure 1.20 : Représentations du système π du benzène. Les orbitales atomiques p sont utilisées pour la représentation. a) Système plan. b) Système incurvé.

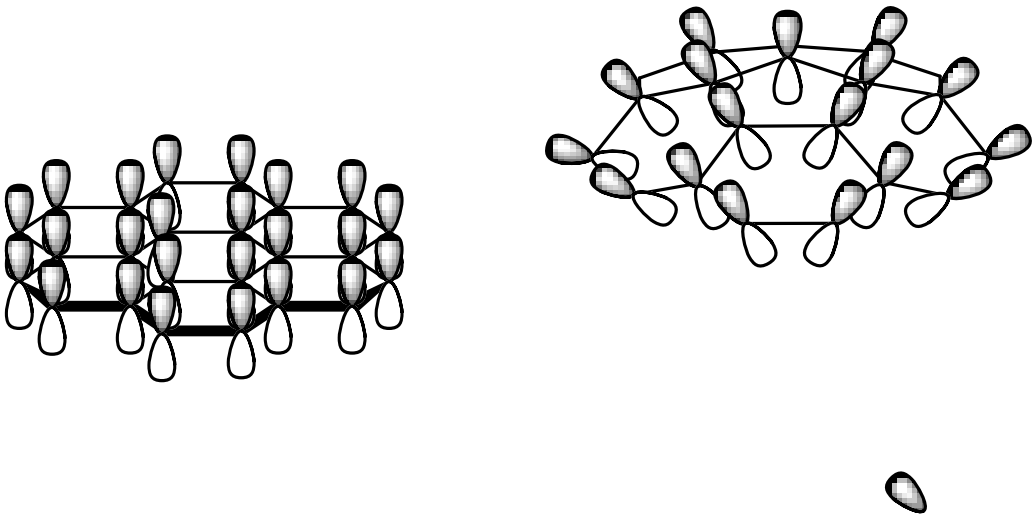

Système π plan Système π incurvé

a b

Figure 1.21 : Représentations des systèmes π. a) Coronène. b) Corannulène.

De nombreuses études computationnelles ont été entreprises dans le but de mieux comprendre et caractériser cette interaction, très souvent en se basant sur le modèle du corannulène.[91-104] Expérimentalement, plusieurs complexes de fullerènes avec un hôte concave ont été rapportés. On catégorise les hôtes concaves en deux groupes : ceux de forme ceinture et ceux de forme bol.

1.4.2 Hôtes de forme ceinture

Le type ceinture (*belt-shaped*) consiste en un macrocycle composé de cycles aromatiques faisant la périphérie du fullerène tel une ceinture. Les cycles aromatiques font face au fullerène de sorte à faire une interaction π-π concave-convexe. On peut y dénombrer les pillar[n]arènes,[105] quoique la déformation de leurs cycles aromatiques soit limitée (Figure 1.22), les macrocycles de dérivés de tétrathiofulvalène (TTF),[106-107] les cyclo-para-phénylacétylènes (Figure 1.23)[108] et les cycloparaphénylènes (Figure 1.24).[109-110]

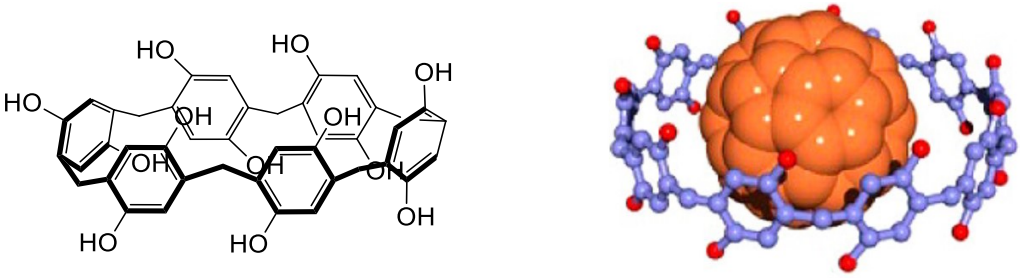

Figure 1.22 : Complexe de C_{60} dans un pillar[10]arène. Image tirée de la référence 105.

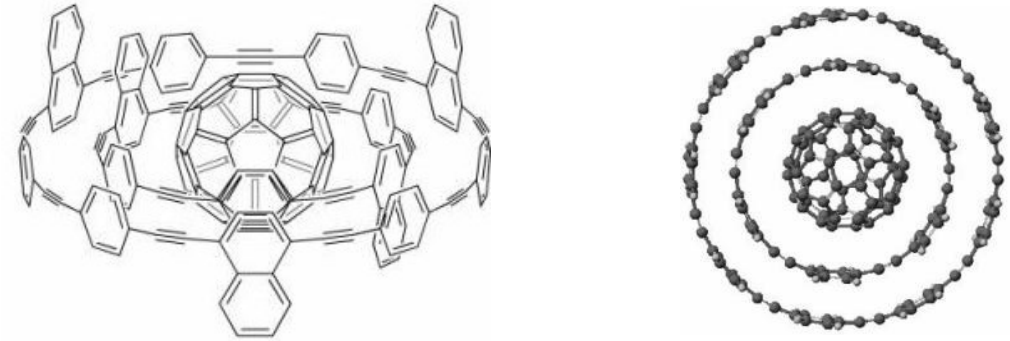

Figure 1.23 : Complexe de type oignon de C_{60} et de cycloparaphénylacétylènes. Image tirée de la référence 108.

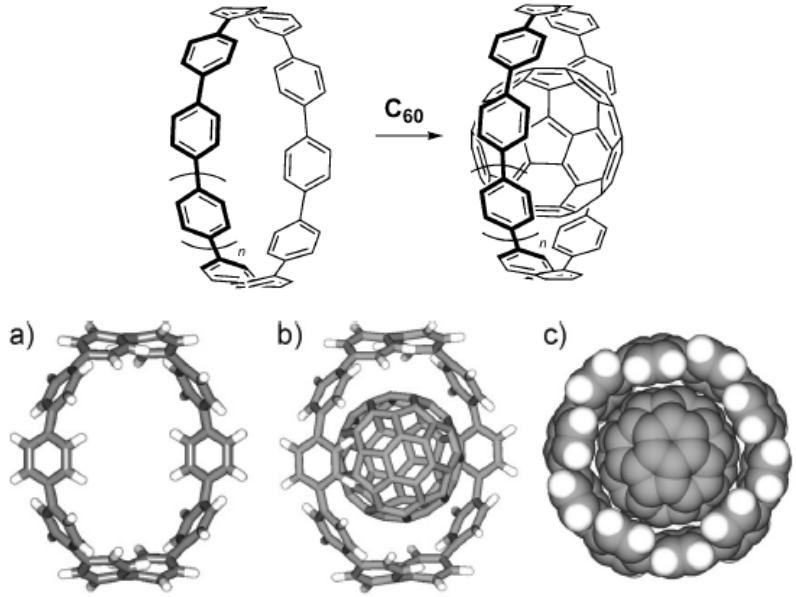

Figure 1.24 : Complexe de C_{60} dans un [10]cycloparaphénylène. Image tirée de la référence 110.

1.4.3 Hôtes de forme bol

Par forme bol, on entend une surface courbe et conjuguée dont la face concave permet d'accueillir le fullerène en le recouvrant partiellement. Plusieurs molécules de cette forme ont été le sujet d'études d'association avec les fullerènes. La majorité de ces bols sont des composés purement hydrocarburés comme le corannulène, le sumanène et le coronène, ou alors leurs dérivés fonctionnalisés. Nous nous pencherons davantage sur les hôtes de cette forme dans le récit de cette thèse.

1.4.3.1 Courbures induites par des cycles à 5 membres : les hémi-fullerènes

Les premiers candidats identifiés pour le mandat d'accueillir les fullerènes à la manière d'un bol furent le corannulène et le sumanène, deux hémi-fullerènes. Ce terme désigne les hydrocarbures polycycliques aromatiques et incurvés correspondant à un fragment de fullerène.[80, 90, 111] En effet, lors de la production de fullerènes, il n'est pas rare d'obtenir un mélange d'hydrocarbures aromatiques pouvant être interprétés comme des fragments ou intermédiaires vers les formes finies de carbone pure que sont les fullerènes. La Figure 1.25 représente une démonstration visuelle de la présence de la structure du corannulène dans le C_{60} et la Figure 1.26 la présence du sumanène.

a b

Figure 1.25 : a) Structure du corannulène. b) Présence de corannulène comme fragment dans le C_{60}.

a b

Figure 1.26: a) Structure du sumanène. b) Présence de sumanène comme fragment dans le C_{60}.

Il a donc semblé naturel d'exploiter des hémi-fullerènes pour y imbriquer un fullerène complet. Il fallait des hémi-fullerènes suffisamment ouverts, et donc des fragments suffisamment petits, comme le corannulène et le sumanène, pour y insérer une molécule de C_{60} ou de C_{70}. Quelques études computationnelles ont déterminé que l'interaction entre corannulène et C_{60} devrait être favorable, du moins en phase gazeuse.[112-113]

En effet, en 1993, Scott, Bohme et leurs associés ont démontré expérimentalement que le corannulène forme un complexe stable en phase gazeuse avec le cation de C_{60}.[114] Cependant, ce postulat a été difficilement prouvé pour les phases solides et en solution. Il y a eu d'abord

des versions altérées du corannulène ayant mené aux complexes en solution ou en phase solide.

Scott, Georghiou et leurs associés introduisent des dérivés thioaryles du corannulène en 2001 et 2005 (Figure 1.27).[115-116] L'incorporation d'atomes de soufre et de groupements aryles supplémentaires a impliqué l'ajout d'interactions de London à l'interaction concave-convexe, favorisant ainsi l'auto-assemblage. Cette stratégie fût reprise également pour le sumanène (Figure 1.28).[117]

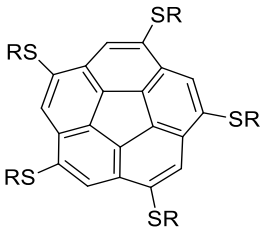

a

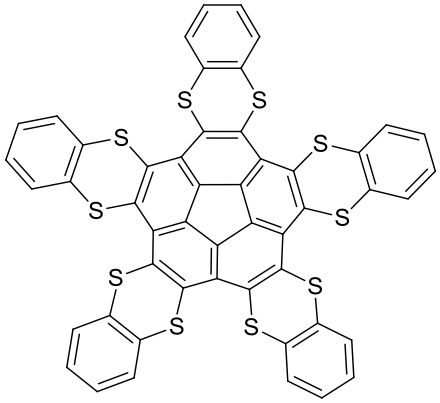

b

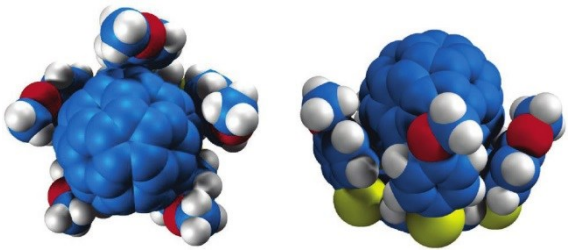

c

Figure 1.27 : a) et b) Dérivés sulfurés du corannulène développés par Georghiou. c) Structure tridimensionnelle hypothétique (n'est pas une image résultant d'une étude par diffraction à rayons X).[115-116] Image c tirée de la référence 116.

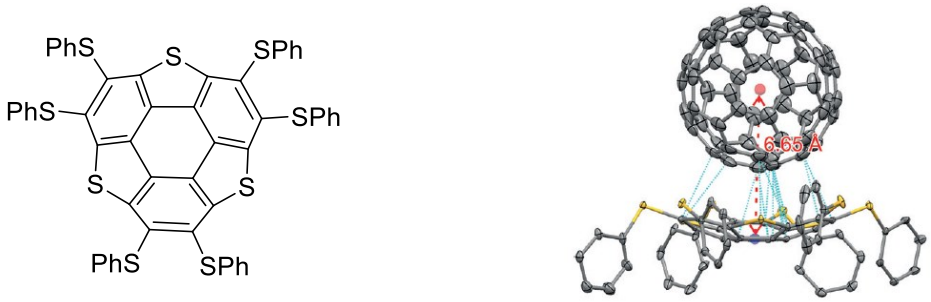

Figure 1.28 : Dérivés thioaryles du sumanène permettant la formation d'un complexe d'inclusion avec le C_{60}. Image tirée de la référence 117.

En 2007, Sygula et ses associés synthétisèrent un récepteur de fullerène constitué de deux unités corannulène reliées par un dibenzocyclooctatétraène, qu'ils nommèrent Buckycatcher (Figure 1.29).[118] Cet hôte de type *tweezer* (pince) mena à l'obtention de cocristaux avec le C_{60}, sans avoir recours à la présence d'hétéroatome électron-riche tel le soufre. Par effet coopératif, les unités corannulène furent en mesure de maintenir le C_{60} en place en formant deux fois plus d'interactions π-π concaves-convexes, tandis que l'unité cyclooctatétraène conféra à la fois suffisamment de flexibilité pour permettre l'ouverture de la cavité, et aussi suffisamment de rigidité pour maintenir la forme de la cavité fermée. L'obtention de ce complexe prouva qu'il est possible d'obtenir des associations purement π-π concaves-convexes entre un fullerène et un hôte PAH incurvé. À travers de nombreuses publications, Sygula et ses associés poursuivirent leurs travaux sur les récepteurs de fullerènes à base de corannulène en variant le groupement pontant et en fonctionnalisant les corannulènes.[94, 119-125] D'autres membres de la

communauté scientifique aux intérêts similaires s'en sont inspirés et ont développé leurs versions de Buckycatcher à base de corannulènes.[126-131]

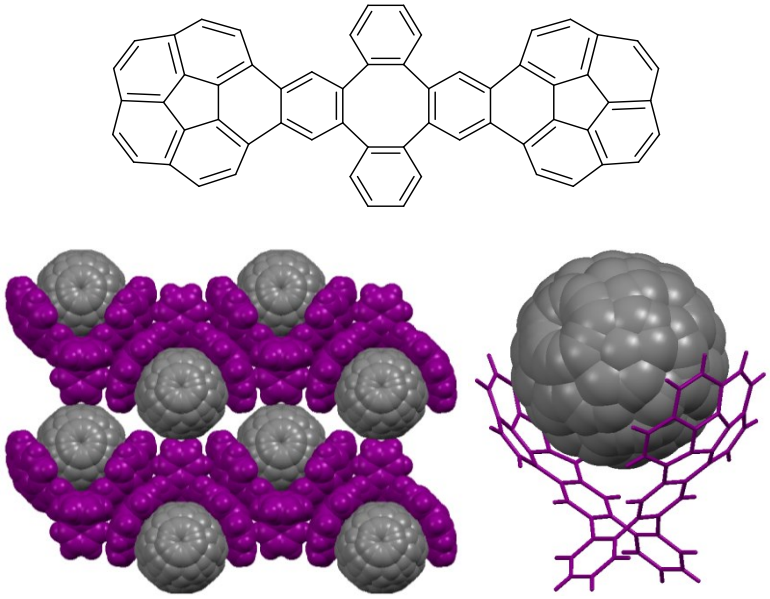

Figure 1.29 : Buckycatcher de Sygula *et al*.[118]

Plus tard, en 2008, Fasel et ses associés rapportèrent avoir réussi à obtenir une complexation du C_{60} avec du corannulène supporté sur une surface de Cu(110) (Figure 1.30) présentant ainsi des interactions π-π concaves-convexes.[132] On se rapprochait alors de l'association du C_{60} avec le corannulène pure et simple.

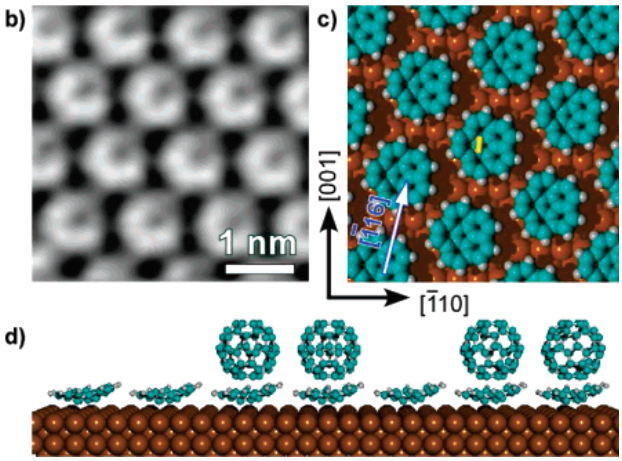

Figure 1.30 : Hôtes corannulène déposés sur une surface de Cu(110). b) Image de microscopie à effet tunnel à haute résolution. c) Modélisation de la surface. d) Schématisation de l'association du C_{60} sur les sites corannulène. Image tirée de la référence 132.

Il a fallu attendre 2012 pour que les premiers cocristaux de C_{60} et de corannulène inaltéré voient le jour grâce aux travaux de Scott, Georghiou et leurs associés.[133] Les conditions de cristallisation rapportées ne sont pas particulières : « les cristaux de prismes rouges furent obtenus par évaporation lente d'une solution équimolaire des deux molécules dans le toluène sur une période de plusieurs semaines ». Dans cet article, les auteurs expliquent que le désordre du C_{60} dans la structure cristallographique indique une absence d'une interaction hôte-invité forte, ce qui pourrait expliquer pourquoi cet auto-assemblage a tardé à être découvert.

La surface du corannulène sans alteration semble trop petite pour permettre un nombre d'interactions approprié pour maintenir le fullerène dans la cavité. Ainsi, un système aromatique plus important tel que la pince de deux corannulènes du Buckycatcher de Sygula semble indiqué. En effet, en 2014, Filatov *et al.* obtinrent des cocristaux avec le

dibenzo[*a,g*]corannulène (Figure 1.31).[134] Les deux cycles aromatiques supplémentaires attachés au cœur corannulène amènent suffisamment d'interactions π-π pour parvenir à la formation d'un cocristal avec le C_{60} assez aisément.

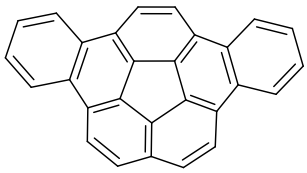

Figure 1.31 : Structure du dibenzo[*a,g*]corannulène présenté dans les travaux de Filatov *et al*.[134]

Une autre raison potentielle expliquant la faible qualité du corannulène inaltéré comme ligand au C_{60} serait le fait que cette molécule n'est pas aussi rigide qu'elle ne parait. En fait, la barrière d'énergie pour son inversion de bol-à-bol est relativement faible (10-11 kcal mol^{-1}). En fait, une analyse cristallographique du corannulène n'affiche pas l'empilement concave-convexe tel qu'attendu.[135] Dans les années 1990, Rabideau, Sygula et leurs collègues[136] ont synthétisé un dérivé fusionnant un cycle à 5 à la structure de base rigidifiant ainsi la molécule. La barrière d'inversion a monté à 27 kcal mol^{-1}, avec une augmentation de la courbure.[137-138] La structure de ce composé déterminée par une analyse cristallographique s'est avérée présenter effectivement l'interaction concave-convexe.[136] Les conclusions tirées de cet article sont que la rigidité moléculaire et la profondeur du bol sont des facteurs importants dans l'empilement des bols à l'état cristallin. Cette rigidification, bien qu'elle ait permis un empilement π du composé pur à l'état cristallin, n'a cependant pas mené à des associations avec des fullerènes.

1.4.3.2 Courbure induite par congestion stérique : autres hydrocarbures polycycliques aromatiques

Mis à part les hémi-fullerènes, on dénombre beaucoup d'autres composés aromatiques incurvés. Nuckolls et ses associés parlent de polycycles aromatiques contorsionnés (*contorted polycyclic aromatics*).[139] Leurs travaux se sont beaucoup penchés sur les dérivés de l'hexabenzocoronène contorsionné (*c*-hexabenzocoronène).[139-153] Les groupements benzo ajoutés au coronène créent des régions baies congestionnées (Figure 1.32). L'encombrement stérique des hydrogènes face-à-face entrainent une contorsion de la molécule, lui conférant une forme doublement concave, avec aucune surface convexe (Figure 1.33).

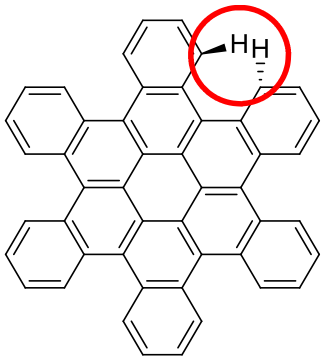

Figure 1.32 : Structure de *c*-hexabenzocoronène. Le cercle rouge indique la zone congestionnée stériquement.

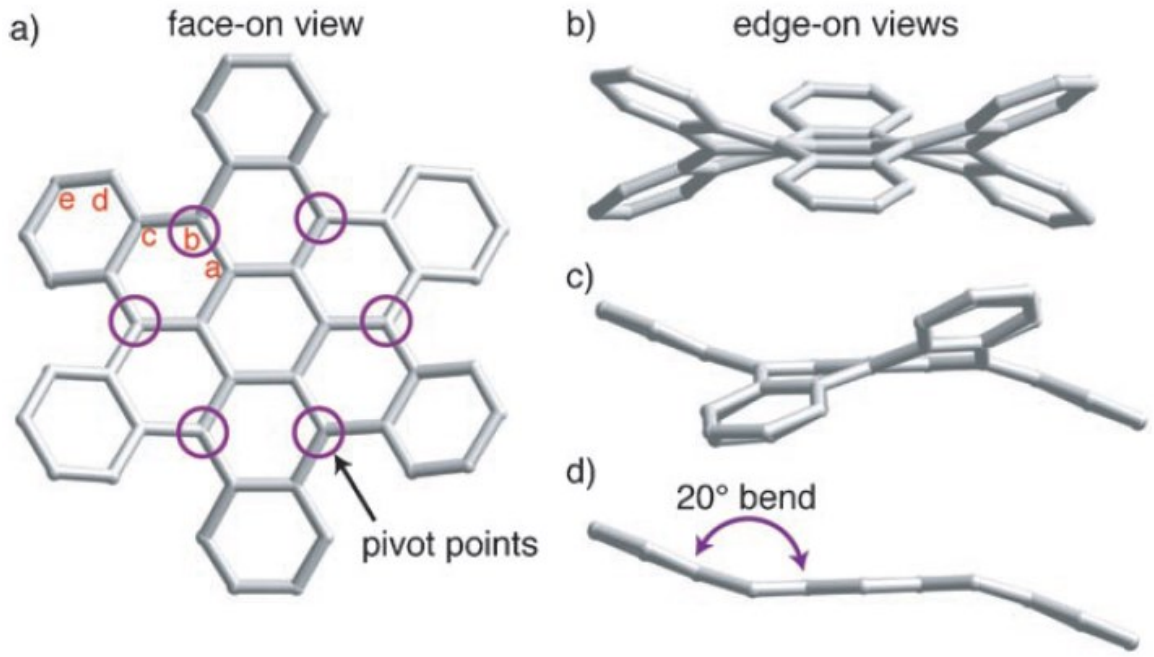

Figure 1.33 : Structure des cristaux de *c*-hexabenzocoronène obtenus dans 1,2,4-trichlorobenzène. Les atomes d'hydrogène ont été soustraits pour plus de clarté. a) Vue de face avec les points de pivots encerclés. b) et c) Vues du côté. d) Vue de côté pour un segment acène où les autres atomes de *c*-hexabenzocoronène ont été retirés. Image tirée de la référence 140.

La forme di-concave de *c*-hexabenzocoronène est maladroite et empêche un empilement concave-convexe dû à l'absence de surface convexe complémentaire. En fait, il n'y a que très peu d'interaction ou même aucune interaction dans la structure cristalline du composé. Ceci fait que cette molécule a à gagner thermodynamiquement en s'associant avec le C_{60} puisque cela lui permettra d'avoir des interactions intermoléculaires (Figure 1.34).

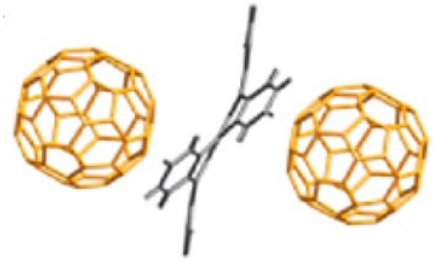

Figure 1.34 : Structure d'un cocristal de *c*-hexabenzocoronène et de C_{60}. Image tirée de la référence 139.

Par ailleurs, les travaux de Nuckolls et ses associés[142, 145, 147] s'inscrivent également dans l'idée de contrôler la morphologie de la couche active des cellules photovoltaïques de type organique. En effet, les auteurs vont au-delà de la simple étude de la cristallisation du C_{60} avec le *c*-hexabenzocoronène et de ses dérivés, en incorporant ces composés dans la couche active des dispositifs photovoltaïques dans le but d'obtenir une morphologie désirée.

Dans une première publication en 2010, Nuckolls et ses collaborateurs décrivent l'emploi d'un mono-cristal résultant de la cocristallisation du C_{60} et de *c*-hexabenzocoronène comme couche active dans un dispositif.[142] Malgré la superposition médiocre du spectre d'absorption de *c*-hexabenzocoronène jouant le rôle de donneur et le spectre solaire, le pourcentage d'efficacité de conversion montait jusqu'à 5.7%, chiffre surprenamment élevé. Par ailleurs, la résistance du matériel a drastiquement diminué lorsqu'exposé à la lumière, indiquant un transfert de charge favorable et résultant en une haute densité de courant (J_{SC} = 3.32 mA/cm²).

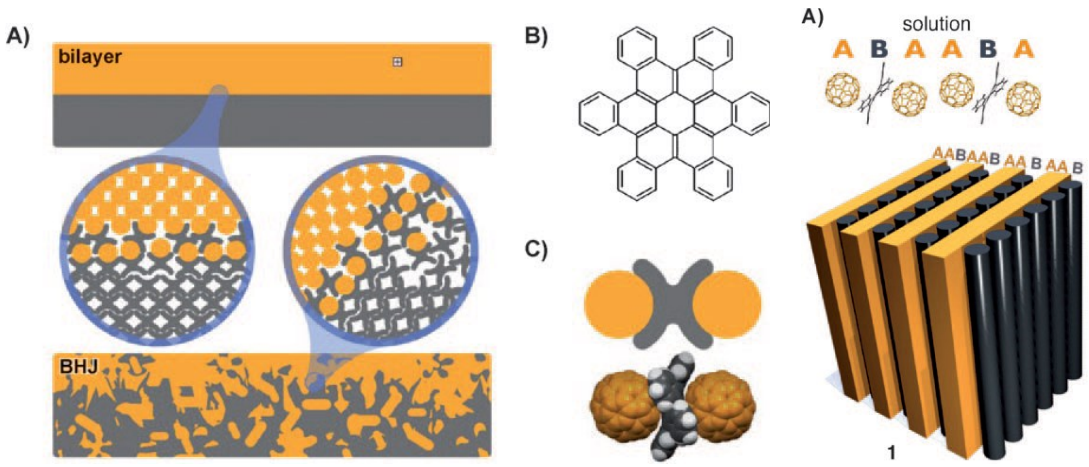

Figure 1.35 : a) Schématisation de l'interface « rotule » (« ball-and-socket ») dans une cellule de type bicouche et de type *bulk heterojunction*. b) Structure de *c*-hexabenzocoronène. c) Corrélation entre la représentation schématique de la rotule et la structure moléculaire réelle obtenue d'un cocristal de *c*-hexabenzocoronène et du C_{60}. d) Organisation dans un cocristal de *c*-hexabenzocoronène et C_{60} tel qu'obtenu par cristallisation à partir d'une solution saturée des deux composantes. Image tirée de la référence 142.

Dans leurs subséquentes recherches,[149] Nuckolls et ses associés ont comparé le *c*-hexabenzocoronène à sa version plane, le *f*-hexabenzocoronène (Figure 1.36). La meilleure interaction obtenue avec le *c*-hexabenzocoronène et le C_{60} permet un transfert de charge plus rapide (15 fs versus 60 fs pour le *f*-hexabenzocoronène). Ainsi, cela se traduit par une dissociation plus rapide des excitons et une diminution de la recombinaison des charges. Par conséquent, les performances photovoltaïques sont alors améliorées.[149] La stratégie d'exploiter l'association concave-convexe afin de contrôler la morphologie nous semble, tout comme pour Nuckolls, particulièrement pertinente.

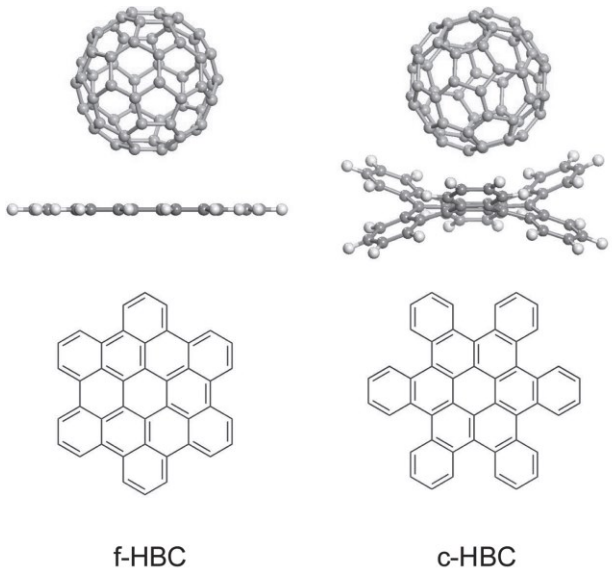

Figure 1.36 : Structures de l'hexabenzocoronène planaire (*f*-hexabenzocoronène) et contorsionné (*c*-hexabenzocoronène). Image tirée de la référence 149.

Plus récemment, en 2018, Cooke, Samuel et leurs collaborateurs ont publié leurs travaux concernant l'emploi du triptycène comme additif supramoléculaire en photovoltaïque organique.[154] Ils ont démontré une augmentation du pourcentage de conversion d'énergie de 60 %. Ils attribuent cette amélioration à, entre autres, l'assistance du triptycène aux interactions entre donneurs et accepteurs induisant ainsi une morphologie de séparation de phases à l'échelle nanoscopique. Ils ont noté également une photostabilité accrue de leurs dispositifs, avec des performances photovoltaïques 30 % meilleure lorsque les dispositifs sont soumis à une illumination prolongée.[154]

1.4.3.3 Courbure induite par un hétéroatome

Mise à part l'inclusion de cycles à 5 ou la congestion stérique, il est possible d'exploiter la géométrie créée par l'incorporation de certains hétéroatomes afin d'induire une courbure à un système qui serait plan autrement. Des exemples notables sont les dérivés de phtalocyanines,[155] subphtalocyanines[101, 156-158] et porphyrines. Les phtalocyanines et porphyrines sont constituées d'un système plan conjugué comportant des atomes d'azote positionnés de façon à ce que les doublets libres pointent vers le centre, favorisant alors la coordination d'un métal ou autre acide de Lewis. À partir du moment que cet atome ne possède pas une géométrie plane telle que le plan carré (pour une porphyrine ou un phtalocyanine) ou la géométrie trigonale (pour les subphtalocyanines), il y a déformation du plan. Dans la Figure 1.37, on voit que le changement de géométrie de l'atome centrale de bore suite à une coordination permet de déformer le plan subphtalocyanine vers une coupe pouvant encapsuler une molécule de C_{60}.[156] Un autre exemple analogue est montré à la Figure 1.38 avec le zinc dans une porphyrine. [159]

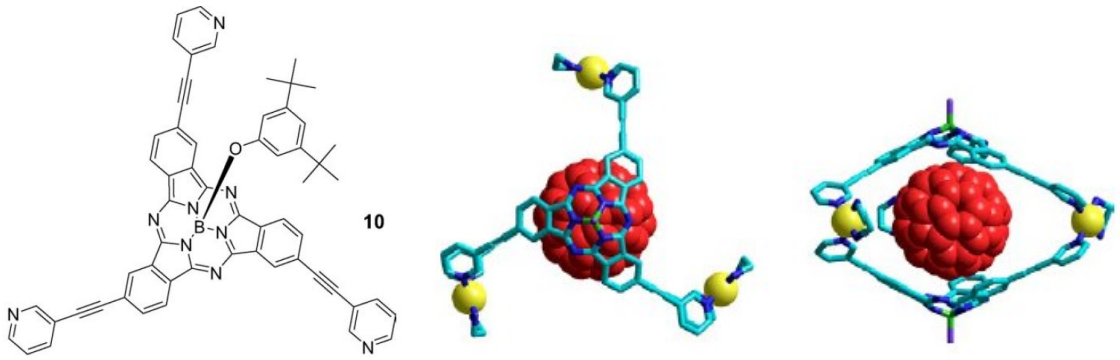

Figure 1.37 : Le changement de géométrie de l'atome central de bore suite à une coordination permet de déformer le plan subphtalocyanine vers une coupe pouvant encapsuler une molécule de C_{60}. Image tirée de la référence 156.

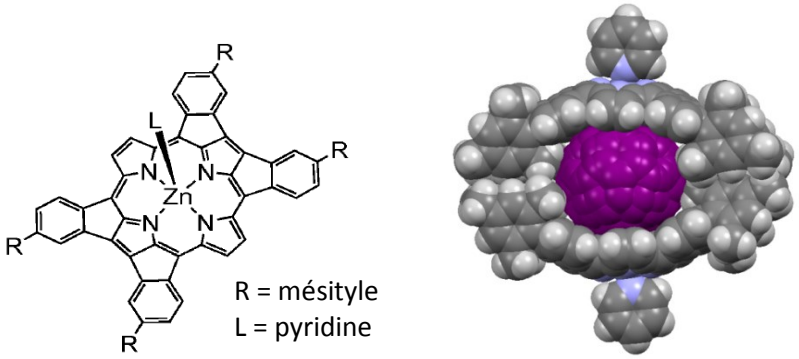

Figure 1.38 : Le changement de géométrie de l'atome centrale de zinc suite à une coordination permet de déformer le plan porphyrine vers une coupe pouvant encapsuler une molécule de C_{60}.

1.4.3.4 Hôtes en forme de bol : conclusions

Il y a donc différents motifs à incorporer à une structure de base afin d'y induire une courbure : 1) un cycle à 5, comme celui du corannulène qui force une tension sur ses cycles voisins hexagonaux, 2) un encombrement stérique, comme celui créé par la région baie du

hexabenzocoronène et 3) un hétéroatome menant à une géométrie non-plane, tel que le bore dans les subphtalocyanines.

La présence d'un système conjugué incurvé n'est pas nécessairement suffisante afin d'avoir des interactions concaves-convexes avec les fullerènes. L'étendue de la surface, sa courbure et sa densité électronique sont des facteurs déterminants à prendre en compte lors de la conception du design moléculaire afin de créer un hôte pouvant se lier efficacement aux fullerènes. Ainsi, dans le but de s'associer avec les buckyballes pour des applications photovoltaïques, nous avons opté pour le phosphangulène, une molécule avec un squelette de base relativement petit, mais électron-riche par la présence de trois atomes d'oxygène et un atome de phosphore.

1.5 Phosphangulène

L'objectif fixé était donc d'étudier une série de composés pouvant agir d'hôte supramoléculaire pour la complexation des fullerènes en étant complémentaires de par leur forme et leur caractère électronique. Il fallait donc une molécule courbe, riche en électrons et facilement fonctionnalisable.

Les travaux relatés dans cette thèse se concentrèrent alors sur le phosphangulène (**1**), une molécule synthétisée pour la première fois par Krebs et ses collaborateurs en 1997.[160] L'étude d'origine était axée sur les propriétés pyroélectriques de ce composé au moment dipolaire notable de 3,3 1± 0,2 D.

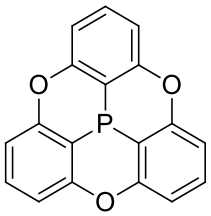

1

Comme de nombreux composés conjugués incurvés, le phosphangulène (**1**) a une tendance à former des piles de bols convexe dans concave, alignant ainsi les moments dipolaires des molécules. À l'état solide cristallin du composé, les piles adjacentes sont orientées avec les moments alignés, conférant des propriétés pyroélectriques au matériau. En regardant la structure cristalline, on comprend que le composé fait des empilements π-π concaves-convexes.

Durant la durée de notre projet débuté en 2013, des travaux de mêmes intérêts furent publiés par Yamamura, Nabeshima et leurs collaborateurs.[161-165] Ils présentèrent un dérivé chiral de l'oxyde de phosphangulène (**1**). L'emploi de groupements phénylacétylène permit un emballage du C_{60} par quatre de leurs molécules (Figure 1.39). Les auteurs ont donc exploité un effet de reconnaissance coopérative obtenue par les interactions C-H···π des groupements phényles entre les quatre molécules hôtes.

Yamamura, Nabeshima et leurs associés ont depuis entrepris quelques autres études sur des dérivés du phosphangulène (**1**). Parmi les dérivés synthétisés dans leurs laboratoires, seuls les composés phénylacétylène-substitués (Figure 1.39) et un composé constitué d'une fusion de deux cœurs modifiés de phosphangulène (Figure 1.40) sont rapportés comme produisant des complexes d'association concave-convexe avec les fullerènes. Ces articles constituent une confirmation que des dérivés de la phosphine sont aptes à faire des interactions π-π concaves-convexes.

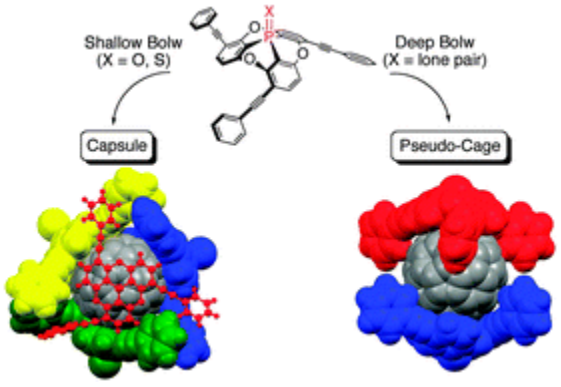

Figure 1.39 : Complexe de C_{60} avec les dérivés phénylacétylène du phosphangulène (1) et de l'oxyde de phosphangulène tel que rapporté par Yamamura et ses associés.[161, 163] Image tirée de la référence 163.

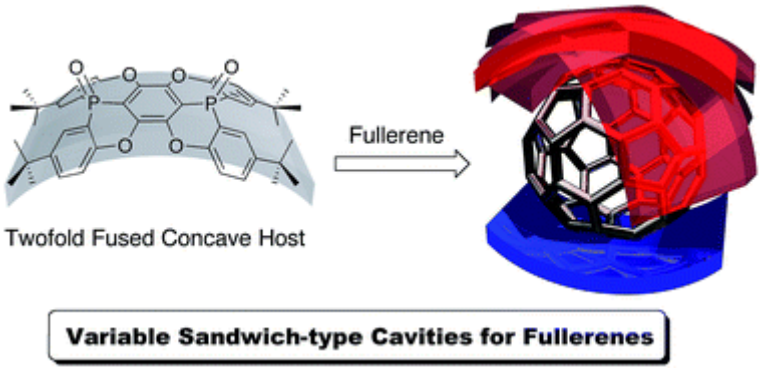

Figure 1.40 : Composé fusionnant deux cœurs altérés du phosphangulène (**1**). Le fullerène est pris en «sandwich» entre deux hôtes représentés en rouge et en bleu. Image tirée de la référence 162.

Mis à part ces études d'association supramoléculaire, le groupe japonais s'est également intéressé à l'étude de la géométrie de la phosphine conique et à l'effet des substituants sur celle-ci.[164-165] L'angle et la profondeur du cône sont des propriétés physiques ayant des répercussions sur la complémentarité de l'hôte sur le fullerène.

1.5.1 Propriétés physiques

1.5.1.1 Angles et profondeurs de cône

Yamamura, Nabeshima et leurs collaborateurs ont déterminé par analyses de diffraction à rayons X que l'angle conique du phosphangulène (**1**) passe d'environ 115° à environ 120° lorsque l'atome de phosphore est substitué (Figure 1.41). Si l'angle de cône augmente pour une longueur d'arrête fixe, la profondeur diminue. C'est ce qui est en effet observé lorsqu'on passe de la phosphine à ses chalcogénures : de 2,45 Å on descend entre 2,12 à 2,22 Å. En quelques mots, la molécule est quelque peu aplatie lorsque le phosphore porte un 4ème substituant.

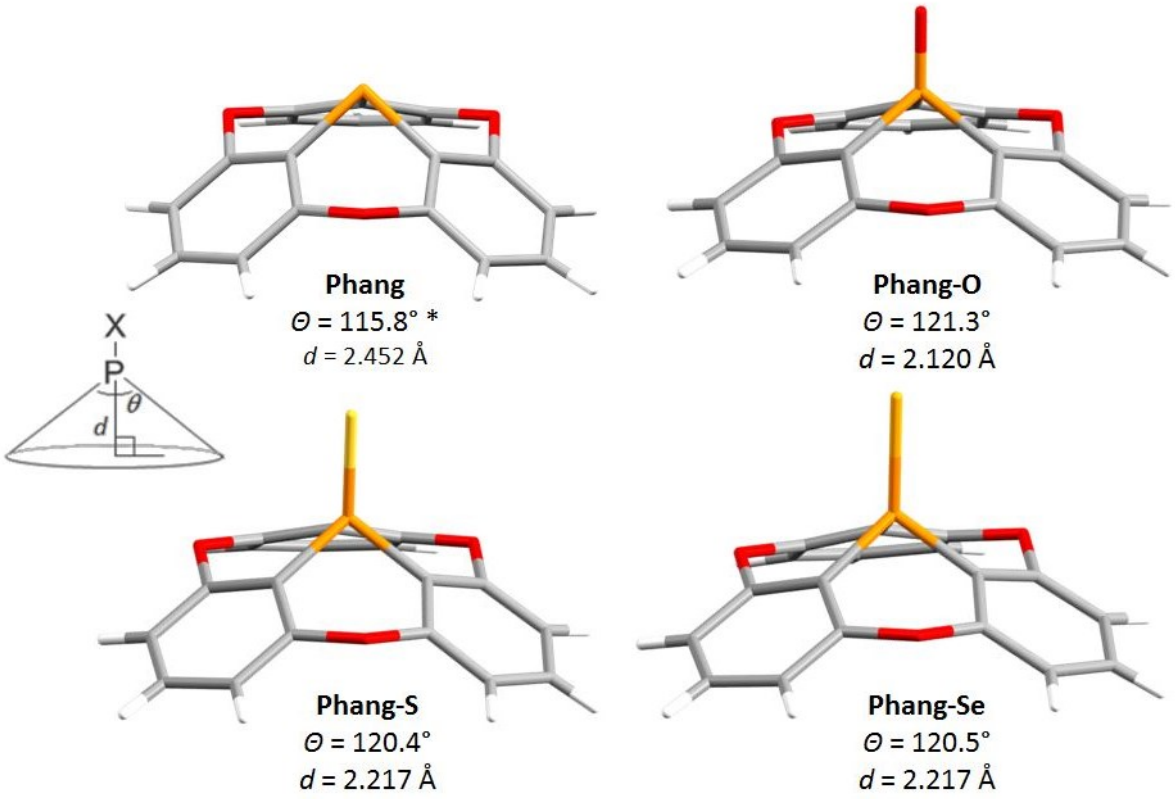

Figure 1.41 : Angles et profondeurs de cône tels que mesurés par Yamamura, Nabeshima et leurs associés[165] pour Phang (phosphangulène); Phang-O, son oxyde; Phang-S, son sulfure; et Phang-Se, son sélénure. *Rapportée par Krebs originellement.[160]

Le groupe japonais s'est aussi intéressé à l'effet qu'une variation des atomes pontant aux aryles pouvait entraîner sur la géométrie du cône.[165] La Figure 1.42 montre comment en remplaçant les oxygènes pontant pour des soufres, on obtient une forme plus aplatie.

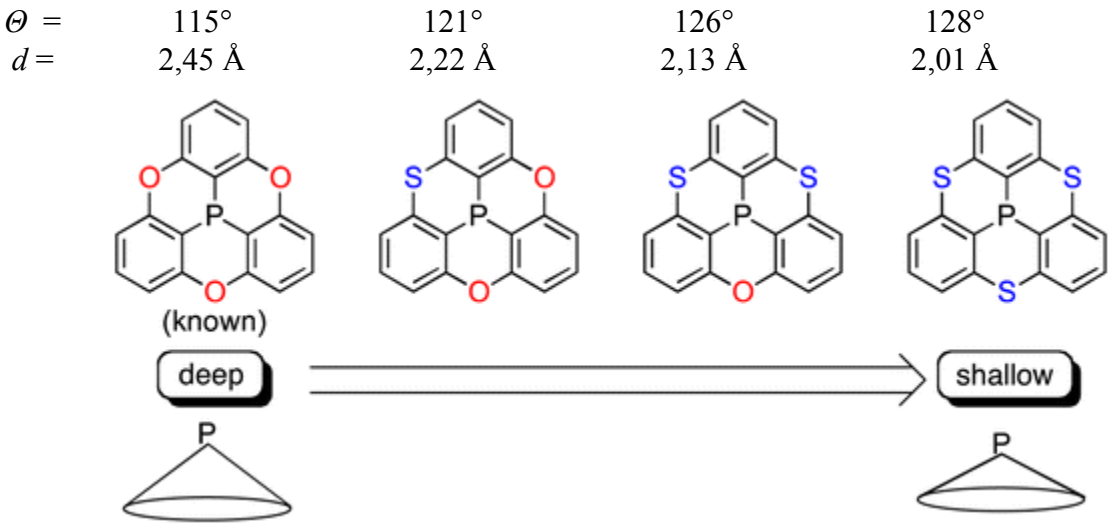

Figure 1.42 : Substitution des oxygènes pontant pour des soufres. Image tirée de la référence 165.

1.5.1.2 Cristallinité

Malgré la forme conique du phosphanulène (**1**), sa cocristallisation avec des fullerènes n'a jamais été rapportée. Afin d'expliquer cette observation, nous proposons que le phosphangulène est parfaitement satisfait à interagir avec lui-même et qu'il n'y a pas d'avantage énergétique de briser ces interactions afin de permettre une cocristallisation avec un fullerène.

On pourrait penser que l'introduction d'atomes de soufre en place des oxygènes du phosphangulène (**1**) permettra à la molécule de s'associer et de cocristalliser avec les fullerènes en agrandissant l'ouverture du cône et en offrant des interactions supplémentaires de van der Waals. Il n'y a cependant pas eu de résultat en ce sens rapporté à ce jour. On peut donc penser que le degré de caractère conique du phosphangulène (**1**) et ses dérivés ne s'agit

pas d'un facteur déterminant dans l'absence de cocristallisation avec les fullerènes. Une autre explication hypothétique serait la cristallinité de l'hôte.

La Figure 1.43 montre les trois formes d'empilement typiques pour les molécules incurvées dans un réseau cristallin : en colonnes parallèles (type A), en colonnes anti-parallèles (type B) et de façon orthogonale ou en pseudo-chevrons (type C). Par exemple, le corannulène emprunte ce dernier type d'empilement comme nous l'avons vu dans la section 1.4.3.1, alors que le phosphangulène (**1**) s'organise en colonnes parallèles du type A (Figure 1.44). Yamamura et Nabeshima ont décrit l'analogue du phosphangulène avec trois atomes de soufre pontant comme appartenant au type B (colonnes anti-parallèles). Les empilements en colonnes sont très efficaces; lorsque la forme moléculaire s'y prête, il est possible de maximiser les interactions moléculaires et diminuer le volume non-occupé. Ainsi, il est possible que la structure cristalline homomoléculaire obtenue soit trop stable thermodynamiquement pour entrevoir une cristallisation hétéromoléculaire. Dans le second chapitre de cette thèse, nous traiterons du polymorphisme des chalcogénures du phosphangulène (**1**) et nous montrerons comment l'introduction d'un atome sur le phosphore empêche l'empilement conique efficace et crée alors une forme maladroite, comparable à un entonnoir, qui est difficile à empiler de sorte à maximiser les interactions moléculaires et à éliminer le vide. Les chalcogénures de phosphangulène n'ont pas d'organisation à l'état cristallin particulièrement stable et sont alors plus susceptibles à cristalliser de façon hétéromoléculaire, avec par exemple un fullerène, de sortes à régler leurs frustrations.

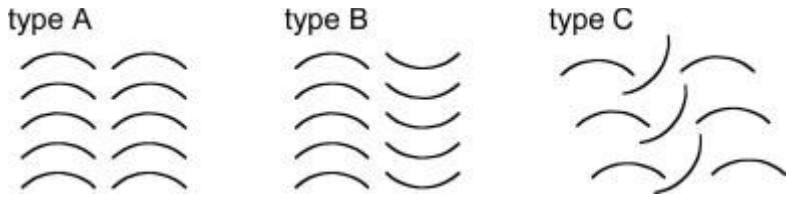

Figure 1.43 : Types d'empilement dans un cristal pour les molécules incurvées. Image tirée de la référence 164.

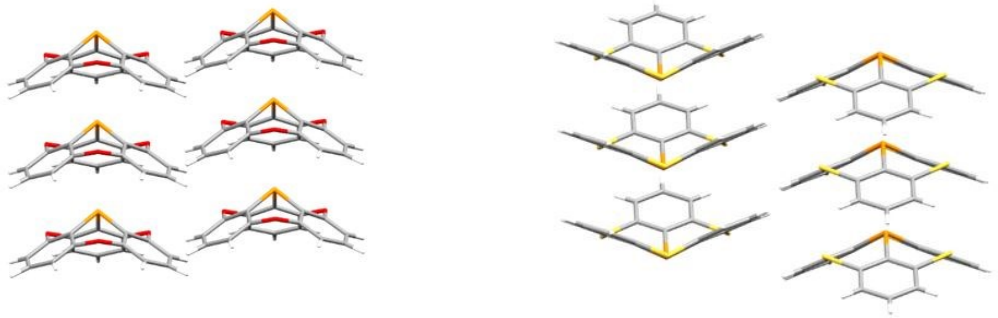

a b

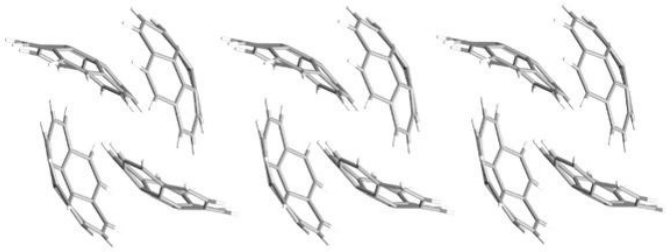

c

Figure 1.44 : Exemples des trois types d'empilement A-C pour les molécules incurvées. a) Colonnes parallèles, illustrées par le cas du phosphangulène (1). b) Colonnes anti-parallèles, illustrées par l'analogue avec trois atomes de soufre. c) Organisation alternative, exemplifiée par le corannulène.

Yamamura et Nabeshima ont obtenu des structures cristallines d'association fullerène-phosphangulène, mais seulement pour des phosphangulènes dont l'empilement homomoléculaire harmonieux a été bloqué par l'introduction de groupements phénylacétylène (Figure 1.39) ou tert-butyles (Figure 1.40). Il n'y a eu à ce jour aucune structure cocristalline obtenue pour le phosphangulène (**1**) lui-même.

Il semble donc que dans ce cas-ci, l'angle et la profondeur du cône ou la présence d'atomes de soufre, bien que des facteurs importants, ne soient pas aussi déterminants que la cristallinité homomoléculaire pour régir les cocristallisations ou associations supramoléculaires avec les fullerènes. Il convient de bloquer ce motif de cristallisation élégante afin d'espérer obtenir des associations hétéromoléculaires. À cette fin, nous avons exploité la réactivité de l'atome de phosphore afin de fonctionnaliser le phosphangulène (**1**) à cette position.

1.5.2 Réactivité du phosphore et du phosphangulène

En principe, la réactivité du phosphangulène (**1**) s'apparente à celles de la plupart des phosphines. En effet, c'est prévu que l'atome de phosphore soit le centre réactif de la molécule, et c'est cette réactivité qui fût le plus exploitée lors de ces travaux de doctorat. Cette section examine la chimie du phosphore de façon générale, qui par extension est valable pour le phosphangulène (**1**).

1.5.2.1 Structure électronique

Le Tableau 1.3 résume les différents modes de coordination des composés phosphorés. La notation $\lambda^n\sigma^m$ sera employée dans cette section afin de décrire la valence des composés, où λ

est la covalence (nombre de liens covalents) et σ le nombre de coordination (nombre de substituants).

1.5.2.1.1 Valences

Le phosphore fait partie du groupe 15, aussi appelé la famille de l'azote ou des pnictogènes. Sa configuration électronique à l'état fondamental est [Ne]$3s^2 3p^3$ (Schéma 1.1a). Sa valence est semblable à celle de l'azote avec trois électrons non-pairés qui peuvent ainsi former trois liens (Tableau 1.3, A). Comme son analogue de la première rangée, le phosphore possède un doublet libre pouvant participer dans une liaison σ dative. L'atome porte alors une charge positive. Si tous les substituants sont neutres, nous sommes alors en présence d'un sel d'ammonium ou de phosphonium (Tableau 1.3, B et Schéma 1.1 b). À la différence de l'azote, le phosphore peut être pentavalent. Selon le modèle *VSEPR*[*], ceci est dû à la possibilité d'hybridation avec les orbitales d du phosphore (Tableau 1.3, E et Schéma 1.1 c).[166-167]

[*] *Valence shell electron pair repulsion*, ou repulsion des paires électroniques de la couche de valence

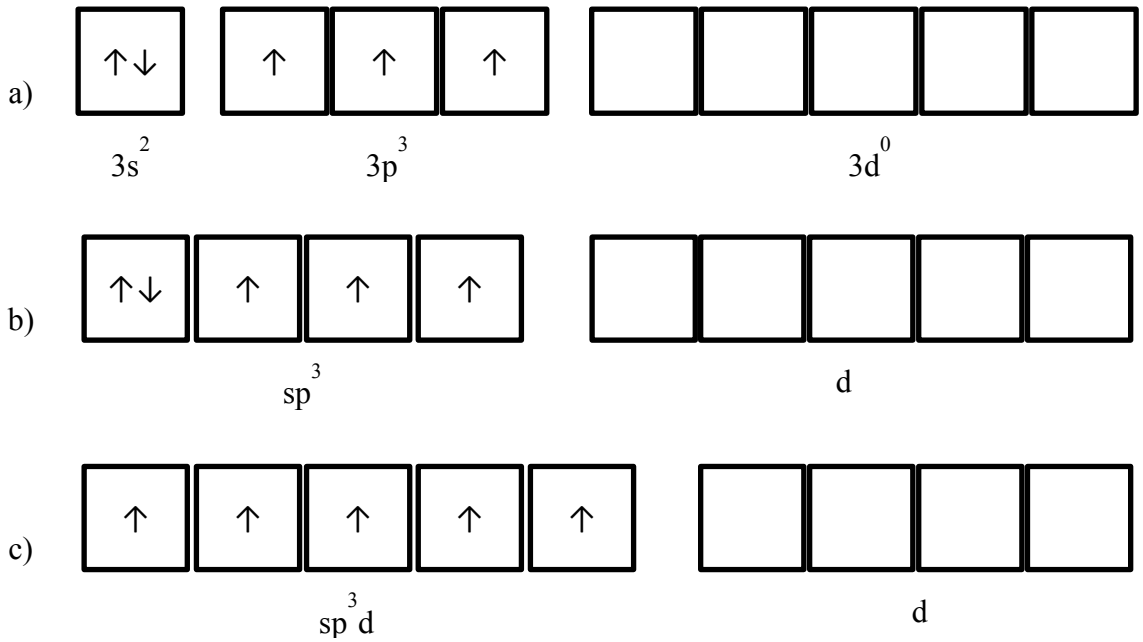

Schéma 1.1 : Configuration électronique de la couche de valence du phosphore. a) État fondamental. b) État trivalent. c) État pentavalent.

Là où la chimie du phosphore devient plus compliquée que celle de l'azote est lorsque le quatrième substituant sur un composé tétraédrique comporte une charge négative (Figure 1.45, II et Tableau 1.3, C). Ce genre d'espèce porte le nom d'ylure. L'extension de la règle de l'octet ayant été pensée comme permise pour les éléments de la troisième période, il a semblé judicieux de suggérer la notation d'un deuxième lien entre ce substituant et le phosphore, afin d'éviter une représentation comportant une séparation de charges.

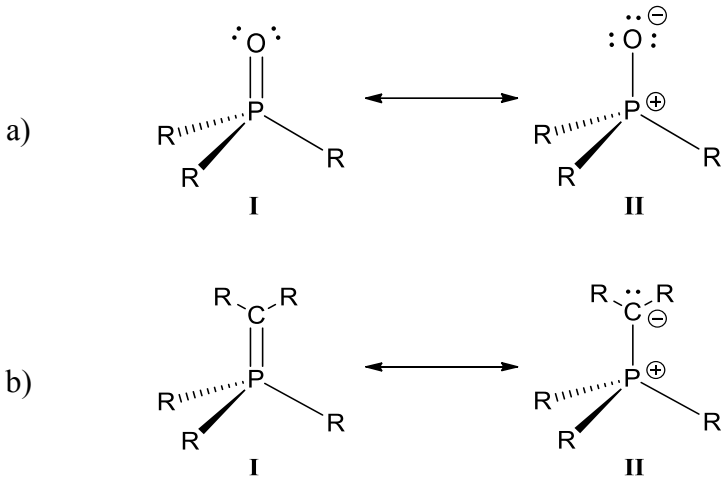

Figure 1.45 : Interprétations du lien P-X chez les composés tétraédriques neutres du phosphore. a) Lien P-O. b) Lien P-C. Forme I = double lien covalent et forme II = lien simple polarisé.

Pendant plusieurs décennies, et encore aujourd'hui, le sujet est matière à débat. Il existe deux écoles de pensée concernant l'interprétation de ce genre de liens. Une possibilité est la représentation par un lien double entre les atomes (forme I de la Figure 1.45) où la liaison π impliquerait une orbitale d du phosphore. L'autre représentation utilise un lien simple covalent avec polarisation de charge résultant en un « deuxième » lien de nature ionique (forme II de la Figure 1.45). Sans rentrer dans le débat, nous résumerons les deux points de vue.

1.5.2.1.2 Liens pπ-dπ

Le postulat selon lequel les éléments de la deuxième rangée du tableau périodique ont accès aux orbitales d qui leur permettent d'enfreindre la règle de l'octet est à l'origine de la représentation de double liaison. Ceci permettrait au phosphore d'accepter une rétrodonation d'une orbitale p du substituant vers une orbitale d vacante (Figure 1.46), résultant en une infraction de la règle de l'octet, car en effet le phosphore serait entouré de 10 électrons. Le lien

entre ce substituant et la charge négative de ce dernier seraient stabilisés ainsi. En effet, il a été observé que l'échange proton-deutérium en milieu aqueux deutéré est beaucoup plus rapide pour le $P(CH_3)_4^+$ que pour le $N(CH_3)_4^+$. Cette différence suggère que le phosphore stabilise mieux le carbanion intermédiaire que l'azote.[167-168]

D'autres observations, particulièrement dans le cas du lien phosphoryle phosphore-oxygène, semblent pointer dans cette direction; la longueur de ce lien dans l'oxyde de triméthylphosphine (Me_3PO) a été mesurée comme étant de 1,46 Å, distance beaucoup plus courte que les 1,71 Å prédits en 1941 par l'équation Schomaker-Stevenson[169] ou la valeur de 1,76 Å prédit par Pyykkö[170] en 2015 pour un lien simple. Cette valeur se rapproche en fait beaucoup plus de la prédiction de ce dernier pour un lien triple, 1,47 Å,[170] ce qui a mené certains scientifiques jusqu'à suggérer un triple lien. Ils prévoient donc que deux paires d'électrons libres dans les orbitales de valence 2p de l'oxygène négativement chargé participeraient dans deux liens π avec deux orbitales d vacantes perpendiculaires du phosphore. Néanmoins, si la force de ce lien est beaucoup plus grande que ce qui serait attendu pour un lien simple, elle n'est pas aussi importante que pour un lien triple traditionnel constitué de liaisons pπ-pπ (Figure 1.46).

Le lien oxygène-phosphore est connu comme étant un des liens les plus forts en chimie. La formation de ce lien est bien souvent la force motrice de nombreuses réactions lorsque celui-ci se retrouve dans les produits.

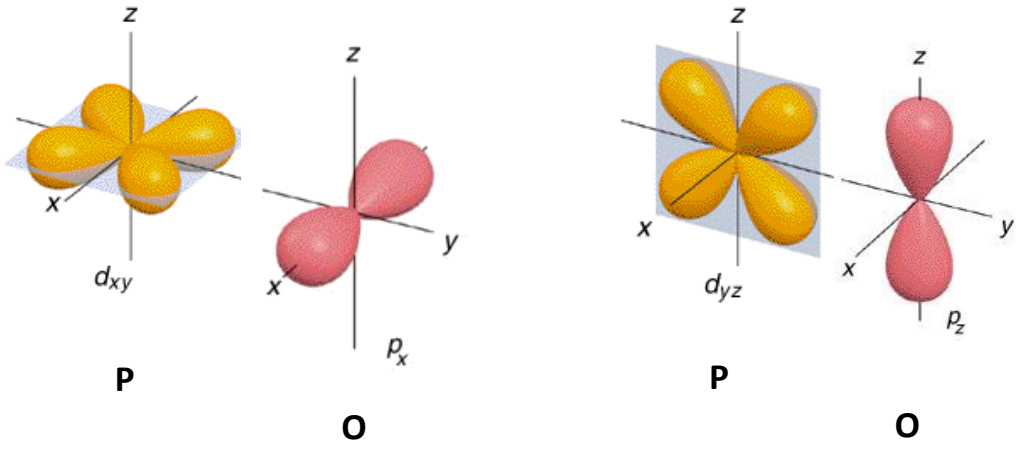

a b

Figure 1.46 : Liens π entre les orbitales 3d vacantes du phosphore et les doublets libres dans les orbitales 2p de l'oxygène. a) Interactions entre les orbitales $3d_{xy}$ du phosphore et $2p_x$ de l'oxygène. b) Interactions entre les orbitales $3d_{yz}$ du phosphore et $2p_z$ de l'oxygène. Image tirée de la référence 171.

1.5.2.1.3 Lien simple polarisé

En s'appuyant sur des calculs, certains scientifiques tels que Magnusson[172-173] considèrent que les orbitales d sont valides uniquement pour les éléments du bloc d ou métaux de transition, et non pas pour le bloc p dont fait partie le phosphore. La règle de l'octet serait alors inviolable même au-delà de la troisième période. Un lien simple polarisé permettrait alors de respecter l'octet.

Une revue approfondie de Gilheany montre que les calculs et les résultats expérimentaux s'accordent avec la notion que le lien P-O chez les oxydes de phosphore (R_3PO) est fort, polaire et plus court qu'un lien double P=O conventionnel.[174] Il a été déterminé à travers des

études *ELF*[†][175-176] menées par Chesnut[177-178] que les doublets libres de l'oxygène sont placés de façon décalée par rapport aux substituants du phosphore (Figure 1.47 a). Cette conformation anti-périplanaire permettrait une rétrodonation de doublets libres de l'oxygène vers l'orbitale anti-liante R-P (Figure 1.47 b). Des résultats analogues ont été obtenus pour le lien P-C chez le H_3PCH_2.[179] Ces conclusions sont consistantes avec la polarisation des doublets libres et avec la nature hautement ionique du lien P-O. Dans cette thèse, nous pencherons davantage pour cette interprétation et nous représenterons ce genre de lien P-O tel un double lien polarisé.

a b

Figure 1.47 : a) Conformation des substituants autour du lien P-O. b) Hyperconjugaison négative d'un des doublets de l'oxygène (en rouge) vers l'orbitale anti-liante P-H (vert).

[†] *Electron Localization Function*, ou fonction de localisation d'électrons.

Tableau 1.3 : Classification des structures ou fonctions du phosphore les plus courantes. La notation de valence indique par λ la covalence et σ le nombre de coordination.

Entrée	Structure	Géométrie	Valence	Hybridation	Nombre d'électrons
A	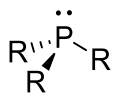	Pyramide trigonale	$\lambda^3\sigma^3$	sp^3	8
B	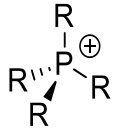	Tétraédrique	$\lambda^4\sigma^4$	sp^3	8
C	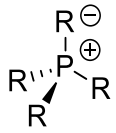	Tétraédrique	$\lambda^4\sigma^4$	sp^3	8
D	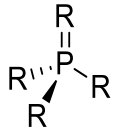	Tétraédrique	$\lambda^5\sigma^4$	sp^3	10
E	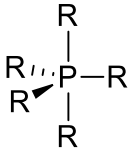	Bipyramide trigonale	$\lambda^5\sigma^5$	sp^3d	10
F	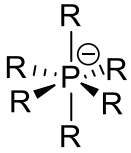	Octaédrique	$\lambda^6\sigma^6$	sp^3d^2	12

1.5.2.2 Réactions

Les réactions ioniques des composés de phosphore peuvent être classifiées en trois catégories selon le rôle du composé phosphoré. Celui-ci peut agir en tant que : [167]

1) Nucléophile : dans le cas du phosphore trivalent de par son doublet libre
2) Électrophile : phosphore trivalent ou pentavalent de par l'accessibilité de ses orbitales d vacantes
3) Intermédiaire dans des réactions n'impliquant pas l'atome de phosphore directement, mais dont la proximité de celui-ci a une influence sur l'issu de la réaction.

On note ainsi que le phosphore trivalent peut être biphilique : il peut agir tant en nucléophile et qu'en électrophile. Ce double caractère est causé par la présence d'un doublet libre conférant la nucléophilicité et d'orbitales d vacantes conférant l'électrophilicité. Les réactions que nous avons exploitées dans ce projet tombent dans l'une des deux premières catégories ou une combinaison des deux.

1.5.2.2.1 Nucléophilicité et basicité de Lewis

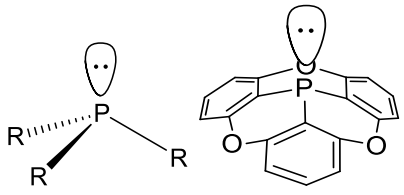

Figure 1.48 : Doublet libre sur les phosphines $\lambda^3\sigma^3$ et le phosphangulène (1).

Le phosphangulène (**1**) est une phosphine de valence $\lambda^3\sigma^3$ possédant ainsi un doublet libre. Le phosphangulène (**1**) réagit comme un nucléophile. Cet aspect réactionnel peut être employé

dans la formation de sels organiques (Schéma 1.2) ou dans le but d'obtenir un intermédiaire activé aux attaques nucléophiles sur l'atome de phosphore (Schéma 1.3).

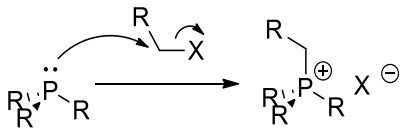

Schéma 1.2 : Substitution électrophile de la phosphine nucléophile produisant un sel organique.

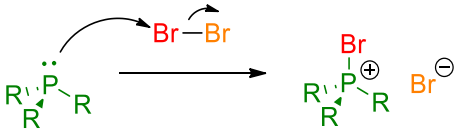

Schéma 1.3 : Activation du phosphore suite à une attaque nucléophile sur le Br_2. L'intermédiaire obtenu est alors plus électrophile et donc susceptible aux attaques nucléophiles.

Par ailleurs, la majorité des phosphines trivalentes ont un caractère de base de Lewis localisé sur le doublet libre de l'atome central de phosphore, lui conférant ainsi l'habilité à se coordonner aux acides de Lewis tels que les métaux de transition et les éléments du groupe 13 (famille du bore) (Figure 1.49). Cette commodité deviendra une opportunité qui sera exploitée afin d'obtenir des complexes métalliques tel que relaté dans le chapitre 4.

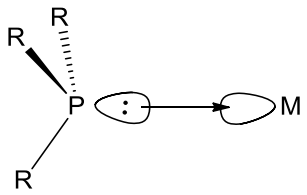

Figure 1.49 : Coordination du doublet libre de la phosphine vers l'orbitale vacante d'un acide de Lewis tel qu'un métal de transition.

Par rapport à la triphénylphosphine, on pourrait s'attendre à ce que le phosphangulène (**1**) soit plus nucléophile et meilleure base de Lewis. Pour justifier cette hypothèse, on pourrait se baser sur l'argument que la présence d'atomes d'oxygène enrichisse le système en densité électronique. Cependant, on pourrait aussi amener le contre-argument que le doublet libre de l'atome de phosphore est beaucoup moins disponible pour le phosphangulène (**1**) que pour la molécule de référence, car l'alignement des orbitales moléculaires π offre une surface conjuguée dans lequel le doublet du phosphore peut participer, ce qui n'est pas le cas pour la triphénylphosphine. Il est également important de noter que la géométrie conique du phosphangulène (**1**) augmente le caractère s de l'orbitale associée au doublet libre, diminuant ainsi la nucléophilie du composé. Nous avons effectué quelques expériences afin de tester la capacité du phosphangulène (**1**) à agir comme nucléophile. Ces expériences sont décrites plus en détails dans le chapitre 4.

Pour les mêmes raisons, les valeurs relatives des constantes d'association métal-phosphine sont difficiles à prédire pour la triphénylphosphine par rapport au phosphangulène (**1**). En principe, le haut caractère s du phosphangulène (**1**) diminuerait sa capacité d'agir comme ligand. Cependant, l'angle de cône est de 128° pour la triphénylphosphine et de 116° pour le

phosphangulène (**1**). Un angle de cône plus petit facilite la coordination d'un ligand sur un métal et favorise des nombres de coordination plus grands. En présence d'un électrophile organique, le phosphangulène (**1**) semble réagir beaucoup moins rapidement dans la substitution nucléophile que la triphénylphosphine. Il semblerait donc que notre phosphine ne soit pas un aussi bon nucléophile que son analogue, mais qu'elle puisse être quand même un bon ligand dans la complexation de métaux de transition pour des raisons stériques. Il est à noter que nous n'avons pas été en mesure de déterminer le pK_a du phosphangulène (**1**), celui-ci n'étant pas assez soluble dans l'eau.

1.5.2.2.2 Électrophilicité et acidité de Lewis

La disponibilité des orbitales d vides pour l'atome de phosphore lui permet d'accepter des électrons. Les halogénures du phosphore sont particulièrement susceptibles aux hydrolyses pour cette raison : au contact de l'humidité de l'air, la phosphine subit typiquement une substitution électrophile. Une élimination de HCl est souvent subséquente (Schéma 1.4).

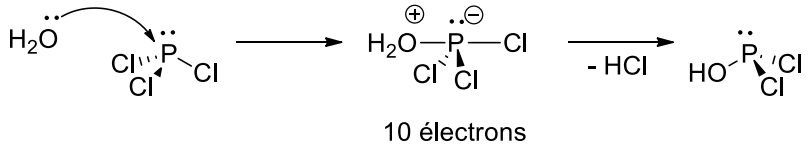

Schéma 1.4 : Substitution nucléophile du PCl_3 par l'eau. Le PCl_3 joue le rôle d'électrophile.

Plus électrophiles encore sont évidemment les espèces cationiques telles qu'obtenues suite à une attaque électrophile sur le phosphore tel que présenté au Schéma 1.3. Le composé ainsi généré est activé et susceptible à des attaques nucléophiles (Schéma 1.5).

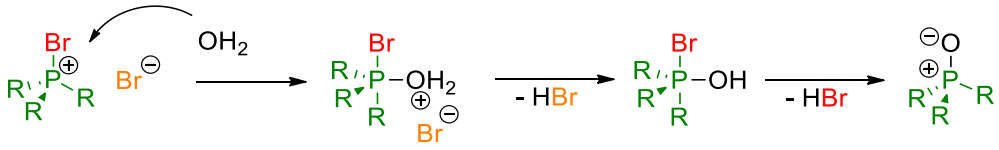

Schéma 1.5 : Attaque nucléophile sur un atome de phosphore cationique et donc activé ($\lambda^4\sigma^4$).

Ainsi, il est possible de faire une attaque nucléophile sur un atome de phosphore préalablement activé suite à une attaque électrophile. Il s'agit d'une stratégie employée entre autres dans la formation des cations de μ-nitrido bis(triphénylphosphore), aussi appelé bis(triphénylphosphine)iminium ou bis(triphénylphosphoranylidène)iminium, ou comme nous l'abrévierons ici par PNP. Le mécanisme exact de la formation d'un composé PNP n'a pas été déterminé expérimentalement. Néanmoins, en se basant sur l'intermédiaire dichlorure (ou dibromure) de triphénylphosphine proposé par Ruff et al.,[180] le mécanisme du Schéma 1.6 nous parait plausible. Les sels de PNP du phosphangulène seront le sujet du cinquième chapitre.

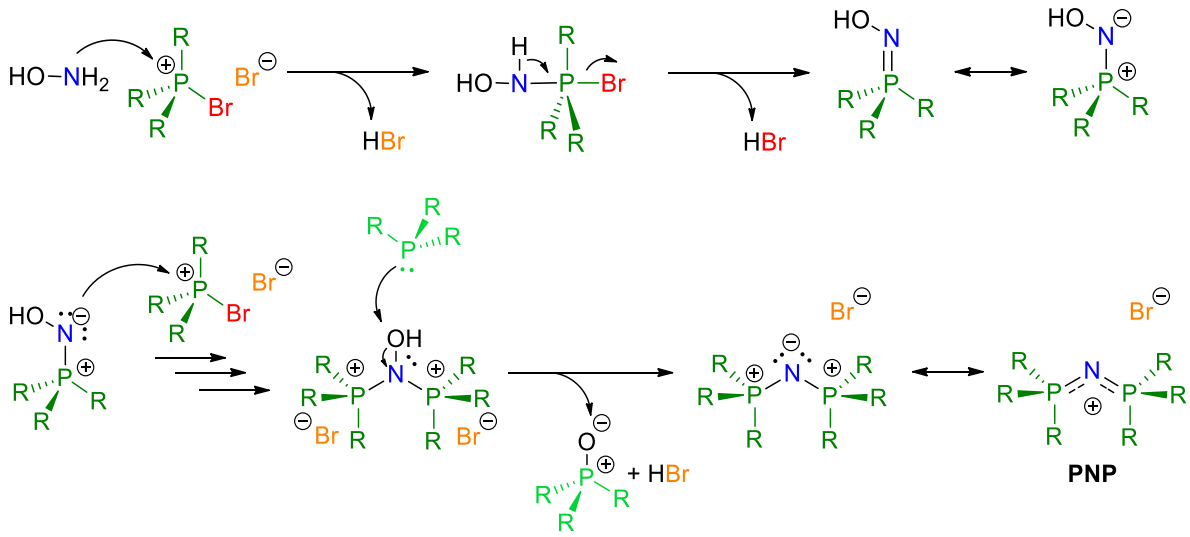

Schéma 1.6 : Mécanisme proposé pour la formation de composés de μ-nitrido bis(triphénylphosphore) (PNP) en se basant sur l'intermédiaire proposé par Ruff *et al.*[180]

Dû à l'oxophilicité de phosphore, il n'est pas rare d'observer une oxydation des phosphines en solution à long terme. Il est d'ailleurs essentiel de prendre soin de travailler en milieu désoxygéné lors des cristallisations et des réactions afin d'éviter une oxydation parasite. L'oxygène fait partie de la famille des chalcogénures où l'on compte le soufre et le sélénium comme éléments. Étant de valence isoélectronique à l'oxygène, ces deux autres éléments réagiront avec le phosphore et formeront des liens similaires. La force du lien chalcogénure-phosphore diminue néanmoins en descendance dans la famille. Ainsi, si un traitement avec le soufre ou le sélénium élémentaire mène au chalcogénure correspondant, il convient cependant de chauffer le milieu réactionnel afin d'obtenir un rendement comparable à celui donné par le traitement au peroxyde d'hydrogène à température ambiante menant à l'oxyde. Les liens chalcogénure-phosphore ainsi obtenus seront tous trois du type ylure. Une série de chalcogénures de phosphangulène (**1**) s'impose donc comme étant la première série de dérivés à cocristalliser avec les fullerènes et à étudier. Il s'agit là du sujet des chapitres 2 et 3 de cette dissertation.

1.6 Objectifs de la thèse

La problématique de morphologie dans les matériaux moléculaires ayant plusieurs composantes différentes, tels qu'illustré par la couche active des cellules solaires organiques d'architecture hétérojonction de masse, fût le point de départ pour nos études. Le projet visait la création d'additifs qui pourraient être employés dans la couche active des cellules solaires typiques afin d'en contrôler la morphologie lorsque des molécules de fullerènes et leurs dérivés sont employés comme accepteurs d'électrons. Dans le cadre de ce doctorat, nous nous sommes concentrés sur les études préliminaires en vue de ce but ultime : la synthèse de nouveaux composés de caractéristiques appropriées et l'étude de ceux-ci dans des cocristaux formés avec les fullerènes. L'incorporation pratique des cibles dans des substrats photovoltaïques n'a pas été étudiée en détail et est laissée à un futur proche dans le cadre d'études plus poussées.

Nous avons mis à profit les principes de la chimie supramoléculaire afin de concevoir des structures moléculaires pouvant remplir le mandat d'interagir avec les unités buckballes présentes dans les électron-accepteurs usuellement employés dans le domaine, tel que le $PC_{61}BM$. Une complémentarité électronique et de forme pour ces fullerènes convexes nous dicte le design d'une molécule avec une surface concave et électron-riche. Le phosphangulène (**1**), qui répond à ces critères et est aisément fonctionnalisable, a été choisi comme structure de base pour la synthèse des cibles.

La présente thèse décrit la synthèse des dérivés du phosphangulène (**1**) et les études cristallographiques des cristaux de ceux-ci ainsi que des cocristaux obtenus avec les fullerènes au travers de quatre articles soumis au courant de ce doctorat. Le premier article décrit la

synthèse des dérivés chalcogénures du phosphangulène (**1**). Ces dérivés-ci présentent de nombreux polymorphes, résultant en de bons candidats pour la cocristallisation. Le second article se concentre sur les cocristaux obtenus par ces dérivés chalcogénures avec le C_{60} et le C_{70}. Dans le troisième article, nous décrivons les complexes métalliques obtenus par coordination du phosphangulène (**1**) sur des métaux de transition. Enfin, dans le quatrième article, nous parlons des sels du μ-nitrido-bis(phosphangulène), un cation organique où deux unités phosphangulène sont pontées par un atome d'azote, ainsi que des cocristaux résultant de la combinaison de ce ligand pontant et du C_{60}.

Références

1. Goetzberger, A.; Hebling, C.; Schock, H.-W. *Mater. Sci. Eng. R Rep.* **2003,** *40* (1), 1-46.
2. Hoppe, H.; Sariciftci, N. S. *J. Mater. Res.* **2004,** *19* (7), 1924-1945.
3. Peumans, P.; Yakimov, A.; Forrest, S. R. *J. Appl. Phys.* **2003,** *93* (7), 3693-3723.
4. Nelson, J. *Curr. Opin. Solid State Mater. Sci.* **2002,** *6* (1), 87-95.
5. Wöhrle, D.; Meissner, D. *Adv. Mater. (Weinheim, Ger.)* **1991,** *3* (3), 129-138.
6. Chamberlain, G. A. *Solar Cells* **1983,** *8* (1), 47-83.
7. Kippelen, B.; Brédas, J.-L. *Energy Environ. Sci.* **2009,** *2* (3), 251-261.
8. Oregan, B.; Gratzel, M. *Nature* **1991,** *353* (6346), 737-740.
9. Bucher, K.; Fricke, J. *Phys. Zeit* **1980,** (21), 237–244.
10. Laboratory, N. R. E. https://www.nrel.gov/pv/. (accédé le 16 décembre 2019).
11. Scharber, M. C.; Sariciftci, N. S. *Prog. Polym. Sci.* **2013,** *38* (12), 1929-1940.
12. Liao, H.-C.; Ho, C.-C.; Chang, C.-Y.; Jao, M.-H.; Darling, S. B.; Su, W.-F. *Materials Today* **2013,** *16* (9), 326-336.
13. Huang, Y.; Kramer, E. J.; Heeger, A. J.; Bazan, G. C. *Chem. Rev.* **2014,** *114* (14), 7006-7043.
14. Chen, W.; Nikiforov, M. P.; Darling, S. B. *Energy Environ. Sci.* **2012,** *5* (8), 8045-8074.
15. Hoppe, H.; Sariciftci, N. S. *J. Mater. Chem.* **2006,** *16* (1), 45-61.
16. Yang, X.; Loos, J. *Macromolecules* **2007,** *40* (5), 1353-1362.
17. Dang, M. T.; Hirsch, L.; Wantz, G.; Wuest, J. D. *Chem. Rev.* **2013,** *113* (5), 3734-3765.

18. Herranz;, Á.; Illescas;, B. M.; Pérez;, E. M.; Martín, N. Supramolecular Assembly of Fullerenes and Carbon Nanotubes Hybrids. In *Chemistry of Nanocarbons*, T. Akasaka, F. W. a. S. N., Ed. 2010; pp 49 - 71.

19. Kroto, H. W.; Heath, J. R.; O'Brien, S. C.; Curl, R. F.; Smalley, R. E. *Nature* **1985,** *318*, 162.

20. Yutaka Matsuo, E. N. Application of Fullerenes to Nanodevices. In *Chemistry of Nanocarbons*, T. Akasaka; Wudl, F.; Nagase, S., Eds. 2010; pp 173 - 187.

21. Rohlfing, E. A.; Cox, D. M.; Kaldor, A. *J. Chem. Phys.* **1984,** *81* (7), 3322-3330.

22. *IETE Technical Review* **1999,** *16* (3-4), 297-310.

23. Smalley, R. E. *Rev. Mod. Phys.* **1997,** *69* (3), 723-730.

24. Tiwari, S. K.; Kumar, V.; Huczko, A.; Oraon, R.; De Adhikari, A.; Nayak, G. C. *Crit. Rev. Solid State Mater. Sci.* **2016,** *41* (4), 257-317.

25. Bernal, A. Canada, Travel 360, Biosphere Montreal. http://www.alessabernal.com/2018/05/17/biosphere-montreal/ (accédé le 21 janvier 2019).

26. Haddon, R. C. *Acc. Chem. Res.* **1992,** *25* (3), 127-133.

27. Charles See, Y.; Ya Kun, C.; Yan Alexander, W. **2011**.

28. Chen, Z.; King, R. B. *Chem. Rev.* **2005,** *105* (10), 3613-3642.

29. Bühl, M.; Hirsch, A. *Chem. Rev.* **2001,** *101* (5), 1153-1184.

30. Schleyer, P. v. R.; Maerker, C.; Dransfeld, A.; Jiao, H.; van Eikema Hommes, N. J. R. *J. Am. Chem. Soc.* **1996,** *118* (26), 6317-6318.

31. Buehl, M.; Thiel, W.; Jiao, H.; Schleyer, P. v. R.; Saunders, M.; Anet, F. A. L. *J. Am. Chem. Soc.* **1994,** *116* (13), 6005-6006.

32. Bühl, M. *Chem. Eur. J.* **1998,** *4* (4), 734-739.

33. Saunders, M.; Jiménez-Vázquez, H. A.; Cross, R. J.; Mroczkowski, S.; Freedberg, D. I.; Anet, F. A. L. *Nature* **1994,** *367* (6460), 256-258.

34. Saunders, M.; Cross, R. J.; Jiménez-Vázquez, H. A.; Shimshi, R.; Khong, A. *Science* **1996,** *271* (5256), 1693-1697.

35. Saunders, M.; Jimenez-Vazquez, H. A.; Cross, R. J.; Billups, W. E.; Gesenberg, C.; Gonzalez, A.; Luo, W.; Haddon, R. C.; Diederich, F.; Herrmann, A. *J. Am. Chem. Soc.* **1995,** *117* (36), 9305-9308.

36. Shabtai, E.; Weitz, A.; Haddon, R. C.; Hoffman, R. E.; Rabinovitz, M.; Khong, A.; Cross, R. J.; Saunders, M.; Cheng, P.-C.; Scott, L. T. *J. Am. Chem. Soc.* **1998,** *120* (25), 6389-6393.

37. Elser, V.; Haddon, R. C. *Nature* **1987,** *325* (6107), 792-794.

38. Prato, M.; Suzuki, T.; Wudl, F.; Lucchini, V.; Maggini, M. *J. Am. Chem. Soc.* **1993,** *115* (17), 7876-7877.

39. Isaacs, L.; Wehrsig, A.; Diederich, F. *Helv. Chim. Acta* **1993,** *76* (3), 1231-1250.

40. Pasquarello, A.; Schlüter, M.; Haddon, R. C. *Science* **1992,** *257* (5077), 1660-1661.

41. Zhou, F.; Jehoulet, C.; Bard, A. J. *J. Am. Chem. Soc.* **1992,** *114* (27), 11004-11006.

42. Ohsawa, Y.; Saji, T. *J. Chem. Soc., Chem. Commun.* **1992,** (10), 781-782.

43. Sternfeld, T.; Hoffman, R. E.; Saunders, M.; Cross, R. J.; Syamala, M. S.; Rabinovitz, M. *J. Am. Chem. Soc.* **2002,** *124* (30), 8786-8787.

44. Haufler, R. E.; Conceicao, J.; Chibante, L. P. F.; Chai, Y.; Byrne, N. E.; Flanagan, S.; Haley, M. M.; O'Brien, S. C.; Pan, C.; Xiao, Z.; Billups, W. E.; Ciufolini, M. A.;

Hauge, R. H.; Margrave, J. L.; Wilson, L. J.; Curl, R. F.; Smalley, R. E. *J. Phys. Chem.* **1990,** *94* (24), 8634-8636.

45. Haddon, R. C.; Hebard, A. F.; Rosseinsky, M. J.; Murphy, D. W.; Duclos, S. J.; Lyons, K. B.; Miller, B.; Rosamilia, J. M.; Fleming, R. M.; Kortan, A. R.; Glarum, S. H.; Makhija, A. V.; Muller, A. J.; Eick, R. H.; Zahurak, S. M.; Tycko, R.; Dabbagh, G.; Thiel, F. A. *Nature* **1991,** *350* (6316), 320-322.

46. Takabayashi, Y.; Prassides, K. *Phil. Trans. R. Soc. A* **2016,** *374* (2076).

47. Hebard, A. F.; Rosseinsky, M. J.; Haddon, R. C.; Murphy, D. W.; Glarum, S. H.; Palstra, T. T. M.; Ramirez, A. P.; Kortan, A. R. *Nature* **1991,** *350* (6319), 600-601.

48. Holczer, K.; Klein, O.; Huang, S.-m.; Kaner, R. B.; Fu, K.-j.; Whetten, R. L.; Diederich, F. *Science* **1991,** *252* (5009), 1154-1157.

49. Fleming, R. M.; Ramirez, A. P.; Rosseinsky, M. J.; Murphy, D. W.; Haddon, R. C.; Zahurak, S. M.; Makhija, A. V. *Nature* **1991,** *352* (6338), 787-788.

50. Tanigaki, K.; Ebbesen, T. W.; Saito, S.; Mizuki, J.; Tsai, J. S.; Kubo, Y.; Kuroshima, S. *Nature* **1991,** *352* (6332), 222-223.

51. Stephens, P. W.; Mihaly, L.; Lee, P. L.; Whetten, R. L.; Huang, S.-M.; Kaner, R.; Deiderich, F.; Holczer, K. *Nature* **1991,** *351* (6328), 632-634.

52. Diederich, F.; Kessinger, R. *Acc. Chem. Res.* **1999,** *32* (6), 537-545.

53. Prato, M.; Maggini, M. *Acc. Chem. Res.* **1998,** *31* (9), 519-526.

54. Bonifazi, D.; Enger, O.; Diederich, F. *Chem. Soc. Rev.* **2007,** *36* (2), 390-414.

55. Makha, M.; Purich, A.; Raston, C. L.; Sobolev, A. N. *Eur. J. Inorg. Chem.* **2006,** *2006* (3), 507-517.

56. Litvinov, A. L.; Konarev, D. V.; Kovalevsky, A. Y.; Neretin, I. S.; Slovokhotov, Y. L.; Coppens, P.; Lyubovskaya, R. N. *CrystEngComm* **2002,** *4* (104), 618-622.

57. Atwood, J. L.; Barbour, L. J.; Heaven, M. W.; Raston, C. L. *Angew. Chem., Int. Ed.* **2003,** *42* (28), 3254-3257.

58. E. Grey, I. *Chem. Commun.* **1999,** (12), 1139-1140.

59. Bond, A. M.; Miao, W.; Raston, C. L.; Ness, T. J.; Barnes, M. J.; Atwood, J. L. *J. Phys. Chem. B* **2001,** *105* (9), 1687-1695.

60. Andrews, P. C.; Atwood, J. L.; Barbour, L. J.; Nichols, P. J.; Raston, C. L. *Chem. Eur. J.* **1998,** *4* (8), 1384-1387.

61. Konarev, D. V.; Neretin, I. S.; Slovokhotov, Y. L.; Yudanova, E. I.; Drichko, N. y. V.; Shul'ga, Y. M.; Tarasov, B. P.; Gumanov, L. L.; Batsanov, A. S.; Howard, J. A. K.; Lyubovskaya, R. N. *Chem. Eur. J.* **2001,** *7* (12), 2605-2616.

62. Olmstead, M. M.; Jiang, F.; Balch, A. L. *Chem. Commun.* **2000,** (6), 483-484.

63. Kawase, T.; Kurata, H. *Chem. Rev.* **2006,** *106* (12), 5250-5273.

64. Kawase, T. Supramolecular Chemistry of Fullerenes: Host Molecules for Fullerenes on the Basis of π-π Interaction. In *Chemistry of Nanocarbons*, Akasaka, T.; Wudl, F.; Nagase, S., Eds. John Wiley & Sons, Ltd.: 2010; pp 189-213.

65. Effing, J.; Jonas, U.; Jullien, L.; Plesnivy, T.; Ringsdorf, H.; Diederich, F.; Thilgen, C.; Weinstein, D. *Angew. Chem., Int. Ed. Engl.* **1992,** *31* (12), 1599-1602.

66. Atwood, J. L.; Koutsantonis, G. A.; Raston, C. L. *Nature* **1994,** *368*, 229.

67. Fa, S.-X.; Wang, L.-X.; Wang, D.-X.; Zhao, L.; Wang, M.-X. *J. Org. Chem.* **2014,** *79* (8), 3559-3571.

68. Rose, K. N.; Barbour, L. J.; Orr, G. W.; Atwood, J. L. *Chem. Commun.* **1998,** (3), 407-408.

69. Steed, J. W.; Junk, P. C.; Atwood, J. L.; Barnes, M. J.; Raston, C. L.; Burkhalter, R. S. *J. Am. Chem. Soc.* **1994,** *116* (22), 10346-10347.

70. Atwood, J. L.; Barnes, M. J.; Gardiner, M. G.; Raston, C. L. *Chem. Commun.* **1996,** (12), 1449-1450.

71. Andersson, T.; Nilsson, K.; Sundahl, M.; Westman, G.; Wennerström, O. *J. Chem. Soc., Chem. Commun.* **1992,** (8), 604-606.

72. Andersson, T.; Westman, G.; Stenhagen, G.; Sundahl, M.; Wennerström, O. *Tetrahedron Lett.* **1995,** *36* (4), 597-600.

73. Andersson, T.; Westman, G.; Wennerström, O.; Sundahl, M. *J. Chem. Soc., Perkin Trans. 2* **1994,** (5), 1097-1101.

74. Sundahl, M.; Andersson, T.; Nilsson, K.; Wennerström, O.; Westman, G. *Synth. Met.* **1993,** *56* (2), 3252-3257.

75. Boulas, P.; Kutner, W.; Jones, M. T.; Kadish, K. M. *J. Phys. Chem.* **1994,** *98* (4), 1282-1287.

76. Canevet, D.; Perez, E. M.; Martin, N. *Angew. Chem., Int. Ed.* **2011,** *50* (40), 9248-9259.

77. Sygula, A. *Eur. J. Org. Chem.* **2011,** (9), 1611-1625.

78. Perez, E. M.; Martin, N. *Chem. Soc. Rev.* **2015,** *44* (18), 6425-6433.

79. Sygula, A. *Synlett* **2016,** *27* (14), 2070-2080.

80. Xu, L.; Feiyu, K.; Michio, I. *Small* **2016,** *12* (24), 3206-3223.

81. Kawase, T. Receptors for Pristine Fullerenes Based on Concave–Convex π–πInteractions. In *Supramolecular Chemistry of Fullerenes and Carbon Nanotubes*, Nierengarten, N. M. J.-F., Ed. Wiley-VCH Verlag GmbH & Co.: 2012; pp 55-78.

82. Hiroto, S. *Bull. Chem. Soc. Jpn.* **2018,** *91* (5), 829-838.

83. Nestoros, E.; Stuparu, M. C. *Chem. Commun.* **2018,** *54* (50), 6503-6519.

84. Saito, M.; Shinokubo, H.; Sakurai, H. *Mater. Chem. Front.* **2018,** *2* (4), 635-661.

85. Selmani, S.; Schipper, D. J. *Chem. Eur. J.* **2019,** *25* (27), 6673-6692.

86. Takeshi, K.; Kenji, T.; Naoki, F.; R., D. H.; Masaji, O. *Angew. Chem., Int. Ed.* **2003,** *42* (14), 1624-1628.

87. Delgado, J. L.; Herranz, M. a. Á.; Martín, N. *J. Mater. Chem.* **2008,** *18* (13), 1417-1426.

88. Haddon, R. C. *Science* **1993,** *261* (5128), 1545-1550.

89. Haddon, R. C. *J. Am. Chem. Soc.* **1997,** *119* (7), 1797-1798.

90. Scott, L. T.; Bronstein, H. E.; Preda, D. V.; Ansems, R. B. M.; Bratcher, M. S.; Hagen, S. *Pure Appl. Chem.* **1999,** *71* (2), 209.

91. Wang, L.; Wang, W. Y.; Zhong, R. L.; Qiu, Y. Q.; Xie, H. M. *J. Phys. Chem. C* **2016,** *120* (45), 26034-26043.

92. Wang, L.; Wang, W. Y.; Fang, X. Y.; Zhu, C. L.; Qiu, Y. Q. *RSC Adv.* **2015,** *5* (97), 79783-79791.

93. Sepúlveda, D.; Guan, Y.; Rangel, U.; Wheeler, S. E. *Org. Biomol. Chem.* **2017,** *15* (28), 6042-6049.

94. Le, V. H.; Yanney, M.; McGuire, M.; Sygula, A.; Lewis, E. A. *J. Phys. Chem. B* **2014,** *118* (41), 11956-11964.

95. Klärner, F.-G.; Panitzky, J.; Preda, D.; Scott, L. T. *J. Mol. Model.* **2000,** *6* (2), 318-327.

96. Kennedy, M. R.; Burns, L. A.; Sherrill, C. D. *J. Phys. Chem. A* **2012,** *116* (48), 11920-11926.

97. Karunarathna, A. A. S.; Saebo, S. *Struct. Chem.* **2014,** *25* (6), 1831-1836.

98. Karunarathna, A. A. S.; Saebo, S. *Struct. Chem.* **2015,** *26* (5-6), 1689-1695.

99. Joko, Y.; Sasaki, R.; Shintani, K. *Phys. Chem. Chem. Phys.* **2017,** *19* (40), 27704-27715.

100. Janowski, T.; Pulay, P.; Karunarathna, A. A. S.; Sygula, A.; Saebo, S. *Chem. Phys. Lett.* **2011,** *512* (4-6), 155-160.

101. Denis, P. A. *New J. Chem.* **2014,** *38* (11), 5608-5616.

102. Calbo, J.; Arago, J.; Boto, R. A.; Sanchez-Marin, J.; Orti, E.; Contreras-Garcia, J. *J. Phys. Chem. A* **2018,** *122* (4), 1124-1137.

103. Cabaleiro-Lago, E. M.; Fernandez, B.; Rodriguez-Otero, J. *J. Comput. Chem.* **2017,** *39* (2), 93-104.

104. Bhattacharyya, K.; Mukhopadhyay, T. K.; Datta, A. *Phys. Chem. Chem. Phys.* **2016,** *18* (22), 14886-14893.

105. Ogoshi, T.; Ueshima, N.; Sakakibara, F.; Yamagishi, T.-a.; Haino, T. *Org. Lett.* **2014,** *16* (11), 2896-2899.

106. Canevet, D.; Gallego, M.; Isla, H.; de Juan, A.; Pérez, E. M.; Martín, N. *J. Am. Chem. Soc.* **2011,** *133* (9), 3184-3190.

107. Mulla, K.; Shaik, H.; Thompson, D. W.; Zhao, Y. *Org. Lett.* **2013,** *15* (17), 4532-4535.

108. Takeshi, K.; Kenji, T.; Nami, S.; Yohko, S.; Masaji, O. *Angew. Chem., Int. Ed.* **2004,** *43* (13), 1722-1724.

109. Yuan, K.; Zhou, C. H.; Zhu, Y. C.; Zhao, X. *Phys. Chem. Chem. Phys.* **2015,** *17* (28), 18802-18812.

110. Iwamoto, T.; Watanabe, Y.; Sadahiro, T.; Haino, T.; Yamago, S. *Angew. Chem., Int. Ed.* **2011,** *50* (36), 8342-8344.

111. Petrukhina, M. A.; Scott, L. T. *Dalton Trans.* **2005,** (18), 2969-2975.

112. Muck-Lichtenfeld, C.; Grimme, S.; Kobryn, L.; Sygula, A. *Phys. Chem. Chem. Phys.* **2010,** *12* (26), 7091-7097.

113. Denis, P. A. *Chem. Phys. Lett.* **2011,** *516* (1), 82-87.

114. Becker, H.; Javahery, G.; Petrie, S.; Cheng, P. C.; Schwarz, H.; Scott, L. T.; Bohme, D. K. *J. Am. Chem. Soc.* **1993,** *115* (24), 11636-11637.

115. Mizyed, S.; Georghiou, P. E.; Bancu, M.; Cuadra, B.; Rai, A. K.; Cheng, P.; Scott, L. T. *J. Am. Chem. Soc.* **2001,** *123* (51), 12770-12774.

116. Georghiou, P. E.; Tran, A. H.; Mizyed, S.; Bancu, M.; Scott, L. T. *J. Org. Chem.* **2005,** *70* (16), 6158-6163.

117. Liu, Y. M.; Xia, D.; Li, B. W.; Zhang, Q. Y.; Sakurai, T.; Tan, Y. Z.; Seki, S.; Xie, S. Y.; Zheng, L. S. *Angew. Chem., Int. Ed.* **2016,** *55* (42), 13047-13051.

118. Sygula, A.; Fronczek, F. R.; Sygula, R.; Rabideau, P. W.; Olmstead, M. M. *J. Am. Chem. Soc.* **2007,** *129* (13), 3842-3843.

119. Abeyratne Kuragama, P. L.; Fronczek, F. R.; Sygula, A. *Org. Lett.* **2015,** *17* (21), 5292-5295.

120. Kobryn, L.; Henry, W. P.; Fronczek, F. R.; Sygula, R.; Sygula, A. *Tetrahedron Lett.* **2009,** *50* (51), 7124-7127.

121. Kuragama, P. L. A.; Fronczek, F. R.; Sygula, A. *Org. Lett.* **2015,** *17* (21), 5292-5295.

122. Yanney, M.; Sygula, A. *Tetrahedron Lett.* **2013,** *54* (21), 2604-2607.

123. Sygula, A.; Yanney, M.; Henry, W. P.; Fronczek, F. R.; Zabula, A. V.; Petrukhina, M. A. *Cryst. Growth Des.* **2014,** *14* (5), 2633-2639.

124. Yanney, M.; Fronczek, F. R.; Sygula, A. *Angew. Chem., Int. Ed.* **2015,** *54* (38), 11153-11156.

125. Upul, K. G.; Kumarasinghe, R.; Fronczek, F. R.; Valle, H. U.; Sygula, A. *Org. Lett.* **2016,** *18* (13), 3054-3057.

126. Yang, D. C.; Li, M.; Chen, C. F. *Chem. Commun.* **2017,** *53* (67), 9336-9339.

127. Álvarez, C. M.; Aullón, G.; Barbero, H.; García-Escudero, L. A.; Martínez-Pérez, C.; Martín-Álvarez, J. M.; Miguel, D. *Org. Lett.* **2015,** *17* (11), 2578-2581.

128. Barbero, H.; Ferrero, S.; Álvarez-Miguel, L.; Gómez-Iglesias, P.; Miguel, D.; Álvarez, C. M. *Chem. Commun.* **2016,** *52* (88), 12964-12967.

129. Takeda, M.; Hiroto, S.; Yokoi, H.; Lee, S.; Kim, D.; Shinokubo, H. *J. Am. Chem. Soc.* **2018,** *140* (20), 6336-6342.

130. Yang, D.-C.; Li, M.; Chen, C.-F. *Chem. Commun.* **2017,** *53* (67), 9336-9339.

131. Yokoi, H.; Hiroto, S.; Sakamaki, D.; Seki, S.; Shinokubo, H. *Chem. Sci.* **2018,** *9* (4), 819-824.

132. Xiao, W.; Passerone, D.; Ruffieux, P.; Aït−Mansour, K.; Gröning, O.; Tosatti, E.; Siegel, J. S.; Fasel, R. *J. Am. Chem. Soc.* **2008,** *130* (14), 4767-4771.

133. Dawe, L. N.; AlHujran, T. A.; Tran, H.-A.; Mercer, J. I.; Jackson, E. A.; Scott, L. T.; Georghiou, P. E. *Chem. Commun.* **2012,** *48* (45), 5563-5565.

134. Filatov, A. S.; Ferguson, M. V.; Spisak, S. N.; Li, B.; Campana, C. F.; Petrukhina, M. A. *Cryst. Growth Des.* **2014,** *14* (2), 756-762.

135. Petrukhina, M. A.; Andreini, K. W.; Mack, J.; Scott, L. T. *J. Org. Chem.* **2005,** *70* (14), 5713-5716.

136. Sygula, A.; Folsom, H. E.; Sygula, R.; Abdourazak, A. H.; Marcinow, Z.; Fronczek, F. R.; Rabideau, P. W. *J. Chem. Soc., Chem. Commun.* **1994,** (22), 2571-2572.

137. Sygula, A.; Abdourazak, A. H.; Rabideau, P. W. *J. Am. Chem. Soc.* **1996,** *118* (2), 339-343.

138. Abdourazak, A. H.; Sygula, A.; Rabideau, P. W. *J. Am. Chem. Soc.* **1993,** *115* (7), 3010-3011.

139. Ball, M.; Zhong, Y.; Wu, Y.; Schenck, C.; Ng, F.; Steigerwald, M.; Xiao, S.; Nuckolls, C. *Acc. Chem. Res.* **2015,** *48* (2), 267-276.

140. Xiao, S. X.; Myers, M.; Miao, Q.; Sanaur, S.; Pang, K. L.; Steigerwald, M. L.; Nuckolls, C. *Angew. Chem., Int. Ed.* **2005,** *44* (45), 7390-7394.

141. Leibfarth, F. A.; Nuckolls, C.; Myers, M. M.; Xiao, S. X. *Abstr. Pap. Am. Chem. Soc.* **2006,** *231*.

142. Tremblay, N. J.; Gorodetsky, A. A.; Cox, M. P.; Schiros, T.; Kim, B.; Steiner, R.; Bullard, Z.; Sattler, A.; So, W.-Y.; Itoh, Y.; Toney, M. F.; Ogasawara, H.; Ramirez, A. P.; Kymissis, I.; Steigerwald, M. L.; Nuckolls, C. *ChemPhysChem* **2010,** *11* (4), 799-803.

143. Whalley, A. C.; Plunkett, K. N.; Gorodetsky, A. A.; Schenck, C. L.; Chiu, C.-Y.; Steigerwald, M. L.; Nuckolls, C. *Chem. Sci.* **2011,** *2* (1), 132-135.

144. Kang, S. J.; Kim, J. B.; Chiu, C. Y.; Ahn, S.; Schiros, T.; Lee, S. S.; Yager, K. G.; Toney, M. F.; Loo, Y. L.; Nuckolls, C. *Angew. Chem., Int. Ed.* **2012,** *51* (34), 8594-8597.

145. Kang, S. J.; Kim, J. B.; Chiu, C.-Y.; Ahn, S.; Schiros, T.; Lee, S. S.; Yager, K. G.; Toney, M. F.; Loo, Y.-L.; Nuckolls, C. *Angew. Chem.* **2012,** *124* (34), 8722-8725.

146. Nuckolls, C. P. *Abstr. Pap. Am. Chem. Soc.* **2012,** *243*.

147. Kang, S. J.; Ahn, S.; Kim, J. B.; Schenck, C.; Hiszpanski, A. M.; Oh, S.; Schiros, T.; Loo, Y.-L.; Nuckolls, C. *J. Am. Chem. Soc.* **2013,** *135* (6), 2207-2212.

148. Kang, S. J.; Kim, J. B.; Chiu, C. Y.; Ahn, S.; Schiros, T.; Lee, S. S.; Yager, K. G.; Toney, M. F.; Loo, Y. L.; Nuckolls, C. *Angew. Chem., Int. Ed.* **2013,** *52* (28), 7063-7063.

149. Schiros, T.; Kladnik, G.; Prezzi, D.; Ferretti, A.; Olivieri, G.; Cossaro, A.; Floreano, L.; Verdini, A.; Schenck, C.; Cox, M.; Gorodetsky, A. A.; Plunkett, K.; Delongchamp, D.; Nuckolls, C.; Morgante, A.; Cvetko, D.; Kymissis, I. *Adv. Energy Mater.* **2013,** *3* (7), 894-902.

150. Xiao, S. X.; Kang, S. J.; Wu, Y.; Ahn, S.; Kim, J. B.; Loo, Y. L.; Siegrist, T.; Steigerwald, M. L.; Li, H. X.; Nuckolls, C. *Chem. Sci.* **2013,** *4* (5), 2018-2023.

151. Xiao, S. X.; Kang, S. J.; Zhong, Y.; Zhang, S. G.; Scott, A. M.; Moscatelli, A.; Turro, N. J.; Steigerwald, M. L.; Li, H. X.; Nuckolls, C. *Angew. Chem., Int. Ed.* **2013,** *52* (17), 4558-4562.

152. Gao, J.; Sengar, N.; Wu, Y.; Jockusch, S.; Nuckolls, C.; Clancy, P.; Loo, Y. L. *Chem. Mater.* **2017,** *29* (2), 595-604.

153. Hiszpanski, A. M.; Woll, A. R.; Kim, B.; Nuckolls, C.; Loo, Y. L. *Chem. Mater.* **2017,** *29* (10), 4311-4316.

154. Krishnan Jagadamma, L.; McCarron, L. J.; Wiles, A. A.; Savikhin, V.; Sajjad, M. T.; Yazdani, M.; Rotello, V. M.; Toney, M. F.; Cooke, G.; Samuel, I. D. W. *ACS Appl. Mater. Interfaces* **2018,** *10* (29), 24665-24678.

155. Qi, D.; Zhang, L.; Wan, L.; Zhao, L.; Jiang, J. *J. Phys. Chem. A* **2012,** *116* (25), 6785-6791.

156. Claessens, C. G.; González-Rodríguez, D.; Iglesias, R. S.; Torres, T. *C. R. Chim.* **2006,** *9* (7), 1094-1099.

157. Nakano, S.; Kage, Y.; Furuta, H.; Kobayashi, N.; Shimizu, S. *Chem. Eur. J.* **2016,** *22* (23), 7706-7710.

158. Sánchez-Molina, I.; Claessens, C. G.; Grimm, B.; Guldi, D. M.; Torres, T. *Chem. Sci.* **2013,** *4* (3), 1338-1344.

159. Yuta, S.; Tomoya, I.; Tatsuhiro, K.; Shigeki, M.; Masaki, K.; Takahiko, K. *Chem. Eur. J.* **2015,** *21* (14), 5302-5306.

160. Krebs, F. C.; Larsen, P. S.; Larsen, J.; Jacobsen, C. S.; Boutton, C.; Thorup, N. *J. Am. Chem. Soc.* **1997,** *119* (6), 1208 - 1216.

161. Yamamura, M.; Saito, T.; Nabeshima, T. *J. Am. Chem. Soc.* **2014,** *136* (40), 14299-14306.

162. Yamamura, M.; Hongo, D.; Nabeshima, T. *Chem. Sci.* **2015,** *6* (11), 6373-6378.

163. Yamamura, M.; Sukegawa, K.; Nabeshima, T. *Chem. Commun.* **2015,** *51* (60), 12080-12083.

164. Yamamura, M.; Hasegawa, T.; Nabeshima, T. *Org. Lett.* **2016,** *18* (4), 816-819.

165. Yamamura, M. N., Tatsuya. *Bull. Chem. Soc. Jpn.* **2016,** *89*, 42-49.

166. Corbridge, D. *Phosphorus*. CRC Press.: Boca Raton, 2013.

167. Kirby, A. J.; Warren, S. G. The Organic Chemistry of Phosphorus. In *Reaction Mechanisms in Organic Chemistry*, Eaborn, C.; Chapman, N. B., Eds. Elsevier Publishing Company: 1967; Vol. 5.

168. von E. Doering, W.; Hoffmann, A. K. *J. Am. Chem. Soc.* **1955,** *77* (3), 521-526.

169. Schomaker, V.; Stevenson, D. P. *J. Am. Chem. Soc.* **1941,** *63* (1), 37-40.

170. Pyykkö, P. *J. Phys. Chem. A* **2015,** *119* (11), 2326-2337.

171. Brown, T. L.; LeMay, H. E.; Bursten, B. E.; Murphy, C.; Woodward, P.; Langford, S.; Sagatys, D.; George, A. Chemistry: The Central Science - 6.6 Representations of Orbitals. http://wps.prenhall.com/wps/media/objects/3311/3390683/blb0606.html (accédé le 16 décembre 2019).

172. Magnusson, E. *J. Am. Chem. Soc.* **1990,** *112* (22), 7940-7951.

173. Magnusson, E. *J. Am. Chem. Soc.* **1993,** *115* (3), 1051-1061.

174. Gilheany, D. G. *Chem. Rev.* **1994,** *94* (5), 1339-1374.

175. Becke, A. D.; Edgecombe, K. E. *J. Chem. Phys.* **1990,** *92* (9), 5397-5403.

176. Silvi, B.; Savin, A. *Nature* **1994,** *371*, 683.

177. Chesnut, D. B.; Savin, A. *J. Am. Chem. Soc.* **1999,** *121* (10), 2335-2336.

178. Chesnut, D. B. *Heteroat. Chem.* **2000,** *11* (1), 73-80.

179. Chesnut, D. B. *Heteroat. Chem.* **2000,** *11* (5), 341-352.

180. Ruff, J. K.; Schlientz, W. J.; Dessy, R. E.; Malm, J. M.; Dobson, G. R.; Memering, M. N. μ-Nitridobis(triphenylphosphorus)(l+) ("PPN") Salts with Metal Carbonyl Anions. In *Inorganic Syntheses*, Parshall, G. W., Ed. McGraw-Hill, Inc.: 1974; Vol. XV, pp 84-90.

Chapitre 2 : Polymorphisme des chalcogénures du phosphangulène

2.1 Introduction

La première série de dérivés synthétisés et étudiés sont les chalcogénures du phosphangulène, soient l'oxyde, le sulfure et le sélénuree. L'introduction d'un seul atome sur la molécule de phosphangulène a une conséquence importante. Alors que la forme conique du phosphangulène lui confère un empilement simple et efficace, il en va tout autrement des chalcogénures qui se retrouvent avec une forme maladroite d'entonnoir. Phosphangulène est une molécule qui cristallise aisément, et ce même sous évaporation rapide d'une solution, pour donner un seul et même polymorphe.

Le manuscrit présenté dans ce chapitre traite du polymorphisme naissant suite au positionnement d'un atome, ici d'éléments de la famille des chalcogénures, sur l'atome de phosphore central. Les différents polymorphes sont traités par une analyse de surface d'Hirshfeld. Ainsi, il est judicieux de commencer par une explication plus détaillée du polymorphisme et une présentation des surfaces d'Hirshfeld. Nous enchaînerons par la suite avec les objectifs des travaux présentés dans ce chapitre.

2.1.1 Polymorphisme

En cristallographie, le polymorphisme est défini comme étant la capacité d'un composé à cristalliser en plus d'un arrangement. On parle souvent de polymorphisme conformationnel lorsqu'entre les différentes formes cristallines il y a un changement important dans la conformation du composé. Néanmoins, parfois, un même conformère peut adopter différentes formes cristallines.

Une structure cristallographique se décrit par la maille élémentaire et le groupe d'espace de l'unité asymétrique. L'unité asymétrique est la plus petite unité répétitive dans un cristal. N'importe quelles opérations de symétrie, telles que des rotations, translations ou des plans d'inversion, peuvent lui être appliquées afin d'obtenir la maille élémentaire, qui est l'unité dont de simples translations décrivent le motif de répétition à travers le réseau cristallin. Le Tableau 2.1 illustre la relation entre les différents termes à l'aide d'un exemple simple en deux dimensions. Alors qu'on dénombre 17 groupes d'espace dans cette dimension appelés « groupe papier-peints », il en existe 230 pour les systèmes cristallins tridimensionnels.

Tableau 2.1 : Exemples en deux dimensions de la construction de réseaux cristallins à partir de l'unité asymétrique et du groupe d'espace.[iii]

Unité asymétrique : Plus petite unité répétitive		
Groupe d'espace : opérations de symétrie pour obtenir la maille élémentaire	pm 1 plan de symétrie	p4g 4 rotations de 90°
Maille élémentaire : Unité décrivant le motif du réseau cristallin		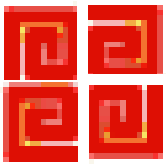
Système cristallin : Forme de la maille élémentaire obtenue	Rectangulaire	Carré
Réseau cristallin	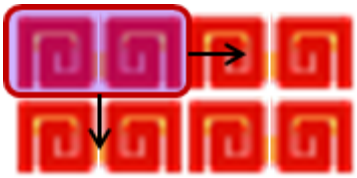	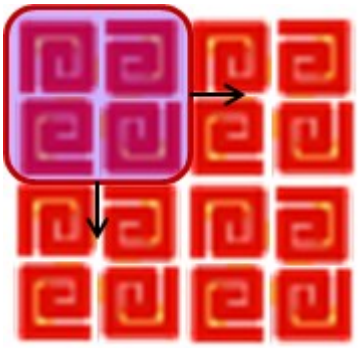

En théorie, il est possible d'organiser dans chacune de ces 230 manières n'importe quel composé. Alors pourquoi n'observons-nous pas 230 polymorphes pour chaque composé

[iii] Zwillinger, D. (Ed.). "Crystallographic Groups." dans *CRC Standard Mathematical Tables,* Boca Raton, FL: CRC Press, pp. 259-264, 1995.

connu? C'est que le modèle purement mathématique des groupes d'espace ne prend pas en compte l'énergie de ceux-ci. La stabilité absolue et relative des différents états possibles déterminent les polymorphes accessibles expérimentalement. Deux éléments régissent l'énergie finale du réseau cristallin : les interactions intermoléculaires et le vide entre les molécules.

La molécule doit tenter d'optimiser l'énergie du réseau cristallin en minimisant le vide et en maximisant les interactions stabilisantes. Dans le cas d'une molécule conique, ces deux aspects d'énergie ne sont pas antagonistes l'un à l'autre, puisque la forme permet un maximum de surface de contact entre les voisins et un minimum de vide. L'entonnoir ne permet pas un contact efficace entre deux individus, rendant plus difficile de balancer le vide et les interactions. En effet, dans la vie commune, il est plus facile d'empiler des chapeaux coniques que des entonnoirs.

Ceci a pour effet que les chalcogénures du phosphangulène devront s'efforcer à trouver un équilibre acceptable et que plusieurs états cristallins possibles sont énergétiquement proches et accessibles, et donc en compétition. On observe donc le phénomène du polymorphisme. Dans le cas du phosphangulène, il semble que les différentes formes ne sont que théoriques. Effectivement, il n'y a qu'un polymorphe connu pour le phosphangulène alors qu'il y en a de nombreux pour l'oxyde. Ceci s'explique par l'opposition des concepts de thermodynamique vs cinétique. Pour le phosphangulène, la forme observée semble être le produit de cristallisation cinétique et thermodynamique. Quant à l'oxyde, il y a une forme qui est thermodynamiquement plus stable que les autres, mais qui n'est pas le produit cinétique, au

moins dans certaines conditions. Le polymorphe stable peut donc se former lentement, possiblement avoir passé par des formes intermédiaires cinétiquement plus accessibles.

2.1.2 Surfaces de Hirshfeld

2.1.2.1 Définition

La surface d'Hirshfeld d'une molécule dans un cristal est un partitionnement de la densité électronique d'un cristal entre celle dérivée de la molécule d'intérêt et celle provenant de toutes les autres molécules présentes dans le cristal. Par exemple, une telle surface pourrait identifier les régions où la densité électronique résultant des atomes de la molécule d'intérêt (dénotée comme la promolécule) est supérieure à la somme des densités électroniques du cristal (le procristal). Cette surface est souvent délimitée comme là où la fonction de masse *w(r)* telle que définie par l'Équation 2.1 est supérieure ou égale à 0.5.[iv] La Figure 2.1a illustre le contour de cette surface pour le benzène comme exemple. Autrement dit, il s'agit donc de la région où la contribution de la promolécule au procristal est supérieure à celles des autres molécules du cristal.

$$\boldsymbol{w(r) = \frac{\rho_{promolécule}(r)}{\rho_{procristal}(r)} = \sum_{A \in molécule} \rho_A(r) \; / \; \sum_{A \in cristal} \rho_A(r)}$$

Équation 2.1 : Masse moléculaire *w(r)* définie par le quotient de la densité électronique d'une promolécule $\rho_{promolécule}(r)$, sur celle du procristal $\rho_{procristal}(r)$. Ces densités sont la somme des

[iv] Spackman, M. A.; Jayatilaka, D., Hirshfeld surface analysis. *CrystEngComm* **2009,** *11* (1), 19-32.

densités électroniques moyennes sphériques des atomes pris individuellement $\rho_A(r)$ respectivement au sein de la molécule et du cristal.

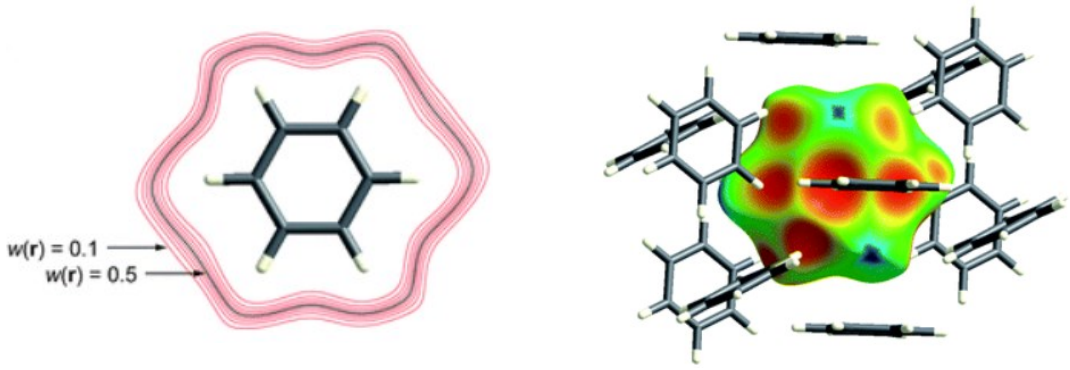

a b

Figure 2.1: Illustration des surfaces de Hirshfeld sur le benzène. a) Contours de la fonction de masse $w_A(r)$ pour des valeurs de 0.1 et 0.5. b) Cartographie de la distance d'un point sur une surface au plus proche atome externe à la surface (de la promolécule) d_e, sur cette surface de Hirshfeld. Le gradient va de la distance d_e la plus courte en rouge à la plus longue en bleu avec le vert pour intermédiaire. Image tirée de : Spackman, M. A.; Jayatilaka, D., Hirshfeld surface analysis. *CrystEngComm* 2009, *11* (1), 19-32.

À partir de cette surface, il est possible d'y cartographier d_e, soit la distance d'un point sur une surface au plus proche atome externe à la surface (la promolécule) et donc d'une autre molécule (Figure 2.1b). Lorsqu'on analyse les distances intermoléculaires en prenant compte de la densité électronique environnant l'atome dans la molécule et dans le cristal, il devient possible d'identifier et de visualiser les régions où il y a des interactions intermoléculaires et leurs importances relatives à l'intérieur du cristal. En ce sens, les surfaces d'Hirshfeld constituent un outil intéressant dans l'analyse des interactions intermoléculaires dans un cristal

en ajoutant une nuance supplémentaire par rapport aux mesures simples des distances interatomiques avec la somme des rayons de van der Waals comme seuil de référence.

2.1.2.2 Fonctions de distance et tracés empreintes digitales

Il existe quelques fonctions de distance employées dans la cartographie des surfaces de Hirshfeld : d_i (distance avec l'atome le plus proche dans la même molécule), d_e (distance avec l'atome le plus proche d'une autre molécule) et d_{norm} (distance de contact normalisée; Équation 2.2) sont les principaux exemples et les premiers à avoir été étudiés.

$$d_{norm} = \frac{d_i - r_i^{vdW}}{r_i^{vdW}} + \frac{d_e - r_e^{vdW}}{r_e^{vdW}}$$

Équation 2.2 : Distance de contact normalisée d_{norm}, définie par la distance d'un point sur une surface au plus proche atome externe à la surface (la promolécule) d_e, la distance d'un point sur une surface au plus proche atome interne à la surface (la promolécule) d_i et le rayon de van der Waals r^{vdW}.[iv]

Spackman, pionnier dans le développement des surfaces d'Hirshfeld comme outil pour l'analyse des interactions moléculaires et la comparaison des polymorphes, et ses collaborateurs ont découvert que de combiner d_e vs d_i dans un graphique de densité de récurrence permet d'obtenir un genre d'empreinte digitale bidimensionnelle plus facile à représenter et à interpréter dans son ensemble que la représentation conventionnelle en 2D de la surface d'Hirshfeld.[v] Le graphique est construit en employant d_e et d_i en guise de coordonnées cartésiennes et en colorant les différents points ou pixels (d_e, d_i) selon leur

[v] Spackman, M. A.; McKinnon, J. J., Fingerprinting intermolecular interactions in molecular crystals. *CrystEngComm* **2002,** *4* (66), 378-392.

récurrence sur la surface d'Hirshfeld tridimensionnelle de la molécule : de bleu pour peu fréquent à rouge pour très fréquent. Ce tracé empreinte digitale, *fingerprint plot*, est devenu un outil visuel standard dans la comparaison des polymorphes.

La **Figure 2.2** présente ces empreintes digitales et démontre leur utilité dans la comparaison et l'analyse des polymorphes pour le cas de l'acide 2-chloro-4-nitrobenzoïque. La forme I (une seule molécule dans l'unité asymétrique) et la forme II (quatre molécules dans l'unité asymétrique) présentent des tracés significativement différents entre eux. Il devient clair que les interactions sont différentes d'une forme à l'autre, et même d'une molécule à l'autre dans une même forme. On constate également et aisément certaines caractéristiques graphiques (« ailettes » ou pointes) dont les coordonnées (d_e, d_i) correspondent à certaines interactions spécifiques.

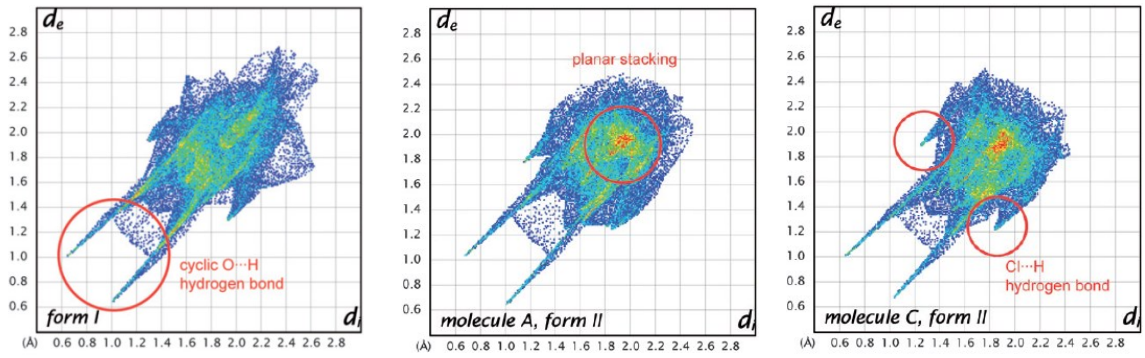

a b

Figure 2.2 : Comparaison des tracés empreintes digitales des surfaces d'Hirshfeld pour l'acide 2-chloro-4-nitrobenzoïque. a) La forme I comportant une seule molécule. b) La forme II comportant quatre molécules différentes dans l'unité asymétrique (seules deux d'entre elles représentées ici). Les interactions intermoléculaires clées sont encerclées et annotées en rouge.

Image tirée de : Spackman, M. A.; Jayatilaka, D., Hirshfeld surface analysis. *CrystEngComm* 2009, *11* (1), 19-32.

2.1.3 Objectifs

Le présent chapitre a pour objet l'étude du phénomène de polymorphisme observé pour les trois chalcogénures synthétisés pour le phosphangulène : l'oxyde, le sulfure et le sélénure. Nous tenterons de comprendre son origine que nous croyons attribuable à la forme maladroite d'entonnoir des dérivés ciblés. Les surfaces d'Hirshfeld cartographiée selon d_e et des tracés empreintes digitales nous servirons d'outils dans l'analyse des divers polymorphes pour les trois chalcogénures, et dans la comparaison entre ceux-ci et avec la molécule parente, le phosphangulène.

Étant donné la faible différence structurelle entre la phosphine et ses dérivés, et l'absence de conformère due à la rigidité du système, peu de variables rentrent en compte dans cette étude. Ainsi, les travaux sur le polymorphisme de ces molécules spécifiquement s'inscrivent dans l'effort à la compréhension du phénomène de polymorphisme en général en isolant un minimum de variables et en réduisant les facteurs pouvant influencer les observations. La cause des problèmes d'empilement à l'état cristallin et du polymorphisme se résumera essentiellement à la forme maladroite obtenue.

2.2 Article 1

Article publié dans

Cryst. Growth Des. **2019**, *19*, 5390-5406.

DOI: 10.1021/acs.cgd.9b00907

(contribution invitée publiée dans un numéro spécial dédié à la mémoire de Joel Bernstein)

Foiling Normal Patterns of Crystallization by Design.

Polymorphism of Phosphangulene Chalcogenides

Alice Heskia, Thierry Maris, and James D. Wuest*

Département de Chimie, Université de Montréal, Montréal, Québec H3C 3J7 Canada

*Author to whom correspondence may be addressed.

E-mail: *james.d.wuest@umontreal.ca*

[a]Dedicated to the memory of the late Joel Bernstein, whose deep understanding of molecular solids and infectious enthusiasm made him a valued friend and colleague

2.2.1 Abstract

Phosphangulene (**1**) has a well-defined hexacyclic structure with a distinctive conical shape and an electron-rich aromatic surface. Molecules of phosphangulene are disposed to crystallize in parallel π-stacks. This preference can be thwarted by adding a single atom and converting phosphangulene into the corresponding oxide (**2a**), sulfide (**2b**), and selenide (**2c**). This change creates an awkward molecular shape that prevents effective stacking. As a consequence, the formation of optimal intermolecular interactions is inhibited, and multiple polymorphs with high values of Z and Z' are formed. The high polymorphism of chalcogenides **2a**–**c** is particularly noteworthy because the compounds have little flexibility. Analysis of the structures of phosphangulene, chalcogenides **2a**–**c**, and related compounds provides deeper understanding of crystallization, including how to design molecules that cannot pack efficiently, are unable to achieve normal patterns of association, and are therefore predisposed to form multiple polymorphs, structures with high values of Z and Z', solvates, solid solutions, and cocrystals.

2.2.2 Introduction

Phosphangulene (**1**) has a characteristic conical shape reminiscent of traditional hats worn in parts of Asia (Figure 2.3). The compound was first reported by Krebs and coworkers, who determined the structure of crystals grown from ethyl acetate.[1] The nonplanarity of phosphangulene gives rise to a dipole moment, determined to be 3.3 ± 0.2 D in $CHCl_3$,[1] which is slightly larger than the moment of triphenylphosphine (1.49 D in benzene).[2,3] On the basis of ab initio calculations and multipolar modeling of X-ray structure factors, the direction of the dipole in phosphangulene is considered to run along the C_3 axis from the apex of the cone (with the atom of phosphorus at the negative end) toward the base (with the peripheral atoms of hydrogen at the positive end).[4]

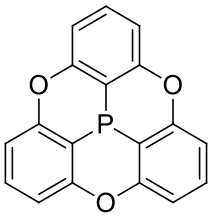

1

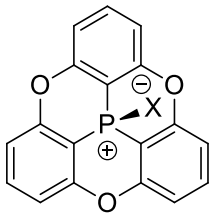

2a (X = O)
2b (X = S)
2c (X = Se)

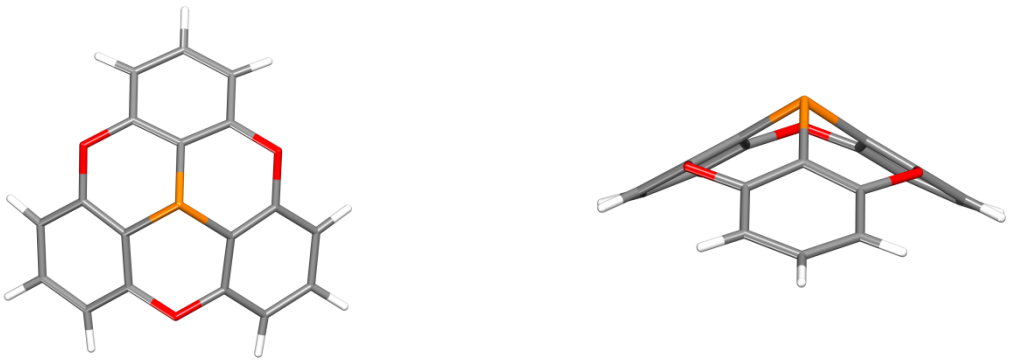

a **b**

Figure 2.3 : Representations of the molecular structure of phosphangulene (1) in crystals grown from ethyl acetate, as viewed along the C_3 axis and perpendicular to the axis. Atoms of carbon appear in gray, hydrogen in white, oxygen in red, and phosphorus in orange.

In crystals of phosphangulene, topology works in harmony with polarity to control molecular packing, which yields π-stacks with dipole moments aligned in parallel (Figure 2.4a). No other polymorph has been reported. Each stack is linked to six neighboring stacks by short C-H···O interactions (2.395 Å), as shown in Figure 2.4. Unexpectedly, the dipole moments of neighboring stacks point in the same direction, thereby yielding *R*3*m* crystals that are polar and pyroelectric. Temporary voltages are generated when pyroelectric materials are heated or cooled, making them suitable for use in high-performance infrared detectors and other devices. Pyroelectric carbon-based materials are uncommon, and their characteristically low densities and small dielectric constants give them advantages not normally shared by inorganic materials. As a consequence, phosphangulene and its derivatives define a structurally intriguing family of compounds with significant potential utility.

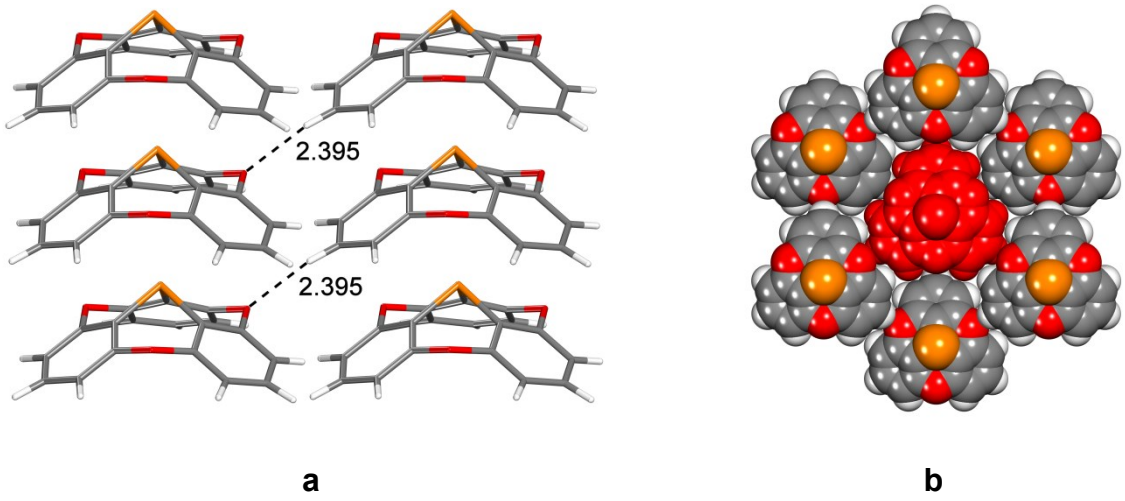

Figure 2.4 : Representations of the structure of crystals of phosphangulene grown from ethyl acetate. (a) View perpendicular to the *c*-axis, showing part of two adjacent π-stacks with aligned dipoles. Principal inter-stack C-H···O interactions are marked by broken lines, with distances given in Å. (b) View along the *c*-axis, showing how a central stack (in red) is surrounded by six others. Unless otherwise indicated, atoms are shown in standard colors.

Key features in the structure of phosphangulene can be highlighted by Hirshfeld surfaces of molecules in the crystal and by the corresponding two-dimensional fingerprint plots.[5,6] Hirshfeld surfaces are typically constructed to show the locus of points around a molecule in a crystal where the calculated electron density contributed by the molecule equals that contributed by all other atoms in the structure. The convex and concave surfaces of phosphangulene are shown in Figure 2.5. The surfaces are colored according to the local value of d_e, which is the distance from the surface to the nearest atomic nucleus in another molecule, and the colors vary from cool (blue) to hot (red) as d_e decreases. Figure 2.5 underscores several key features, including (1) the C_{3v} molecular symmetry of phosphangulene, (2) the presence of six significant C-H···O interactions per molecule, denoted by conspicuous red

spots located on the convex surface near each atom of oxygen, and (3) the weak affinity of the convex and concave π-surfaces, as indicated by the high proportion of blue and green around the center of each molecule. The primary driving forces for stacking appear to be topology and dipolar alignment rather than π-π interactions, and stacked molecules are separated by a relatively long distance (4.259 Å), which corresponds to the length of the unit cell along the *c*-axis.

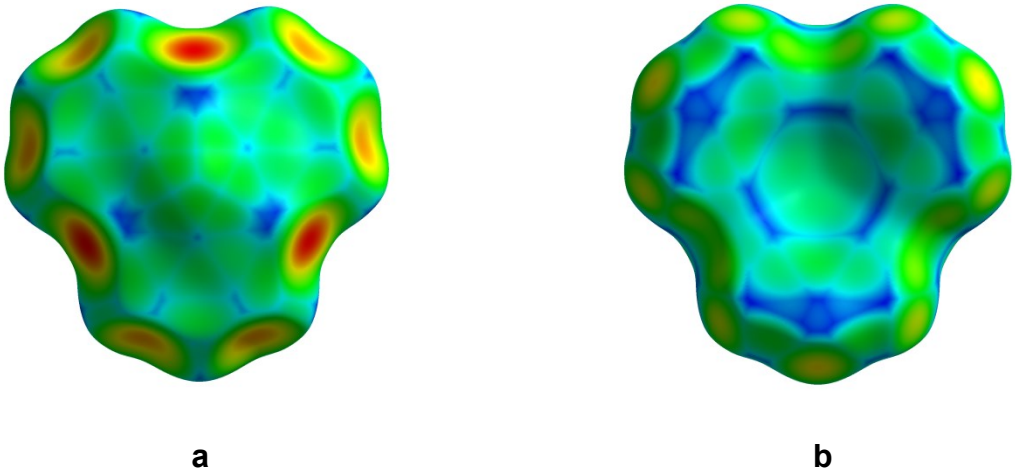

Figure 2.5 : (a) Hirshfeld surface of the convex face of a molecule of phosphangulene in crystals grown from ethyl acetate. The surface is colored according to the local value of d_e (distance from the surface to the nearest atomic nucleus in another molecule), and the colors range from cool (blue) to hot (red) as d_e decreases. (b) Corresponding surface of the concave face.

The fingerprint plot in Figure 2.6 provides complementary information by showing the frequency of finding points on the Hirshfeld surface with particular values of d_e (distance to the nearest external atomic nucleus) and d_i (distance to the nearest internal atomic nucleus). Colors at each point on the plot range from cool (blue) to hot (red) as the frequency increases.

Two long spikes in Figure 2.6 denote the presence of important intermolecular C-H···O interactions, and the reddish area near $d_i \approx d_e \approx 1.9$ Å reflects the significant contribution made by π-stacking, although the distances are relatively long. In addition, the absence of points near $d_i \approx d_e \approx 1.2$ Å confirms that H···H interactions are of minor importance; similarly, the lack of points near $(d_i, d_e) \approx (1.7, 1.1)$ or $(d_i, d_e) \approx (1.1, 1.7)$ demonstrates that C-H···π interactions are not significant. Together, the Hirshfeld surface and fingerprint plot suggest that the conical topology of phosphangulene allows molecules to be stacked with a degree of efficiency, despite low mutual affinity arising from any specific interactions other than dipolar alignment.

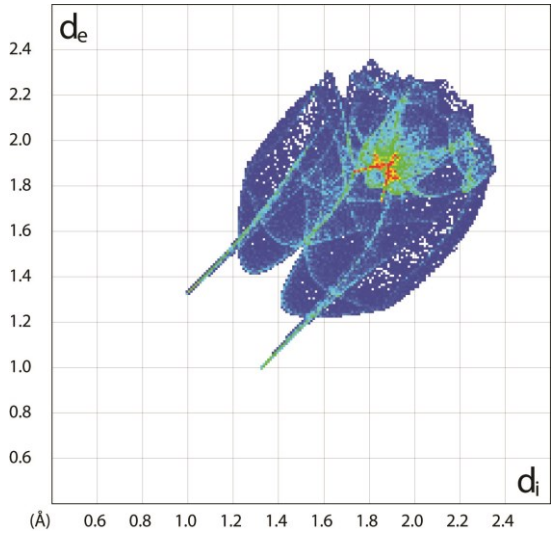

Figure 2.6 : Two-dimensional fingerprint plot of the Hirshfeld surface for molecules of phosphangulene in crystals grown from ethyl acetate. The plot shows the frequency of finding points on the surface with particular values of d_e and d_i (distances to the nearest external and internal atomic nuclei). The colors at each point range from cool (blue) to hot (red) as the frequency increases.

As noted by Yamamura and Nabeshima,[7] converting phosphangulene into the corresponding oxide, sulfide, and selenide (**2a–c**) makes the cone angle slightly less acute, possibly as a result of decreases in the s-character of the orbital of phosphorus involved in the P-chalcogenide bonds. In addition, forming the chalcogenides adds only one atom to phosphangulene but changes the topology markedly, creating awkwardly-shaped molecules that are no longer predisposed to stack. These intriguing early observations suggested to us that further analysis of phosphangulene, its chalcogenides, and related compounds offered a unique opportunity to explore what we have called the "dark side of crystal engineering," which focuses on what happens when normal patterns of crystallization are thwarted.[8–11] This approach has begun to yield materials with unusual properties, as well as deeper understanding of subtle factors controlling molecular organization. Previous studies of chalcogenides **2a–c** and analogues confirmed the intuitive expectation that their awkward shape prevents stacking, but other important questions have not been answered, such as what new patterns of organization emerge as alternatives to stacking or what the observed structures reveal about molecular crystallization in general. We have now found that analysis of structural options available to phosphangulene, its chalcogenides, and related compounds sheds light on enduring mysteries, including the origin of high levels of polymorphism, unusually large numbers of molecules in unit cells, and pronounced tendencies to form solvates, solid solutions, and cocrystals.

2.2.3 Results and Discussion

Syntheses of Phosphangulene and its Chalcogenides. Phosphangulene was synthesized by a modification of the method reported by Krebs and coworkers (Scheme 1).[1] Protection of 3-

fluorophenol (**3**) as its tetrahydropyranyl (THP) ether (**4**) was achieved efficiently in neat dihydropyran with pyridinium *p*-toluenesulfonate (PPTS) as the acidic catalyst. Metalation of THP ether **4** and subsequent reaction with PBr_3 afforded triarylphosphine **5**, as described by Krebs and coworkers,[1] and the protective group was then removed by acid-catalyzed methanolysis to give phosphine **6**. Krebs and coworkers reported preparing phosphangulene in 86% yield by heating intermediate **6** with KO-*t*-Bu in *N*-methylpyrrolidinone at 200 °C, but we obtained lower yields despite various attempts to use the reported method. Instead, we turned to an intramolecular Ullmann-type coupling of the type described by Zhang and coworkers.[12] Treatment of intermediate **6** with Cs_2CO_3 and CuI in DMF gave phosphangulene conveniently and reproducibly in 56% yield. Further experiments showed that CuI was necessary and that its use with other bases such as KO-*t*-Bu or K_2CO_3 gave lower yields. Chalcogenides **2a**–**c** were obtained in high yields from phosphangulene by modifications of published methods (Scheme 1).[1,7] Specifically, oxide **2a** was prepared by treatment with 30% aqueous hydrogen peroxide, sulfide **2b** by heating with elemental sulfur in xylene, and selenide **2c** by an analogous reaction with elemental selenium.

Scheme 1

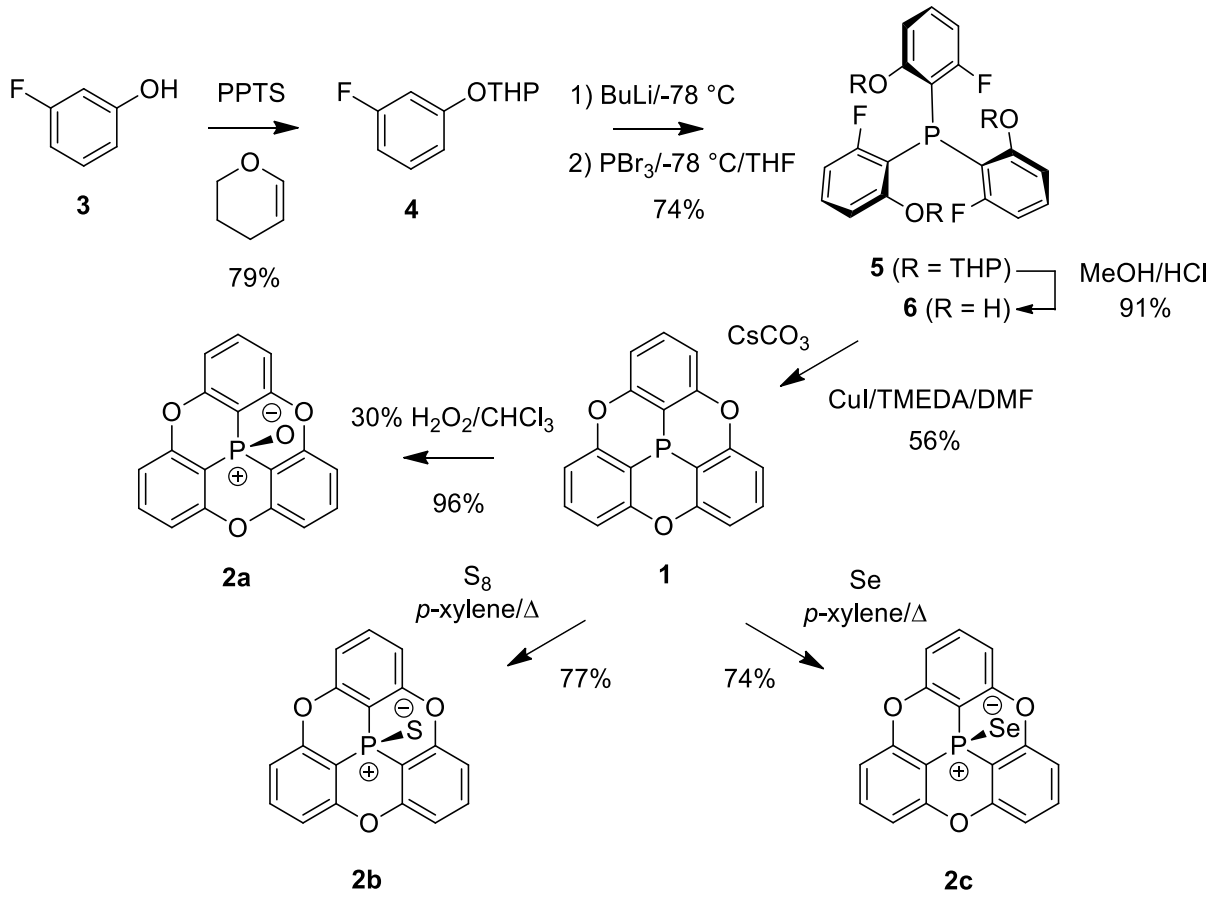

Polymorphs of Phosphangulene Oxide. The characteristic stacking of molecules of phosphangulene cannot be maintained in crystals of chalcogenides **2a**–**c**. The added *P*-chalcogen bonds alter the dipole moment of phosphangulene and create awkward molecular shapes that retain C_{3v} molecular symmetry but can no longer form efficiently packed conical stacks. Confirmation is provided by the earlier work of Krebs, Yamamura, and their coworkers, who reported the structure of crystals of phosphangulene oxide (**2a**) grown from ethyl acetate (polymorph A).[7,13] More thorough analysis has revealed four new polymorphs B–

E. The new polymorphs are described below, after a summary of the structure of known polymorph A to allow comparison.

Polymorph A of Oxide 2a. Crystals grown from ethyl acetate belong to the monoclinic space group $P2_1/n$, with $Z = 4$ and $Z' = 2$. The same structure is also produced by crystallization from anhydrous ethanol. Other crystallographic data are summarized in Table 2.1, and views of the structure are presented in Figures 2.7-2.9. Conical stacking is not observed; instead, the structure consists of pairs of symmetry-inequivalent molecules of oxide **2a** (Figure 2.7), held in an offset clamshell arrangement by multiple C-H···π interactions despite a locally unfavorable orientation of molecular dipoles. Adjacent pairs form C-H···O interactions involving atoms of oxygen bonded to phosphorus (2.505 Å in the illustrated pairs), as well as unusually short C···O contacts (2.987 Å) involving atoms of oxygen in the phosphangulene rings.

Table 2.1 : Crystallographic data for polymorphs A, B, C, D, and E of phosphangulene oxide (**2a**).

Polymorph	A[a]	B	C	D	E
crystallization medium	EtOAc	EtOH	EtOH	EtOH	EtOH
formula	$C_{18}H_9O_4P$	$C_{18}H_9O_4P$	$C_{18}H_9O_4P$	$C_{18}H_9O_4P$	$C_{18}H_9O_4P$
crystal system	monoclinic	monoclinic	orthorhombic	orthorhombic	monoclinic
space group	$P2_1/n$	$P2_1/c$	$Pbca$	$Pca2_1$	$P2_1$
a (Å)	10.0356(15)	28.5547(11)	12.0850(6)	11.6101(3)	9.9199(5)
b (Å)	25.043(4)	16.6794(6)	7.4412(4)	16.6814(5)	11.8932(5)
c (Å)	10.6453(16)	11.6200(4)	29.7220(16)	28.2286(8)	11.8950(6)
α (°)	90	90	90	90	90
β (°)	94.420(1)	98.990(1)	90	90	101.879(3)
γ (°)	90	90	90	90	90
V (Å^3)	2667.4(7)	5466.3(3)	2672.8(2)	5467.1(3)	1373.31(11)
Z	8	16	8	16	4
Z'	2	4	1	4	1
F(000)	1312	2624	1312	2624	656
T (K)	120	150	150	150	150
ρ_{calc} (g cm^{-3})	1.595	1.556	1.592	1.556	1.549
λ (Å)	0.71073	1.34139	1.34139	1.34139	1.34139
μ (mm^{-1})	0.226	1.282	1.307	1.279	1.272
measured reflections	30172	131053	21867	64961	25072
independent reflections	6042	12534	3063	11716	6277
R_{int}	0.0229	0.0351	0.0512	0.0399	0.0362
R_σ	0.0145	0.0133	0.0325	0.0294	0.0299
observed reflections	5812	12089	2650	10862	5983
R_1, $I > 2\sigma(I)$	0.0332	0.0417	0.0491	0.0475	0.0420
R_1, all data	0.0343	0.0426	0.0561	0.0519	0.0447
wR_2, $I > 2\sigma(I)$	0.0889	0.1078	0.1238	0.1217	0.1068
wR_2, all data	0.0904	0.1090	0.1310	0.1266	0.1099
GoF	1.033	1.055	1.088	1.026	1.025
Max/Min	0.434/-0.352	0.428/-0.497	0.563/-0.51	0.590/-0.391	1.190/-0.274
Flack parameter	N/A	N/A	N/A	0.006(17)	0.08(3)

[a]Data taken from the work of Krebs, Yamamura, and coworkers[7,13]

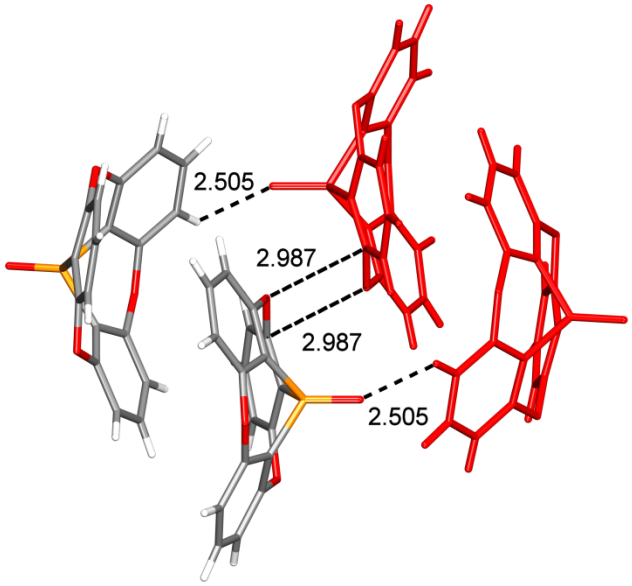

Figure 2.7 : Representation of the structure of crystals of phosphangulene oxide (**2a**) grown from ethyl acetate (polymorph A). Two molecules that interact to form an offset clamshell pair are highlighted in red, and a second pair is shown with atoms in normal colors. Selected C-H···O interactions and C···O contacts are marked by broken lines, with distances given in Å.

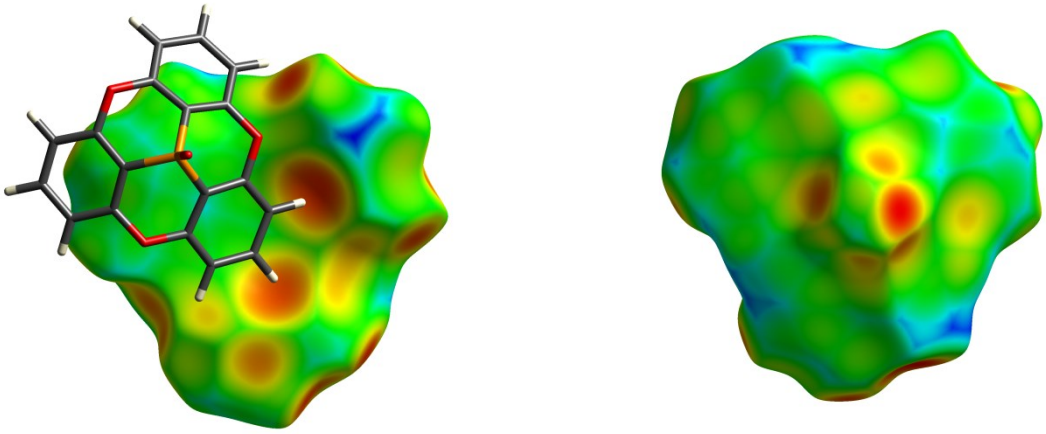

a **b**

Figure 2.8 : (a) Hirshfeld surface colored by d_e, showing an offset clamshell pair formed by two molecules of oxide **2a** in polymorph A. (b) Corresponding surface of one of the convex faces of the pair.

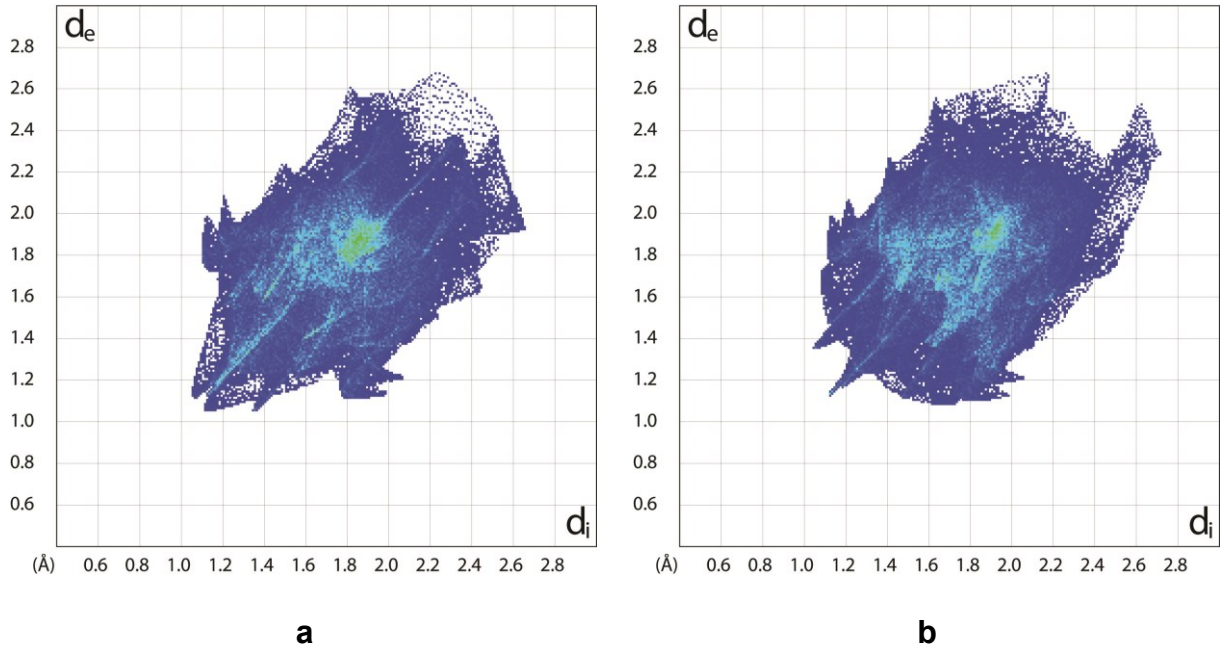

Figure 2.9 : Fingerprint plots of Hirshfeld surfaces for the two symmetry-inequivalent molecules of oxide **2a** in polymorph A.

Key features of the structure are highlighted by the Hirshfeld surfaces shown in Figure 2.8. In particular, conspicuous red spots on the concave surface (Figure 2.8a) arise from multiple C-H···π interactions, and red spots near the center of the convex surface reflect the formation of C-H···O interactions involving atoms of oxygen bonded to phosphorus (Figure 2.8b). The striking dissimilarity of the structures of phosphangulene and oxide **2a** is underscored by the fingerprint plots in Figure 2.9. The two symmetry-inequivalent molecules in the asymmetric unit of polymorph A engage in closely similar interactions, as demonstrated by the overall resemblance of Figures 2.9a and 2.9b. Features of particular interest that distinguish the plots

from that of phosphangulene (Figure 2.6) are (1) numerous H···H interactions, as indicated by the density of points near $d_i \approx d_e \approx 1.1$ Å, (2) significant wings near (d_i, d_e) ≈ (1.8, 1.1) and (d_i, d_e) ≈ (1.1, 1.8), which correspond to C-H···π interactions, and (3) the many large values of d_i and d_e observed in Figure 2.9, which extend to approximately 2.7 Å. In sharp contrast, the plot corresponding to phosphangulene is compact and bounded by $d_i \approx d_e \approx 2.3$ Å (Figure 2.6).

Together, the Hirshfeld surfaces and fingerprint plots suggest that oxide **2a** has no compelling reason to crystallize in any particular way, despite its relatively rigid and symmetric molecular structure. Instead, crystallization is forced to produce a structure with many sub-optimal interactions, and multiple molecules are used to create a unit cell with acceptable packing. The high frequency of large intermolecular separations in the fingerprint plots of Figure 2.9, as indicated by the density of points with coordinates exceeding 2.3 Å, reveals that the behavior of oxide **2a** resembles that of classic clathrate-forming compounds such as hydroquinone and Dianin's compound. Both enclose suitable guests but can also form guest-free *R*-3 crystals with significant unoccupied volume.[14,15] Fingerprint plots of the Hirshfeld surfaces of molecules in such structures are strikingly extended.

The markedly different packing of phosphangulene and its oxide can also be underscored by comparing voids in their structures, as assessed by using spheres of variable radius to probe accessible volumes lying between the van der Waals surfaces of the constituent molecules. For crystals of phosphangulene and polymorph A of oxide **2a**, the Kitaigorodsky packing coefficients are similar (0.689 and 0.705, respectively, at 293 K), but the structure of oxide **2a** incorporates much larger voids. For example, a probe sphere of radius 0.8 Å can occupy 6% of the volume of crystals of polymorph A but cannot be accommodated anywhere within the

structure of phosphangulene. Adding an atom of oxygen to phosphangulene interferes substantially with molecular packing, as expected, whereas such changes do not result routinely when triarylphosphines are converted into the corresponding oxides. For example, the structures of the triclinic $P\bar{1}$ polymorph of triphenylphosphine[16] and the orthorhombic *Pbca* form of its oxide[17] are related, as confirmed by comparing the fingerprint plots in Figure 2.10, which are bounded by similar values of d_i and d_e.

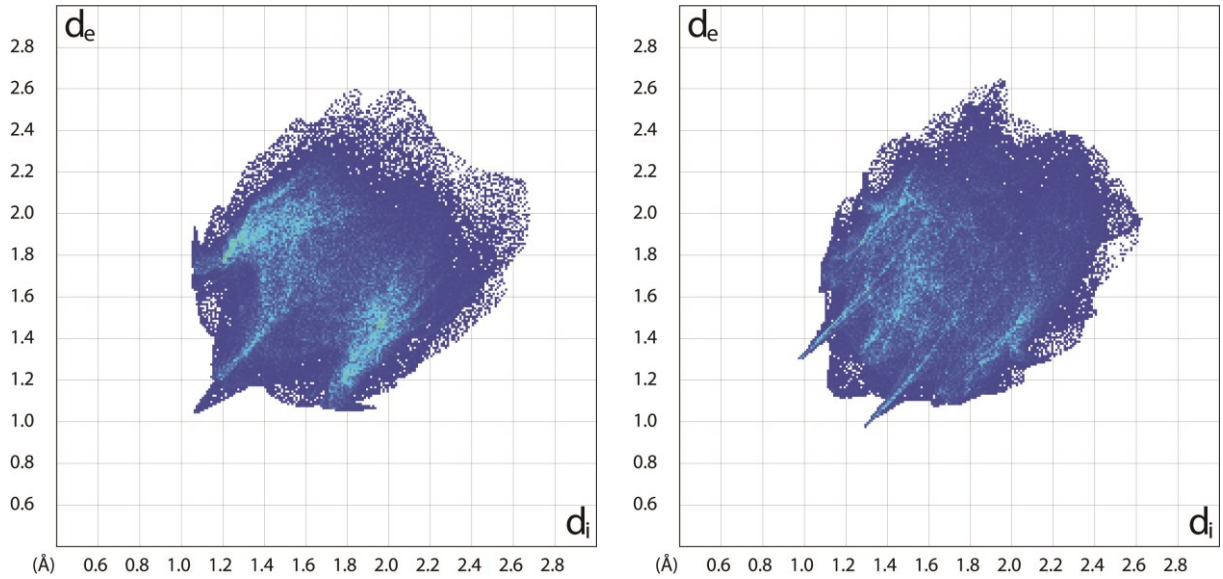

Figure 2.10 : (a) Representative fingerprint plot of the Hirshfeld surface of one of the four symmetry-inequivalent molecules of triphenylphosphine in the triclinic $P\bar{1}$ polymorph. (b) Fingerprint plot of the Hirshfeld surface of a molecule of triphenylphosphine oxide in the orthorhombic *Pbca* form.

Polymorph B of Oxide 2a. We observed that crystallizing phosphangulene oxide from anhydrous ethanol yielded crystals with different morphologies. Blocks proved to correspond to known polymorph A, whereas needles were shown to be new polymorph B, which

crystallized in the monoclinic space group $P2_1/c$ with $Z = 16$ and $Z' = 4$. Additional crystallographic data are provided in

Table 2.1 2.1, and representations of the structure are shown in Figures 2.11-2.12. Again, oxide **2a** forms offset clamshell pairs like those observed in polymorph A (Figure 2.11a). The resemblance of the pairs in the two polymorphs can be highlighted by superimposition (Figure 2.11b) and by comparison of the Hirshfeld surfaces (Figure 2.8a and Figure 2.12a). Conspicuous red spots on the concave surface of molecules in polymorph B reflect C-H···π interactions that help hold the pairs together, and the structure is also maintained by π-stacking, dipolar alignment, and various C-H···O interactions, including those with H···O distances as short as 2.329 Å (C-H···O-P) and 2.426 Å (C-H···O-C). Portraying structural details is complicated by the high value of *Z'*, and the representative view in Figure 2.11 highlights only the shortest C-H···O-P distance between adjacent inequivalent clamshell pairs of oxide **2a**.

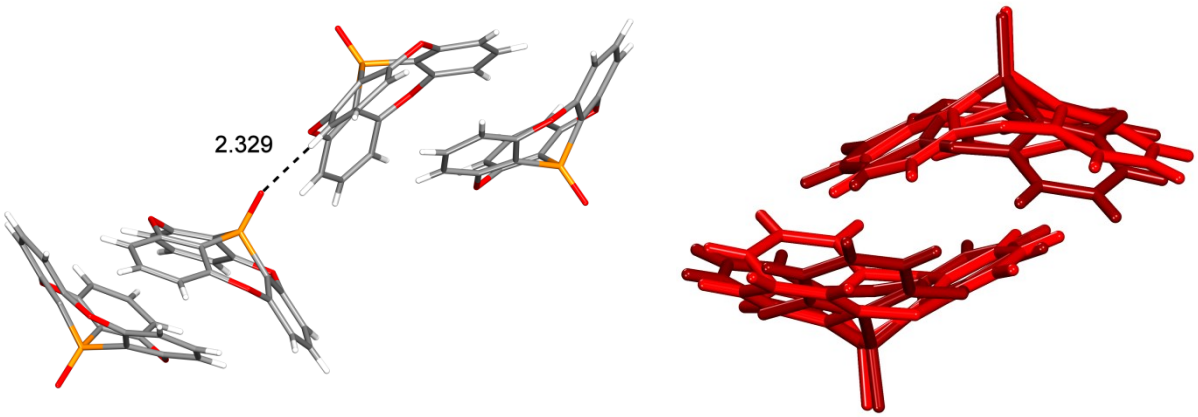

Figure 2.11 : (a) Representation of the structure of needle-shaped crystals of oxide 2a grown from anhydrous ethanol (polymorph B). Two adjacent inequivalent clamshell pairs are shown with atoms in normal colors. The shortest C-H···O interaction between pairs is marked by a

broken line, with the distance given in Å. (b) Superposition of representative clamshell pairs in the structures of polymorphs A and B, with different pairs shown in shades of red.

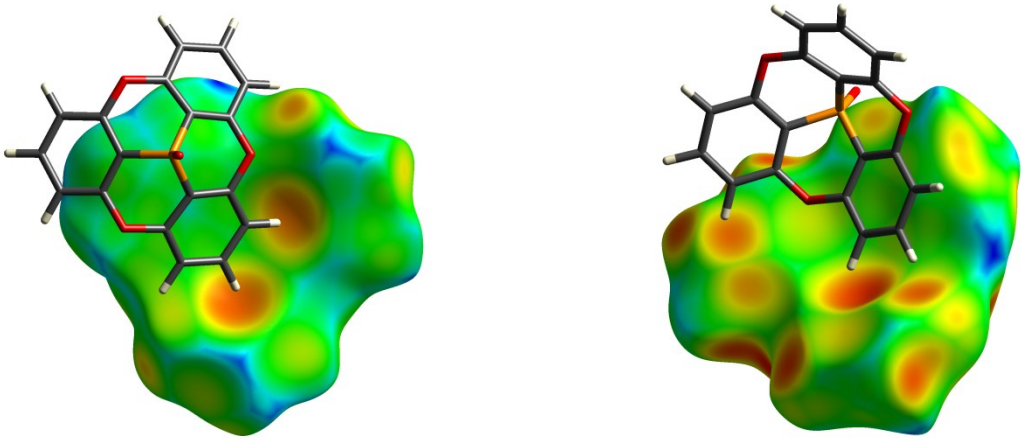

a **b**

Figure 2.12 : (a) Hirshfeld surface colored by d_e, showing a representative offset clamshell pair of molecules of oxide **2a** in polymorph B. (b) Corresponding surface of adjacent molecules of oxide **2a** in a slipped stack in polymorph C.

All four inequivalent molecules of oxide **2a** in the asymmetric unit of polymorph B have very similar environments, and the single fingerprint plot in Figure 2.13a is representative.[18] Moreover, the plot closely resembles those of molecules of oxide **2a** in polymorph A (Figure 2.9). In both polymorphs A and B, molecules of oxide **2a** produce similar fingerprints arising from H···H interactions (area near $d_i \approx d_e \approx 1.0$–$1.2$ Å), C-H···π interactions (small wings near $(d_i, d_e) \approx (1.8, 1.1)$ and $(d_i, d_e) \approx (1.1, 1.8)$), and distant π-stacking (light blue area centered on $d_i \approx d_e \approx 1.8$ Å). Of special note is the highly extended nature of all plots, which reach out to $d_i \approx d_e \approx 2.7$ Å. This supports the notion that the molecular structure of oxide **2a** prevents

efficient stacking and forces crystallization to occur in various alternative ways, none particularly favorable.

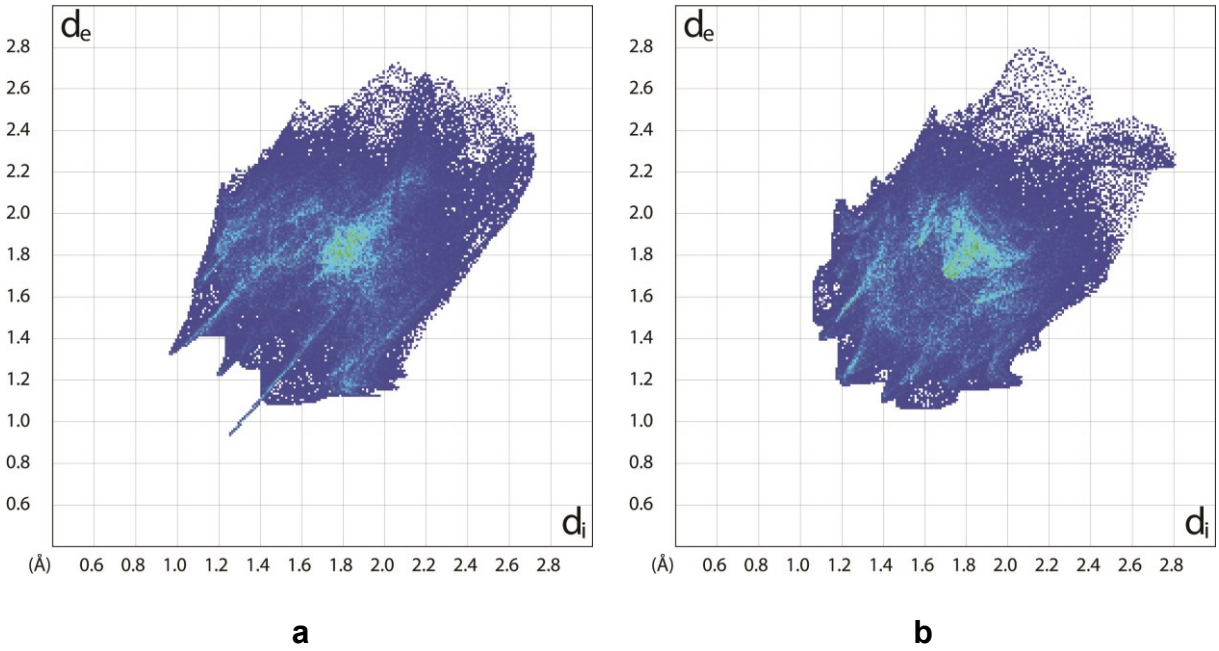

Figure 2.13 : (a) Representative fingerprint plot of the Hirshfeld surface corresponding to one of the four symmetry-inequivalent molecules of oxide **2a** in polymorph B. (b) Fingerprint plot for molecules of oxide **2a** in polymorph C.

Polymorph C of Oxide 2a. Further evidence for this idea is provided by the existence of polymorph C, which is produced concomitantly with polymorphs A and B during crystallization from anhydrous ethanol.[19] Crystals of polymorph C proved to belong to the orthorhombic space group *Pbca* with $Z = 8$ and $Z' = 1$.

Table 2**.1** summarizes additional crystallographic data, and Figure 2.14 provides a view of the structure, which can be considered to consist of slipped stacks of molecules of oxide **2a** with their dipoles aligned approximately along the *b*-axis. Each stack is surrounded by six others, which are oriented so that there is no net dipole along the *b*-axis.

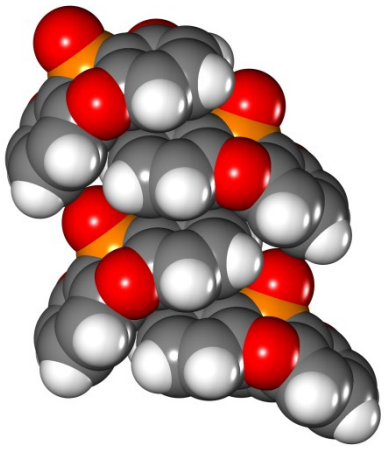

Figure 2.14 : Space-filling representation of part of a slipped stack observed in the structure of polymorph C of oxide **2a**. Atoms are shown in normal colors.

The Hirshfeld surface (Figure 2.12b) shows two adjacent molecules in a slipped stack and demonstrates the presence of multiple C-H···π interactions. The close similarity of the fingerprint plot (Figure 2.13b) to those of molecules in polymorphs A and B confirms the notion that oxide **2a** cannot be packed efficiently in ways that create optimal interactions. In particular, H···H and C-H···π distances are long, and π-stacking is weak, as shown by reddish areas in the fingerprint plot near $d_i \approx d_e \approx 1.8$ Å. In addition, the plot is notably extended and reveals a high frequency of coordinates with large values of d_i or d_e ranging up to 2.8 Å. The

inability of oxide **2a** to crystallize in ways that allow its constituent atoms to engage in normal intermolecular interactions leads to the formation of multiple unappealing polymorphs with nearly equal stabilities, as demonstrated by the concomitant crystallization of forms A, B, and C.

Polymorph D of Oxide 2a. Additional polymorph D was produced when oxide **2a** was crystallized from anhydrous ethanol or from thiophene. Crystals of polymorph D were found to belong to the orthorhombic space group $Pca2_1$ with $Z = 16$ and $Z' = 4$. Other crystallographic data are summarized in Table 2.1, and representations of the structure are provided in Figures 2.15a and 2.16a. Again, the structure consists of offset clamshell pairs similar to those observed in polymorphs A and B (Figure 2.15a), and fingerprint plots reveal a high frequency of large intermolecular distances (Figure 2.16a).

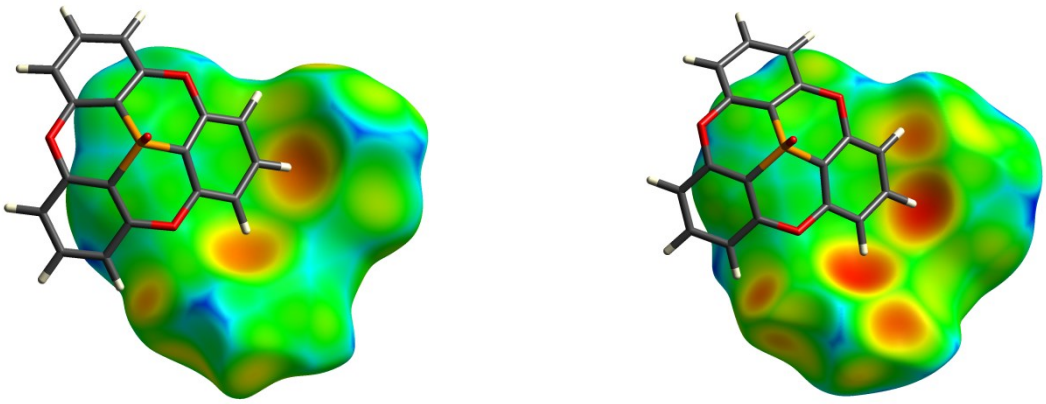

a **b**

Figure 2.15 : (a) Hirshfeld surface colored by d_e, showing a representative offset clamshell pair formed by two molecules of oxide **2a** in polymorph D. (b) Corresponding surface of an offset clamshell pair in polymorph E of oxide **2a**.

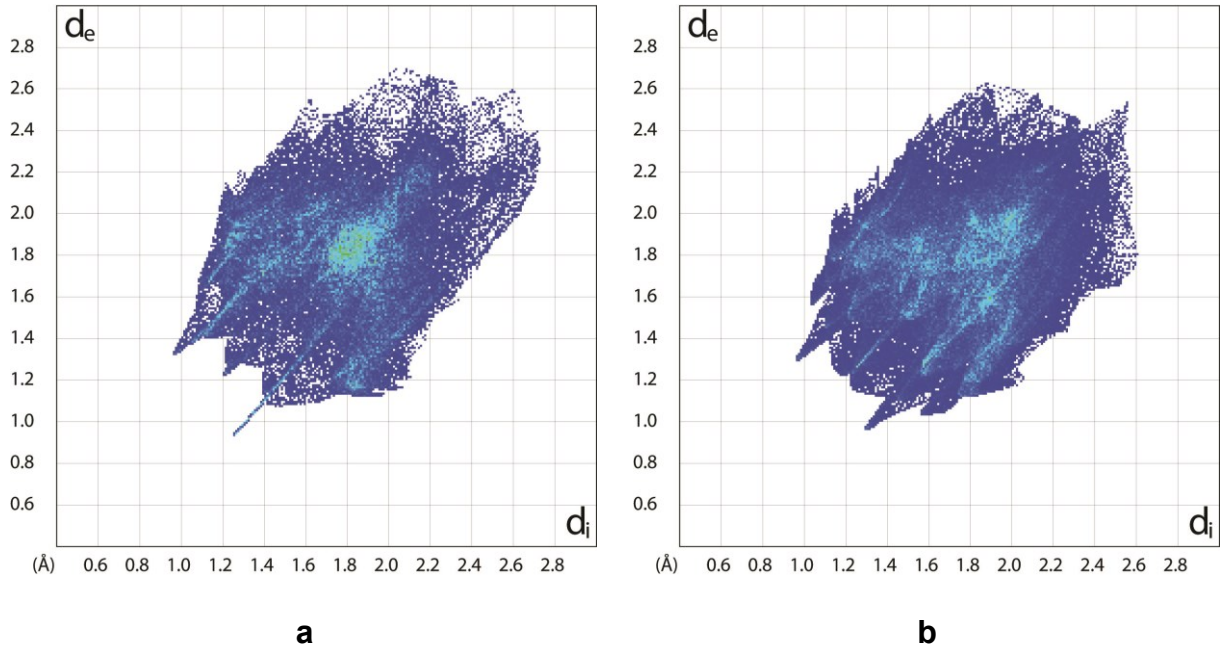

Figure 2.16 : (a) Representative fingerprint plot of the Hirshfeld surface for one of the four symmetry-inequivalent molecules of oxide **2a** in polymorph D. (b) Fingerprint plot for molecules of oxide **2a** in polymorph E.

Polymorph E of Oxide 2a. A fifth form (polymorph E) resulted when oxide **2a** was crystallized from anhydrous ethanol or from CS_2. Crystals of polymorph E proved to belong to the monoclinic space group $P2_1$ with $Z = 4$ and $Z' = 1$.

Table 2**.1** includes additional crystallographic data, and Figures 2.15b and 2.16b provide representations of the structure, which show the presence of offset clamshell pairs like those present in polymorphs A, B, and D (Figure 2.15b), as well as a similarly high frequency of abnormally long intermolecular separations (Figure 2.16b).

No polymorph of oxide **2a** adopts efficient conical stacking of the type observed in crystals of phosphangulene **1** itself. This underscores the disruptive effect of introducing a well-placed atom of oxygen. Adding oxygen also alters the dipole moment and gives rise to new C-H···O-P interactions in all five polymorphs. The repeated observation of high values of Z' and Z (8, 16, 8, 16, and 4 in polymorphs A, B, C, D, and E, respectively) reinforces the hypothesis that the inherently awkward shape of oxide **2a** prevents crystallization from yielding structures in which the constituent atoms have normal intermolecular interactions. This favors the formation of multiple polymorphs that are similar in energy and must use multiple inequivalent molecules to ensure satisfactory packing.[20–22] In essence, oxide **2a** is condemned to crystallize in ways that reflect unsatisfactory compromises: in particular, the conical aromatic surface cannot be packed efficiently in the manner of phosphangulene, nor can it engage fully in H···H, C-H···π, and π···π interactions of the type that stabilize stacks and herringbone arrangements of planar aromatic analogues.

As shown in Figure 2.17, various intermolecular interactions make similar contributions to the Hirshfeld surfaces of all of the polymorphs of oxide **2a**, whereas the contributions differ widely from those observed in the structure of phosphangulene **1**. The crystallographic parameters in Table 2.1, along with other observations such as the formation of all five polymorphs A–E during crystallization from anhydrous ethanol,[19] do not provide definitive

evidence for placing the polymorphs in any particular order of thermodynamic stability. However, the low densities, high values of *Z*, and relatively low Kitaigorodsky packing coefficients (0.704–0.707 at 150 K) found for polymorphs B, D, and E suggest that they are the least stable. Moreover, we observed the transformation of polymorph B into polymorphs A and C during extended exposure to anhydrous ethanol. Concomitant crystallizations and polymorphic interconversions prevented us from obtaining pure samples for more detailed analysis by differential scanning calorimetry. In principle, computational approaches can be used to estimate lattice energies and to compare the stabilities of polymorphs; however, current methods cannot be expected to provide reliable guidance in the case of forms A–E of oxide **2a**, which have high values of *Z*/*Z*' and closely similar energies, as demonstrated by their coexistence under equilibrating conditions.[23]

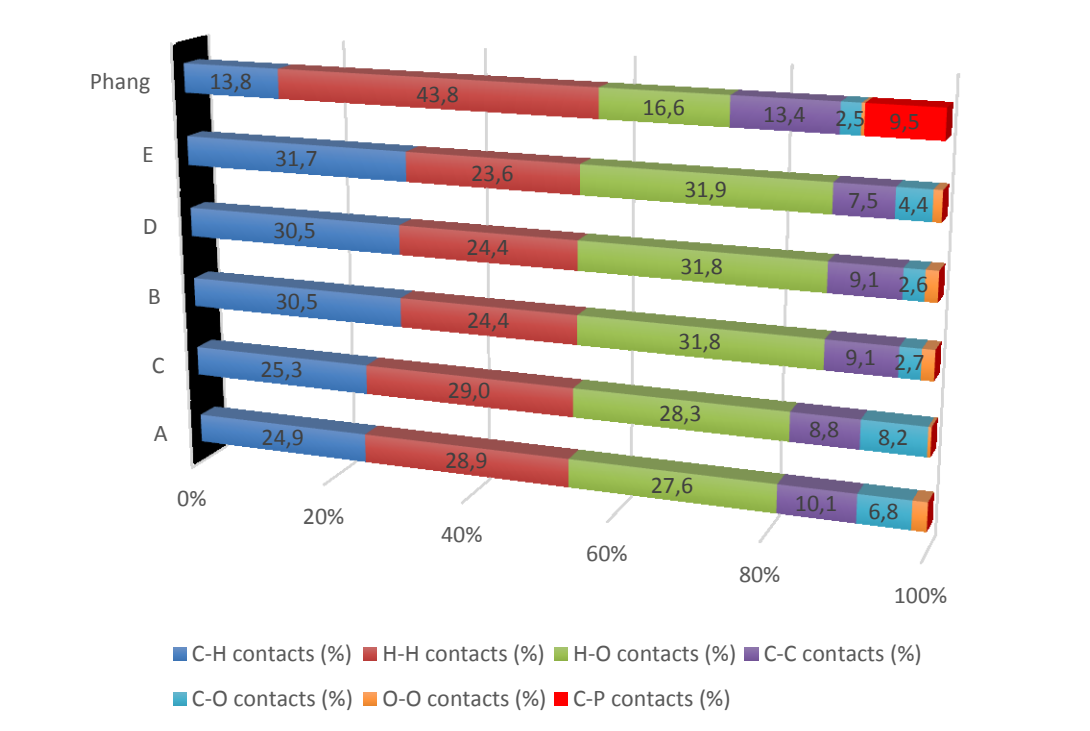

Figure 2.17 : Percentage contributions made by various intermolecular interactions to the Hirshfeld surfaces of representative molecules in the structures of phosphangulene and oxide **2a** (polymorphs A–E). Phosphangulene is shown as Phang, and polymorphs A–E appear in order of the importance of C-H interactions.

Only one polymorph of phosphangulene has been reported, and earlier workers noted a single form of oxide **2a**. In this context, we were surprised to observe four new polymorphs, without making any systematic effort to find others. Oxide **2a** is less highly polymorphic than the intensively studied compound 5-methyl-2-[(2-nitrophenyl)amino]-3-thiophenecarbonitrile (ROY), which exists in 10 fully characterized forms and remains one of the most highly polymorphic substances in the Cambridge Structural Database (CSD).[24–27] Unlike ROY, however, oxide **2a** is a hexacyclic molecule with a well-defined shape, so its rich polymorphic diversity does not arise from an ability to adopt multiple conformations. The CSD now includes more than one million entries, but recent analyses have identified only 13 compounds that are known to exist in more than four fully characterized polymorphic forms.[26] Nearly all of these special molecules are flexible and crystallize as different conformers. Oxide **2a** is among the rare examples that are both highly polymorphic and virtually inflexible. As a result, oxide **2a** and its analogues allow the origin of polymorphism to be probed in the absence of other contributing factors. Our observations suggest that the awkward topology of these compounds makes efficient stacking impossible and forces crystallization to occur in ways that lead to many sub-optimal intermolecular contacts, thereby expanding the scope for producing polymorphic forms with similar energies. It is also possible that the conical topology and polarity of oxide **2a** inhibit displacements and reorientations needed to convert metastable arrangements into forms of lower energy.

Previous statistical analyses of the CSD have led to assertions that molecular flexibility and the incidence of polymorphism are not correlated.[28–30] Nevertheless, the quest to identify general structural features favoring polymorphism and high values of Z/Z' remains an active area of study. If predisposing features exist and can be identified, their discovery would have a significant practical impact by expanding the range of different ordered materials that can be derived from a single molecular entity. However, the notion that compounds with multiple polymorphic forms or high values of Z/Z' are exceptional and may have underlying shared features is not universally accepted. Dissenting opinions include those of McCrone, who famously stated "…that every compound has different polymorphic forms and that, in general, the number of forms known for a given compound is proportional to the time and energy spent in research on that compound."[31] In addition, Gavezzotti has suggested that each case of elevated values of Z' "…may be a story in itself."[32]

Much of what is believed to be true about high levels of polymorphism and large values of Z/Z' reflects purely statistical analyses of the CSD or smaller sets of data, often related to drugs and intermediates used in their synthesis, which do not represent the full scope of molecular diversity. In contrast, surprisingly little effort has been devoted to close comparative scrutiny of the structures of highly polymorphic substances or to experimental studies of compounds specifically devised to test conjectures about the origins of polymorphism and high values of Z/Z'. Of the 13 compounds recently highlighted because they are known to exist in more than four polymorphic forms,[26] only the 4-chloro-1,2,3,5-dithiadiazolyl radical (**7a**)[33,34] and 1,8-dihydroxyanthraquinone (**8**)[35,36] resemble oxide **2a** by existing primarily in a single conformation.

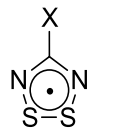

7a (X = Cl)
7b (X = F)
7c (X = Br)

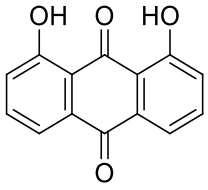

8

This places compounds **2a**, **7a**, and **8** in an intriguing subset of elite highly polymorphic compounds and challenges chemists to identify specific structural features that explain their special behavior. The polymorphic diversity of radical **7a** presumably arises in part from its strong self-association, which creates isomeric dimers that resemble distinct covalently-bonded species and therefore crystallize differently. Notably, however, the behavior of radical **7a** does not extend to close analogues such as fluoride **7b** and bromide **7c**, which have not yielded multiple polymorphs despite efforts to make them.[33] As a result, the example of radical **7a** is "a story in itself" that does not tell how to design any other highly polymorphic compounds, even those with a close structural relationship.

1,8-Dihydroxyanthraquinone (**8**) is a natural product derived from glycosides that have long been used as laxatives. Its high polymorphism has complex origins, including the ability to engage in multiple intermolecular O-H···O hydrogen-bonding motifs. However, none of the observed structures exhibits any clear signs of inefficient packing. In particular, the values of Z' are generally small (1, 2, 4, 1, and 0.5 for the five known polymorphs), and the fingerprint plots are compact, with a low frequency of abnormally long distances to atoms in neighboring molecules (beyond $d_i \approx d_e \approx 2.4$ Å). As in the case of radical **7a,** the behavior of anthraquinone **8** does not point unerringly to any other compounds that would also be expected to be highly

polymorphic. The examples of compounds **7a** and **8** thereby provide grounds for the gloomy conjecture that "polymorphism is unpredictable on the basis of molecular structure."[30]

Phosphangulene chalcogenides **2a**–**c** have let us put this notion to a stringent experimental test. The special features that appear to induce oxide **2a** to form multiple polymorphs with high values of *Z*/*Z*' remain essentially unchanged in analogues **2b**–**c**; in particular, the retained awkward topology is expected to continue to prevent crystallization from occurring in fully satisfactory ways. If polymorphism is in fact unpredictable, however, then sulfide **2b** and selenide **2c** should not necessarily behave like oxide **2a**.

Polymorphs of Phosphangulene Sulfide. Yamamura and Nabeshima previously solved the structure of crystals of sulfide **2b** grown from CH_2Cl_2/hexane, which will be referred to as polymorph A.[7] By crystallizing sulfide **2b** from anhydrous ethanol, we obtained new polymorph B. Its structure is described below, after a brief analysis of known polymorph A to allow comparison.

Polymorph A of Sulfide 2b. Crystals of known form A belong to the monoclinic space group $P2_1/c$ with Z = 8 and *Z*' = 2. Additional crystallographic data are provided in Table 2.2, and representative views of the structure are shown in Figure 2.18 and Figure 2**.19**a. Conical stacking is prevented, as expected, and molecules form offset clamshell pairs like those present in multiple polymorphs of oxide **2a** (Figure 2.18). This observation suggests that pairing is a fundamental preference of all phosphangulene chalcogenides, not a phenomenon resulting uniquely from C-H···O-P interactions in oxide **2a**. The Hirshfeld surface of paired molecules of sulfide **2b** (Figure 2.19a) closely resembles the corresponding surfaces of various

polymorphs of oxide **2a** and shows that the pairs are again joined by multiple C-H···π interactions. The fingerprint plot in Figure 2.20a demonstrates that the structure of polymorph A of sulfide **2b** is maintained by various interactions, including π-stacking, C-H···π interactions, C-H···O interactions, and C-H···S interactions. As in the case of polymorphs A–E of oxide **2a**, the fingerprint plot is notably extended and shows a high frequency of coordinates with values of d_i or d_e as large as 2.8 Å. The plot thereby confirms that sulfide **2b**, like oxide **2a**, is forced by topology to pack in ways that poorly exploit the potential of the constituent atoms to engage in stabilizing intermolecular contacts. As a result, small changes in structural parameters can be accommodated without incurring significant energetic penalties, and the range of accessible polymorphs is broadened.

Table 2.2 : Crystallographic data for polymorphs A and B of phosphangulene sulfide (**2b**) and for polymorphs A, B, and C of phosphangulene selenide (**2c**).

Compound	Sulfide **2b** Polymorph A[a]	Sulfide **2b** Polymorph B	Selenide **2c** Polymorph A[a]	Selenide **2c** Polymorph B	Selenide **2c** Polymorph C
crystallization medium	CH_2Cl_2 / hexane	EtOH	$CHCl_3$/ hexane	CS_2	CS_2
crystal system	monoclinic	orthorhombic	orthorhombic	monoclinic	monoclinic
space group	$P2_1/c$	*Pbca*	*Pbca*	$P2_1/c$	$I2/a$
a (Å)	15.112(5)	14.7446(3)	12.9896(19)	15.0217(6)	14.1307(8)
b (Å)	13.276(4)	13.0971(3)	15.120(2)	13.5252(5)	6.9551(4)
c (Å)	14.291(5)	14.9443(3)	14.872(2)	14.4528(5)	29.079(2)
α (°)	90	90	90	90	90
β (°)	93.096 (3)	90	90	93.393(2)	90.359(2)
γ (°)	90	90	90	90	90
V (Å³)	2863.1(16)	2885.92(11)	2920.8(8)	2931.25(19)	2857.9(3)
Z	8	8	8	8	8
Z'	2	1	1	2	1
F(000)	1376	1376	1520	1520	1520
T (K)	120	105	120	150	150
ρ_{calc} (g cm^{-3})	1.560	1.548	1.743	1.737	1.781
λ (Å)	0.71073	1.34139	0.71073	1.34139	1.34139
μ (mm^{-1})	0.350	2.049	2.692	3.046	3.124
measured reflections	32254	30130	15435	78953	52256
independent reflections	6592	3574	3339	6425	3240
R_{int}	0.0425	0.0274	0.0301	0.0536	0.0464
R_σ	0.0345	0.0154	0.0216	0.0232	0.0183
observed reflections	5294	3406	2877	5234	3158
R_1, I > 2σ(I)	0.0336	0.0294	0.0512	0.0320	0.0632
R_1, all data	0.0521	0.0306	0.0563	0.0456	0.0647
wR_2, I > 2σ(I)	0.0863	0.0847	0.1339	0.0745	0.1756
wR_2, all data	0.0934	0.0857	0.1409	0.0825	0.1775
GoF	1.034	1.051	1.059	1.056	1.054
Max/Min	0.474/-0.348	0.456/-0.222	2.369/-0.494	0.397/-0.564	3.205/-1.56

[a]Data taken from the work of Yamamura and Nabeshima[7]

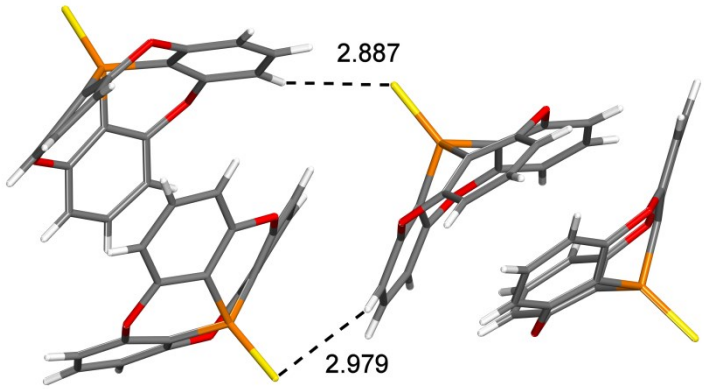

Figure 2.18 : Representation of the structure of crystals of sulfide **2b** (polymorph A). Two adjacent offset clamshell pairs of molecules are illustrated with atoms of carbon in gray, hydrogen in white, oxygen in red, phosphorus in orange, and sulfur in yellow. C-H···S interactions are marked by broken lines, with the distances given in Å.

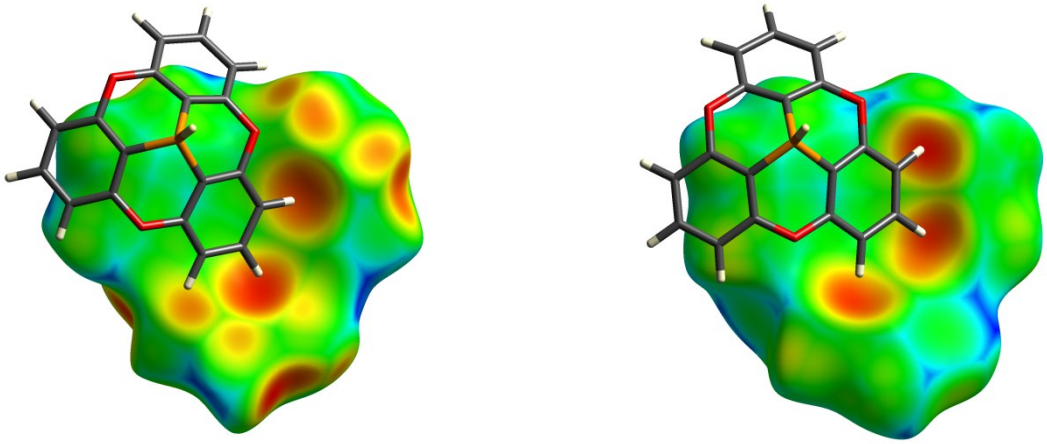

Figure 2.19 : (a) Hirshfeld surface colored by d_e, showing a representative offset clamshell pair formed by two molecules of sulfide **2b** in polymorph A. (b) Corresponding surface of an offset clamshell pair in polymorph B of sulfide **2b**.

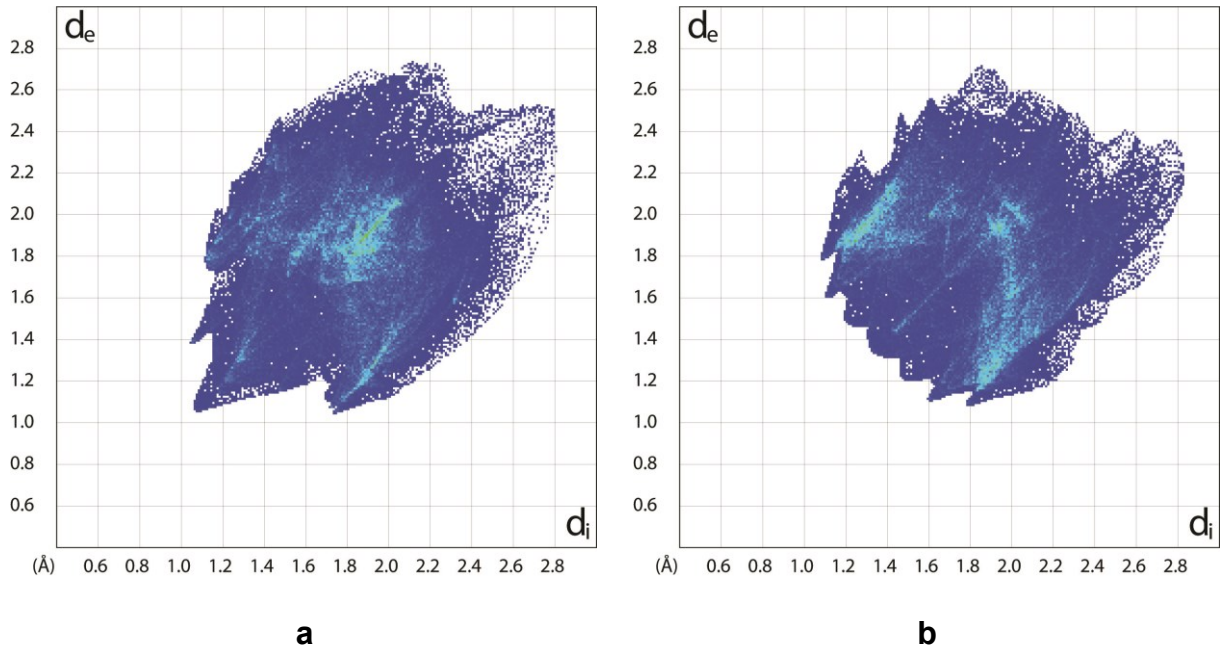

Figure 2.20 : (a) Representative fingerprint plot of the Hirshfeld surface for one of the two symmetry-inequivalent molecules of sulfide **2b** in polymorph A. (b) Fingerprint plot for molecules of sulfide **2b** in polymorph B.

Polymorph B of Sulfide 2b. Crystallization of sulfide **2b** from anhydrous ethanol yielded a new form, polymorph B. The crystals were found to belong to the orthorhombic space group *Pbca* with Z = 8 and Z' = 1, and other crystallographic data are summarized in Table 2.2. The Hirshfeld surface in Figure 2.19b confirms that polymorph B incorporates offset clamshell pairs joined by multiple C-H···π interactions, as found in polymorph A of sulfide **2b** and in polymorphs A, B, D, and E of oxide **2a**. Unlike polymorph A of sulfide **2b**, however, polymorph B does not have any C-H···O or C-H···S contacts shorter than the sum of the van der Waals radii. The fingerprint plot (Figure 2.20b) reveals that intermolecular separations in polymorph B are unusually large; in particular, there are no points on the Hirshfeld surface

with values of d_i or d_e less than 1.3 Å. Polymorph A is denser than polymorph B and therefore appears to be more stable.

Polymorphs of Phosphangulene Selenide. With the polymorphism of sulfide **2b** established, we did not search systematically for other forms, but instead examined the crystallization of selenide **2c**. We were confident that the coherent behavior of oxide **2a** and sulfide **2b**, including their polymorphism, formation of crystals with large values of *Z*/*Z*', and abnormally high frequencies of long intermolecular distances, reflected basic principles of molecular design and organization that would also govern the properties of selenide **2c**. In previous work, Yamamura and Nabeshima reported the structure of crystals of selenide **2c** grown from $CHCl_3$/hexane, which will be referred to as polymorph A.[7] We have found that new polymorphs result when selenide **2c** is crystallized under other conditions. Their structures are described below, following an analysis of known polymorph A to allow comparison.

Polymorph A of Selenide 2c. Crystals of selenide **2c** grown from $CHCl_3$/hexane belong to the orthorhombic space group *Pbca* with Z = 8 and Z' = 1. Table 2.2 summarizes additional crystallographic data, and Figure 2.21a provides a representative view of the structure. Polymorph A of selenide **2c** and polymorph B of sulfide **2b** are isostructural. Conical stacking is obstructed, as expected, and molecules of selenide **2c** form offset clamshell pairs like those produced by oxide **2a** and sulfide **2b**. Molecular association in the structure is governed primarily by C-H···π and C-H···O interactions, as shown by the Hirshfeld surface of paired molecules in Figure 2.22a. Again, the fingerprint plot is abnormally extended, with values of d_i or d_e reaching out beyond 2.7 Å.

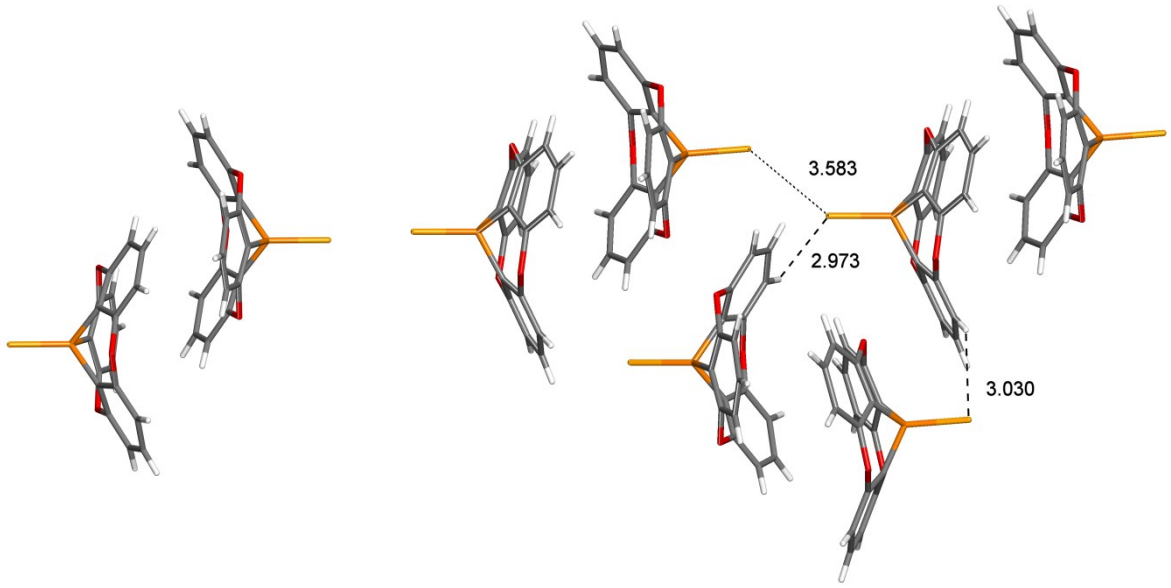

Figure 2.21 : Representations of the structures of crystals of selenide **2c** grown from $CHCl_3$/hexane (polymorph A) and from CS_2 (polymorph B). (a) Offset clamshell pair observed in polymorph A. (b) Three adjacent offset clamshell pairs in polymorph B. Both images show atoms of carbon in gray, hydrogen in white, oxygen in red, phosphorus in orange, and selenium in yellow. Selected C-H···Se and Se···Se interactions are marked by broken lines, with the distances given in Å.

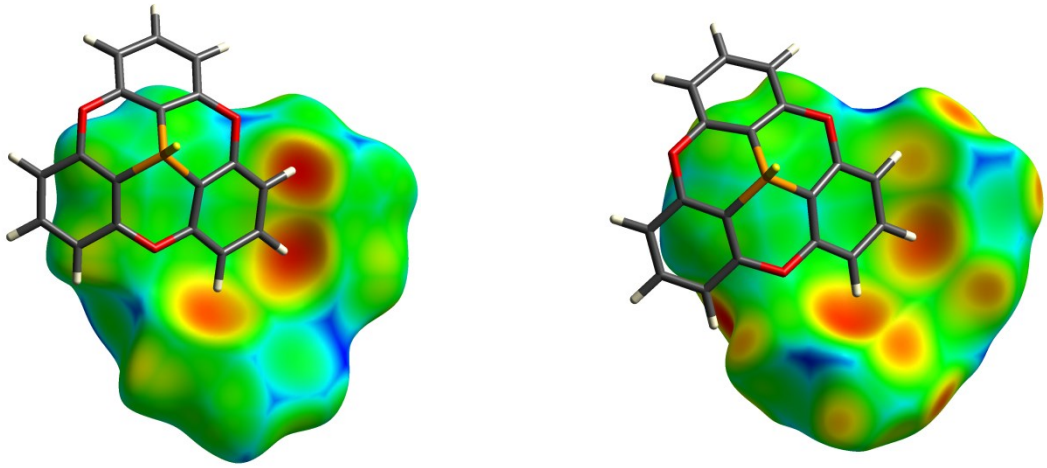

a **b**

Figure 2.22 : (a) Hirshfeld surface colored by d_e, showing an offset clamshell pair formed by molecules of selenide **2c** in polymorph A. (b) Corresponding surface of a representative offset clamshell pair in polymorph B of selenide **2c**.

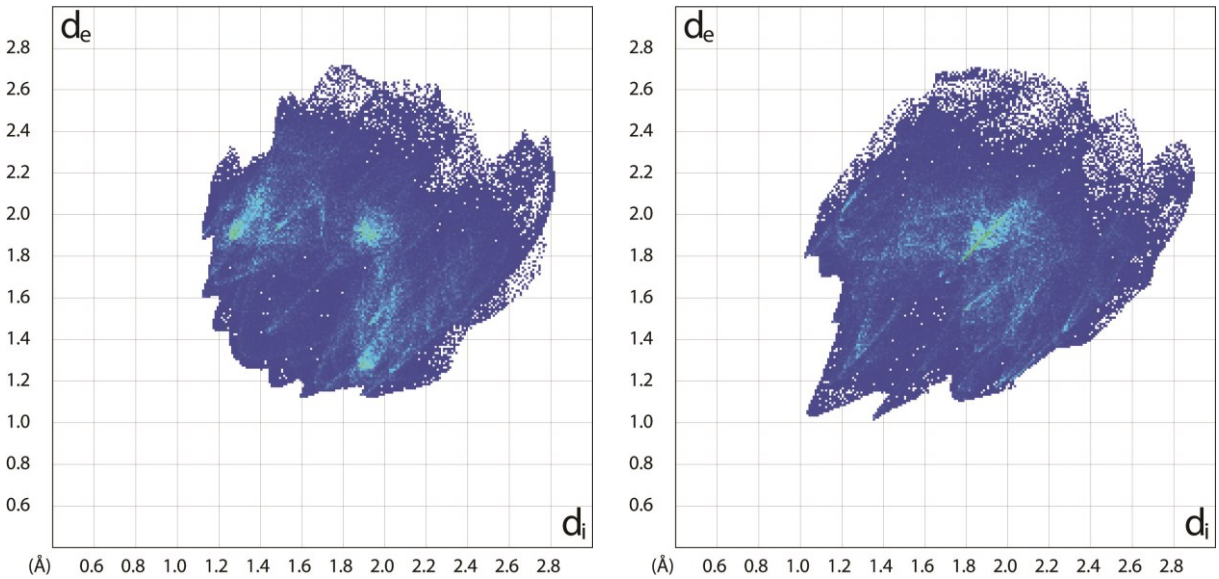

a **b**

Figure 2.23 : (a) Representative fingerprint plot of the Hirshfeld surface for one of the two symmetry-inequivalent molecules of selenide **2c** in polymorph A. (b) Fingerprint plot for molecules of selenide **2c** in polymorph B.

Polymorph B of Selenide 2c. New polymorphs B and C were obtained concomitantly by crystallizing selenide **2c** from CS_2. Crystals of form B proved to belong to the monoclinic space group $P2_1/c$ with Z = 8 and Z' = 2. Table 2.2 summarizes additional crystallographic data, and Figure 2.21b shows that the structure is composed of offset clamshell pairs like those formed by polymorph A of selenide **2c** and by various polymorphs of oxide **2a** and sulfide **2b**. Form B of selenide **2c** and form A of sulfide **2b** are isostructural. The Hirshfeld surface corresponding to form B of selenide **2c** confirms that the pairs are held together by multiple C-H···π interactions (Figure 2.22b). Other contacts shorter than the sum of the van der Waals radii include C-H···Se interactions (2.973 and 3.030 Å) and Se···Se interactions (3.583 Å), as illustrated in Figure 2.21b. The fingerprint plot (Figure 2.23b) is even more extended than that of polymorph A of selenide **2c**, and values of d_i reach 2.9 Å.

Polymorph C of Selenide 2c. Crystals of concomitant polymorph C were found to belong to the monoclinic space group $I2/a$ with Z = 8 and Z' = 1. Other crystallographic details appear in Table 2.2, and a view of the structure is provided in Figure 2.24. The structure is devoid of noteworthy interactions, and it can be considered to be composed of adjacent columns in which widely separated molecules (6.955 Å) are stacked with their P-Se bonds aligned approximately with the *b*-axis. The convex and concave faces of the Hirshfeld surface (Figure 2.25) indicate that the structure is maintained in part by C-H···π interactions between columns, and the corresponding fingerprint plot extends to large values of d_i and d_e.

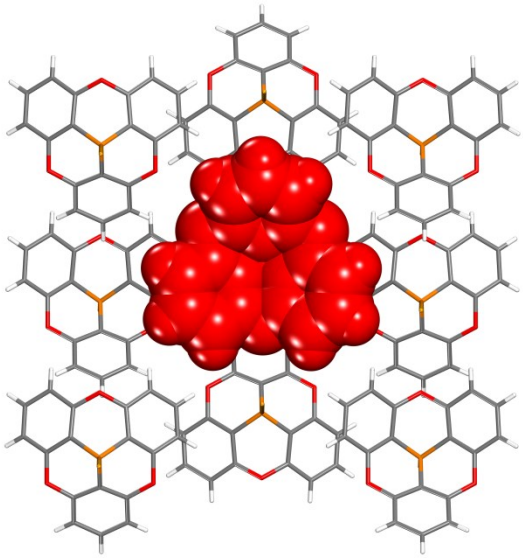

Figure 2.24 : Representation of the structure of crystals of selenide **2c** (polymorph C). View along the *b*-axis, showing how a central column of widely separated molecules (in red) is surrounded by eight other loose stacks. Unless otherwise indicated, atoms are shown in normal colors.

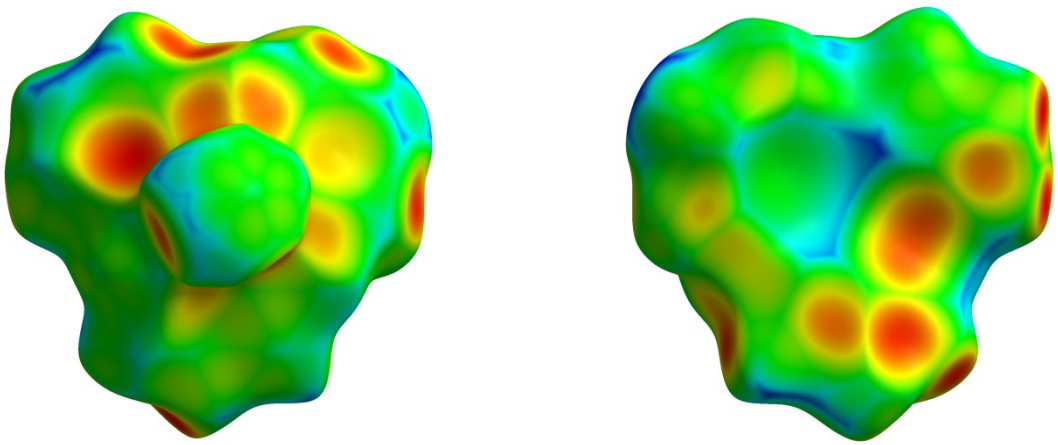

Figure 2.25 : (a) Hirshfeld surface colored by d_e, showing the convex face of a molecule of selenide **2c** in polymorph C. (b) Corresponding concave face.

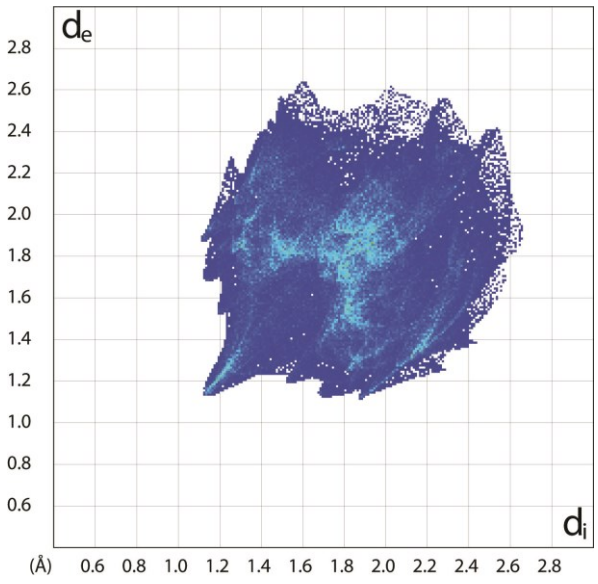

Figure 2.26 : Fingerprint plot for molecules of selenide **2c** in polymorph C.

The inability to form stacks like those favored by phosphangulene forces chalcogenides **2a**–**c** to accept unattractive alternatives, particularly structures built from offset clamshell pairs held together by multiple C-H···π interactions. Figure 2.27 shows the superimposition of six representative pairs that are present in the structures of oxide **2a** (polymorphs A and B), sulfide **2b** (polymorphs A and B), and selenide **2c** (polymorphs A and B). The figure confirms that similar association is conserved throughout the series, but the structural details vary substantially. This suggests that chalcogenides **2a**–**c** are highly polymorphic partly because they can form a multitude of pairs that have slightly differing geometries, closely similar energies, and numerous ways to pack in crystal lattices.

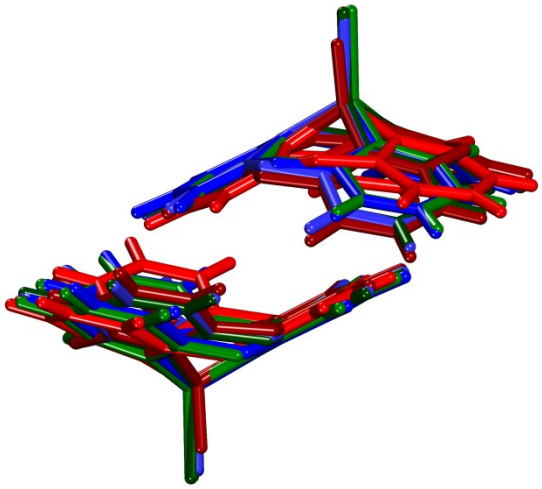

Figure 2.27 : Superimposition of six representative offset clamshell pairs present in the structures of oxide **2a** (polymorphs A and B in red and dark red), sulfide **2b** (polymorphs A and B in blue and dark blue), and selenide **2c** (polymorphs A and B in green and dark green).

Ability of Phosphangulene Chalcogenides 2a–c to Form Crystalline Solid Solutions, Pseudopolymorphs, and Cocrystals. The distinctive shape of chalcogenides **2a–c** prevents efficient packing and forces crystallization to occur in ways that are significantly flawed, with high frequencies of long intermolecular contacts. Polymorphism is thereby favored, and multiple molecules are needed to construct unit cells with acceptable packing. We reasoned that if chalcogenides **2a–c** cannot in fact crystallize in fully satisfactory ways, then they should be disposed to form structures that accommodate other molecules.

To test this notion, we crystallized equimolar mixtures of phosphangulene and oxide **2a** from ethyl acetate, and we observed the formation of both needles and blocks. The needles proved to be phosphangulene uncontaminated by oxide **2a**. This indicates that crystallization of phosphangulene by stacking is kinetically favorable, as well as topologically attractive, and

that the lattice effectively excludes molecules of oxide **2a**, which are larger and awkwardly shaped. Concurrently formed block-shaped crystals were found to have the structure of polymorph C of oxide **2a**, but they contained ratios of oxide **2a** and phosphangulene that varied according to the changing composition of the mother liquors. Blocks appearing early in the crystallization were shown to have the 1:1 composition of the initial mother liquors, whereas crystals formed later were progressively enriched in oxide **2a** as pure phosphangulene was gradually removed from the liquid phase. The observation of crystalline solid solutions strengthens the hypothesis that the solid-state behavior of oxide **2a** has a clear-cut structural basis, rooted in its odd shape and inability to avoid suboptimal intermolecular interactions. As a result, its crystallization is prone to errors in which molecules of oxide **2a** are replaced by other compounds. A particularly attractive substitute is phosphangulene itself, which is identical in symmetry, topologically related, and smaller.

When isostructural compounds cocrystallize, the unit cell parameters typically vary linearly as the ratio of the components changes. This relationship, which is known as Vegard's law,[37–39] unexpectedly also describes the behavior of mixtures of phosphangulene and oxide **2a**, even though they are far from isostructural. Figure 2.28 shows that the volume of the unit cell measured for single crystals of polymorph C of oxide **2a** decreases linearly as the amount of incorporated phosphangulene increases.

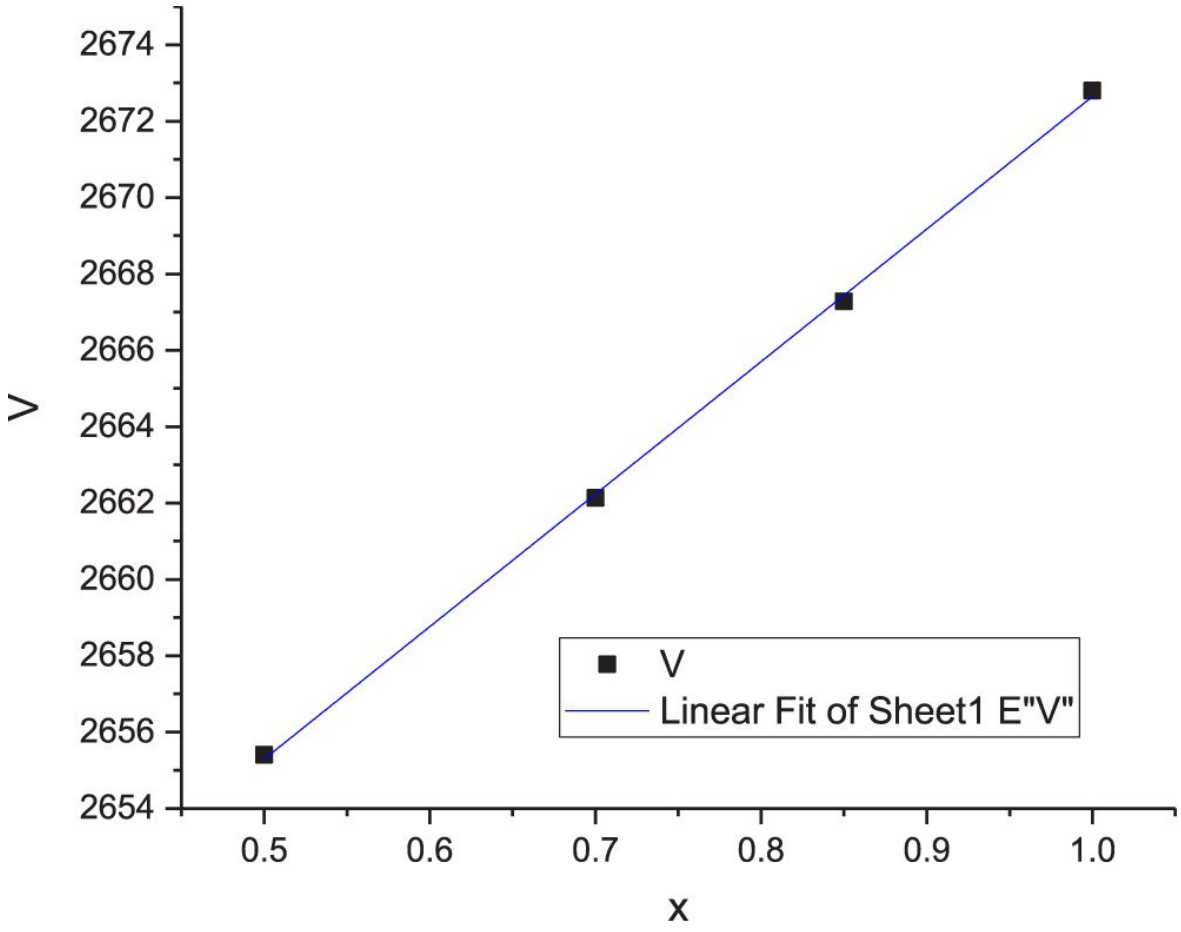

Figure 2.28 : Graph showing that the unit cell volume *V* (in $Å^3$) measured for single crystals of polymorph C of oxide **2a** decreases linearly as the molar fraction (1-χ) of incorporated phosphangulene increases.

The rapid high-fidelity crystallization of phosphangulene differs sharply from the promiscuous behavior of oxide **2a**. The contrast is an impressive example of how patterns of molecular organization can be altered substantially by simple structural modifications. The ability of oxide **2a** to include phosphangulene over a wide range of compositions is noteworthy because crystals of the pure components are not isomorphous, isostructural, or even structurally similar. The special tendency of oxide **2a** to form solid solutions appears to have the same

origin as its high degree of polymorphism: specifically, the awkward shape inhibits effective packing, weakens intermolecular interactions, and broadens the opportunities to produce crystals in which the orientation and even the identity of adjacent molecules can be varied without imposing a significant energetic penalty.

These conclusions are reinforced by the results of related experiments. For example, crystallization of equimolar mixtures of oxide **2a** and sulfide **2b** from CH_2Cl_2/hexane yielded crystals of oxide **2a** incorporating approximately 28% of sulfide **2b**. This surprising observation reveals that packing in the lattice of oxide **2a** is so susceptible to variations that sulfide **2b** can be accommodated, even though it is a larger molecule. Remarkably, examination of multiple mixed crystals showed that they all had similar compositions but formed two different structures. One corresponded to known polymorph A of oxide **2a** (monoclinic $P2_1/n$), but the other appears to be a new polymorph of oxide **2a** (monoclinic $P2_1/c$) that we have not yet been able to prepare in pure form. This observation suggests that further study of oxide **2a** will yield more polymorphs, beyond the five forms A–E already characterized in detail. Moreover, the promiscuous formation of mixed crystals is not a phenomenon limited to a single polymorph but rather is a more general consequence of the peculiar structural features of chalcogenides **2a**–**c**. The finding that oxide **2a** can be induced to crystallize in new ways by traces of additives provides further evidence that its molecular organization can be altered with unusual facility.

Chalcogenides **2a**–**c** also readily form pseudopolymorphs incorporating molecules of various solvents, as well as cocrystals with diverse partners.[40] We have found that particularly suitable partners are fullerenes such as C_{60} and C_{70}, which have convex surfaces that are topologically

and electronically complementary to the concave faces of phosphangulene and its derivatives.[40–43] The related propensity of triphenylphosphine oxide to cocrystallize with many partners has been noted in previous work and attributed in part to a strong capacity to accept hydrogen bonds.[44] Phosphangulene oxide (**2a**) promises to be an even more effective agent for promoting cocrystallizations, because it cannot crystallize effectively by itself in ways that properly exploit its latent ability to form hydrogen bonds and other interactions.

2.2.4 Conclusions

The distinctive conical shape of phosphangulene allows efficient molecular packing and helps direct crystallization by favoring the formation of π-stacks. As confirmed earlier by Krebs, Yamamura, and their coworkers, this preferred mode of association can be foiled by converting phosphangulene into the corresponding oxide **2a**, sulfide **2b**, or selenide **2c**. Only one atom is added, but molecular packing is altered profoundly. The shape of chalcogenides **2a**–**c** consistently disfavors efficient stacking and forces crystallization to occur in other ways. Detailed structural analysis of multiple polymorphs shows that none of the alternatives is particularly favorable, and the frequency of large intermolecular separations is always abnormally high. Chalcogenides **2a**–**c** are structurally unable to exploit the full potential of their constituent atoms to engage in stabilizing intermolecular contacts. A high degree of polymorphism is favored because various structural alterations can be accommodated without incurring significant energetic penalties, and the unit cells and asymmetric units of crystals must typically include large numbers of molecules to allow acceptable packing to be achieved.

Phosphangulene chalcogenides **2a**–**c** are richly polymorphic despite having little conformational flexibility. Statistical analysis of the CSD has established that molecular

compounds exhibit polymorphism in only about 37% of the single-component crystals examined;[30] moreover, only two inflexible compounds in the entire CSD (0.0002%) are known to exist in more than four polymorphic forms. As a result, the consistently unusual behavior of all three compounds **2a**–**c** is statistically improbable and refutes the notion that there are no correlations between molecular structure and high levels of polymorphism.

Our work builds on earlier investigations of phosphangulene and its derivatives but extends these previous studies in unexpected ways. Our observations reveal that the behavior of the compounds is not merely a curiosity, but rather a source of broadly useful new understanding of molecular crystallization overlooked in earlier work. Phosphangulene and its chalcogenides may appear to be exotic compounds, but they are not odd exceptions to normal molecular behavior. In fact, the series of compounds is aptly chosen to help reveal how molecular organization can be altered and controlled. Crystallization is an undeniably complex phenomenon, but our findings confirm that it is not futile to seek to identify specific structural features that underlie particular solid-state behavior. The approach used in our study of phosphangulene and its chalcogenides is based on purposeful interference with established patterns of crystallization, followed by extensive analysis of the consequences. Our results confirm that the approach is an effective way to probe the origins of molecular organization and to engineer materials with useful properties that arise predictably from structural features present in the individual molecular components.

Our results underscore the shortcomings of efforts to understand molecular crystallization based solely on statistical analyses of the CSD and other structural databases. Previous surveys have failed to identify any specific molecular features that predictably underlie high levels of

polymorphism. Reported structures with high values of Z/Z' are also diverse, although certain organizing principles have been identified.[20] However, the guidelines are far too vague to allow confident extrapolation from the behavior of one compound to that of an analogue. We are not aware of any previous study in which the origin of high polymorphism and elevated values of Z/Z' has been traced back to specific structural features in a set of compounds, in the way that we have probed the behavior of phosphangulene chalcogenides **2a**–**c**. Moreover, the correlation we observe between molecular structure and crystalline organization is tight, allowing key features of the solid-state behavior of the entire set of compounds to be predicted with confidence, on the basis of the properties of a single example. This has not been achieved in previous efforts to understand the origin of polymorphism and elevated values of Z/Z'. Analyses of large databases are valuable tools for discovery, but they must be complemented by parallel experimental studies, using molecules purposefully devised to reveal and test principles of organization in crystals. Mining databases, however large, cannot yet replace sound chemical intuition as a way to locate promising areas for exploration within the infinite realm of molecular structures.

2.2.5 Experimental Section

All reagents and solvents were obtained from commercial sources and used without further purification unless otherwise indicated. Phosphangulene and chalcogenides **2a**–**c** were prepared by modifications of published procedures, as described below.[1,7,13]

2-(3-Fluorophenoxy)tetrahydro-2*H*-pyran (4). To a stirred solution of pyridinium *p*-toluenesulfonate (0.305 g, 1.39 mmol) in 3,4-dihydro-2*H*-pyran (50 mL) was slowly added 3-fluorophenol (12.5 mL, 138 mmol) at 25 °C under N_2. After 30 min, the resulting mixture was concentrated by evaporating volatile components under reduced pressure, and ethyl acetate (200 mL) was added to the residue. The organic phase was washed with saturated aqueous $NaHCO_3$ (200 mL), water (200 mL), and brine (200 mL). The washed solution was then dried over Na_2SO_4 and filtered. Evaporation of volatiles under reduced pressure left an oily residue that was purified by flash chromatography (hexane, silica gel) to afford ether **4** as a colorless solid (21.6 g, 110 mmol, 79%). The ^1H and ^{13}C NMR spectra matched those reported previously.[1]

Tris[2-fluoro-6-(tetrahydro-2*H*-pyran-2-yloxy)phenyl]phosphine (5). A stirred solution of ether **4** (20.7 g, 105 mmol) in dry THF (320 mL) was cooled to -85 °C under N_2 and treated dropwise with a solution of n-BuLi (42 mL, 2.5 M in hexane, 110 mmol) during 15 min. After 1 h at -85 °C, freshly distilled PBr_3 (9.23 g, 34.1 mmol) was added dropwise during 10 min. The resulting mixture was stirred for 2.5 h at -85 °C, then MeOH (5.5 mL) was added, and the temperature was allowed to rise to 25 °C. The quenched mixture was poured into brine (300 mL), and the mixture was extracted with diethyl ether (3 × 200 mL). The combined extracts were dried over Na_2SO_4 and filtered. Evaporation of volatiles under reduced pressure left a

residue of solid, which was purified by trituration with boiling MeOH or by recrystallization from a boiling mixture of MeOH (1000 mL) and $CHCl_3$ (50–100 mL). The resulting solid was washed with MeOH and dried under vacuum to give phosphine **5** as a colorless solid (15.6 g, 25.3 mmol, 74%). The ^{1}H and ^{13}C NMR spectra matched those reported previously.[1]

2,2',2''-Phosphinetriyltris(3-fluorophenol) (6). Phosphine **5** (8.00 g, 13.0 mmol) was suspended in N_2-sparged MeOH (800 mL), and 36% aqueous HCl (16 mL, 190 mmol) was added. The mixture was stirred at 25 °C under N_2 until a solution was formed (about 1–1.5 h), and then volatile components were removed by evaporation under reduced pressure. The residue was dissolved in N_2-sparged $CHCl_3$ (300 mL), and N_2-sparged aqueous $NaHCO_3$ (1 *N*, 300 mL) was added. The two phases were vigorously stirred for 2 h under N_2 and then separated. The aqueous phase was extracted with diethyl ether (2 × 100 mL), and the combined organic phases were dried over Na_2SO_4 and filtered. Volatiles were removed by evaporation under reduced pressure, and the residue was then dissolved in boiling toluene (about 125 mL). Subsequent careful addition of heptane (200 mL) caused a colorless solid to precipitate. The resulting suspension was kept overnight at -25 °C to induce further precipitation. The product was separated by filtration, washed with hexane, and dried under vacuum to afford phosphine **6** as a colorless solid (4.31 g, 11.8 mmol, 91%). The ^{1}H and ^{13}C NMR spectra matched those reported previously.[1]

Phosphangulene (1). Under dry N_2, a mixture of phosphine **6** (1.82 g, 5.00 mmol), Cs_2CO_3 (12.2 g, 37.5 mmol), and CuI (0.0952 g, 0.500 mmol) was treated with dry DMF (75 mL) and freshly distilled tetramethylethylenediamine (TMEDA; 38 μL, 0.25 mmol). The mixture was heated at reflux for 2 days and then allowed to cool. Water was added until no more

precipitate was formed. The solid was separated by filtration, washed thoroughly with water, and dried under vacuum at 25 °C. Decolorization could be achieved by dissolving the solid in CH_2Cl_2 and passing the solution through a pad of silica. This yielded phosphangulene (**1**) as a colorless solid (0.850 g, 2.79 mmol, 56%). The ^{1}H and ^{13}C NMR spectra matched those reported previously.[1]

Phosphangulene Oxide (2a). A solution of phosphangulene (**1**; 304 mg, 1.00 mmol) in $CHCl_3$ (8 mL) was treated with 30% aqueous hydrogen peroxide (10 mL), and the mixture was stirred vigorously at 25 °C for 12 h. The phases were separated, and the organic phase was dried over sodium sulfate and filtered. Removal of volatiles by evaporation under reduced pressure left a residue that was recrystallized from anhydrous ethanol to afford phosphangulene oxide (**2a**) as a colorless solid (307 mg, 0.959 mmol, 96% yield). The ^{1}H and ^{13}C NMR spectra matched those reported previously.[7]

Phosphangulene Sulfide (2b). A solution of phosphangulene (**1**; 304 mg, 1.00 mmol) in *p*-xylene (3 mL) was sparged with N_2, and elemental sulfur was added (48.1 mg, 1.50 mmol). The resulting suspension was stirred and heated at reflux for 12 h. Volatiles were then removed by evaporation under reduced pressure, and the residue was purified by elution with hexane through a short column of silica. Crystallization of the product from anhydrous ethanol afforded phosphangulene sulfide (**2b**) as a colorless solid (259 mg, 0.770 mmol, 77%). The ^{1}H and ^{13}C NMR spectra matched those reported previously.[7]

Phosphangulene Selenide (2c). A solution of phosphangulene (**1**; 304 mg, 1.00 mmol) in *p*-xylene (3 mL) was sparged with N_2, and elemental selenium was added (118.4 mg, 1.50

mmol). The resulting suspension was stirred and heated at reflux for 12 h. Volatiles were then removed by evaporation under reduced pressure, and the residue was purified by elution with hexane through a short column of silica. Crystallization of the product from anhydrous ethanol afforded phosphangulene selenide (**2c**) as a colorless solid (283 mg, 0.738 mmol, 74%). The ^{1}H and ^{13}C NMR spectra matched those reported previously.[7]

Supporting Information Available: Supplementary two-dimensional fingerprint plots of Hirshfeld surfaces and additional crystallographic details, including ORTEP drawings. Structural data have been deposited with the Cambridge Crystallographic Data Centre in CIF form (1912956-1912970).

Acknowledgments. We are grateful to the Natural Sciences and Engineering Research Council of Canada, the Ministère de l'Éducation du Québec, the Canada Foundation for Innovation, the Canada Research Chairs Program, and Université de Montréal for financial support.

Notes. The authors declare no competing financial interest.

2.2.6 References

1. Krebs, F. C.; Larsen, P. S.; Larsen, J.; Jacobsen, C. S.; Boutton, C.; Thorup, N. Synthesis, Structure, and Properties of 4,8,12-Trioxa-12c-phospha-4,8,12,12c-tetrahydrodibenzo[*cd*,*mn*]pyrene, a Molecular Pyroelectric. *J. Am. Chem. Soc.* **1997**, *119*, 1208–1216.

2. Carlson, R. R.; Meek, D. W. Dipole Moments of Several Tertiary Phosphine Oxides, Sulfides, and Selenides and of Some Tertiary Arsine Oxides and Sulfides. *Inorg. Chem*. **1974**, *13*, 1741–1747.

3. Cumper, C. W. N.; Foxton, A. A.; Read, J.; Vogel, A. I. Physical Properties and Chemical Constitution. Part XXXIX. The Electric Dipole Moments of Some Tri-n-alkylphosphines, of Triphenylphosphine, and of their Oxides. *J. Chem. Soc.* **1964**, 430–434.

4. Madsen, G. K. H.; Krebs, F. C.; Lebech, B.; Larsen, F. K. Evaluation of the Solid State Dipole Moment and Pyroelectric Coefficient of Phosphangulene by Multipolar Modeling of X-ray Structure Factors. *Chem. Eur. J.* **2000**, *6*, 1797–1804.

5. Hirshfeld surfaces and two-dimensional fingerprint plots were generated by using CrystalExplorer17. Turner, M. J.; McKinnon, J. J.; Wolff, S. K.; Grimwood, D. J.; Spackman, P. R.; Jayatilaka, D.; Spackman, M. A. *CrystalExplorer17*; University of Western Australia, 2017.

6. McKinnon, J. J.; Spackman, M. A.; Mitchell, A. S. Novel Tools for Visualizing and Exploring Intermolecular Interactions in Molecular Crystals. *Acta Crystallogr. B* **2004**, *60*, 627–668.

7. Yamamura, M.; Nabeshima, T. Relationship between the Bowl-Shaped Geometry of Phosphangulene and an Axial Group on the Phosphorus Atom. *Bull. Chem. Soc. Jpn.* **2016,** *89*, 42–49.

8. Maly, K. E.; Gagnon, E.; Wuest, J. D. Engineering Molecular Crystals with Abnormally Weak Cohesion. *Chem. Commun.* **2011**, 5163−5165.

9. Gagnon, E.; Halperin, S. D.; Métivaud, V.; Maly, K. E.; Wuest, J. D. Tampering with Molecular Cohesion in Crystals of Hexaphenylbenzenes. *J. Org. Chem.* **2010**, *75*, 399−406.

10. Zhou, H.; Dang, H.; Yi, J.-H.; Nanci, A.; Rochefort, A.; Wuest, J. D. Frustrated 2D Molecular Crystallization. *J. Am. Chem. Soc.* **2007**, *129*, 13774−13775.

11. Lebel, O.; Maris, T.; Perron, M.-È.; Demers, E.; Wuest, J. D. The Dark Side of Crystal Engineering: Creating Glasses from Small Symmetric Molecules that Form Multiple Hydrogen Bonds. *J. Am. Chem. Soc.* **2006**, *128*, 10372−10373.

12. Zhang, X.; Liu, F.; Wei, Z.; Wang, Z. Synthesis of Diaryl Ethers by CuI-Catalyzed C-O Bond Formation via Ullman Coupling: Assessing the Reactivity of Aryl Halides. *Lett. Org. Chem.* **2013,** *10*, 31–36.

13. Faldt, A.; Krebs, F. C.; Thorup, N. Synthesis, Structure and Properties of Various Molecules Based on the 4,8,12-Trioxa-4,8,12,12c-tetrahydrodibenzo[*cd*,*mn*]pyrene System with an Evaluation of the Effect Differing Molecular Substitution Patterns has on the Space Group Symmetry. *J. Chem. Soc., Perkin Trans 2* **1997**, 2219–2227.

14. Eikeland, E.; Thomsen, M. K.; Overgaard, J.; Spackman, M. A.; Iversen, B. B. Intermolecular Interaction Energies in Hydroquinone Clathrates at High Pressure. *Cryst. Growth Des.* **2017**, *17*, 3834–3846.

15. Lee, J. J.; Fuller, R. O.; Sobolev, A. N.; Clausen, H. F.; Overgaard, J.; Koutsantonis, G. A.; Iversen, B. B.; Spackman, M. A. Temperature-Dependent Crystal Structure of the Isopropanol Clathrate of Dianin's Compound. *Chem. Commun.* **2011**, *47*, 2029–2031.

16. Kooijman, H.; Spek, A. L.; van Bommel, K. J. C.; Verboom, W.; Reinhoudt, D. N. A Triclinic Modification of Triphenylphosphine. *Acta Crystallogr. C* **1998**, *54*, 1695–1698.

17. Brock, C. P.; Schweizer, W. B.; Dunitz, J. D. Internal Molecular Motion of Triphenylphosphine Oxide: Analysis of Atomic Displacement Parameters for Orthorhombic and Monoclinic Crystal Modifications at 100 and 150 K. *J. Am. Chem. Soc*. **1985**, *107*, 6964–6970.

18. Views of the structures of other inequivalent molecules in the asymmetric unit are provided in the Supporting Information.

19. Bernstein, J.; Davey, R. J.; Henck, J.-O. Concomitant Polymorphs. *Angew. Chem. Int. Ed.* **1999**, *38*, 3440–3461.

20. Brock, C. P. High-Z' Structures of Organic Molecules: Their Diversity and Organizing Principles. *Acta Crystallogr. B* **2016**, *72*, 807–821.

21. Steed, K. M.; Steed, J. W. Packing Problems: High Z' Crystal Structures and Their Relationship to Cocrystals, Inclusion Compounds, and Polymorphism. *Chem. Rev.* **2015**, *115*, 2895–2933.

22. Bernstein, J.; Dunitz, J. D.; Gavezzotti, A. Polymorphic Perversity: Crystal Structures with Many Symmetry-Independent Molecules in the Unit Cell. *Cryst. Growth. Des.* **2008**, *8*, 2011–2018.

23. Thomas, S. P.; Spackman, P. R.; Jayatilaka, D.; Spackman, M. A. Accurate Lattice Energies for Molecular Crystals from Experimental Crystal Structures. *J. Chem. Theory Comput*. **2018**, *14*, 1614–1623.

24. Zeidan, T. A.; Trotta, J. T.; Tilak, P. A.; Oliviera, M. A.; Chiarella, R. A.; Foxman, B. M.; Almarsson, Ö.; Hickey, M. B. An Unprecedented Case of Dodecamorphism: The Twelfth Polymorph of Aripiprazole Formed by Seeding with its Active Metabolite. *CrystEngComm* **2016**, *18*, 1486–1488.

25. Gnutzmann, T.; Thi, Y. N.; Rademann, K.; Emmerling, F. Solvent-Triggered Crystallization of Polymorphs Studied in Situ. *Cryst. Growth. Des*. **2014**, *14*, 6445–6450.

26. López-Mejías, V.; Kampf, J. W.; Matzger, A. J. Nonamorphism in Flufenamic Acid and a New Record for a Polymorphic Structure with Solved Structures. *J. Am. Chem. Soc.* **2012**, *134*, 9872–9875.

27. Yu, L. Polymorphism in Molecular Solids: An Extraordinary System of Red, Orange, and Yellow Crystals. *Acc. Chem. Res*. **2010**, *43*, 1257–1266.

28. Brás, E. M.; Henriques, M. S. C.; Paixão, J. A.; Fausto, R. High Z' Crystal Structure of a New Polymorph of a Thioimidazole Disulfide: Importance of Conformational Flexibility. *Cryst. Growth Des*. **2018**, *18* 4167–4173.

29. Kersten, K.; Kaur, R.; Matzger, A. Survey and Analysis of Crystal Polymorphism in Organic Structures. *IUCrJ* **2015**, *5*, 124–129.

30. Cruz-Cabeza, A. J.; Reutzel-Edens, S. M.; Bernstein, J. Facts and Fictions about Polymorphism. *Chem. Soc. Rev*. **2015**, *44*, 8619–8635.

31. McCrone, W. C. In *Polymorphism in Physics and Chemistry of the Organic Solid State*. Fox, D.; Labes, M. M.; Weissenberg, A., eds. Interscience, New York, 1965, vol. II, pp. 726.

32. Gavezzotti, A. Structure and Energy in Organic Crystals with Two Molecules in the Asymmetric Unit: Causality or Chance? *CrystEngComm* **2008**, *10*, 389−398.

33. Knapp, C.; Lork, E.; Gupta, K.; Mews, R. Structure Investigations on 4-Halo-1,2,3,5-dithiadiazolyl Radicals XCNSSN$^{\bullet}$ (X = F, Cl, Br): The Shortest Intradimer S···S Distance in Dithiadiazolyl Dimers. *Z. Anorg. Allg. Chem.* **2005**, *631*, 1640−1644.

34. Clarke, C. S.; Pascu, S. I.; Rawson, J. M. Further Studies on the Polymorphic Dithiadiazolyl Radical, ClCNSSN. *CrystEngComm* **2004**, *6*, 79−82.

35. Cheuk, D.; Khamar, D.; McArdle, P.; Rasmuson, Å. C. Solid Forms, Crystal Habits, and Solubility of Danthron. *J. Chem. Eng. Data* **2015**, *60*, 2110−2118.

36. Rohl, A. L.; Moret, M.; Kaminsky, W.; Claborn, K.; McKinnon, J. J.; Kahr, B. Hirshfeld Surfaces Identify Inadequacies in Computations of Intermolecular Interactions in Crystals: Pentamorphic 1,8-Dihydroxyanthraquinone. *Cryst. Growth Des.* **2008**, *8*, 4517−4525.

37. Lusi, M. Engineering Crystal Properties through Solid Solutions. *Cryst. Growth Des.* **2018**, *18*, 3704−3712.

38. Vegard, L. Die Konstitution der Mischkristalle und die Raumfüllung der Atome. *Z. Phys.* **1921**, *5*, 17−26.

39. Vegard, L.; Shelderup, H. Die Konstitution der Mischkristalle. *Phys. Z.* **1917**, *18*, 93−96.

40. Heskia, A.; Maris, T.; Wuest, J. D. Putting Fullerenes in Their Place: Cocrystallizing C_{60} and C_{70} with Phosphangulene Chalcogenides. *Cryst. Growth Des.* **2019**, *19*, in press (DOI: 10.1021/acs.cgd.9b00954).

41. Yamamura, M.; Hongo, D.; Nabeshima, T. Twofold Fused Concave Hosts Containing Two Phosphorus Atoms: Modules for the Sandwich-Type Encapsulation of Fullerenes in Variable Cavities. *Chem. Sci.* **2015**, *6*, 6373–6378.

42. Yamamura, M.; Sukegawa, K.; Nabeshima, T. Tuning the Depth of Bowl-Shaped Phosphine Hosts: Capsule and Pseudo-Cage Architectures in Host–Guest Complexes with C_{60} Fullerene. *Chem. Commun*. **2015**, 51, 12080–12083.

43. Yamamura, M.; Saito, T.; Nabeshima, T. Phosphorus-Containing Chiral Molecule for Fullerene Recognition Based on Concave/Convex Interaction. *J. Am. Chem. Soc.* **2014**, *136*, 14299–14306.

44. Etter, M. C.; Baures, P. W. Triphenylphosphine Oxide as a Crystallization Aid. *J. Am. Chem. Soc.* **1988**, *110*, 639–640.

2.2.7 Table of Contents Graphic

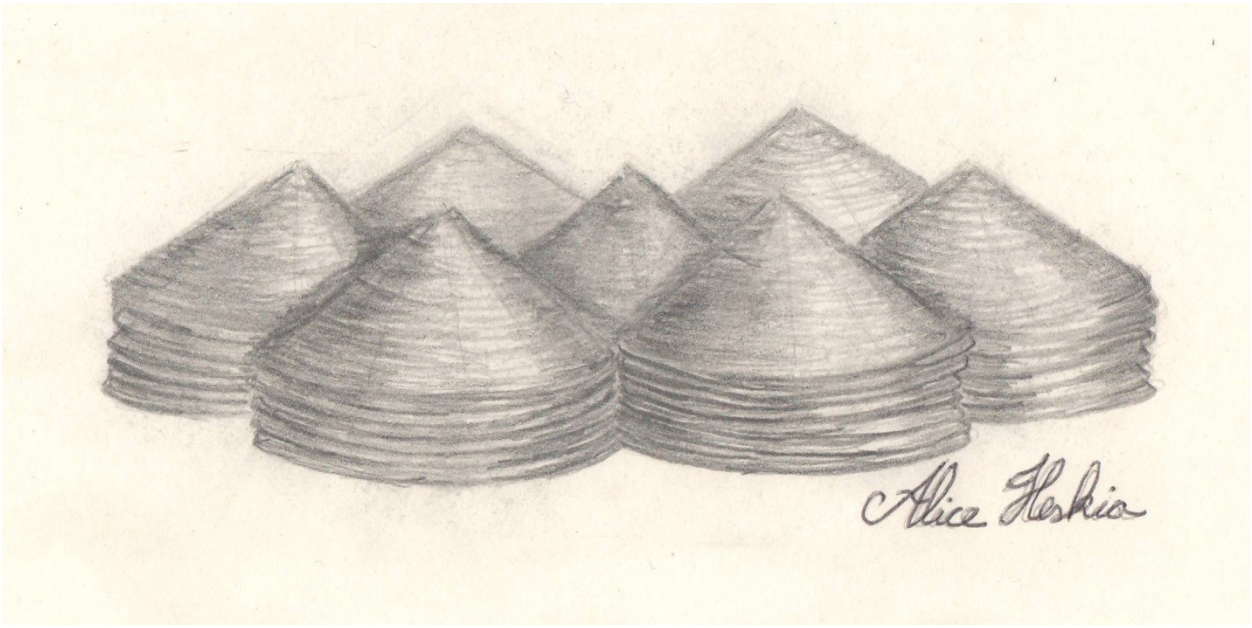

Synopsis

The structures of derivatives of phosphangulene, a hexacyclic phosphine with a conical shape, help reveal how to design molecules that cannot pack efficiently or achieve normal patterns of association, leading to the formation of multiple polymorphs, structures with high values of Z and Z', solvates, solid solutions, and cocrystals.

2.3 Conclusions

En quelques mots, l'harmonieux réseau cristallin du phosphangulène peut être perturbé par l'introduction d'un seul atome qui changera significativement la forme moléculaire de sorte à diminuer l'efficacité de l'empilement dans l'espace tridimensionnel. L'ajout de cette étude à la compréhension globale du phénomène de polymorphisme, dû aux particularités du système isolant un minimum de variables, mérite d'être noté. Cette analyse de polymorphes avec des valeurs de Z et Z' élevées constitue un point de départ dans nos démarches vers la cocristallisation avec les fullerènes. En effet, les problèmes d'empilement dans un homocristal (entre des molécules d'une seule et même nature) et la surface concave disponible pour ces composés, rendent notre première série de dérivés des candidats idéaux comme partenaires de cocristallisation avec les fullerènes.

Chapitre 3 : Cocristaux entre les chalcogénures du phosphangulène et les fullerènes

3.1 Introduction

Nous avons ciblé le phosphangulène comme sujet de recherche dû à la surface concave et conjuguée que la molécule offre, faisant d'elle une excellente candidate comme partenaire de cocristallisation avec les fullerènes via des interactions concaves-convexes. Cependant, nous n'avons pu obtenir quelque cocristal que ce soit avec la phosphine originale, et à ce jour, la littérature n'en a pas rapporté plus. En fait, les premiers cocristaux de fullerènes produits dans ce projet furent obtenus avec les chalcogénures de phosphangulène.

Précédemment, nous avons présenté le polymorphisme des chalcogénures du phosphangulène. Nous avons démontré que le polymorphisme de cette série de composés est causé par l'ajout d'un simple atome. Cette petite modification a eu comme conséquence de changer significativement la forme de la phosphine, la rendant maladroite.

Il existe un lien entre la propension d'un composé à produire des polymorphes, des structures de nombre *Z'* élevé et des cocristaux.[vi] Ces trois phénomènes observables sont causés par un problème d'empilement de la molécule, attribuable à la forme dans ce cas-ci. Phosphangulène et ses dérivés sont d'excellents exemples illustrant cette idée.

[vi] Steed, K. M.; Steed, J. W., Packing Problems: High Z′ Crystal Structures and Their Relationship to Cocrystals, Inclusion Compounds, and Polymorphism. *Chem. Rev.* **2015,** *115* (8), 2895-2933.

3.1.1 Problèmes d'empilement : polymorphisme, *Z'* élevé et cocristaux

Les composés présentant plus d'un polymorphe ont également tendance à avoir un nombre de molécules dans l'unité asymétrique (Z') supérieur à un, et un nombre de molécules dans la maille élémentaire (Z) élevé (> 2). Cela est relié à la difficulté du composé à trouver un état cristallin stable. N'y arrivant pas avec une unité moléculaire ($Z' = 1$), une association de molécules ($Z' > 1$) lui permettra d'obtenir une nouvelle unité d'une forme plus pratique.

Une association de molécules, dans le cas des polymorphes, implique qu'il s'agit d'un seul composé. Néanmoins, il est possible d'extrapoler et d'y voir une possibilité d'association avec d'autres composés. Les cocristaux peuvent être vus comme étant le résultat de la même stratégie. Lorsqu'une molécule a une forme peu commode pour l'empilement, il lui est possible de s'associer à d'autres, qu'il s'agisse de composés de même nature ou non, afin de former une unité qui résoudra ses problèmes. On peut donc croire qu'un composé ayant une forme inadéquate à l'entassement et ayant plusieurs polymorphes, dont plusieurs avec un nombre Z' supérieur à un, sera plus enclin à cristalliser avec un composé de nature différente qu'un analogue de forme plus empilable.

3.1.2 Objectifs

Le but des travaux décrits dans le présent chapitre était de produire des cocristaux avec les fullerènes (C_{60} et C_{70}) pour la série des chalcogénures de phosphangulène (l'oxyde, le sulfure et le sélénure). Les résultats qui y seront présentés appuient l'idée selon laquelle le polymorphisme, les structures avec un Z' élevé et les cocristaux sont liés et tirent leur origine des problèmes d'empilement à l'état solide.

3.2 Article 2

Article publié dans

Cryst. Growth Des. **2019**, *19*, 5418-5428.

DOI: 10.1021/acs.cgd.9b00954

(contribution invitée publiée dans un numéro spécial sur « Crystalline Molecular Materials: From Structure to Function »)

Putting Fullerenes in Their Place:

Cocrystallizing C_{60} and C_{70} with Phosphangulene Chalcogenides

Alice Heskia, Thierry Maris, and James D. Wuest*

Département de Chimie, Université de Montréal, Montréal, Québec H3C 3J7 Canada

*Author to whom correspondence may be addressed.

E-mail: *james.d.wuest@umontreal.ca*

3.2.1 Abstract

The distinctive conical shape and electron-rich aromatic surface of phosphangulene (**1**) and its derivatives offer geometric and electronic complementary to the convex electron-poor surface of fullerenes such as C_{60} and C_{70}. In crystals of phosphangulene itself, molecules form π-stacks that are efficiently packed. In contrast, the corresponding oxide (**2a**), sulfide (**2b**), and selenide (**2c**) have an awkward shape that prevents effective stacking and forces crystallization to produce structures with abnormally large intermolecular separations. As a result, chalcogenides **2a**–**c** are strongly disposed to form cocrystals with C_{60} and C_{70}. Structural studies of a series of cocrystals show that compounds **2a**–**c** disrupt the normal organization of fullerenes and reposition them in diverse new ways that introduce a degree of separation but do not eliminate fullerene-fullerene contacts needed to ensure direct electronic communication.

3.2.2 Introduction

Phosphangulene (**1**) has many intriguing properties. It was first synthesized by Krebs and coworkers, who also determined the structure of crystals grown from ethyl acetate.[1] The well-defined conical shape of phosphangulene, shown in Figure 3.1, favors the formation of efficiently packed crystals built from π-stacks. The nonplanarity of phosphangulene gives rise to a dipole moment, determined to be 3.3 ± 0.2 D in $CHCl_3$.[1] Ab initio calculations and multipolar modeling of X-ray structure factors have established that the dipole runs along the C_3 axis from the apex of the cone (with the atom of phosphorus at the negative end) to the base (with the peripheral atoms of hydrogen defining the positive end of the dipole).[2]

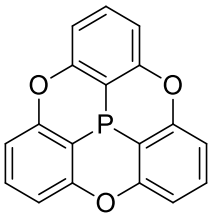

1

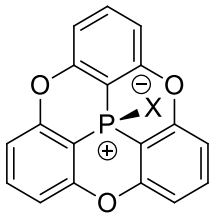

2a (X = O)
2b (X = S)
2c (X = Se)

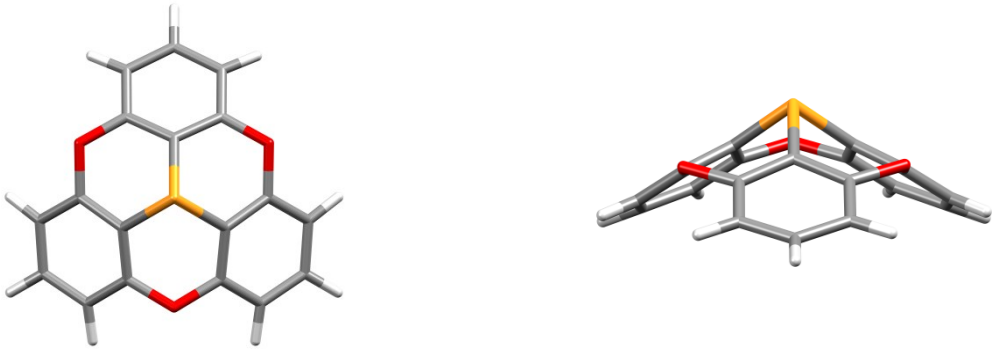

Figure 3.1 : Two views of the structure of phosphangulene (**1**), one along the C_3 axis and the other perpendicular. Atoms of carbon appear in gray, hydrogen in white, oxygen in red, and phosphorus in orange.

Molecular polarity and topology work in harmony to help direct the crystallization of phosphangulene by favoring the formation of π-stacks with dipole moments aligned (Figure 3.2). No other polymorph has been reported. Each stack forms short C-H···O interactions (2.395 Å) with six parallel stacks. Unexpectedly, the dipole moments of all stacks point in the same direction, thereby producing *R*3*m* crystals that are polar and pyroelectric.

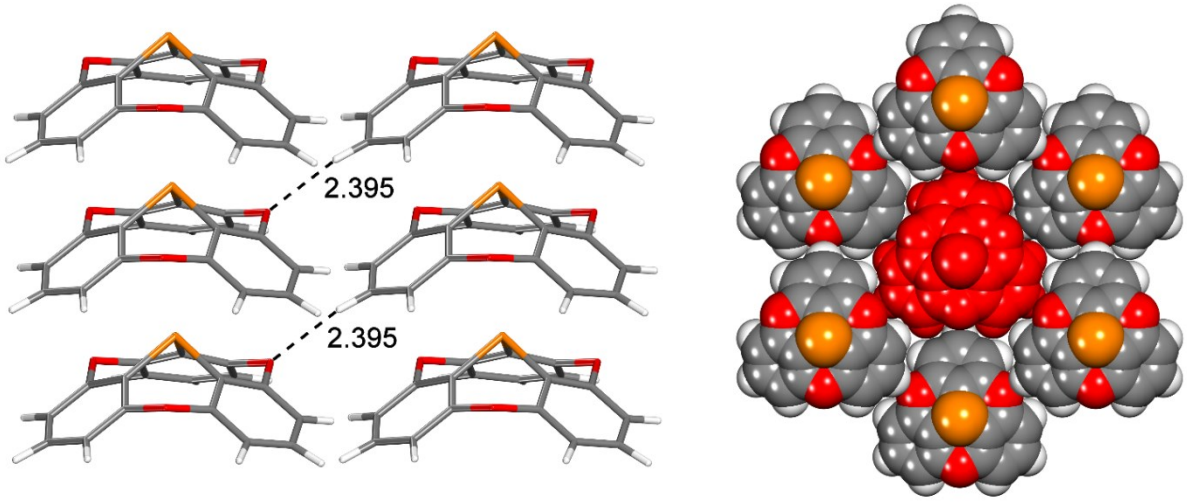

Figure 3.2 : Representations of the structure of crystals of phosphangulene grown from ethyl acetate. (a) View perpendicular to the *c*-axis, illustrating part of two adjacent π-stacks with aligned dipoles. Significant inter-stack C-H···O interactions are marked by broken lines, and H···O distances are given in Å. (b) View along the *c*-axis, showing a central stack (in red) surrounded by six others. Unless indicated otherwise, atoms are shown in standard colors.

Converting phosphangulene into the corresponding chalcogenides changes the molecular structure by adding only one atom. However, the modification disrupts the normal crystallization of phosphangulene, prevents the formation of efficiently packed π-stacks, and leads to alternative modes of organization, none particularly attractive.[3–5] As a result, chalcogenides **2a–c** form multiple polymorphs, require large numbers of molecules to construct unit cells and asymmetric units with acceptable packing, and produce structures with abnormally high frequencies of long intermolecular contacts. These properties suggested to us

that chalcogenides **2a–c** are strongly disposed to form cocrystals, particularly with partners incorporating convex aromatic surfaces.

Especially attractive partners for cocrystallization are fullerenes and their derivatives, which define a unique class of carbon-based molecular structures with convex electron-poor π-surfaces. Fullerenes and their derivatives can serve as electron acceptors and are widely used as components of the active layers in thin-film molecule-based optoelectronic devices such as solar cells. When properly positioned relative to other components of the layers,[6–8] fullerenes and their derivatives can accept electrons from the excited states of neighboring chromophores and then convey electrons to the cathode through chains of fullerene-fullerene contacts. Moreover, suitably oriented fulleride anions in crystalline salts can even give rise to high-temperature superconductivity, as exemplified by the face-centered cubic phase and body-centered cubic phase of Cs_3C_{60}.[9] Such applications require suitably ordered materials, in which fullerenes occupy specific positions with respect to neighboring molecules.

For these reasons, learning how to control the organization of fullerenes and their derivatives in materials is an important goal. Useful guidance can come from analyzing the structures of fullerene cocrystals. Despite the inherently inefficient packing of globular objects, fullerenes have characteristically low solubility,[10] which reflects poor solvation, as well as stabilization of their crystal lattices by extensive intermolecular aromatic interactions. Nevertheless, many cocrystals of fullerenes have been reported, often with partners that incorporate extended hinged or curved aromatic surfaces.[11–13] In particular, Yamamura, Nabeshima, and coworkers have prepared complex derivatives of phosphangulene that form cocrystals with C_{60} and C_{70}.[14–16]

The goal of many efforts to devise suitable partners for forming cocrystals or complexes with fullerenes has been to envelop a substantial part of their surface. Such work is inherently interesting but typically requires making large molecules by challenging multistep routes. Moreover, when encapsulation is achieved, fullerene-fullerene contacts are necessarily absent, and the resulting materials cannot have useful properties of conductivity or superconductivity arising from direct electronic interaction of the fullerene components. Advances in fullerene-based electronic technologies are more likely to result from creating simple molecules that can control how fullerenes and related compounds are organized, without eliminating contacts altogether.

In designing molecules of this type, we reasoned that the best candidates would have two key attributes: (1) An accessible concave electron-rich aromatic surface with a suitable radius of curvature and (2) an inherent inability to form effectively-packed crystals without the aid of partners. Phosphangulene and chalcogenides **2a**–**c** allowed us to test this hypothesis. Phosphangulene satisfies the first criterion but not the second, because it forms well-packed structures by itself; in contrast, the closely related chalcogenides **2a**–**c** meet both criteria. As a result, we were optimistic that chalcogenides **2a**–**c** and fullerenes would cocrystallize rather than form separate single-component crystals, with inherently inefficient packing and many abnormally long distances between neighboring molecules. Moreover, the concave aromatic face of a single molecule of compounds **2a**–**c** can envelop only about one-fourth of the surface of C_{60}. For these reasons, we expected chalcogenides **2a**–**c** to interfere with the normal aggregation of fullerenes and to yield cocrystals with novel structures, without necessarily

eliminating significant fullerene-fullerene contacts of the type required for conductivity and superconductivity.

3.2.3 Results and Discussion

Syntheses of Phosphangulene and Chalcogenides 2a–c. Phosphangulene and chalcogenides **2a**–**c** were made by recently reported methods.[5]

Attempted Cocrystallizations of C_{60} and C_{70} with Phosphangulene. Despite multiple attempts, we have not obtained cocrystals of C_{60} or C_{70} with phosphangulene. This observation supports the notion that the conical shape and dipole moment of phosphangulene work in tandem to direct the formation of well-packed molecular stacks. Fullerenes are thereby excluded, despite their complementary shapes. In addition, the conical topology of phosphangulene is flattened somewhat in chalcogenides **2a**–**c** as a result of decreases in the *s*-character of the orbital of phosphorus involved in the *P*-chalcogenide bonds.[4,5] The more acute cone angle of phosphangulene may also help disfavor cocrystallization by decreasing the aromatic surface area that each molecule can place in contact with fullerenes.

Cocrystallizations of C_{60} with Phosphangulene Oxide (2a)

2a • C_{60} • PhCl. In attempts to cocrystallize fullerenes, we typically used phosphangulene chalcogenides **2a**–**c** in excess to favor encapsulation. Allowing PhCl to evaporate slowly from a solution containing oxide **2a** and C_{60} in a 2.2:1 ratio yielded dark red crystals. Analysis by X-ray diffraction established that they have the composition **2a** • C_{60} • PhCl and belong to the monoclinic space group *Pn*. Other crystallographic data are provided in Table 3.1, and views

of the structure are shown in Figures 3.3-3. Each molecule of C_{60} is capped by only one molecule of oxide **2a** (Figure 3.3), despite the presence of an excess during crystallization. If the radius of C_{60} and the separation of layers in graphite are taken to be 3.55 Å and 3.35 Å, respectively, then 6.90 Å can be considered to be the distance between the centroid of C_{60} and an atom of carbon in van der Waals contact.[17,18] In the cocrystal, the measured distances between the centroid of C_{60} and the centroids of the three capping aromatic rings of oxide **2a** are significantly shorter (6.631–6.852 Å), suggesting that topological and electronic complementarities work together to favor cocrystallization. In the resulting structure, interstitial volumes not occupied by oxide **2a** and C_{60} accommodate molecules of PhCl (Figure 3.3), and their aromatic centroids are separated from the centroids of the closest molecules of C_{60} by 6.77 Å.

Table 3.1 : Crystallographic Data for Cocrystals of Phosphangulene Oxide (**2a**) with C_{60}

Compound	**2a** • C_{60} • PhCl	3 **2a** • C_{60} • 3 *o*-xylene	2 **2a** • C_{60} • PhMe	6 **2a** • 4 C_{60} • MeOH
crystallization medium	PhCl	*o*-xylene	PhMe	PhMe/MeOH
formula	$C_{84}H_{14}ClO_4P$	$C_{138}H_{57}O_{12}P_3$	$C_{103}H_{26}O_8P_2$	$C_{349}H_{58}O_{25}P_6$
crystal system	monoclinic	monoclinic	monoclinic	monoclinic
space group	*Pn*	$P2_1/c$	$P2_1/n$	$P2_1/n$
a (Å)	10.0298(4)	27.1567(14)	10.0466(3)	18.3952(9)
b (Å)	22.4623(8)	13.6785(7)	22.0937(6)	13.3563(6)
c (Å)	10.1970(4)	27.0976(13)	13.3309(4)	39.9166(19)
(°)	90	90	90	90
β (°)	96.888(2)	119.1907(19)	96.709(1)	94.304(2)
γ (°)	90	90	90	90
V (Å³)	2280.73(15)	8787.4(8)	2938.75(15)	9779.5(8)
Z	2	4	2	2
Z'	1	1	0.5	0.5
T (K)	105	100	150	150
ρ_{calc} (g cm^{-3})	1.679	1.512	1.642	1.642
λ (Å)	1.34139	1.34139	1.34139	1.34139
μ (mm^{-1})	1.074	0.815	0.855	0.821
R_1, I > 2σ(I)	0.0785	0.1029	0.0657	0.1280
R_1, all data	0.1105	0.1291	0.0718	0.1439
wR_2, I > 2σ(I)	0.1942	0.2865	0.1638	0.3899
wR_2, all data	0.2202	0.3189	0.1702	0.4139
measured reflections	42649	178590	43087	146950
independent reflections	8349	39117	6759	22467
observed reflections	6150	30259	6068	18020
GoF	1.025	1.069	1.048	1.556

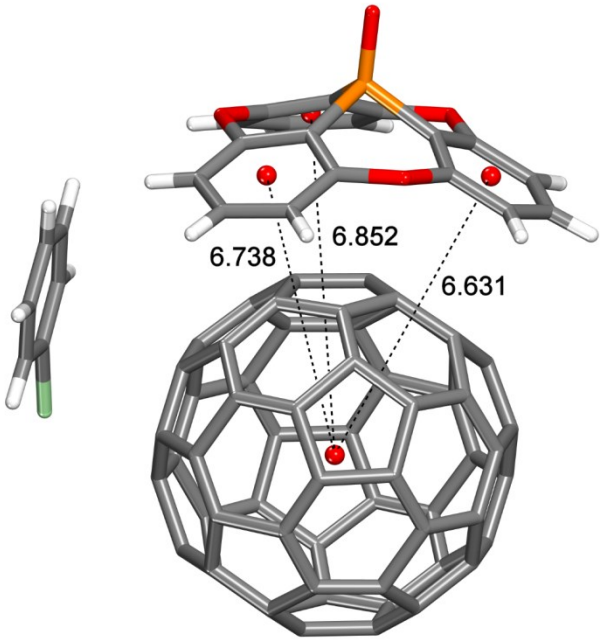

Figure 3.3 : Representation of the asymmetric unit in the structure of 1:1 cocrystals of phosphangulene oxide (**2a**) and C_{60} grown from PhCl. Atoms of carbon appear in gray, hydrogen in white, oxygen in red, chlorine in green, and phosphorus in orange. The centroids of C_{60} and the aromatic rings of oxide **2a** are marked by red circles, and key interactions are identified by broken lines, with distances given in Å. Molecules of C_{60} are disordered in the structure, and only a single representative orientation is shown.

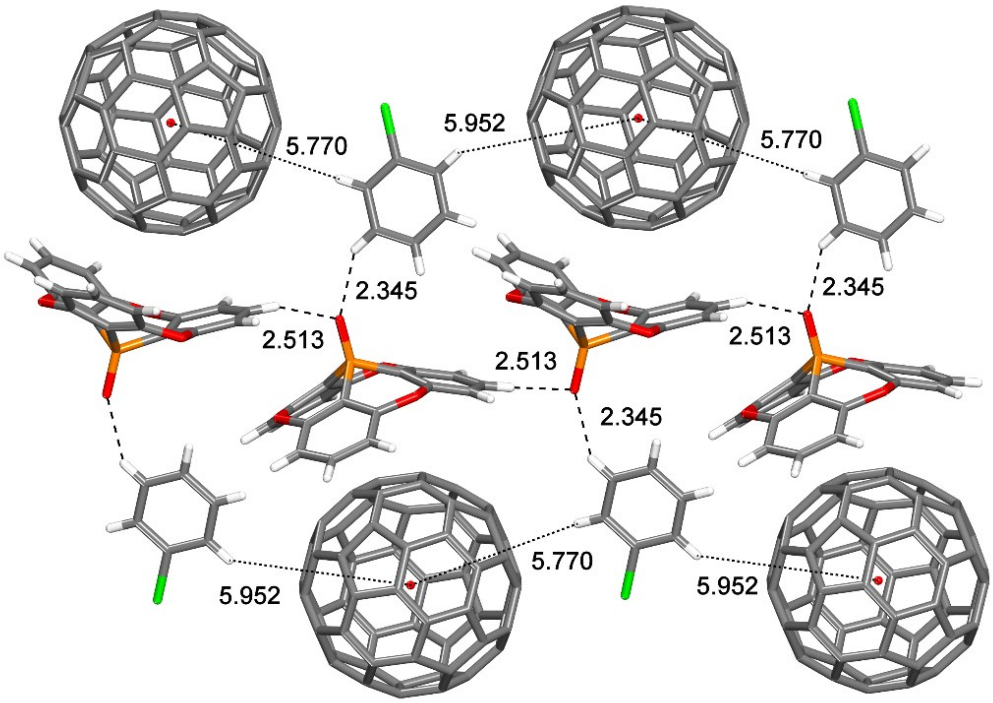

Figure 3.4 : Representation of the structure of 1:1 cocrystals of phosphangulene oxide and C_{60} grown from PhCl. View along the *ac*-diagonal showing how fullerene-rich regions (top and bottom) are separated by intervening layers of oxide **2a**. The structure is maintained by multiple C-H···O-P and C-H···π interactions (identified by broken lines, with distances given in Å), as well as by the aromatic interactions shown in **Figure 3.3**. Atoms are shown in their standard colors. Molecules of C_{60} are disordered and are shown using a simplified representation. Their centroids are marked by red circles.

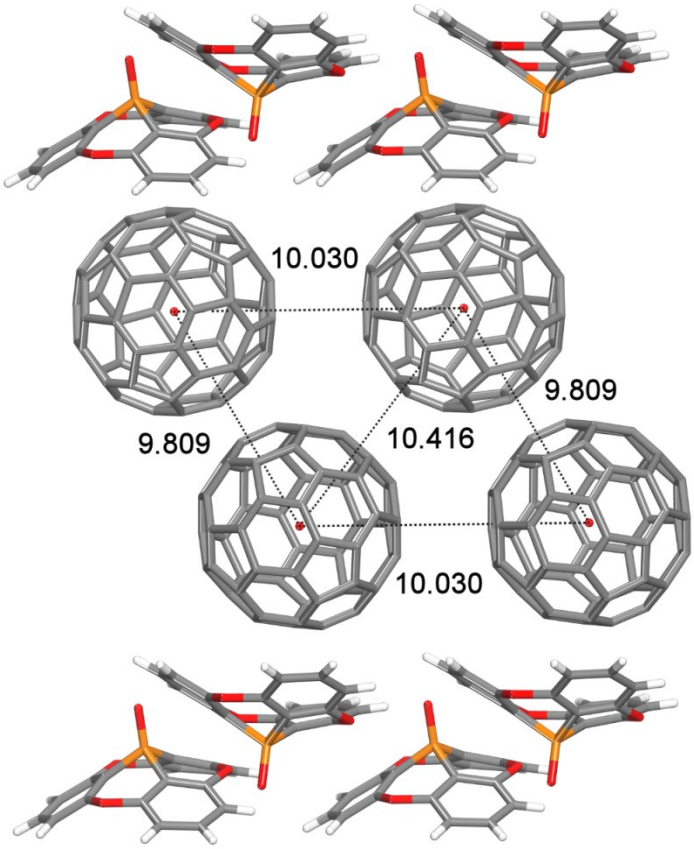

Figure 3.5 : Bilayers of C_{60} in the structure of 1:1 cocrystals of phosphangulene oxide and C_{60} grown from PhCl. Each molecule of C_{60} is surrounded by one molecule of oxide **2a** and by eight other molecules of C_{60} with centroid-centroid distances less than 10.45 Å. Atoms are shown in their standard colors. Molecules of C_{60} are disordered and are shown using a simplified representation. Their centroids are marked by red circles, and illustrative centroid-centroid distances are shown in Å. Guest molecules of PhCl are omitted for clarity.

Figures 3.4-3.5 reveal that the cocrystals contain fullerene-rich regions and intervening layers of phosphangulene oxide. Molecules of the oxide pack with their dipoles opposed and are also linked by C-H···O-P interactions (H···O distance = 2.513 Å). Further structural cohesion is provided by C-H···O-P interactions between PhCl and oxide **2a** (2.345 Å), as well as by C-

H···π interactions between PhCl and C_{60} (H···centroid distances = 5.770 and 5.952 Å). As shown in Figure 3.5, C_{60} is packed in bilayers perpendicular to the *b*-axis. Molecules of C_{60} can be considered to be in van der Waals contact if their centroids are separated by 10.45 Å,[18] and shorter distances signify stronger bonding interactions or the compressive effects of molecular packing. In the structure of cocrystals of oxide **2a** and C_{60} grown from PhCl, each molecule of C_{60} in the bilayers is surrounded by one molecule of compound **2a** and by eight other molecules of C_{60} with centroid-centroid distances in the range 9.809–10.416 Å.

The observation that phosphangulene oxide cocrystallizes with C_{60} shows that small curved molecules can be designed to interfere with the normal self-association and crystallization of fullerenes. The fullerenes can thereby be repositioned in new ways that introduce a degree of separation but do not eliminate fullerene-fullerene contacts altogether. The resulting cocrystals feature a unique segregation of fullerenes in distinct layers. Direct electronic interactions can presumably take place within those layers but are blocked in the perpendicular direction by intervening layers of oxide **2a**.

3 2a • C_{60} • 3 *o*-xylene. Inclusion of PhCl in cocrystals of phosphangulene oxide and C_{60} suggests that the peculiar molecular topologies of the partners cannot be packed efficiently even when combined, despite their complementary shapes. Distinctly different structures result when oxide **2a** and C_{60} are cocrystallized from other solvents. Slow evaporation of *o*-xylene from a solution containing oxide **2a** and C_{60} in a 2.2:1 ratio yielded dark red crystals that were shown by X-ray diffraction to have the composition 3 **2a** • C_{60} • 3 *o*-xylene and to belong to the monoclinic space group $P2_1/c$. .

Table 3.1 summarizes additional crystallographic data, and Figures 3.6-3.7 provide views of the structure. C_{60} is partially enveloped by two of the three molecules of oxide **2a** in the asymmetric unit, and the distances between the centroid of C_{60} and the centroids of the aromatic rings of oxide **2a** all lie in the range 6.599−6.865 Å (Figure 3.6). These values are shorter than the distance signifying van der Waals contact (6.90 Å), suggesting again that topological and electronic complementarities work in tandem to promote cocrystallization. The third molecule of oxide **2a** in the asymmetric unit does not cap C_{60}, but instead forms only a single O···C interaction (O···centroid distance = 6.561 Å). In the structure, molecules of *o*-xylene fill interstitial volumes not occupied by oxide **2a** and C_{60}. The structure is maintained by multiple C-H···O and C-H···π interactions, in addition to the aromatic C···C interactions involving C_{60}, oxide **2a**, and *o*-xylene. A particularly short C-H···O-P interaction (2.437 Å) is shown in Figure 3.6.

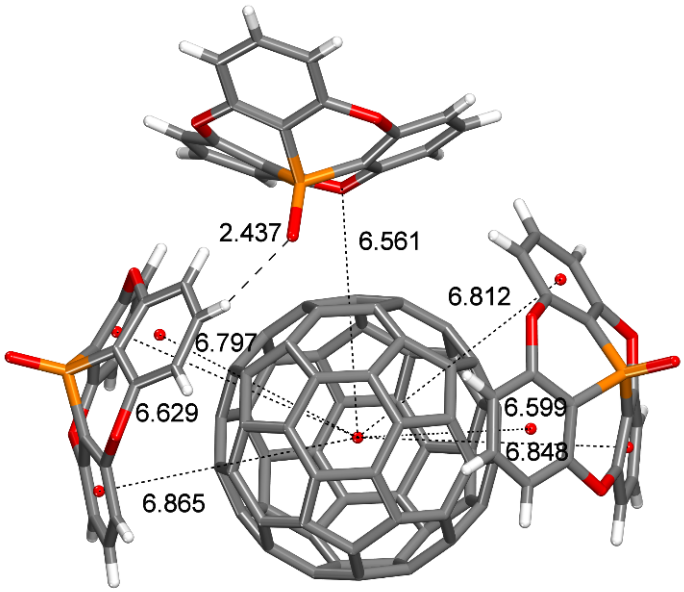

Figure 3.6 : Representation of the asymmetric unit in the structure of 3:1 cocrystals of phosphangulene oxide and C_{60} grown from *o*-xylene. Atoms are shown in their standard colors. Centroids of C_{60} and the aromatic rings of oxide **2a** are marked by red circles, and key interactions are identified by broken lines, with distances given in Å. Guest molecules of *o*-xylene are omitted for clarity.

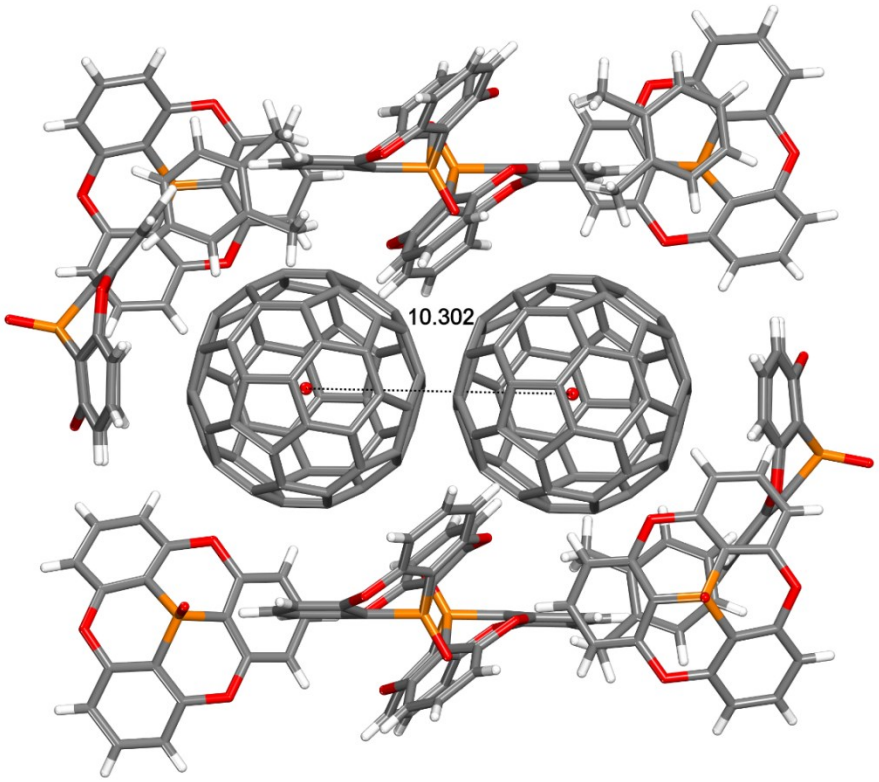

Figure 3.7 : Representation of the structure of 3:1 cocrystals of phosphangulene oxide and C_{60} grown from *o*-xylene. The view shows paired molecules of C_{60} in a cavity bounded by molecules of oxide **2a** and *o*-xylene. Atoms are shown in their standard colors. Their centroids are marked by red circles, and the centroid-centroid distance is given in Å.

The structure is noteworthy because it incorporates isolated pairs of C_{60}, which are separated from neighboring pairs by surrounding molecules of oxide **2a** and *o*-xylene (Figure 3.7). The distance between the centroids of the pairs (10.302 Å) is shorter than the distance corresponding to van der Waals contact (10.45 Å). All other fullerene-fullerene distances in the structure exceed 13.6 Å. These observations highlight the special ability of oxide **2a** to disrupt the normal crystallization of fullerenes and favor new modes of self-association.

2 2a • C_{60} • PhMe. Additional cocrystals were obtained by mixing phosphangulene oxide with C_{60} in PhMe. The cocrystals proved to have the composition 2 **2a** • C_{60} • PhMe and to belong to the monoclinic space group $P2_1/n$. Other crystallographic data are presented in Table 3.1, and views of the structure appear in Figures 3.8-3.9. Each molecule of C_{60} is capped by two diametrically opposed symmetry-equivalent molecules of oxide **2a** (Figure 3.8), and the centroids of C_{60} and the aromatic rings of oxide **2a** are separated by normal distances (6.774−6.849 Å). The structure incorporates columns of molecules of C_{60} aligned with the *a*-axis and separated by centroid-centroid distances of 10.046 Å (Figure 3.9).

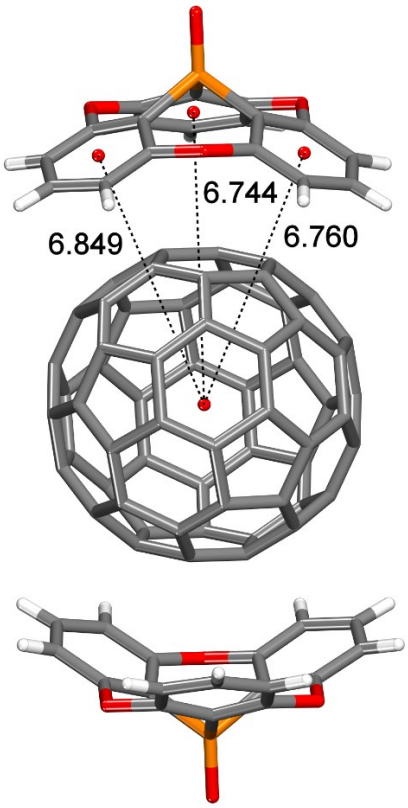

Figure 3.8 : Representation of the structure of 2:1 cocrystals of phosphangulene oxide and C_{60} grown from PhMe. Atoms are shown in their standard colors. The centroids of C_{60} and the aromatic rings of oxide **2a** are marked by red circles, and centroid-centroid distances are given in Å. Guest molecules of PhMe are omitted for clarity.

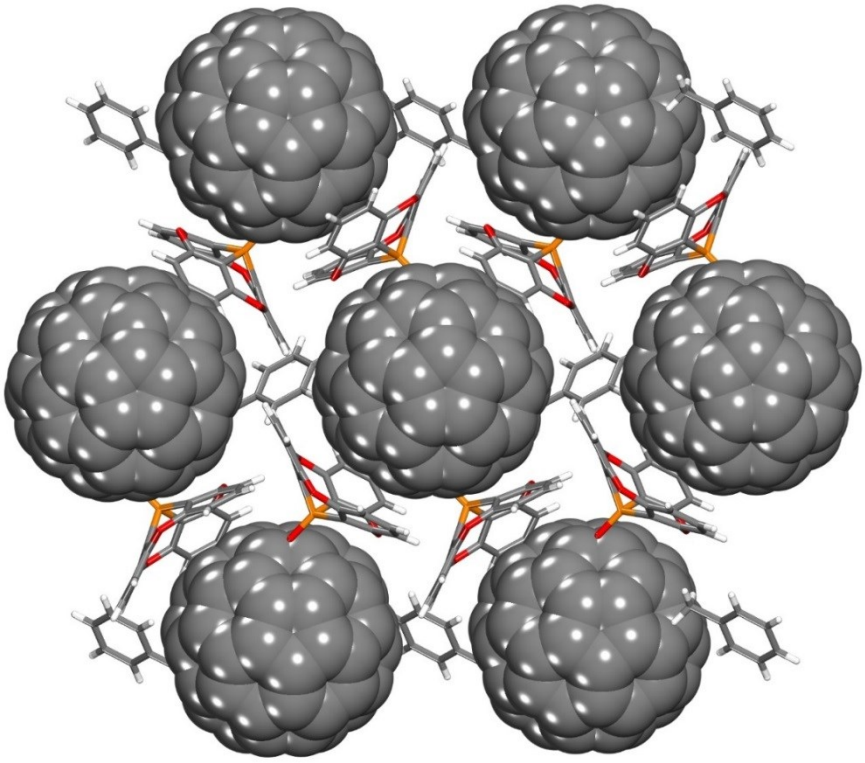

Figure 3.9 : View along the *a*-axis showing the structure of 2:1 cocrystals of phosphangulene oxide and C_{60} grown from PhMe. Fullerenes are aligned in contact along the *a*-axis to form a hexagonal array of columns surrounded by molecules of oxide **2a** and PhMe. Atoms are shown in their standard colors. Molecules of PhMe are disordered and are shown using simplified representations.

3 2a • 2 C_{60} • 0.5 MeOH. Mixing phosphangulene oxide with C_{60} in PhMe/MeOH in a 2.2:1 ratio yielded additional cocrystals, which were found to have the composition 6 **2a** • 4 C_{60} • MeOH and to belong to the monoclinic space group $P2_1/n$. Table 3.1 summarizes other crystallographic data, and Figures 3.10-3.11 provide views of the structure. One of the two symmetry-inequivalent molecules of C_{60} is capped by two molecules of oxide **2a** (Figure 3.10), and the centroids of C_{60} and the aromatic rings of oxide **2a** are separated by distances

close to the normal range (6.629−6.897 Å). The other symmetry-inequivalent molecule of C_{60} is singly capped. The doubly-capped molecule of C_{60} is in close contact with five neighboring fullerenes (centroid-centroid distances in the range 10.001−10.191 Å), whereas the singly-capped fullerene has four close neighbors. Fullerene-rich layers lie parallel to the *ab*-plane and are separated by layers of oxide **2a** and MeOH (Figure 3.11).

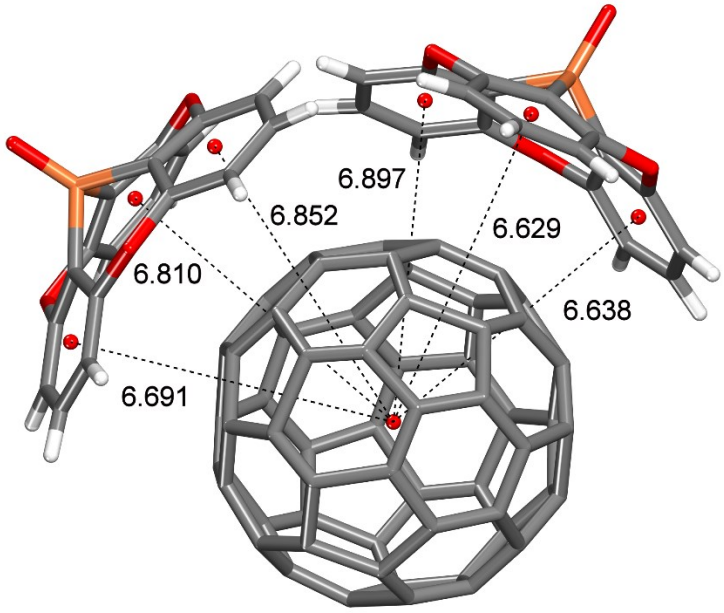

Figure 3.10 : View of the structure of 6:4 cocrystals of phosphangulene oxide and C_{60} grown from PhMe/MeOH. The view shows only one symmetry-inequivalent molecule of C_{60} capped by two molecules of oxide **2a**. Atoms are shown in their standard colors. The centroids of C_{60} and the aromatic rings of oxide **2a** are marked by red circles, and centroid-centroid distances are given in Å. C_{60} is disordered and is shown using a simplified representation. Guest molecules of MeOH are omitted for clarity.

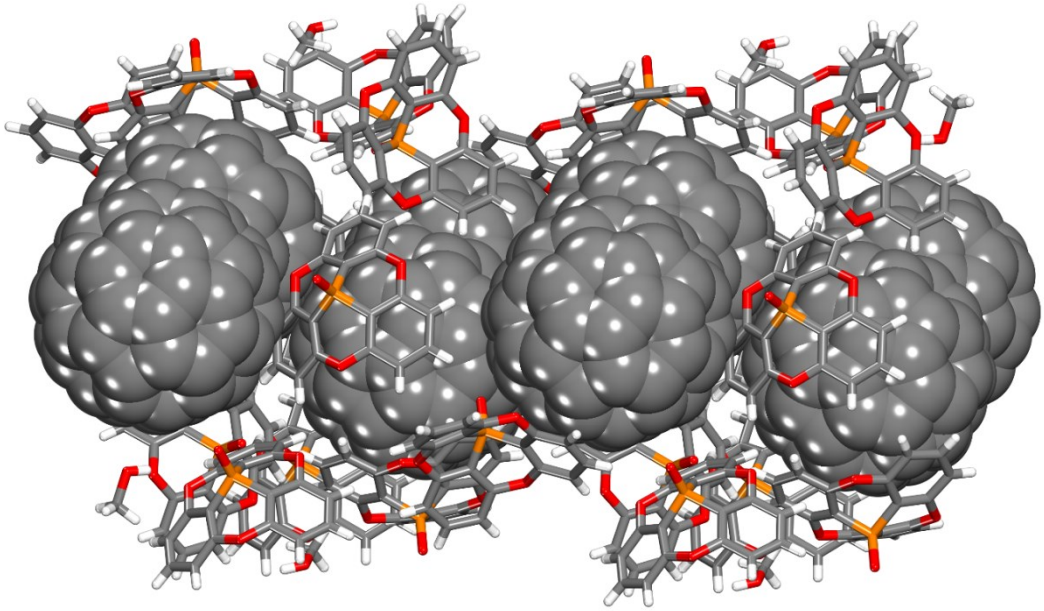

Figure 3.11 : Representation of the structure of 6:4 cocrystals of phosphangulene oxide and C_{60} grown from PhMe/MeOH. The view shows a fullerene-rich layer in the *ab*-plane and adjacent layers comprised of molecules of oxide **2a** and MeOH. Atoms are shown in their standard colors. Molecules of C_{60} are disordered and are shown using a simplified representation.

In $Pa\bar{3}$ crystals of pure C_{60}, each molecule is surrounded in three dimensions by twelve close neighbors, with centroid-centroid distances in the range 9.577−10.235 Å.[19] Cocrystallization with phosphangulene oxide reduces the density of fullerene-fullerene contacts. In 1:1 cocrystals grown from PhCl, the number of close C_{60} neighbors decreases to eight, all located in single layers, and the range of centroid-centroid distances increases to 9.778–10.416 Å. In 6:4 cocrystals grown from PhMe/MeOH are layers of C_{60} in which each fullerene has 4–5 close neighbors. In 2:1 cocrystals grown from PhMe, fullerenes are aligned in columns, and the number of close neighbors drops to two, with a centroid-centroid separation of 10.046 Å.

In 2:1 cocrystals grown from *o*-xylene, fullerenes form isolated pairs, and the number of close neighbors thereby decreases to one, with a centroid-centroid distance of 10.302 Å.

Together, these observations show that phosphangulene oxide has an affinity for C_{60}, consistently induces it to cocrystallize, and helps assemble molecules of C_{60} in diverse ways, including layers, columns, and isolated pairs, without eliminating fullerene-fullerene contacts altogether. As a result, oxide **2a** is a promising candidate for use as an additive that can help organize fullerenes in ways that enhance the performance of thin-film devices such as solar cells.[20–22] The cocrystals confirm that C_{60} can accommodate one or two capping molecules of oxide **2a**, but no examples with more than two have been observed, despite the use of excess oxide. As the number of capping molecules increases, the number of neighboring molecules of C_{60} generally decreases, as expected, and the shortest fullerene-fullerene distances become longer.

Cocrystallizations of C_{60} and C_{70} with Phosphangulene Sulfide (2b)

2b • C_{60} • CS_2. The consistent formation of cocrystals from solutions containing fullerenes and phosphangulene oxide suggests that the normal crystallization of fullerenes can be disrupted reliably by small molecules that have complementary shapes and cannot crystallize effectively by themselves. As a result, we were confident that phosphangulene sulfide (**2b**) would also interfere with the crystallization of fullerenes. Dark red crystals were obtained when CS_2 was allowed to evaporate slowly from a solution containing sulfide **2b** and C_{60} in a 2.2:1 ratio. X-ray diffraction established that the crystals have the composition **2b** • C_{60} • CS_2 and belong to

the monoclinic space group $P2_1$. Additional crystallographic data are summarized in Table 3.2, and views of the structure are shown in Figures 3.12-3.15.

Table 3.2 : Crystallographic Data for Cocrystals of Phosphangulene Sulfide (**2b**) with C_{60} and C_{70}

Compound	**2b** • C_{60} • CS_2	**2b** • C_{60} • *m*-xylene	**2b** • C_{70} • CS_2
crystallization medium	CS_2	*m*-xylene	CS_2
formula	$C_{79}H_9O_3PS_3$	$C_{86}H_{19}O_3PS$	$C_{89}H_9O_3PS_3$
crystal system	monoclinic	triclinic	monoclinic
space group	$P2_1$	$P\bar{1}$	$P2_1$
a (Å)	13.0898(8)	13.0855(6)	13.2521(15)
b (Å)	14.0998(9)	13.4725(7)	14.4547(15)
c (Å)	13.3595(8)	15.6662(7)	25.261(3)
α (°)	90	76.899(3)	90
β (°)	118.467(3)	87.109(3)	90.153(6)
γ (°)	90	61.864(2)	90
V (Å³)	2167.6(2)	2367.0(2)	4838.9(9)
Z	2	2	4
Z'	1	1	2
T (K)	100	100	100
ρ_{calc} (g cm^{-3})	1.736	1.632	1.720
λ (Å)	1.34139	1.34139	1.34139
μ (mm^{-1})	1.609	0.965	1.486
R_1, I > 2σ(I)	0.0563	0.0653	0.0926
R_1, all data	0.0657	0.0951	0.1001
wR_2, I > 2σ(I)	0.1201	0.1272	0.2402
wR_2, all data	0.1286	0.1415	0.2470
measured reflections	31921	58054	211874
independent reflections	9390	10631	9738
observed reflections	8529	8001	8708
GoF	1.134	1.080	1.068

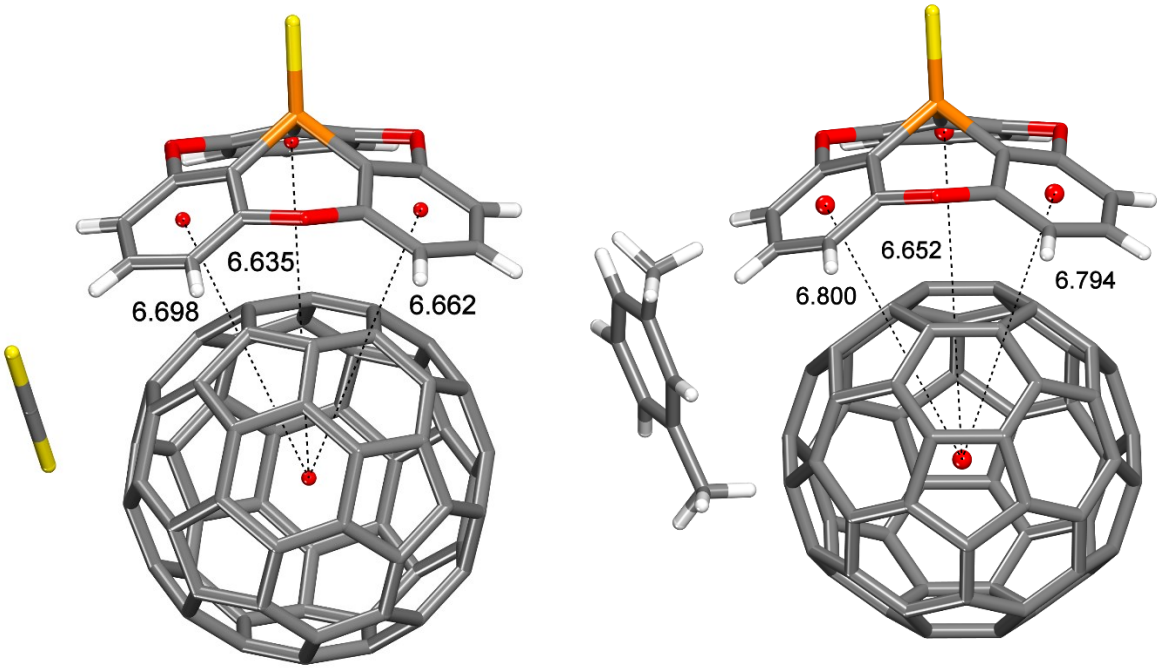

Figure 3.12 : (a) View showing how C_{60} is singly capped by phosphangulene sulfide in the structure of 1:1 cocrystals grown from CS_2. (b) Analogous view of the structure of 1:1 cocrystals grown from *m*-xylene. Atoms of carbon are shown in gray, hydrogen in white, oxygen in red, phosphorus in orange, and sulfur in yellow. Centroids of C_{60} and the aromatic rings of sulfide **2b** are marked by red circles, and centroid-centroid distances are given in Å.

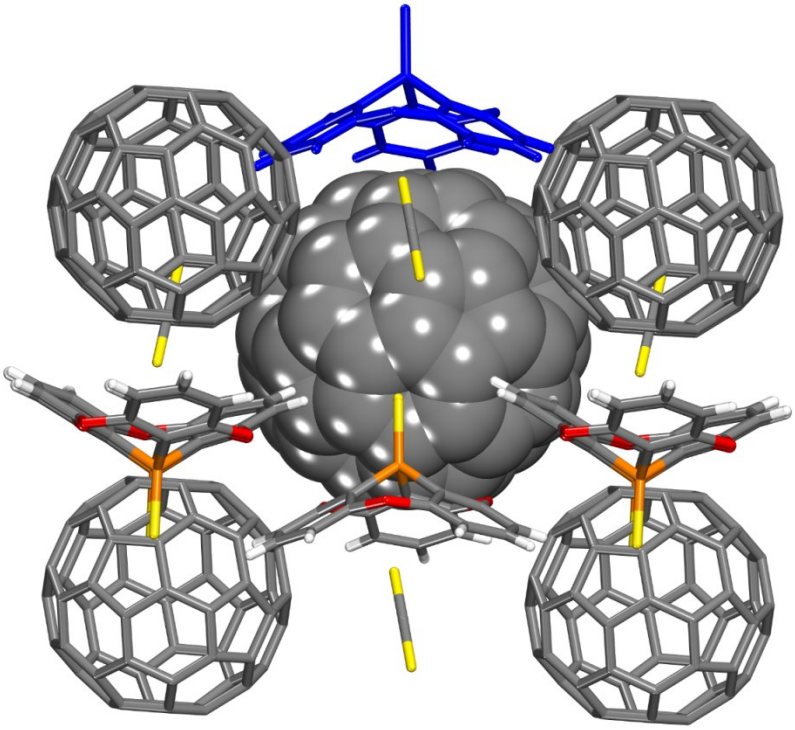

Figure 3.13 : Representation of the structure of 1:1 cocrystals of phosphangulene sulfide and C_{60} grown from CS_2, showing the environment of a central molecule of C_{60} (space-filling image), with a capping molecule of sulfide **2b** (blue), four contacting molecules of C_{60}, and various other interacting molecules of sulfide **2b** and CS_2. Unless indicated otherwise, atoms are shown in their standard colors.

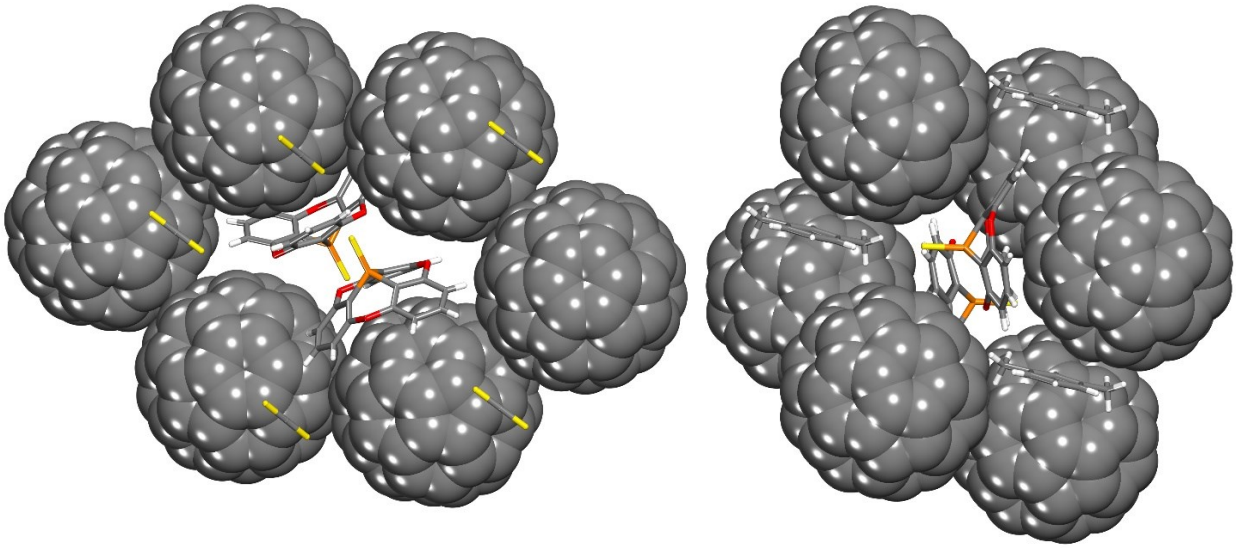

a **b**

Figure 3.14 : (a) View along the *b*-axis showing the structure of 1:1 cocrystals of phosphangulene sulfide and C_{60} grown from CS_2. Hexagonally-arranged columns of fullerenes separated by molecules of CS_2 lie along the *b*-axis and define channels that include capping molecules of sulfide **2b.** (b) Analogous view along the *c*-axis portraying the closely related structure of 1:1 cocrystals of sulfide **2b** and C_{60} grown from *m*-xylene. Atoms are shown in their standard colors.

Each molecule of C_{60} is singly capped by sulfide **2b** (Figure 3.12), and the distances between the centroids of C_{60} and the aromatic rings of the capping sulfide are normal (6.635−6.698 Å). As shown in Figure 3.13, each molecule of C_{60} also takes part in many other interactions, including π-stacking with the convex face of a second molecule of sulfide **2b** (centroid···centroid distance = 6.734 Å), multiple C-H···π interactions with four other nearby molecules of sulfide **2b** (H···centroid distances in the range 5.946−6.226 Å), and various S···π

interactions with an additional molecule of sulfide **2b** and included molecules of CS_2. In these interactions, the S···centroid distances (6.853−6.929 Å) are shorter than those signifying van de Waals contact between sulfur and C_{60} (7.05 Å). In addition, Figure 3.13 shows that each molecule of C_{60} interacts with four neighboring molecules of C_{60}, with centroid···centroid distances (10.200 and 10.397 Å) shorter than the separation corresponding to van der Waals contact (10.45 Å). These interactions define separated layers of connected fullerenes parallel to the *bc*-plane. As shown in Figure 3.14, columns of fullerenes separated by single molecules of CS_2 are aligned with the *b*-axis in a hexagonal pattern that creates channels for the inclusion of capping molecules of sulfide **2b**. In the channels, adjacent molecules of sulfide **2b** are oriented with their dipoles opposed, and they take part in C-H···S interactions with an H···S distance (2.768 Å) shorter than the separation indicating van der Waals contact (3.00 Å). Cocrystallization confirms that phosphangulene oxide and sulfide both have an affinity for C_{60} and are able to disrupt its normal association, without eliminating fullerene-fullerene contacts completely.

2b • C_{60} • *m*-xylene. We observed closely similar structural features in crystals grown by allowing *m*-xylene to evaporate slowly from a solution containing sulfide **2b** and C_{60} in a 2.2:1 ratio. The crystals proved to have the composition **2b** • C_{60} • *m*-xylene and to belong to the triclinic space group $P\bar{1}$. Table 3.2 summarizes additional crystallographic data, and Figures 3.12b, 3.14b and 3.15 provide views of the structure. Again, each molecule of C_{60} is capped by a single molecule of sulfide **2b** (Figure 3.12b), and the distances between the centroids of C_{60} and the aromatic rings of the capping sulfide **2b** are normal (6.652−6.800 Å). Each molecule of C_{60} also forms multiple C-H···π, S···π, and O···π interactions with five other nearby

molecules of sulfide **2b** and with a molecule of *m*-xylene (Figure 3.15). In addition, each molecule of C_{60} interacts with four neighboring fullerenes, with centroid···centroid distances (9.859−10.080 Å) shorter than the separation corresponding to van der Waals contact (10.45 Å). The images in Figures 14a and 14b highlight the close structural similarity of cocrystals of sulfide **2b** and C_{60} grown from CS_2 and *m*-xylene. In both cases, hexagonal arrays of columns consisting of molecules of C_{60} separated by molecules of solvent define channels that include capping molecules of sulfide **2b**.

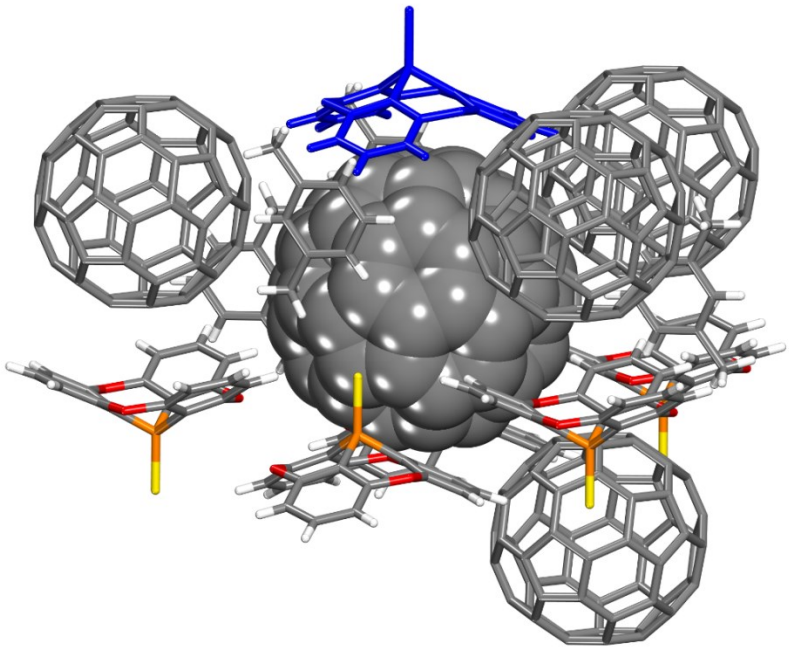

Figure 3.15 : Representation of the structure of 1:1 cocrystals of phosphangulene sulfide and C_{60} grown from *m*-xylene, showing the environment of a central molecule of C_{60} (space-filling image), with a capping molecule of sulfide **2b** (blue), four close C_{60} neighbors, and various other interacting molecules of sulfide **2b** and *m*-xylene. Unless indicated otherwise, atoms are

shown in their standard colors. C_{60} is disordered and is shown using a simplified representation.

2b • C_{70} • CS_2. We reasoned that factors underlying the cocrystallization of C_{60} with phosphangulene oxide and sulfide, including their complementary shapes and inability to form efficiently packed structures by themselves, would also favor cocrystallizations with other fullerenes. Allowing CS_2 to evaporate slowly from a solution containing sulfide **2b** and C_{70} in a 2.2:1 ratio yielded crystals were found to have the composition **2b** • C_{70} • CS_2 and to belong to the monoclinic space group $P\bar{1}$. Other crystallographic data appear in Table 3.2, and views of the structure are provided in Figures 3.16-3.17. C_{70} is shaped like a prolate spheroid, with a long axis, an equator, and two poles. Intermolecular distances were therefore assessed by defining three centroids, one at the molecular center (shown in red in Figure 3.16) and two pseudocentroids (blue) slightly displaced along the axis toward each pole, at the centroids of imaginary C_{60} subunits created by removing C_{10} from the poles of C_{70} (the C_5 ring and the five directly attached atoms of carbon). In this way, intermolecular distances at the poles can be compared directly with those at the equator, as well as with those measured for C_{60} in other structures.

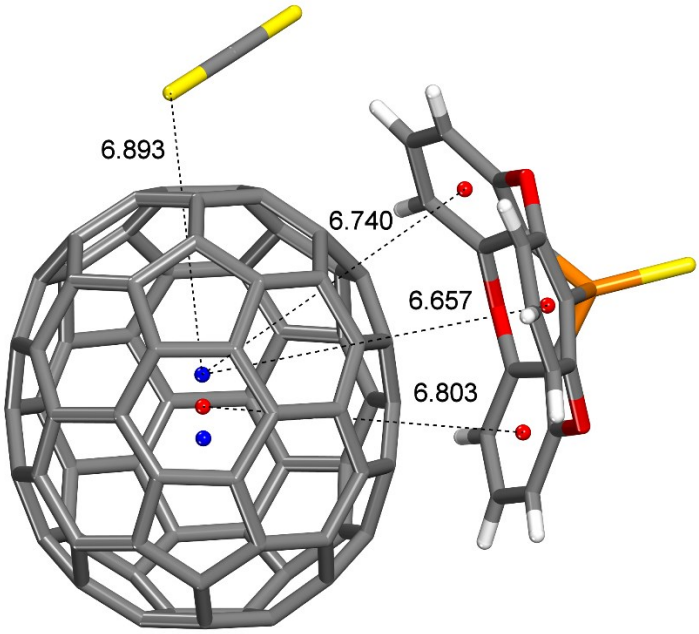

Figure 3.16 : Representative view of the structure of 1:1 cocrystals of phosphangulene sulfide and C_{70} grown from CS_2. The view shows one of two symmetry-inequivalent molecules of C_{70} capped near the equator by a molecule of sulfide **2b**. An interacting molecule of CS_2 is also shown. Atoms are drawn in their standard colors. The centroids of C_{70} and the aromatic rings of sulfide **2b** are indicated by red circles, and two pseudocentroids in blue correspond to C_{60} subunits of the fullerene. Interactions are represented by broken lines, and distances are given in Å.

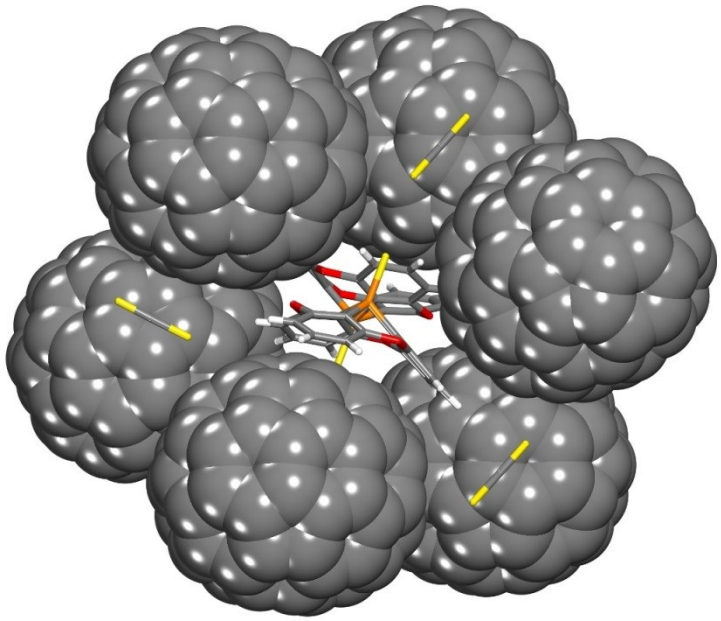

Figure 3.17 : View along the *b*-axis showing the structure of 1:1 cocrystals of phosphangulene sulfide and C_{70} grown from CS_2. Hexagonally-arrayed columns of fullerenes separated by molecules of CS_2 lie along the *b*-axis and define channels that include capping molecules of sulfide **2b**. Atoms are shown in their standard colors.

Each of the two symmetry-inequivalent molecules of fullerene in the asymmetric unit is capped near the equator by a single molecule of sulfide **2b** (Figure 3.16), and the distances between the centroids of the aromatic rings of the capping sulfide **2b** and the closest centroid of C_{70} lie in the normal range. Each molecule of C_{70} also forms C-H···π, π···π, S···π, and O···π interactions with nearby non-capping molecules of sulfide **2b**. In addition, each molecule of C_{70} interacts with six neighboring fullerenes, with centroid···centroid distances shorter than the separation corresponding to van der Waals contact. As shown in Figure 3.17,

cocrystals of sulfide **2b** with C_{70} are structurally similar to those formed with C_{60}. In all cases observed, columns of fullerenes separated by molecules of solvent are arrayed hexagonally along a single crystallographic axis, thereby forming channels that accommodate capping molecules of sulfide **2b**. Cocrystallization with both C_{60} and C_{70} shows that phosphangulene chalcogenides are generally effective agents for prying fullerenes apart, without separating them altogether.

Cocrystallizations of C_{60} with Phosphangulene Selenide (2c)

2c • C_{60} • CS_2. The consistent behavior of phosphangulene oxide and sulfide shows that the normal crystallization of fullerenes can be foiled reliably by small molecular additives, when they are designed to have complementary shapes and to be unable to crystallize effectively by themselves. We therefore expected the corresponding selenide **2c** to form cocrystals with fullerenes. Slow evaporation of CS_2 from a solution containing selenide **2c** and C_{60} in a 2.2:1 ratio yielded dark red crystals that proved to have the composition **2c** • C_{60} • CS_2, to belong to the monoclinic space group $P2_1$, and to be isostructural with cocrystals formed by sulfide **2b** under analogous conditions. Table 3.3 presents additional crystallographic data, and Figures 3.12-3.14 provide views of the corresponding isostructural cocrystals formed by sulfide **2b**. Again, each molecule of C_{60} is capped by a single molecule of phosphangulene chalcogenide, and the distances between the centroids of C_{60} and the aromatic rings of the capping selenide **2b** (6.639−6.701 Å) are all shorter than the separation corresponding to van der Waals contact (6.90 Å). Each molecule of C_{60} interacts with four neighboring molecules of C_{60}, with centroid to centroid distances (10.214−10.439 Å) shorter than the separation corresponding to van der Waals contact (10.45 Å).

Table 3.3 : Crystallographic Data for Cocrystals of Phosphangulene Selenide (**2c**) with C_{60}

Compound	**2c** • C_{60} • CS_2	2 **2c** • 2 C_{60} • PhCl
crystallization medium	CS_2	PhCl
formula	$C_{79}H_9O_3PS_2Se$	$C_{162}H_{23}ClO_6P_2Se_2$
crystal system	monoclinic	monoclinic
space group	$P2_1$	$P2_1/c$
a (Å)	13.0971(4)	15.7478(5)
b (Å)	14.1629(4)	13.2732(4)
c (Å)	13.3737(4)	42.7568(13)
α (°)	90	90
β (°)	118.4105(11)	98.284(2)
γ (°)	90	90
V (Å³)	2181.95(11)	8844.3(5)
Z	2	4
Z'	1	1
T (K)	100	100
ρ_{calc} (g cm^{-3})	1.796	1.742
λ (Å)	1.34139	1.34139
μ (mm^{-1})	1.945	1.527
R_1, I > 2σ(I)	0.0648	0.1393
R_1, all data	0.0688	0.2034
wR_2, I > 2σ(I)	0.1768	0.3330
wR_2, all data	0.1824	0.3816
measured reflections	82538	28233
independent reflections	10019	19868
observed reflections	9245	11911
GoF	1.081	1.054

2 2c • 2 C_{60} • PhCl. Similar structural features were observed in crystals produced by the slow evaporation of PhCl from a solution containing selenide **2c** and C_{60} in a 2.2:1 ratio. Crystals grown under these conditions were found to have the composition 2 **2c** • 2 C_{60} • PhCl and to belong to the monoclinic space group $P2_1/c$. Additional crystallographic data appear in Table 3.3, and views of the structure are shown in Figures 3.18-3.19. Again, each of the two symmetry-inequivalent molecules of C_{60} in the asymmetric unit is capped by a single molecule

of selenide **2c** (Figure 3.18), with distances between the centroids of C_{60} and the aromatic rings of the capping selenide **2c** lying in the normal range (6.706−6.855 Å in the case shown in Figure 3.18). Each molecule of C_{60} also interacts with five other molecules of selenide **2c** in various ways that place atoms of H, C, and S at distances shorter than the sum of the van de Waals radii of C_{60} (5.22 Å) and the atoms involved (Figure 3.19). In addition, Figure 3.19 shows that each molecule of C_{60} interacts with five neighboring molecules of C_{60}, with centroid to centroid distances shorter than the separation corresponding to van der Waals contact (10.45 Å).

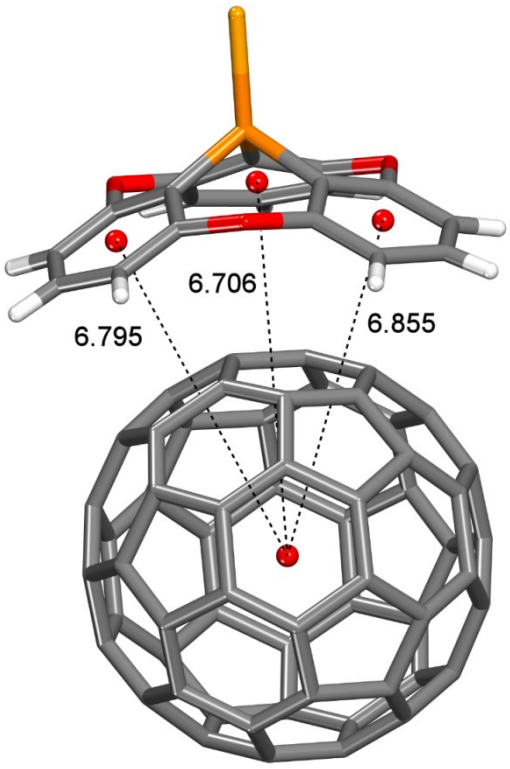

Figure 3.18 : Representative view of the structure of 1:1 cocrystals of phosphangulene selenide and C_{60} grown from PhCl, showing how one of the symmetry-inequivalent molecules of C_{60} is capped by selenide **2c**. Atoms of carbon are shown in gray, hydrogen in white, oxygen in red, phosphorus in orange, and selenium in yellow-orange. Centroids of C_{60} and the aromatic rings of selenide **2c** are marked by red circles, and centroid-centroid distances are given in Å. C_{60} is disordered and is shown using a simplified representation. Guest molecules of PhCl are omitted for clarity.

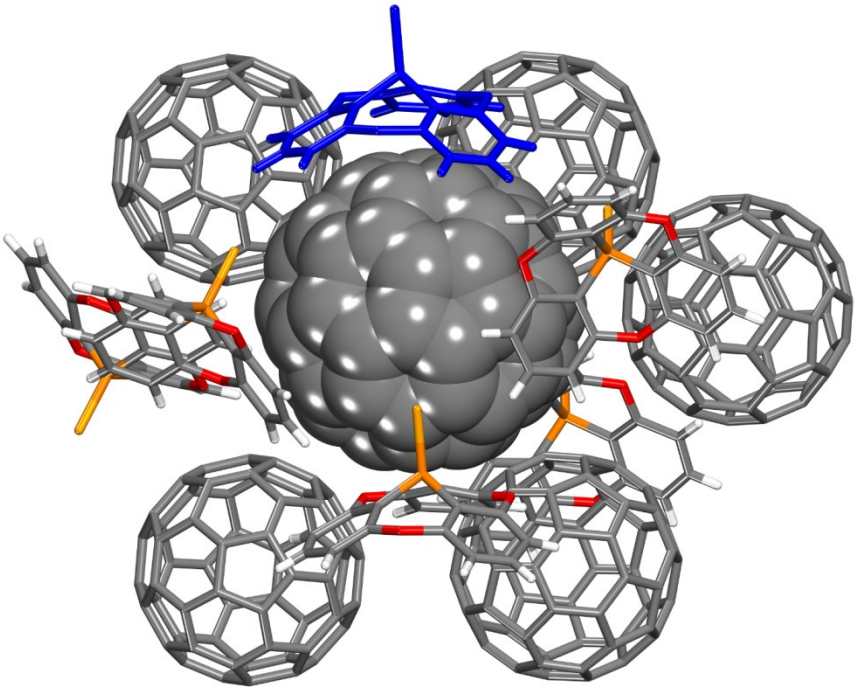

Figure 3.19 : Representative view of the structure of 1:1 cocrystals of phosphangulene selenide (**2c**) and C_{60} grown from PhCl, showing the environment of a central molecule of C_{60} (space-filling image), a capping molecule of selenide **2c** (blue), five neighboring molecules of C_{60}, and various other interacting molecules of selenide **2c** and PhCl. Unless indicated

otherwise, atoms are shown in their standard colors. Molecules of C_{60} are disordered and are shown using a simplified representation. Guest molecules of PhCl are omitted for clarity.

3.2.4 Conclusions

Fullerenes and their derivatives are unique globular molecules with convex electron-deficient aromatic surfaces. Their self-association and packing in crystals are subjects of inherent interest. In addition, the compounds are widely used as electron-accepting components in the active layers of carbon-based optoelectronic devices such as solar cells. Optimizing the performance of these devices normally requires preventing fullerenes and related compounds from associating extensively in ways that lead to undesirable phase separation and subsequent crystallization. At the same time, however, a degree of order featuring strong fullerene-fullerene contacts must be maintained to facilitate electronic mobility. Striking the proper balance between favoring and disfavoring fullerene-fullerene contacts is the key to achieving optimal performance.

One way to meet this challenge is to employ agents that interfere with the normal association of fullerenes and their derivatives, thereby reducing fullerene-fullerene contacts but not eliminating them altogether. To better understand how such agents can be created, we have examined the cocrystallization of fullerenes with small molecules that have concave aromatic surfaces designed to be topologically and electronically complementary to the convex surfaces of fullerenes.[18] Particularly promising agents are those that are not merely complementary, but are also specifically devised so that they cannot crystallize effectively by themselves and have no attractive options except to associate with fullerenes. Our results suggest that phosphangulene chalcogenides **2a**–**c** are agents of this type. Despite their small size, all three

compounds cocrystallize with C_{60} and C_{70} to form structures in which the fullerenes are forced to accept a degree of separation, but fullerene-fullerene contacts are not eliminated completely.

Our study of phosphangulene chalcogenides **2a**–**c** helps reveal how to design other small molecular agents that obstruct the normal crystallization of fullerenes and induce them to adopt new structures. In particular, compounds **2a**–**c** have topologies that block efficient stacking and prevent crystallization from occurring according to the pattern established by phosphangulene. In addition, the concave surfaces of compounds **2a**–**c** are geometrically and electronically complementary to the convex surfaces of fullerenes but are too small to envelop them completely. Fullerene-fullerene contacts are thereby partially interrupted in the resulting cocrystals, but the structures typically incorporate fullerene-rich regions in which continuous close contact is maintained. This offers vast scope for engineering new periodic arrangements of connected fullerenes, as suggested by the varied patterns observed in cocrystals formed by phosphangulene oxide and C_{60}, which include layers, columns, and even isolated pairs (Figure 3.20).

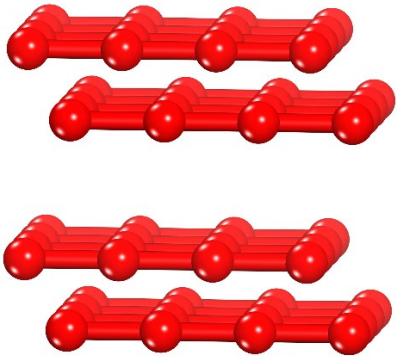

C_{60} Layers

(**2a** • C_{60} • PhCl)

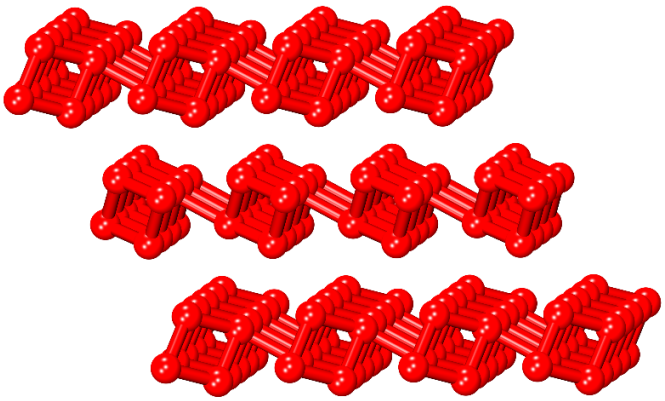

C_{60} Layers

(6 **2a** • 4 C_{60} • MeOH)

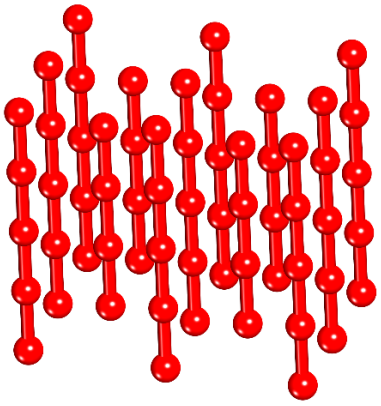

C_{60} Columns

(2 **2a** • C_{60} • PhMe)

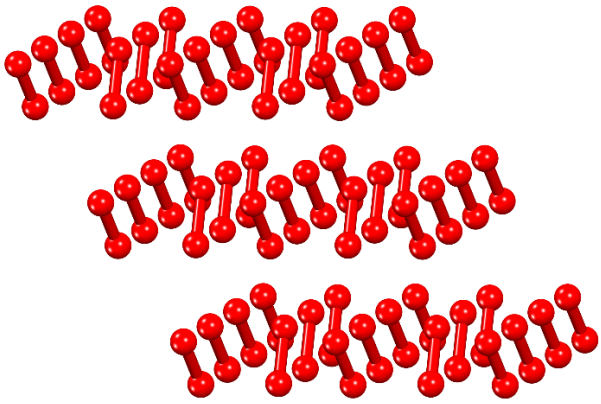

C_{60} Pairs

(3 **2a** • C_{60} • 3 *o*-xylene)

Figure 3.20 : Ordered arrangements of connected fullerenes observed in cocrystals formed by phosphangulene oxide and C_{60}. In each image, fullerenes are represented by red spheres and their connections by red sticks.

In nearly all of the cocrystals studied, phosphangulene chalcogenides **2a**–**c** place fullerenes in continuous contact, as required for effective bulk heterojunctions in solar cells. We are therefore optimistic that chalcogenides **2a**–**c** or other sets of compounds devised according to similar principles can be used as additives to help create or maintain productive organization of fullerenes in various complex material. In addition, sets of cocrystals such as those produced by chalcogenides **2a**–**c** provide libraries of well-defined related materials in which fullerenes in direct contact are positioned in varying ways. As a result, these materials offer an opportunity to probe systematically how conductivity and other properties depend on molecular organization.

3.2.5 Experimental Section

All reagents and solvents were obtained from commercial sources and used without further purification unless otherwise indicated. Phosphangulene and chalcogenides **2a**–**c** were prepared by published procedures.[5]

General procedure for cocrystallizations

Cocrystallizations of phosphangulene chalcogenides **2a**–**c** with fullerenes were achieved by a combinatorial approach using 60 different conditions. Stock solutions of the three chalcogenides (oxide **2a**, sulfide **2b**, and selenide **2c**) and two fullerenes (C_{60} and C_{70}) were prepared in ten different solvents in which fullerenes have relatively high solubilities (toluene, *m*-xylene, *o*-xylene, *p*-xylene, mesitylene, chlorobenzene, *o*-dichlorobenzene, 1,1,2,2-tetrachloroethane, CS_2, and thiophene). The stock solutions, with concentrations of 5.2 mM (phosphangulene chalcogenides) and 2.4 mM (fullerenes), were combined to give mixtures

with chalcogenide:fullerene ratios of 2.2:1. The resulting mixtures were placed in stoppered vials, and slow partial evaporation at 25 °C over the course of several weeks afforded precipitates. From these samples, single crystals were selected for analysis by X-ray diffraction. Cocrystals of composition 6 **2a** • 4 C_{60} • MeOH were grown by adding MeOH to a mixture of stock solutions prepared in toluene, followed by slow evaporation.

Each cocrystallization trial used a combined mass of only 5-6 mg (chalcogenide + fullerene), and the primary objectives were to obtain single crystals and to confirm by structural analysis that cocrystallization had occurred. As a result, bulk precipitates obtained in various trials were not subjected to further study, such as by examining their structural uniformity, nor could we establish yields or characterize cocrystals by methods other than structural analysis. In future work, we plan to examine the conductivity and other properties of individual cocrystals, and we will explore the bulk synthesis of uniform samples of any cocrystals deemed to be of special interest.

Supporting Information Available: Additional crystallographic details, including ORTEP drawings. This material is available free of charge via the Internet at http://pubs.acs.org.

Accession Codes. CCDC 1941637-1941645 contain the supplementary crystallographic data for this paper. These data can be obtained free of charge via www.ccdc.cam.ac.uk/data_request/cif, by emailing data_request@ccdc.cam.ac.uk, or by contacting The Cambridge Crystallographic Data Centre, 12 Union Road, Cambridge CB2 1EZ, UK; fax: +44 1223 336033.

Acknowledgments. We are grateful to the Natural Sciences and Engineering Research Council of Canada, the Ministère de l'Éducation du Québec, the Canada Foundation for Innovation, the Canada Research Chairs Program, and Université de Montréal for financial support.

Notes. The authors declare no competing financial interest.

3.2.6 References

1. Krebs, F. C.; Larsen, P. S.; Larsen, J.; Jacobsen, C. S.; Boutton, C.; Thorup, N. Synthesis, Structure, and Properties of 4,8,12-Trioxa-12c-phospha-4,8,12,12c-tetrahydrodibenzo[*cd*,*mn*]pyrene, a Molecular Pyroelectric. *J. Am. Chem. Soc.* **1997**, *119*, 1208–1216.
2. Madsen, G. K. H.; Krebs, F. C.; Lebech, B.; Larsen, F. K. Evaluation of the Solid State Dipole Moment and Pyroelectric Coefficient of Phosphangulene by Multipolar Modeling of X-ray Structure Factors. *Chem. Eur. J.* **2000**, *6*, 1797–1804.
3. Faldt, A.; Krebs, F. C.; Thorup, N. Synthesis, Structure and Properties of Various Molecules Based on the 4,8,12-Trioxa-4,8,12,12c-tetrahydrodibenzo[*cd*,*mn*]pyrene System with an Evaluation of the Effect Differing Molecular Substitution Patterns has on the Space Group Symmetry. *J. Chem. Soc., Perkin Trans 2* **1997**, 2219–2227.
4. Yamamura, M.; Nabeshima, T. Relationship between the Bowl-Shaped Geometry of Phosphangulene and an Axial Group on the Phosphorus Atom. *Bull. Chem. Soc. Jpn.* **2016,** *89*, 42–49.
5. Heskia, A.; Maris, T.; Wuest, J. D., Foiling Normal Patterns of Crystallization by Design. Polymorphism of Phosphangulene Chalcogenides. *Cryst. Growth Des.* **2019,** *19* (9), 5390-5406.
6. Lee, H.; Park, C.; Sin, D. H.; Park, J. H.; Cho, K. Recent Advances in Morphology Optimization for Organic Photovoltaics. *Adv. Mater.* **2018**, *30*, 1800453.
7. Lai, Y.-Y.; Cheng, Y.-J.; Hsu, C.-S. Applications of Functional Fullerene Materials in Polymer Solar Cells, *Energy Environ. Sci.* **2014**, *7*, 1866–1883.

8. Dang, M. T.; Hirsch, L.; Wantz, G.; Wuest, J. D. Controlling the Morphology and Performance of Bulk Heterojunctions in Solar Cells. Lessons Learned from the Benchmark Poly(3-hexylthiophene):[6,6]-Phenyl-C_{61}-butyric Acid Methyl Ester System. *Chem. Rev.* **2013**, *113*, 3734–3765.

9. Ganin, A. Y.; Takabayashi, Y.; Jeglič, P.; Arčon, D.; Potočnik, A.; Baker, P. J.; Ohishi, Y.; McDonald, M. T.; Tzirakis, M. D.; McLennan, A.; Darling, G. R.; Takata, M.; Rosseinsky, M. J.; Prassides, K. Polymorphism Control of Superconductivity and Magnetism in Cs_3C_{60} Close to the Mott Transition. *Nature* **2010**, *466*, 221–225.

10. Ruoff, R. S.; Tse, D. S.; Malhotra, R.; Lorents, D. C. Solubility of Fullerene (C_{60}) in a Variety of Solvents. *J. Phys. Chem*. **1993**, *97*, 3379–3383.

11. Macovez, R. Physical Properties of Organic Fullerene Cocrystals. *Front. Mater.* **2018**, *4*, 46.

12. Wang, L. Solvated Fullerenes, a New Class of Carbon Materials Suitable for High-Pressure Studies: A Review. *J. Phys. Chem. Solids* **2015**, *84*, 85–95.

13. Neretin, I. S.; Slovokhotov, Yu. L. Chemical Crystallography of Fullerenes. *Russ. Chem. Rev.* **2004**, *73*, 455–486.

14. Yamamura, M.; Hongo, D.; Nabeshima, T. Twofold Fused Concave Hosts Containing Two Phosphorus Atoms: Modules for the Sandwich-Type Encapsulation of Fullerenes in Variable Cavities. *Chem. Sci.* **2015**, *6*, 6373–6378.

15. Yamamura, M.; Sukegawa, K.; Nabeshima, T. Tuning the Depth of Bowl-Shaped Phosphine Hosts: Capsule and Pseudo-Cage Architectures in Host–Guest Complexes with C_{60} Fullerene. *Chem. Commun*. **2015**, *51*, 12080–12083.

16. Yamamura, M.; Saito, T.; Nabeshima, T. Phosphorus-Containing Chiral Molecule for Fullerene Recognition Based on Concave/Convex Interaction. *J. Am. Chem. Soc.* **2014**, *136*, 14299–14306.

17. Johnson, R. D.; Bethune, D. S.; Yannoni, C. S. Fullerene Structure and Dynamics: A Magnetic Resonance Potpourri. *Acc. Chem. Res*. **1992**, *25*, 169−175.

18. Langis-Barsetti, S.; Maris, T.; Wuest, J. D. Molecular Organization of 2,1,3-Benzothiadiazoles in the Solid State. *J. Org. Chem.* **2017**, *82*, 5034−5045.

19. Bürgi, H.-B.; Blanc, E.; Schwarzenbach, D.; Liu, S.; Lu, Y.-j.; Kappes, M. M.; Ibers, J. A. The Structure of C_{60}: Orientational Disorder in the Low-Temperature Modification of C_{60}. *Angew. Chem. Int. Ed.* **1992**, *31*, 640−643.

20. Molina-Ontoria, A.; Gallego, M.; Echegoyen, L.; Pérez, E. M.; Martín, N. Organic Solar Cells Based on Bowl-Shaped Small-Molecules. *RSC Adv.* **2015**, *5*, 31541−31546.

21. Dang, M. T.; Wuest, J. D. Using Volatile Additives to Alter the Morphology and Performance of Active Layers in Thin-Film Molecular Photovoltaic Devices Incorporating Bulk Heterojunctions. *Chem. Soc. Rev.* **2013**, *42*, 9105−9126.

22. Schiros, T.; Kladnik, G.; Prezzi, D.; Ferretti, A.; Olivieri, G.; Cossaro, A.; Floreano, L.; Verdini, A.; Schenck, C.; Cox, M.; Gorodetsky, A. A.; Plunkett, K.; Delongchamp, D.; Nuckolls, C.; Morgante, A.; Cvetko, D.; Kymissis, I. Donor-Acceptor Shape Matching Drives Performance in Photovoltaics. *Adv. Energy Mater*. **2013**, *3*, 894−902.

3.2.7 Table of Contents Graphic

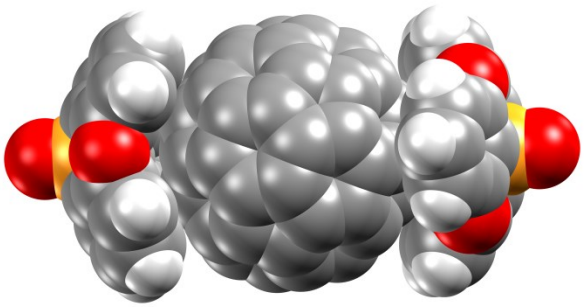

3.3 Conclusions

Nous avions comme objectif de produire des cocristaux avec des fullerènes pour la série des chalcogénures. Nous avons postulé que, parce que ces dérivés du phosphangulène sont hautement polymorphiques et que les structures cristallines de ceux-ci ont souvent un paramètre *Z'* élevé, nous récolterions des cocristaux.

C'est effectivement ce que nos travaux rapportent. Nous avons obtenu une dizaine de cocristaux pour les trois dérivés de la série. Les diverses structures décrites présentent des morphologies variées en ce qui a trait à l'empilement des fullerènes (colonnes, feuillets, doublets isolés et d'autres organisations). Ceci s'inscrit dans le cadre de l'objectif plus large vers le contrôle morphologique des matériaux à base de fullerènes.

À partir de ce point dans le projet, le concept de la surface concave difficile à empiler a été poussé plus loin vers la production de composés présentant plusieurs de ces surfaces où pourront se nicher les fullerènes.

Chapitre 4 : Complexes de coordination du phosphangulène sur les métaux de transition

4.1 Introduction

Après avoir obtenu des associations concave-convexe avec des molécules présentant une surface concave conjuguée, nous nous sommes fixés un objectif plus ambitieux : de produire des composés comportant plusieurs de ces surfaces propices à l'association avec les fullerènes. Une stratégie simple pour atteindre cet objectif consiste à associer plusieurs molécules de phosphangulène ensemble en utilisant l'atome de phosphore comme site de liaison.

Les phosphines offrent une réactivité très intéressante à exploiter en ce sens de par leur atome de phosphore, qui font d'elles des nucléophiles et des bases de Lewis. Ces caractéristiques furent en effet exploitées depuis bon nombre de décennies dans la chimie de coordination où les phosphines constituent des ligands de choix pour la complexation de métaux.

4.1.1 Les phosphines comme ligands

L'emploi des phosphines comme ligands est répandu depuis longtemps. Comme l'azote, le phosphore fait partie de la famille des pnictogènes. Le phosphore (III) possède un doublet libre qui peut participer dans la formation de nouvelles liaisons telles les liens datifs entre les pairs base et acide de Lewis. Les amines et les phosphines ont souvent une géométrie pyramidale. Alors qu'à température pièce, les amines procèdent normalement à des inversions rapides de la géométrie pyramidale, le processus est plus lent pour les phosphines analogues et la barrière d'inversion est plus élevée. Ceci a pour conséquence de leur conférer une structure plus fixe. Le doublet libre d'électrons localisé sur le pnictogène est également plus disponible chez la phosphine que chez l'amine. Cette différence structurelle est la raison pourquoi les phosphines sont en général de meilleurs ligands.[vii]

Il existe de nombreuses phosphines disponibles commercialement vendues à des fins de ligands dans des réactions catalytiques. La nature de la phosphine peut avoir une influence sur l'issue de la catalyse. Certains de ces ligands sont (1) bidentates afin de forcer une disposition cis sur d'autres substituants du complexe, (2) chiraux dans le but d'obtenir sélectivement un seul énantiomère, ou (3) massifs afin d'induire un encombrement stérique autour du métal. Parmi les paramètres intrinsèques au ligand pouvant influencer ses performances de coordination, on compte l'encombrement stérique, l'angle de cône et les propriétés électroniques.

[vii] Downing, J. H.; Smith, M. B., 1.12 - Phosphorus Ligands. Dans *Comprehensive Coordination Chemistry II*, McCleverty, J. A.; Meyer, T. J., Eds. Pergamon: Oxford, 2003; pp 253-296.

Un des ligands les plus répandus dans la famille des phosphines est la triphénylphosphine. Sa simplicité la rend facile à synthétiser et peu coûteuse. Il s'agit également d'un composé facile à manipuler dû au fait qu'il est solide à température ambiante et assez stable à l'air. En effet, de nombreuses phosphines tertiaires s'oxydent rapidement à l'air et peuvent parfois même être pyrophoriques. Tout comme la triphénylphosphine, le phosphangulène est une triarylphosphine avec trois cycles benzèniques. Il nous a semblé approprié de nous inspirer de la chimie de coordination de la triphénylphosphine afin de prédire le comportement du phosphangulène. Ainsi, les complexes métalliques que nous traiterons dans le présent chapitre sont basés sur des complexes de triphénylphosphine, qui constituent ainsi des références à des fins de comparaison. Quoique divers métaux peuvent être coordonnés par des phosphines, dans cette étude préliminaire nous avons étudié surtout la complexation de Ag(I) et de Cu(I), qui sont connus pour former un grand nombre de complexes avec la triphénylphosphine.

4.1.2 Objectifs

La branche du projet de thèse décrit dans ce chapitre traite d'une série de complexes métalliques composés du phosphangulène. Dans un premier temps, les présents travaux auront pour buts (1) de synthétiser et d'étudier des complexes analogues à ceux de la triphénylphosphine et (2) de comparer les qualités de ligand du phosphangulène avec celles de la molécule de référence, la triphénylphosphine. L'objectif ultime étant de produire des complexes d'association avec les fullerènes, nous tenterons d'obtenir des structures dans lesquelles les fullerènes viendront se loger dans les cavités créées par les multiples surfaces concaves présentes chez les complexes métalliques du phosphangulène.

4.2 Article 3

Article publié dans

J. Am. Chem. Soc. **2019**, *141*(47), 18740-18753.

Building Large Structures with Curved Aromatic Surfaces by Complexing Metals with Phosphangulene

Alice Heskia, Thierry Maris, Pedro M. Aguiar, and James D. Wuest*

Département de Chimie, Université de Montréal, Montréal, Québec H3C 3J7 Canada

*Author to whom correspondence may be addressed.

E-mail: *james.d.wuest@umontreal.ca*

4.2.1 Abstract

Phosphangulene (**1**) is a hexacyclic triarylphosphine with a distinctive conical shape and an electron-rich aromatic surface that is geometrically and electronically complementary to fullerenes such as C_{60} and C_{70}. As a result, suitable derivatives of phosphangulene can cocrystallize with fullerenes or even bind them in solution. Surprisingly, previous work has largely overlooked the potential of phosphangulene to form complexes with metals, which offers a simple way to create large molecular structures with curved aromatic surfaces. To explore this approach, we have prepared and characterized a series of complexes of phosphangulene with Ag^+ and Cu^+. Our results show that Phang ligands are exceptional for many reasons. In particular, they can yield metal complexes with unique coordination, and the metal centers hold the concave aromatic surfaces of multiple ligands in various divergent arrays. Moreover, the rigid conical structure of phosphangulene gives the complexes an awkward shape that cannot be packed efficiently without complementary partners. As a result, metal complexes of phosphangulene are predisposed to cocrystallize with fullerenes, thereby yielding materials in which metals and fullerenes are brought together in ordered arrangements.

4.2.2 Introduction

Phosphangulene (**1**) is a hexacyclic triarylphosphine first reported by Krebs and coworkers in 1997.[1] Molecules of the compound have a well-defined conical shape and an electron-rich aromatic surface (Figure 4.1). Studies of phosphangulene and its derivatives during the last twenty years have reflected a preoccupation with the effects of their distinctive non-planar topology.[1–11] For example, the shape helps induce molecules of phosphangulene to crystallize as parallel π-stacks.[2] In addition, the concave electron-rich aromatic surface of phosphangulene is geometrically and electronically complementary to the convex electron-poor surfaces of fullerenes such as C_{60} and C_{70}. As a result, various derivatives of phosphangulene have been used to bind fullerenes in solution and to produce cocrystals that control how fullerenes are positioned in the solid state.[7–10] For such reasons, phosphangulene and related compounds have drawn the attention of chemists, and the seminal early work of Krebs and coworkers has led to a surge of creative new studies in recent years, particularly by the group of Nabeshima.[5–11]

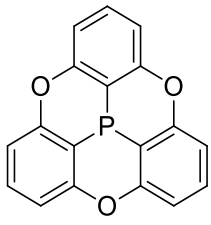

1

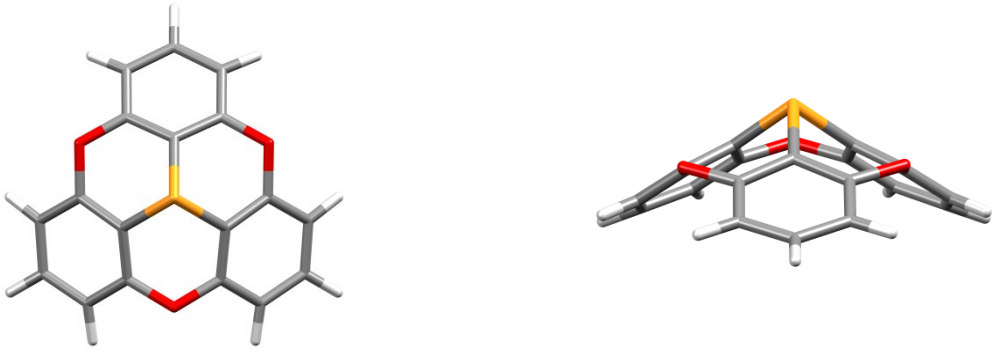

Figure 4.1 : Representations of the molecular structure of phosphangulene (**1**) in crystals grown from ethyl acetate,[1] as viewed along the C_3 axis and perpendicular to the axis. Atoms of carbon are shown in gray, hydrogen in white, oxygen in red, and phosphorus in yellow-orange.

Motivation to learn how to bind fullerenes and control their arrangement in complex materials springs in part from the widespread use of C_{60} and related structures as electron acceptors in the active layers of thin-film molecule-based optoelectronic devices such as solar cells. When properly arranged with respect to other components of the layers,[12–14] fullerenes and their derivatives can accept electrons from the excited states of nearby chromophores and then serve as a conduit for transporting electrons to the cathode via chains of fullerene-fullerene contacts. In addition, crystalline salts of fulleride anions can act as high-temperature superconductors, as shown by the face-centered cubic phase and body-centered cubic phase of Cs_3C_{60}.[15] These examples show the importance of being able to control how fullerenes are positioned in complex materials. One possible way to manipulate organization is by using shape-complementary additives, such as derivatives of phosphangulene.[10,16]

By focusing on the conical shape of phosphangulene, previous work has not fully exploited other useful properties of the compound. In particular, researchers have largely overlooked its ability to form complexes with transition metals, which offers a simple way to create complex molecular structures with curved aromatic surfaces for binding fullerenes. This strategy is appealing for two main reasons: (1) It gives access to an unlimited range of complexes with concave electron-rich aromatic surfaces that diverge from metals in geometrically predictable ways, using a one-step procedure in which phosphangulene is combined with various inorganic or organometallic precursors; and (2) the strategy promises to yield materials with uniquely ordered structures that incorporate both metals and unfunctionalized fullerenes. Other metal-fullerene networks are known, but they have typically been constructed not from fullerenes, but from derivatives that have been exohedrally functionalized to add sites of coordination.[17–19]

When multiple molecules of phosphangulene are bound to a metallic core, the total aromatic surface area of the complex will be large, and it will be subdivided into patches contributed by each ligand. Each bound phosphangulene can surround only about one-fourth of the total surface of C_{60}, as shown by the structures of cocrystals of phosphangulene chalcogenides with fullerenes.[10] As a result, complexes of phosphangulene are well designed to interact with neighboring fullerenes without completely enveloping them. In contrast, many previous efforts to devise suitable partners for binding fullerenes have targeted ways to surround them.[20,21] When encapsulation is achieved, however, fullerene-fullerene contacts are severely reduced or even eliminated, along with properties of conductivity or superconductivity that require extensive electronic communication between fullerenes. For this reason, it is important to

learn how to devise compounds that can interact with fullerenes and control how they are positioned, but do not eliminate fullerene-fullerene contacts altogether.

We based our choice of targets for initial study on the notion that phosphangulene would yield metal complexes similar in stoichiometry and structure to those formed by triphenylphosphine. In fact, however, phosphangulene and triphenylphosphine differ geometrically and electronically in significant ways. The geometric differences can be assessed by comparing cone angles defined by $\theta = 2\cos^{-1}(d/R)$, where d is the distance from the atom of phosphorus to the plane defined by the three most distant atoms of carbon in the aryl rings, and R is the average distance from phosphorus to the same three atoms. Measured in this way using molecular geometries observed in the crystal structures of unbound ligands, θ is approximately 116° for phosphangulene,[45] 132° for triphenylphosphine (triclinic form),[22] and 138° for tris(2,6-dimethoxyphenyl)phosphine.[23] In addition, the average C-P-C angles in the three structures are 93.0°, 102.1°, and 104.4°, respectively, and the average C-P distances are 1.80 Å, 1.84 Å, and 1.84 Å. The similarity of the cone angles, C-P-C angles, and C-P distances of triphenylphosphine and tris(2,6-dimethoxyphenyl)phosphine suggests that *ortho*-substitution by methoxy does not lead to major changes in geometry involving the central atom of phosphorus. Nevertheless, triphenylphosphine forms 4:1 complexes with Ag(I) and Cu(I),[24] whereas the slightly more bulky tris(2,4,6-trimethoxyphenyl)phosphine yields 2:1 complexes.[25]

Previous work has established that phosphangulene, triphenylphosphine, and oxygenated derivatives such as tris(2,6-dimethoxyphenyl)phosphine also differ electronically, as assessed by computational studies and by experimental measurements of basicity, nucleophilicity, and

ease of oxidation. The notably small average C-P-C angle in phosphangulene (93.0°) establishes that the lone pair orbital has high *s* character, and cyclic voltammetry has shown that the compound undergoes irreversible oxidation at 1.55 V (1 M Bu_4N^+ ClO_4^- in CH_2Cl_2), whereas triphenylphosphine is more easily oxidized (1.05 V).[5] The conjugate acid of tris(2,6-dimethoxyphenyl)phosphine (pK_a 9.33)[26] is much weaker than that of triphenylphosphine (pK_a 2.73).[27] Similarly, tris(2,6-dimethoxyphenyl)phosphine is a stronger Lewis base than triphenylphosphine, as measured by their reactions with benzhydryl cations.[28] Moreover, the S_N2 reaction of tris(2,6-dimethoxyphenyl)phosphine with BuBr is 620 times faster than that of triphenylphosphine under standard conditions,[29] and tris(2,6-dimethoxyphenyl)phosphine also reacts faster in other nucleophilic substitutions.[30] Together, these data suggested to us that the reduced bulk and high oxygen-substitution of phosphangulene would help make it an effective ligand for susceptible metals; however, the high *s* character of the lone pair orbital prepared us to observe behavior atypical of triarylphosphines.

4.2.3 Results and Discussion

Syntheses of Phosphangulene and its Metal Complexes. Phosphangulene was made by a modification of the original method of Krebs and coworkers.[1,11] Solutions containing various ratios of phosphangulene and metal salts were prepared, and complexes were induced to crystallize by partial evaporation. To simplify describing the composition of complexes, phosphangulene will be abbreviated as Phang. In certain cases, the isolated solids consisted largely of a single crystalline phase, could be obtained in satisfactory yields, and were characterized by selected spectroscopic methods, in addition to being subjected to structural analysis by X-ray diffraction. In general, however, crystals were obtained in small quantities,

and their structures do not necessarily reveal the identity of the major solid product of each reaction. Complexes of various metals were crystallized and characterized, but the present paper describes only the binding of Ag(I) and Cu(I) by Phang.

$[Ag(Phang)_4]^+$ BF_4^-. The coordination of Ag(I) by phosphines has been studied for many decades, and the subject has been reviewed.[31] Tetracoordination of Ag(I) to give $[Ag(PPh_3)_4]^+$ was first reported in 1960,[21] and the structures of many salts have been published.[32-41] As a result, we began by targeting the preparation of salts of $[Ag(Phang)_4]^+$. Single crystals of the BF_4^- salt were obtained by combining $AgBF_4$ with phosphangulene in CH_2Cl_2 in a 1:4 ratio, followed by slow evaporation of solvent under N_2 in the dark. Analysis by X-ray diffraction established that crystals formed under these conditions have the composition $[Ag(Phang)_4]^+$ BF_4^-. Other crystallographic data are provided in Table 4.1, and views of the structure are shown in Figure 4.2. As in $[Ag(PPh_3)_4]^+$, the coordination of Ag(I) in $[Ag(Phang)_4]^+$ is approximately tetrahedral, and the P-Ag-P bond angles lie in the range 107.5–112.2°, with an average of 109.5°. The average length of Ag-P bonds in $[Ag(Phang)_4]^+$ is 2.456 Å, which is substantially shorter than the Ag-P bonds in $[Ag(PPh_3)_4]^+$ (2.60–2.68 Å).[32-41] The difference can be attributed to the smaller cone angle of phosphangulene, which reduces repulsive intra-complex ligand-ligand interactions created when the ligand approaches the metal more closely.

Table 4.1 : Crystallographic Data for Salts of $[Ag(Phang)_4]^+$ and $[Cu(Phang)_4]^+$

Compound	$[Ag(Phang)_4]^+ BF_4^-$	$[Cu(Phang)_4]^+ BF_4^-$	$[Cu(Phang)_4]^+ PF_6^- \bullet 3$ MeOH
crystallization medium	CH_2Cl_2	EtOH	MeOH
formula	$C_{72}H_{36}AgBF_4O_{12}P_4$	$C_{72}H_{36}BCuF_4O_{12}P_4$	$C_{75}H_{48}CuF_6O_{15}P_5$
crystal system	monoclinic	monoclinic	orthorhombic
space group	$P2_1/c$	$P2_1/c$	$Pna2_1$
a (Å)	12.2303(3)	12.0917(2)	13.6619(5)
b (Å)	14.1157(3)	14.0561(3)	37.9460(14)
c (Å)	34.8230(8)	34.6177(7)	13.6696(6)
α (°)	90	90	90
β (°)	98.635(1)	98.119(1)	90
γ (°)	90	90	90
V (Å^3)	5943.7(2)	5824.7(2)	7086.5(5)
Z	4	4	4
Z'	1	1	1
F(000)	2848	2776	3104
T (K)	150	150	150
ρ_{calc} (g cm^{-3})	1.577	1.559	1.426
λ (Å)	1.34139	1.34139	1.34139
μ (mm^{-1})	2.967	3.162	2.821
measured reflections	165886	82853	89528
independent reflections	13649	13385	11920
R_{int}	0.0287	0.0343	0.0755
R_σ	0.0124	0.0254	0.0552
observed reflections	13263	12351	10287
R_1, $I > 2\sigma(I)$	0.0357	0.0735	0.0708
R_1, all data	0.0366	0.0772	0.0835
wR_2, $I > 2\sigma(I)$	0.0918	0.1984	0.1874
wR_2, all data	0.0924	0.2020	0.1970
GoF	1.225	1.053	1.068
Max/Min	1.125/-0.963	1.895/-1.018	0.724/-0.519
Flack parameter	N/A	N/A	0.140(9)

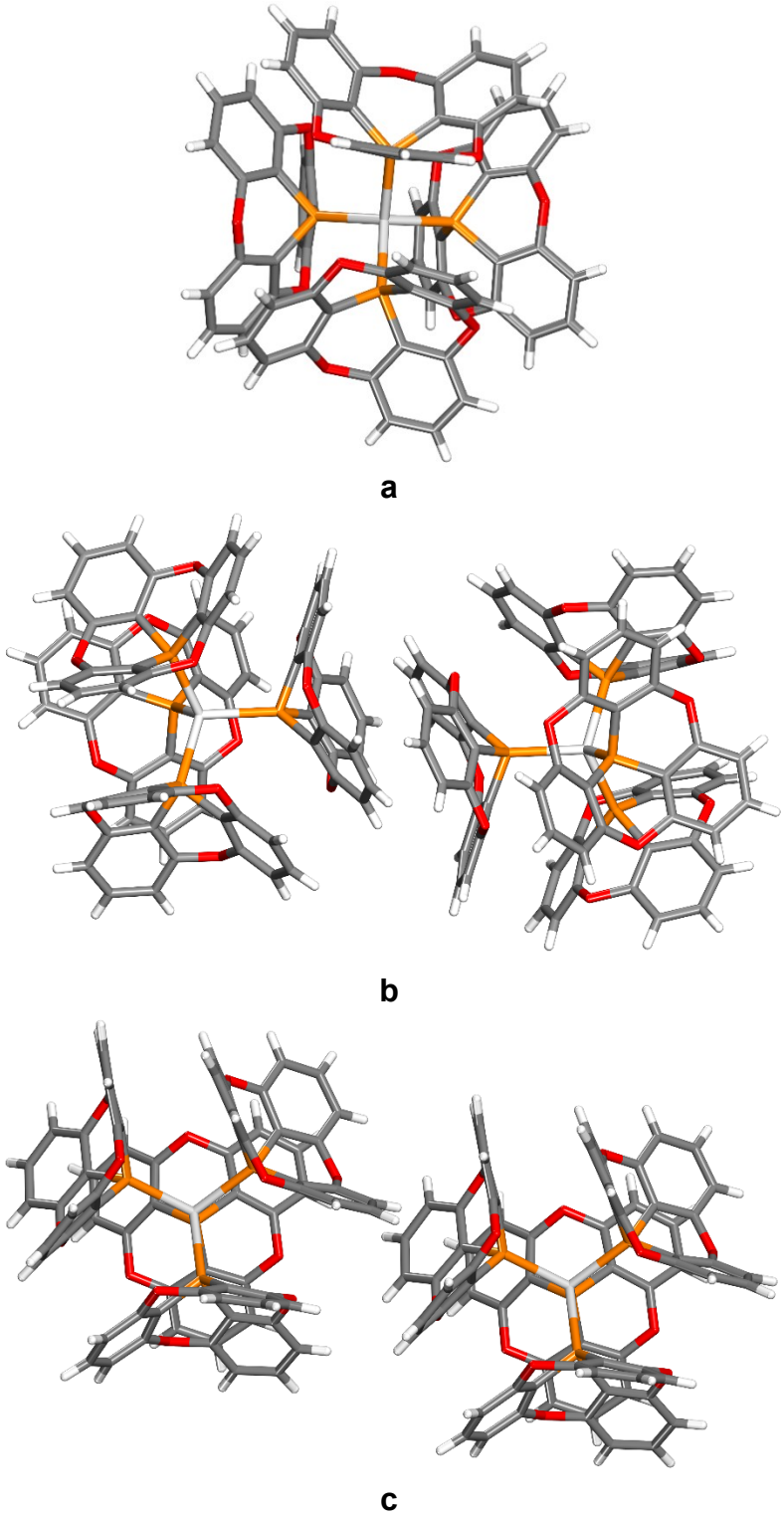

Figure 4.2 : Representations of the structure of crystals of $[Ag(Phang)_4]^+$ BF_4^- grown from CH_2Cl_2. (a) Image showing the approximately tetrahedral coordination of Ag(I). (b) View of

neighboring $[Ag(Phang)_4]^+$ cations linked by an offset clamshell pair of Phang ligands. (c) View of neighboring cations joined by a distorted pair of Phang ligands. Atoms of carbon appear in gray, hydrogen in white, oxygen in red, phosphorus in yellow-orange, and silver in light gray. BF_4^- ions are omitted for clarity.

As defined by $\theta = 2\cos^{-1}(d/R)$, the average cone angle for the Phang ligands in $[Ag(Phang)_4]^+$ (117°) is virtually the same as in uncomplexed phosphangulene (116°). Nevertheless, coordination has a small geometric effect, as revealed by a larger average C-P-C bond angle (from 93.0° in phosphangulene itself to 95.8° in bound Phang ligands), as well as by a shorter average C-P bond length (from 1.80 Å in phosphangulene itself to 1.78 Å in bound Phang ligands). Similarly, coordination of triphenyphosphine to form $[Ag(PPh_3)_4]^+$ BF_4^- has only minor geometric consequences, and the average cone angle, C-P-C bond angle, and C-P bond length in the complex are similar to those in the unbound ligand.[33]

Previous crystallographic studies of salts of $[Ag(PPh_3)_4]^+$ have analyzed the coordination of Ag(I) in detail but have not fully examined other interactions that help determine the overall structures. Closer study reveals that the surface of each cation is rich in phenyl groups that engage in C-H···aromatic interactions, both within a single cation and between neighboring cations. Ph_3P groups and analogues such as trityl are known to form characteristic patterns of C-H···aromatic interactions known as phenyl embraces.[42-45] To form a classic sixfold phenyl embrace, two Ph_3P groups or analogues must adopt propeller-shaped conformations of opposite configuration and then interdigitate to create a cyclic array of six phenyl rings. Within this array, each ring of each Ph_3P group or analogue engages simultaneously in edge-to-face C-H···aromatic interactions with two rings provided by the other group, often across a

center of inversion. In addition to being able to form sixfold embraces, Ph_3P groups and analogues can also engage in related but less extensive fourfold embraces, as well as simple edge-to-face pairing and other standard aromatic interactions. When examined from this perspective, the reported structures of salts of $[Ag(PPh_3)_4]^+$ can be seen to include many embraces, both within each cation and between adjacent cations.

In contrast, the rigid shape and small cone angle of phosphangulene prevent $[Ag(Phang)_4]^+$ from taking part in similar interdigitated phenyl embraces. Significant ligand-ligand interactions within each cation are eliminated, and the number of C-H···aromatic interactions formed between adjacent cations is severely reduced. Instead, neighboring cations are typically linked by what have been called "offset clamshell pairs," in which two Phang ligands are held together by mutual C-H···aromatic interactions involving only the concave surfaces (Figure 4.2b).[11] The corresponding convex surfaces are screened by the other three Phang ligands in $[Ag(Phang)_4]^+$ and cannot participate extensively in inter-cation interactions. Each cation is joined to three neighbors by offset clamshell pairing as shown in Figure 4.2b, and a fourth neighbor is linked by the distorted pairing illustrated in Figure 4.2c.

Analogous clamshell pairing is a widespread feature of the structures of simple derivatives of phosphangulene such as oxide **2** (Figure 4.3a),[11] whereas π-stacking is favored in crystals of phosphangulene itself (Figure 4.3b).[1] Interactions that give rise to these different modes of association can be highlighted by comparing Hirshfeld surfaces of molecules in crystals of phosphangulene and oxide **2**, as well as by examining the corresponding two-dimensional fingerprint plots.[46,47] Hirshfeld surfaces are normally constructed to show where the calculated electron density contributed by a molecule in a crystal equals the density resulting from all

other atoms in the structure. The concave surfaces of molecules of phosphangulene and oxide **2** (in a representative polymorph) are shown in Figure 4.3c–d. The surfaces are colored according to the local value of d_e, which is the distance from the surface to the nearest atomic nucleus in another molecule, and the colors show a variation from cool (blue) to hot (red) as d_e decreases. Phosphangulene and oxide **2** have nearly identical molecular structures, but their Hirshfeld surfaces differ markedly. The conspicuous red spots on the concave face of oxide **2** (Figure 4.3c) denote multiple C-H···π interactions, whereas the high proportion of blue and green on the corresponding face of phosphangulene reflects weak π-stacking directed largely by the conical molecular topology (Figure 4.3c).

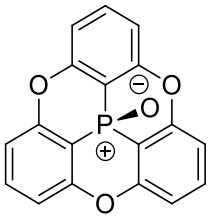

2

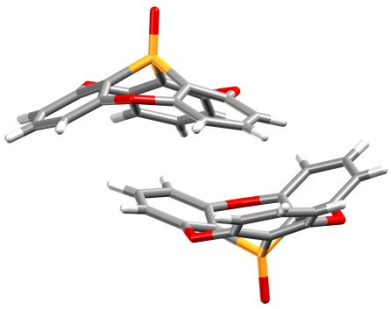

a

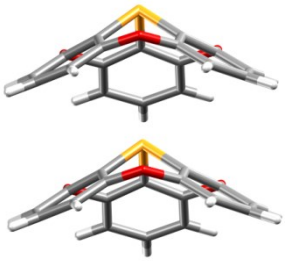

b

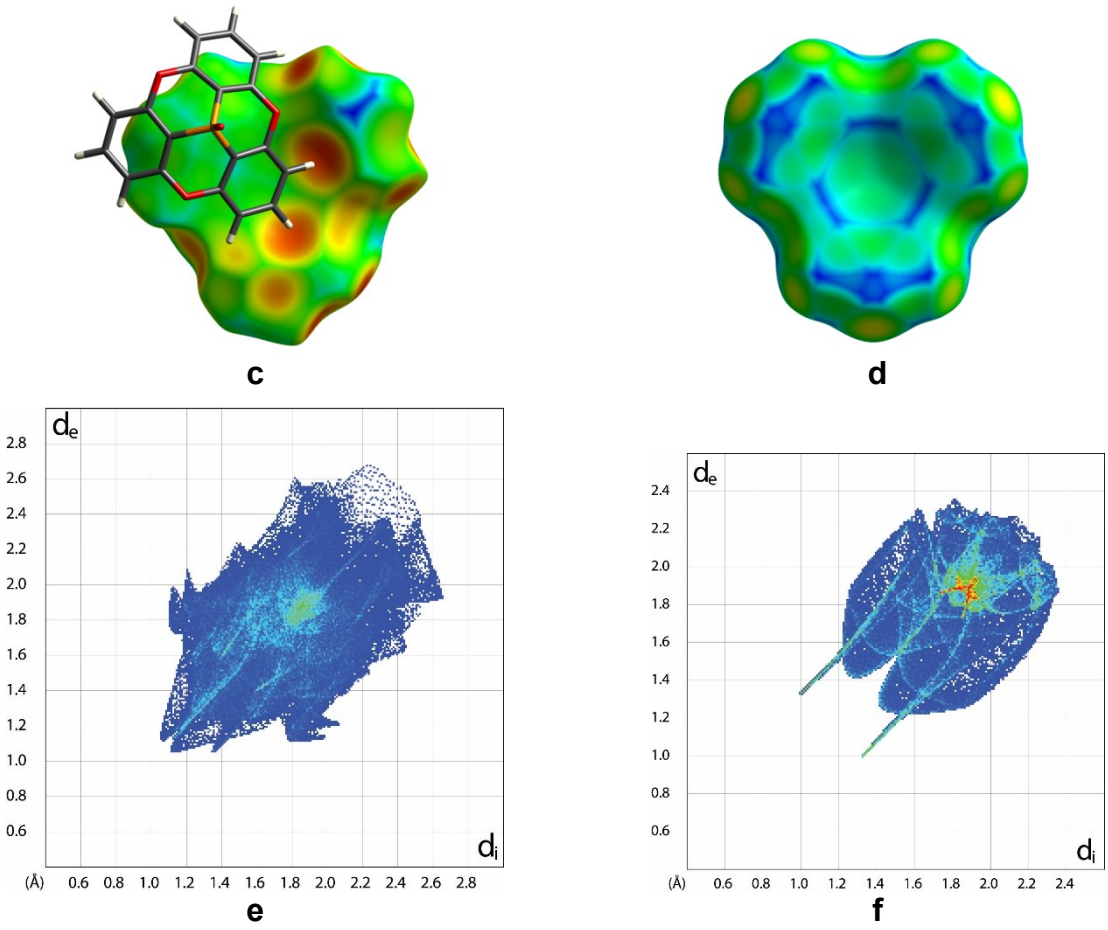

Figure 4.3 : Comparisons of molecular organization in crystals of phosphangulene and oxide **2**. (a) Offset clamshell pair formed by molecules of oxide **2** in crystals of a representative polymorph. (b) Stacking of molecules of phosphangulene.[1] (c) Hirshfeld surface showing a representative concave surface in paired molecules of oxide **2**. (d) Hirshfeld surface of the concave face of stacked molecules of phosphangulene. (e) Two-dimensional fingerprint plot of the surface of oxide **2**. (e) Fingerprint plot of the surface of phosphangulene. Colors of the Hirshfeld surfaces range from cool (blue) to hot (red) as d_e decreases. The colors at each point in the fingerprint plots vary from cool (blue) to hot (red) as the frequency of particular values of d_e and d_i increases. In Figures 3a–b, atoms are shown in normal colors.

The corresponding two-dimensional fingerprint plots in Figure 4.3e–f allow further analysis of the structures of phosphangulene and oxide **2** by showing the probability of locating points on the Hirshfeld surfaces with particular values of d_e (distance to the nearest external atomic nucleus) and d_i (distance to the nearest internal atomic nucleus). Colors at each point on the plots range from cool (blue) to hot (red) as the frequency increases. The two plots differ markedly, thereby confirming that adding a single atom of oxygen to phosphangulene changes molecular organization significantly. In particular, many points on the Hirshfeld surface of oxide **2** have values of d_i or d_e as large as 2.7 Å (Figure 4.3e), whereas the fingerprint plot corresponding to phosphangulene is compact and bounded by $d_i \approx d_e \approx 2.3$ Å (Figure 4.3f). Oxide **2** has an awkward molecular shape that prevents effective stacking and forces crystallization to occur in alternative ways that lead inevitably to unsatisfactory structures with abnormally long intermolecular separations. As a result, oxide **2** and related derivatives of phosphangulene are disposed to form multiple polymorphs, structures with high values of Z and Z', solid solutions, solvates, and cocrystals.[11]

These comparisons are relevant because similar factors help direct the crystallization of salts of $[Ag(Phang)_4]^+$. Although $[Ag(PPh_3)_4]^+$ and $[Ag(Phang)_4]^+$ are closely related species, in which Ag^+ is tetrahedrally coordinated by similar triarylphosphines, the incorporation of topologically unique Phang ligands leads to major differences in inter-complex interactions. These differences can be highlighted by comparing the Hirshfeld surfaces and corresponding fingerprint plots of $[Ag(PPh_3)_4]^+$ and $[Ag(Phang)_4]^+$ in crystals of their BF_4^- salts (Figure 4.4).[33] Abundant red spots on the surface of $[Ag(PPh_3)_4]^+$ reflect the importance of C-H···aromatic interactions resulting from phenyl embraces (Figure 4a), whereas the surface of

$[Ag(Phang)_4]^+$ shows little participation in C-H···aromatic interactions, except those resulting from clamshell pairing of Phang ligands. The fingerprint plot corresponding to $[Ag(PPh_3)_4]^+$ is largely bounded by $d_i \approx d_e \approx 2.6$ Å (Figure 4.4c); in contrast, the plot of the surface of $[Ag(Phang)_4]^+$ is much more extended, with values of d_i or d_e reaching 3.0 Å.

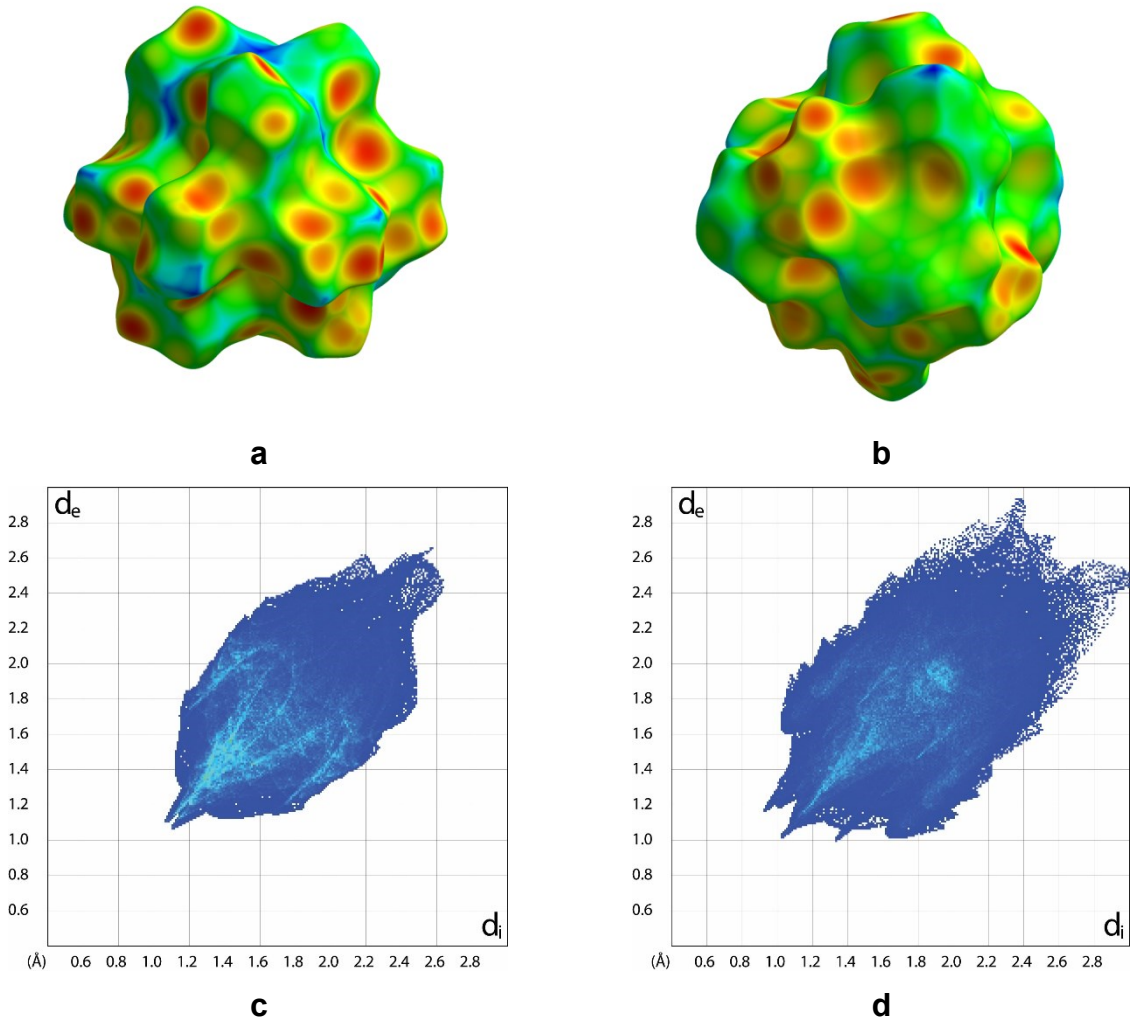

Figure 4.4 : Hirshfeld surfaces and two-dimensional fingerprint plots corresponding to $[Ag(PPh_3)_4]^+$ and $[Ag(Phang)_4]^+$ in crystals of their BF_4^- salts. (a) View of the Hirshfeld surface of $[Ag(PPh_3)_4]^+$ along the direction of a representative P-Ag bond. (b) Corresponding view of the surface of $[Ag(Phang)_4]^+$. (c) Fingerprint plot of the surface of $[Ag(PPh_3)_4]^+$. (d)

Fingerprint plot of the surface of $[Ag(Phang)_4]^+$. The Hirshfeld surfaces and fingerprint plots are colored in the normal ways.

The behavior of phosphangulene, oxide **2**, and salts of $[Ag(Phang)_4]^+$ illustrates aspects of what we have called "the dark side of crystal engineering," which includes efforts to design molecules that cannot adopt normal patterns of crystallization.[48–51] Converting phosphangulene into oxide **2** and other chalcogenides adds only one atom but creates an awkward topology that prevents effective π-stacking and diverts crystallization toward less attractive alternatives.[11] Similarly, salts of $[Ag(Phang)_4]^+$ are forced by the peculiar shape of the ligands to form crystals without stabilizing interactions present in the structures of analogous salts of $[Ag(PPh_3)_4]^+$. Our observations suggest that phosphangulene may serve in a general way by introducing problems of packing whenever it is included as a component of larger structures. If so, metal complexes with multiple concave aromatic surfaces derived from phosphangulene should be unable to pack efficiently and should therefore be highly effective agents for producing cocrystals, particularly with complementary partners such as fullerenes.

$[Ag(Phang)_4]^+$ BF_4^- precipitated in 59% yield when $AgBF_4$ and phosphangulene (4 equiv) were mixed in CH_2Cl_2, followed by the addition of hexane. Powder X-ray diffraction confirmed that the bulk solid was uniformly crystalline, with the same structure determined by analyzing single crystals grown from CH_2Cl_2.[52] Obtaining $[Ag(Phang)_4]^+$ as the major product suggested that the cation might also be present in solution. In earlier work, the formation of $[Ag(PPh_3)_4]^+$ was confirmed by ^{31}P NMR spectroscopy at 193 K, using solutions in CH_2Cl_2 prepared by mixing $AgPF_6$ with increasing amounts of triphenylphosphine.[53,54] Under these conditions, well-resolved signals attributed to $[Ag(PPh_3)_n]^+$ (n = 1–4) appear as distinctive

pairs of doublets resulting from coupling with ^{107}Ag and ^{109}Ag. The dominant cation in the presence of 4 equiv of triphenylphosphine is $[Ag(PPh_3)_4]^+$, characterized by δ ^{31}P = -5.6 and a coupling constant of ^1J (^{107}Ag, ^{31}P) = 224 Hz.

The results of an analogous low-temperature experiment with $AgBF_4$ and phosphangulene are shown in Figure 4.5. All spectra resulting from the addition of 1–4 equiv of phosphangulene revealed a sharp pair of doublets near δ ^{31}P = -110, with ^1J (^{107}Ag, ^{31}P) = 264 Hz. The relative importance of this feature increased as phosphangulene was added, suggesting that it corresponds to $[Ag(Phang)_4]^+$. Broadened signals appearing in spectra recorded after the addition of 1–2 equiv of phosphangulene can be assigned to various species $[Ag(Phang)_n]^+$ where n = 1–3. Detection of free phosphangulene (singlet at δ ^{31}P = -134) after the addition of 3–4 equiv indicates that formation of $[Ag(Phang)_4]^+$ is not complete, and exchanges involving coordinatively unsaturated species $[Ag(Phang)_n]^+$ (n = 1–3) are faster than in analogous complexes with triphenylphosphine. The slower exchange of $[Ag(Phang)_4]^+$ can be attributed to the fact that it is coordinatively saturated. Together, these observations support the conclusion that the high *s* character of the lone pair orbital makes phosphangulene weaker than triphenylphosphine as a ligand, base, and nucleophile. The low nucleophilicity of phosphangulene was confirmed qualitatively by observing that its S_N2 reaction with EtI (acetone-d_6, 338 K) is much slower than that of triphenylphosphine.

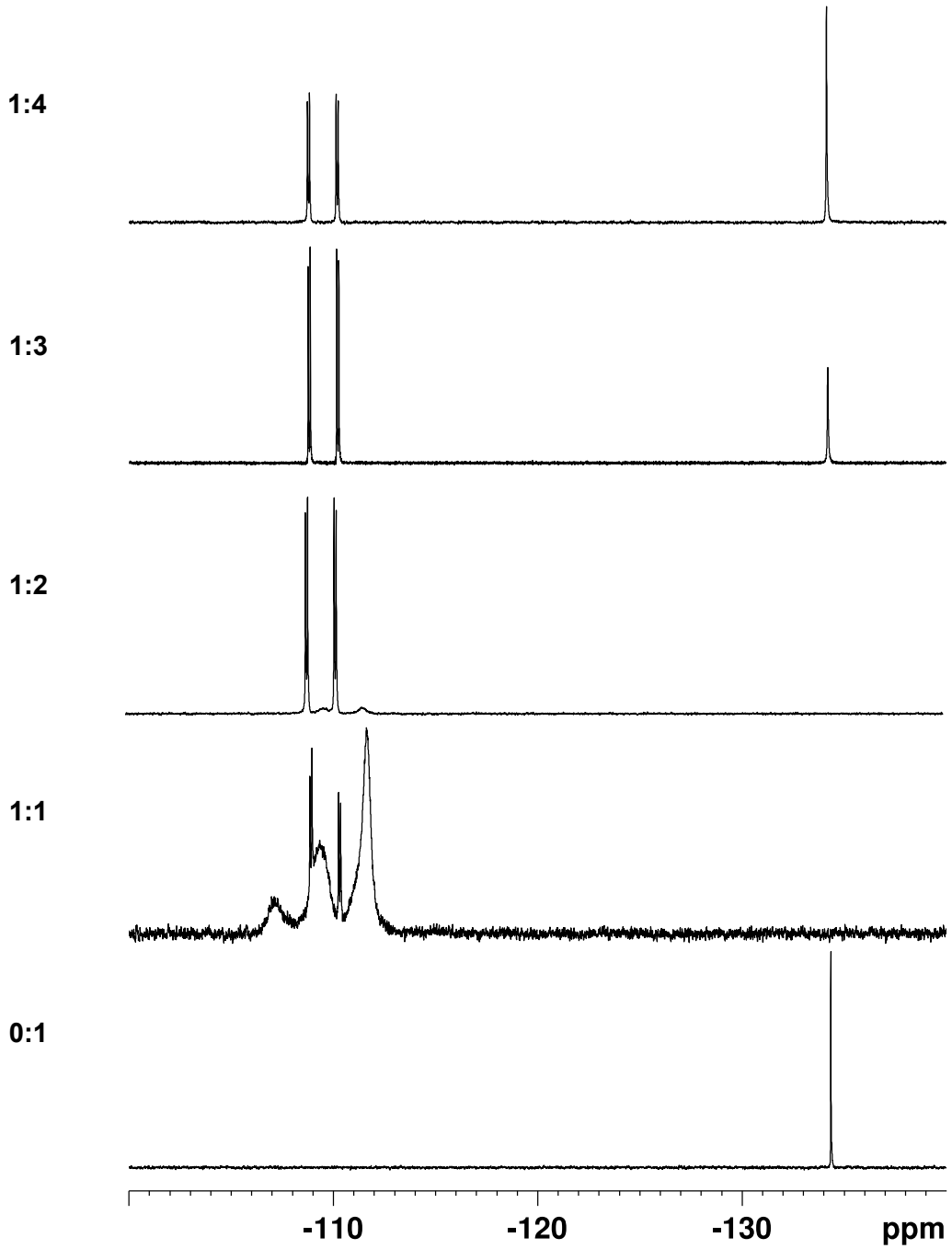

Figure 4.5 : Low-temperature (183 K) ^{31}P NMR spectra of solutions prepared by mixing phosphangulene and $AgBF_4$ in CH_2Cl_2/diethyl ether, with the ratios shown on the left. The bottom spectrum corresponds to pure phosphangulene. Chemical shifts are relative to external 85% aqueous H_3PO_4.

We were confident that the sharp pair of doublets in low-temperature ^{31}P NMR spectra (Figure 4.5) were correctly assigned to $[Ag(Phang)_4]^+$. However, the size of ^1J (^{107}Ag, ^{31}P) reflects the number of coordinated phosphines, and we noted that the observed value (^1J = 264 Hz) lies between those reported for tetracoordinated $[Ag(PPh_3)_4]^+$ (^1J = 224 Hz) and tricoordinated $[Ag(PPh_3)_3]^+$ (^1J = 319 Hz).[53] We confirmed our assignment by analyzing the solid-state ^{31}P NMR spectrum of crystalline $[Ag(Phang)_4]^+$ BF_4^-, in which Ag(I) is known to be tetracoordinated. The analysis is presented in detail in the Supporting Information.

$[Cu(Phang)_4]^+$ BF_4^-. Like Ag(I), Cu(I) has a strong affinity for phosphines. Tetracoordination of Cu(I) to give $[Cu(PPh_3)_4]^+$ was first described in 1960,[24] and the structure of the ClO_4^- salt has been reported.[40] To make the BF_4^- salt of $[Cu(Phang)_4]^+$, $[Cu(MeCN)_4]^+$ BF_4^- was mixed with phosphangulene in a 1:4 ratio in CH_2Cl_2/MeCN (3:1), volatiles were removed by evaporation, and the residual solid was crystallized from anhydrous EtOH. The resulting crystals proved to be isomorphous with those of $[Ag(Phang)_4]^+$ BF_4^-, and Table 4.1 summarizes additional crystallographic data. Isomorphism has also been reported in pairs of closely related complexes of triphenylphosphine such as the ClO_4^- salts of $[Ag(PPh_3)_4]^+$ and $[Cu(PPh_3)_4]^+$.[39] The coordination of Cu(I) in $[Cu(Phang)_4]^+$ is approximately tetrahedral, and the P-Cu-P bond angles lie in the range 107.2–111.3°, with an average of 109.5°. The average Cu-P bond length in $[Cu(Phang)_4]^+$ is 2.290 Å, which is much shorter than the average (2.58 Å) observed in the case of $[Cu(PPh_3)_4]^+$ ClO_4^-.[40] The short metal-P bonds in both $[Ag(Phang)_4]^+$ and $[Cu(Phang)_4]^+$ can be attributed to the small cone angle of phosphangulene, even though it is a weaker ligand than triphenylphosphine.

Crystals of composition $[Cu(Phang)_4]^+ PF_6^- \bullet 3$ MeOH were obtained under related conditions and proved to have a similar structure, which is described in greater detail in the Supporting Information. Other crystallographic data are summarized in Table 4.1. Bulk solids that precipitated when $[Cu(MeCN)_4]^+ BF_4^-$ and phosphangulene were mixed in solution in a 1:4 ratio proved to be crystalline; however, they did not have the same structure as single crystals grown from EtOH and were not examined further.

$Cu_2Cl_2(Phang)_4$. Phosphine complexes of Cu(I) halides have been studied intensively and shown to exhibit remarkable structural diversity, which reflects the capacity of Cu(I) to accommodate different coordination numbers, as well as the ability of halides to serve as terminal ligands or as bridges with varying geometries.[55] Special motivation for studying these complexes is provided by their luminescence, which has been attributed to halide-to-Cu charge transfer, Cu-to-ligand charge transfer, and effects arising from short Cu···Cu distances.[55] Halide-bridged triphenylphosphine Cu(I) complexes of stoichiometry $Cu_2X_2(PPh_3)_3$ (X = Cl, Br, I) are particularly well known and have been prepared by the direct reaction of CuX with triphenylphosphine. Multiple structures of this type have been reported,[55-64] and the complexation has also been analyzed in solution.[65] Despite decades of studies of this type, however, the isolation and characterization of fully coordinated complexes $Cu_2X_2(PPh_3)_4$ have never been reported.

Expecting on this basis to obtain $Cu_2Cl_2(Phang)_3$, we combined CuCl and phosphangulene in CH_2Cl_2/EtOH and crystallized the resulting solid from hot EtOH. To our surprise, analysis of the crystals by X-ray diffraction revealed the formation of $Cu_2Cl_2(Phang)_4$. Table 4.2 summarizes crystallographic data, and Figure 4.6 provides views of the structure. The

geometric parameters for the $Cu_2Cl_2P_4$ core of the complex are generally similar to those observed for the tetracoordinated center in structures of $Cu_2Cl_2(PPh_3)_3$.[55–64] In particular, the average Cu-P bond length in $Cu_2Cl_2(Phang)_4$ is 2.264 Å, whereas the value for the corresponding Cu-P bonds in the triclinic form of $Cu_2Cl_2(PPh_3)_3$ is 2.260 Å.[59] Metal-P bond lengths observed in salts of $[M(Phang)_4]^+$ (M = Ag, Cu) are much shorter than those in salts of $[M(PPh_3)_4]^+$, but the phenomenon is not general, and the differences in bond length can be smaller when fewer phosphines are bound, presumably because PPh_3 can then approach as closely as Phang despite having a larger cone angle. The transannular Cu···Cu distance in $Cu_2Cl_2(Phang)_4$ is long (3.138 Å) and identical to the one found in $Cu_2Cl_2(PPh_3)_3$,[59] so metal-metal bonding is insignificant. The only noteworthy structural difference related to the tetracoordinated centers of the complexes of phosphangulene and triphenylphosphine is the P-Cu-P bond angle, which is 110.4° in $Cu_2Cl_2(Phang)_4$ but expands to 130.4° in $Cu_2Cl_2(PPh_3)_3$, presumably because PPh_3 has a larger cone angle.

Table 4.2 : Crystallographic Data for Complexes of Phosphangulene with Cu(I) Halides

Compound	$Cu_2Cl_2(Phang)_4$	$Cu_2I_2(Phang)_4$ • 1 toluene	$Cu_2Cl_2(Phang)_3$
crystallization medium	EtOH	EtOH/toluene	EtOH
formula	$C_{72}H_{36}Cl_2Cu_2O_{12}P_4$	$C_{79}H_{44}Cu_2I_2O_{12}P_4$	$C_{54}H_{27}Cl_2Cu_2O_9P_3$
crystal system	monoclinic	tetragonal	triclinic
space group	$P2_1/n$	$P4_2/m$	$P\bar{1}$
a (Å)	12.1132(3)	13.9038(7)	10.8679(4)
b (Å)	13.9653(3)	13.9038(7)	13.9505(5)
c (Å)	18.1189(4)	17.3483(9)	17.0453(6)
α (°)	90	90	105.882(2)
β (°)	107.042(1)	90	105.468(2)
γ (°)	90	90	105.195(2)
V (Å^3)	2930.49(12)	3353.7(4)	2233.61(14)
Z	2	2	2
Z'	0.5	0.25	1
F(000)	1432	1676	1120
T (K)	150	150	150
ρ_{calc} (g cm^{-3})	1.603	1.673	1.651
λ (Å)	1.34139	1.34139	1.34139
μ (mm^{-1})	5.537	9.346	6.892
measured reflections	47052	50926	51082
independent reflections	6726	4020	9402
R_{int}	0.0261	0.0650	0.0500
R_σ	0.0161	0.0287	0.0402
observed reflections	6539	3665	7897
R_1, $I > 2\sigma(I)$	0.0285	0.0458	0.0465
R_1, all data	0.0293	0.0486	0.0622
wR_2, $I > 2\sigma(I)$	0.0776	0.1340	0.0847
wR_2, all data	0.0782	0.1377	0.0914
GoF	1.056	1.094	1.038
Max/Min	0.495/-0.392	1.596/-0.889	0.457/-0.520

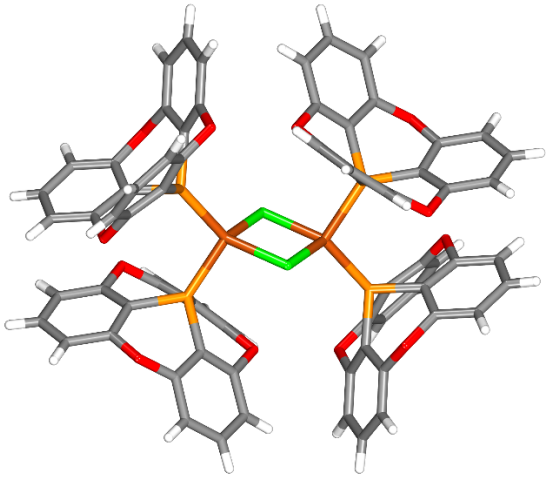

a

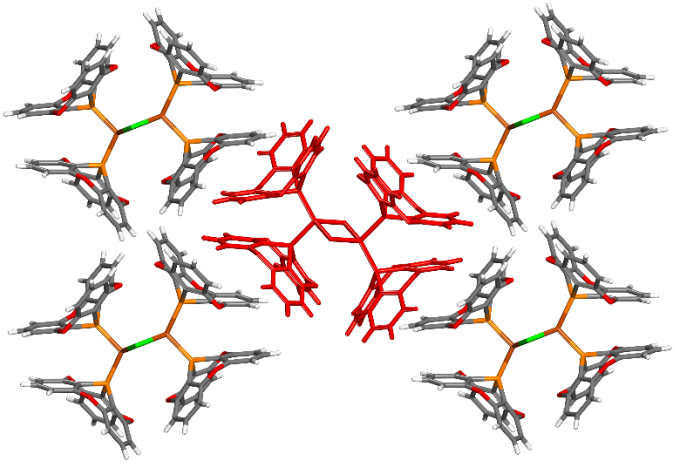

b

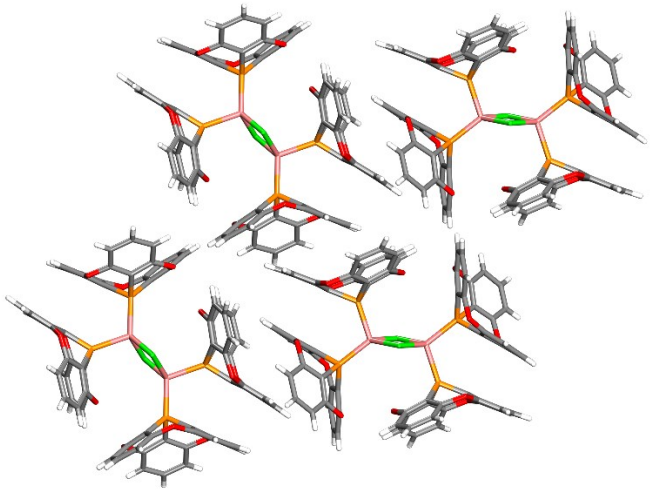

c

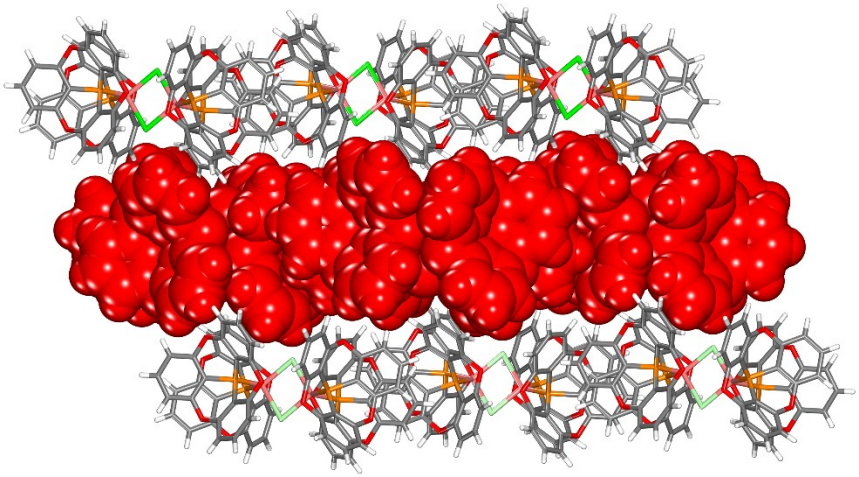

d

Figure 4.6 : Representations of the structure of crystals of $Cu_2Cl_2(Phang)_4$ grown from EtOH. (a) Image showing a single complex. (b) View of a central complex (in red) linked to four coplanar neighbors by offset clamshell pairs of Phang ligands. (c) Image showing a cyclic quartet joined by pairing of Phang ligands. (d) Side view of part of a sheet (in red) and two adjacent layers. Unless indicated otherwise, atoms of carbon appear in gray, hydrogen in white, oxygen in red, phosphorus in yellow-orange, copper in orange, and chlorine in green.

By positioning four Phang ligands in a tetragonal orientation, each molecule of $Cu_2Cl_2(Phang)_4$ is predisposed to have four coplanar neighbors, all linked by the formation of offset clamshell pairs (Figure 4.6b). This pattern of assembly gives rise to the formation of sheets built from cyclic quartets (Figure 4.6c–d), and adjacent sheets are held together by various forces, including C-H···aromatic, C-H···O, and C-H···Cl interactions. The inability of *P*-substituted derivatives of phosphangulene to form π-stacks forces them to accept less efficient modes of packing. Offset clamshell pairing appears to be the best of these alternatives, because it is observed in the structures of a wide spectrum of compounds, ranging from simple derivatives of phosphangulene (such as oxide **2**) to complexes with multiple

divergent Phang units (such as $Cu_2Cl_2(Phang)_4$ and salts of $[Ag(Phang)_4]^+$ and $[Cu(Phang)_4]^+$). The observation of paired Phang groups in all of these structures suggests that the motif exerts a reliable directing effect that can be used to position molecules predictably. In contrast, analogous PPh_3 groups engage in a wide rande of intermolecular interactions and do not control organization in ways that are easy to foresee.[42-45]

Crystals of a closely related iodide-bridged complex, $Cu_2I_2(Phang)_4$ • 1 toluene, were obtained by an analogous procedure. Crystallographic data are presented in Table 4.2, and the structure is described in more detail in the Supporting Information. The two halide-bridged $Cu_2X_2(Phang)_4$ complexes show that Phang ligands are exceptional for two reasons: (1) They can yield metal complexes with unique coordination, and (2) they can direct organization in the solid state in foreseeable ways, based on offset clamshell pairing. Phosphangulene reacts with CuCl to form the unprecedented tetracoordinated complex $Cu_2Cl_2(Phang)_4$, but the same conditions also yield crystals of the tricoordinated complex $Cu_2Cl_2(Phang)_3$, which is analogous to the well-known compound $Cu_2Cl_2(PPh_3)_3$. Table 4.2 summarizes crystallographic data, and the structure is described in greater detail in the Supporting Information.

$[Ag(O_3SCF_3)(H_2O)(Phang)]_2$. The widespread use of trifluoromethanesulfonates (triflates) of Ag(I), Cu(I), and other metals as stoichiometric reagents and catalysts led us to examine their complexes with phosphangulene.[66] Crystallization was induced by combining AgO_3SCF_3 and phosphangulene in EtOH/toluene, followed by slow evaporation of solvent. Crystallographic data are compiled in Table 4.3, and views of the structure appear in Figure 4.7. Two Ag(I) centers, each coordinated to H_2O and phosphangulene, are doubly bridged by triflate to form

an eight-membered $Ag_2O_4S_2$ ring. Even though triflates of Ag(I) and Cu(I) are familiar reagents in chemistry, few crystallographic studies of complexes have been reported, and only the structure of $[Ag(O_3SCF_3)(PPh_3)_2]_2$ is directly related.[67,68] Comparison with the structure of $[Ag(O_3SCF_3)(H_2O)(Phang)]_2$ is instructive. In both cases, bridging by triflate is unsymmetric, and the two Ag-O bond lengths differ significantly (2.508 Å and 2.720 Å in the Phang complex, versus 2.416 Å and 2.578 Å in the PPh_3 complex). The coordination of Ag(I) in $[Ag(O_3SCF_3)(H_2O)(Phang)]_2$ is best described as trigonal bipyramidal (Figure 4.7), with approximately axial Phang and H_2O ligands, and with three basal atoms of oxygen, two derived from triflate and the third contributed by a Phang ligand in a neighboring complex (Ag···O distance = 2.956 Å). The lengths of the Ag-P and Ag-OH_2 bonds are 2.361 Å and 2.221 Å, respectively, and the corresponding P-Ag-O bond angle is 158.6°. In contrast, the average Ag-P bond length in $[Ag(O_3SCF_3)(PPh_3)_2]_2$ is longer (2.432 Å), and the P-Ag-P bond angle is 131.2°, so the coordination of Ag(I) is distorted tetrahedral. Molecules of $[Ag(O_3SCF_3)(H_2O)(Phang)]_2$ are linked to form chains by normal clamshell pairing of Phang ligands (Figure 4.7c), and the chains are linked by hydrogen bonds involving bound H_2O.

Table 4.3 : Crystallographic Data for Complexes Formed by the Reaction of Phosphangulene with Ag(I) Trifluoromethanesulfonate and Perchlorate

Compound	$[Ag(O_3SCF_3)(H_2O)(Phang)]_2$	$[Ag(O_3SCF_3)(toluene)(Phang)]_2$	$[Ag(ClO_4)(toluene)(Phang)]_2$	$[Ag(ClO_4)(MeCN)_2(Phang)]_2$	$[Ag(O_3SCF_3)(toluene)(Phang)_2] \cdot 2\ C_{60} \cdot 3$ toluene
crystallization medium	EtOH/toluene	EtOH/toluene	MeCN/toluene	MeCN/toluene	EtOH/toluene
formula	$C_{38}H_{22}Ag_2F_6O_{14}P_2S_2$	$C_{52}H_{34}Ag_2F_6O_{12}P_2S_2$	$C_{25}H_{17}AgClO_7P$	$C_{44}H_{30}Ag_2Cl_2N_4O_{14}P_2$	$C_{229}H_{76}Ag_2F_6O_{18}P_4S_2$
crystal system	triclinic	monoclinic	monoclinic	triclinic	triclinic
space group	$P\bar{1}$	$P2_1/c$	$P2_1/n$	$P\bar{1}$	$P\bar{1}$
a (Å)	6.9434(6)	21.711(1)	11.8082(7)	8.6233(3)	10.1347(9)
b (Å)	12.0474(10)	11.6334(6)	16.1007(9)	9.8147(3)	17.4030(14)
c (Å)	12.4915(10)	20.2589(10)	12.8381(7)	13.9858(5)	20.810(2)
α (°)	81.860(4)	90	90	73.587(2)	86.369(4)
β (°)	77.662(4)	104.999(2)	108.495(2)	75.133(2)	80.154(5)
γ (°)	77.572(4)	90	90	86.914(2)	89.061(4)
V (Å^3)	991.84(14)	4942.5(4)	2314.7(2)	1097.22(7)	3609.0(6)
Z	1	4	4	1	1
Z'	0.5	1	1	0.5	0.5
F(000)	572	2608	1208	592	1834
T (K)	150	150	150	150	150
ρ_{calc} (g cm^{-3})	1.939	1.756	1.732	1.797	1.671
λ (Å)	1.34139	1.34139	1.34139	1.34139	1.34139
μ (mm^{-1})	7.126	5.754	6.153	6.498	2.425
measured reflections	31684	60590	31981	8480	12677
independent reflections	4574	10157	4417	4101	12677*
R_{int}	0.0655	0.0591	0.0558	0.0393	0.0861
R_σ	0.0331	0.0374	0.0301	0.0348	0.0543
observed reflections	4127	8289	4135	3883	10127
R_1, $I > 2\sigma(I)$	0.0593	0.0709	0.0601	0.0725	0.1053
R_1, all data	0.0638	0.0852	0.0623	0.0742	0.1208
wR_2, $I > 2\sigma(I)$	0.1735	0.1913	0.1632	0.2240	0.2958
wR_2, all data	0.1793	0.2074	0.1663	0.2264	0.3192
GoF	1.115	1.100	1.041	1.114	1.129
Max/Min	1.348/-1.292	1.641/-2.000	1.235/-0.759	2.195/-1.054	1.543/-1.950

*Reflections were not merged, and the sample was refined as a two-component twin.

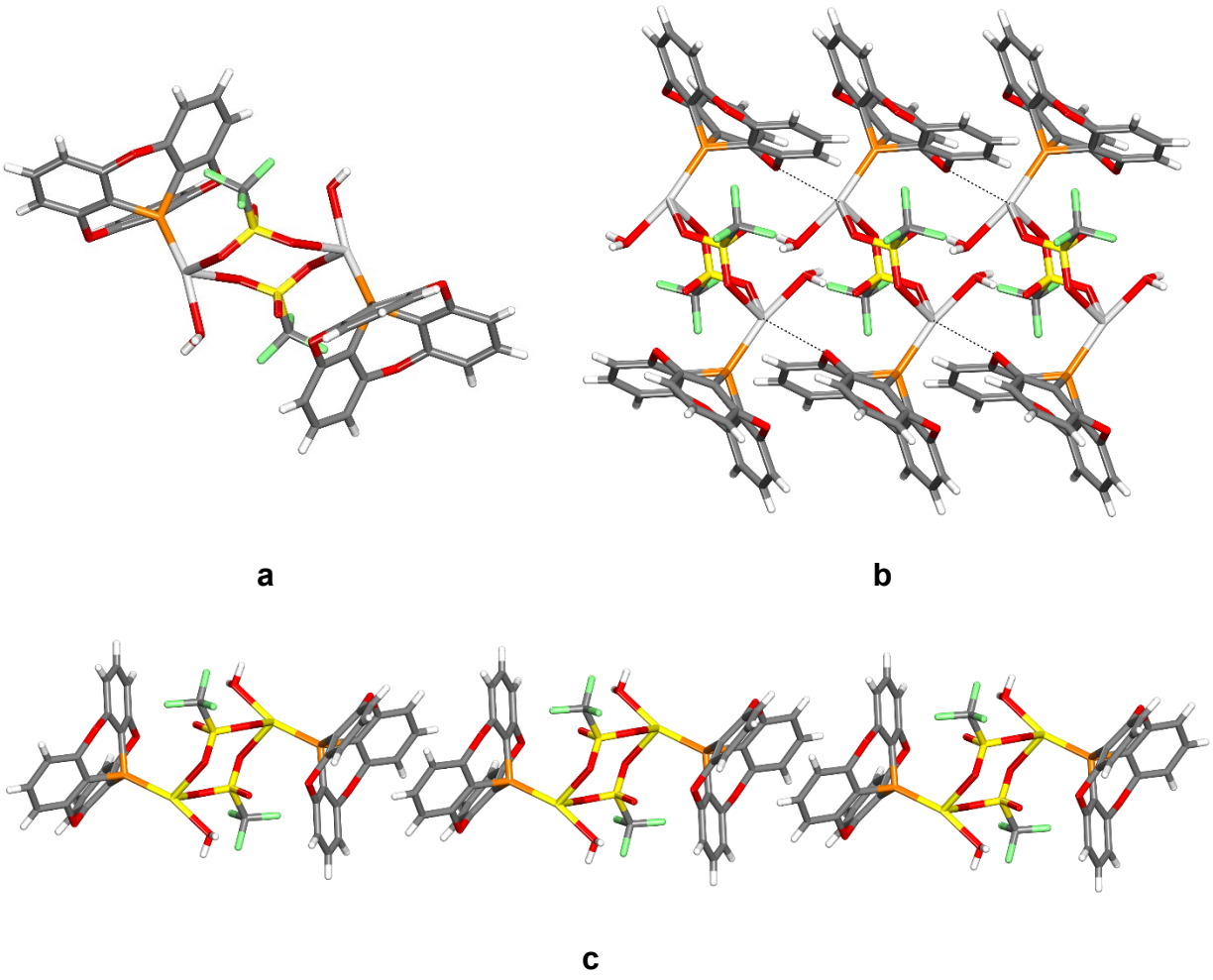

Figure 4.7 : Representations of the structure of crystals of $[Ag(O_3SCF_3)(H_2O)(Phang)]_2$ grown from EtOH/toluene. (a) View of a single molecule of the complex. (b) Image showing how inter-complex Ag···O interactions complete the trigonal bipyramidal coordination of Ag(I). (c) View showing a chain of complexes linked by pairing of Phang ligands. Atoms of carbon appear in gray, hydrogen in white, oxygen in red, fluorine in yellow-green, phosphorus in yellow-orange, sulfur in yellow, and silver in light gray. Selected intermolecular interactions are represented by broken lines.

[Ag(O_3SCF_3)(toluene)(Phang)]$_2$. A closely related complex, [Ag(O_3SCF_3)(toluene)(Phang)]$_2$, crystallized under the same conditions. Table 4.3 summarizes crystallographic data, and the structure is described in greater detail in the Supporting Information. Toluene is bound according to Mulliken's model,[69] with Ag(I) positioned directly above one of the carbon atoms in the aromatic ring, and molecules of the complex are joined to form chains by standard clamshell pairing of Phang ligands.

[Ag(ClO_4)(toluene)(Phang)]$_2$. We also examined how phosphangulene binds Ag(I) when triflate is replaced by perchlorate, another weakly coordinating anion. Slow evaporation of a solution prepared by mixing $AgClO_4$ and phosphangulene in MeCN/toluene yielded crystals of a perchlorate-bridged analogue of the triflate-bridged complex [Ag(O_3SCF_3)(toluene)(Phang)]$_2$. Crystallographic data are compiled in Table 4.3, and a view of the structure and additional information are provided in the Supporting Information. Of special note is the fact that the Ag-P bond length (2.259 Å) is shorter than the one found in [Ag(O_3SCF_3)(toluene)(Phang)]$_2$ (2.389 Å) and shorter those observed in all reported complexes of triphenylphosphine and Ag(I) perchlorate.[70-72] In fact, the Ag-P bond in [Ag(ClO_4)(toluene)(Phang)]$_2$ is shorter than those found in all but two reported complexes of Ag(I) with simple monodentate triarylphosphines.[73,74] Molecules of the complex are linked into chains by normal clamshell pairing, nicely underscoring the dual ability of Phang ligands to bind metals in unique ways and to direct molecular organization reliably.

[Ag(ClO_4)($MeCN)_2$(Phang)]$_2$. Crystals of another unusual Phang complex of $AgClO_4$ were formed under the same conditions. Table 4.3 presents crystallographic data, and Figure 4.8 provides a view of the structure. The structure can be described as two trigonal

$[Ag(MeCN)_2(Phang)]^+$ cations joined directly by an argentophilic Ag···Ag interaction (3.187 Å)[75] and capped by two weakly bonded perchlorate anions. Argentophilic interactions have been reported in many structures, but the structure of $[Ag(ClO_4)(MeCN)_2(Phang)]_2$ is noteworthy because the proximity of the two interacting Ag(I) centers is not enforced by a bridging ligand.[76-78] Bond angles at Ag within $[Ag(MeCN)_2(Phang)]_2$ are in the range 104.1–134.6°, the Ag-P bond length is 2.404 Å, and the Ag-O distance to the capping perchlorate anions is 2.813 Å. As in related structures, the complexes are joined to form chains by standard clamshell pairing of Phang ligands.

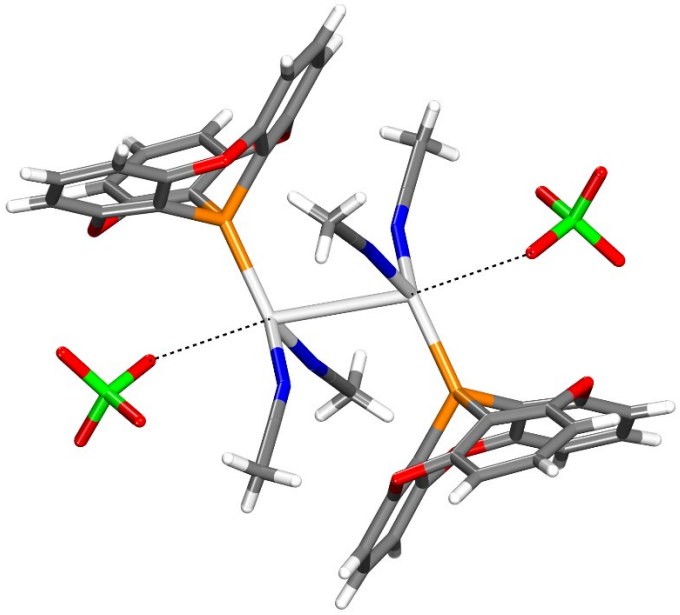

Figure 4.8 : Representation of a molecule of $[Ag(ClO_4)(MeCN)_2(Phang)]_2$ in the structure of crystals grown from MeCN/toluene. Atoms of carbon appear in gray, hydrogen in white, nitrogen in blue, oxygen in red, phosphorus in yellow-orange, chlorine in green, and silver in light gray.

Phosphangulene yields complexes with unique metal-ligand binding. In addition, Phang ligands exert special effects not only on individual complexes, but also on their collective properties of association in the solid state. The distinctive shape of Phang ligands forces association to occur in particular ways, thereby allowing complexes to be used as modules for building materials with predetermined structures. Furthermore, the patterns of association are inherently inefficient, and the presence of Phang ligands prevents complexes from packing in ways that allow the formation of normal intermolecular interactions. As a result, phosphangulene provides complexes with multiple concave electron-rich aromatic surfaces and with topologies inherently resistant to effective packing without suitable partners. This sets the stage for producing cocrystals in which metals and unfunctionalized fullerenes are brought together in ordered arrays. The desire to make materials of this type was part of our initial motivation to study the coordination chemistry of phosphangulene, and we have carried out proof-of-concept experiments that establish the feasibility of using metal complexes of phosphangulene to form cocrystals with fullerenes.

$[Ag(O_3SCF_3)(toluene)(Phang)_2]_2$ • 2 C_{60} • 3 toluene. Crystallization was induced by slow evaporation of a solution prepared by mixing AgO_3SCF_3, phosphangulene, and C_{60} in EtOH/toluene. Crystallographic data are summarized in Table 4.3, and views of the structure appear in Figure 4.9. In the complex, bonding of Ag(I) to triflate does not have pronounced ionic character, as indicated by a normally short Ag-O bond length (2.375 Å). Standard values are also observed for the distance from Ag(I) to the centroid of the bound molecule of toluene (2.857 Å), the average Ag-P bond length for the two Phang ligands (2.440 Å), and the P-Ag-P bond angle (118.3°). Each Phang ligand in the complex caps a cocrystallized molecule of C_{60}

(Figure 4.9a). If 3.55 Å is taken to be the radius of C_{60} and 3.35 Å is the separation of layers in graphite,[79,80] then 6.90 Å can be considered to be the distance separating the centroid of C_{60} from an atom of carbon in van der Waals contact. In the cocrystal, the measured distances between the centroid of C_{60} and the centroids of the capping aromatic rings of the Phang ligands are all shorter (6.735–6.872 Å), suggesting that cocrystallization is favored by the combined effect of topological and electronic complementarities. Similar distances are observed in cocrystals of fullerenes with phosphangulene oxide (**2**) and related compounds, so coordination to metals does not prevent Phang ligands from interacting with fullerenes.

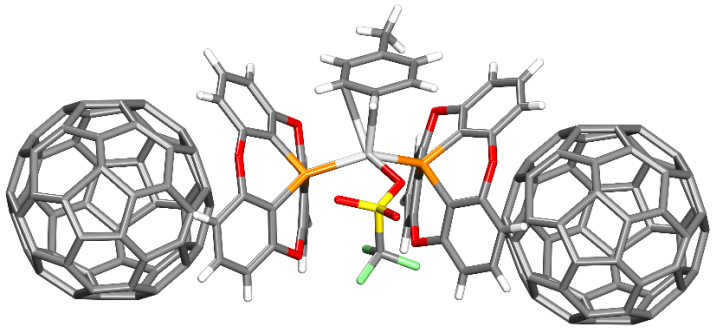

a

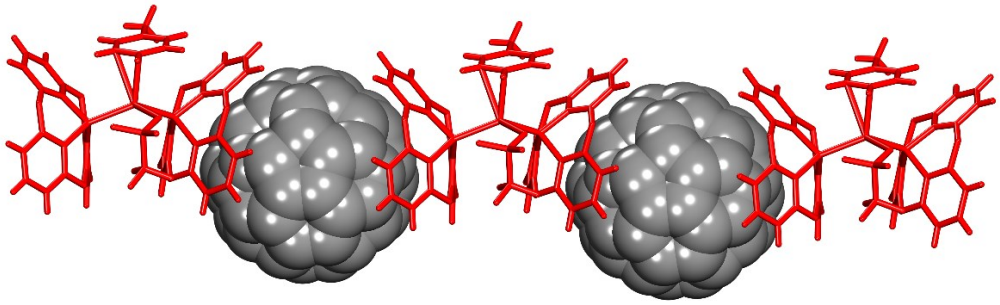

b

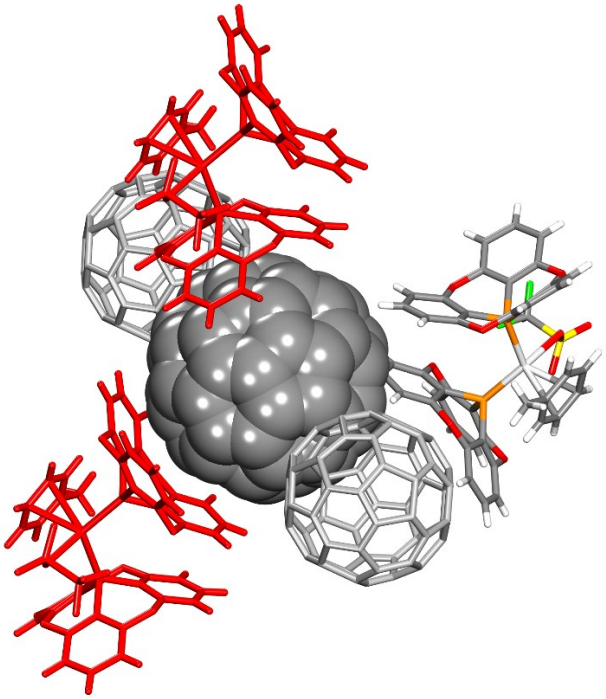

c

Figure 4.9 : Representations of the structure of crystals of $[Ag(O_3SCF_3)(toluene)(Phang)_2]_2 \bullet 2\ C_{60} \bullet 3$ toluene grown from EtOH/toluene. (a) View showing an individual complex and two adjacent molecules of C_{60} capped by Phang ligands. (b) Image showing how complexes (in red) and molecules of C_{60} are linked to form alternating zig-zag chains. (c) View showing a central molecule of C_{60} and its immediate environment, including two neighboring fullerenes aligned with the *a*-axis, two capping complexes (in red), and a third molecule of the complex that forms C-H···π interactions with the central fullerene. Unless stated otherwise, atoms of carbon appear in gray, hydrogen in white, oxygen in red, fluorine in yellow-green, phosphorus in yellow-orange, sulfur in yellow, and silver in light gray. Guest molecules of toluene are omitted for clarity.

In the structure, each molecule of C_{60} is capped on two sides by Phang ligands from different complexes, thereby creating zig-zag chains in which complexes and interacting molecules of

fullerene alternate along the *b*-axis (Figure 4.9b). Each molecule of C_{60} also forms multiple C-H···π interactions with the Phang ligands of a third molecule of the complex (Figure 4.9c). In this way, Phang ligands provided by three molecules of the complex create a belt around the equator of each molecule of C_{60}, and the poles accommodate two adjacent molecules of fullerene to form columns along the *a*-axis (Figure 4.9c). Molecules of C_{60} can be considered to be in van der Waals contact when the distance between their centroids is 10.45 Å,[80] and shorter separations may reveal the presence of stronger bonding interactions. In crystals of $[Ag(O_3SCF_3)(toluene)(Phang)_2]_2 \bullet 2\ C_{60} \bullet 3$ toluene, the centroids of adjacent molecules of C_{60} in the columns are separated by 10.135 Å.

The observed structure confirms that Phang complexes can disrupt the self-association of C_{60} and produce cocrystals that bring metals and fullerenes together in ordered arrays. As intended, the Phang ligands partially surround each molecule of C_{60} but do not eliminate fullerene-fullerene contacts entirely, so electronic interactions of the type needed to ensure conductivity are retained.

4.2.4 Conclusions

Our work establishes that phosphangulene is an effective ligand for binding metals. Its properties are related to those of other triarylphosphines, but its characteristic conical shape, small cone angle, and low basicity and nucleophilicity give rise to complexes with unique features. As a result, the use of phosphangulene as a ligand is a promising subject for further research in coordination chemistry, catalysis, and other areas. In particular, using phosphangulene to bind metals is a powerful one-step way to construct molecules with multiple concave electron-rich aromatic surfaces. The awkward molecular shape of simple *P*-

substituted derivatives of phosphangulene prevents them from forming π-stacks and forces them to accept less efficient modes of packing. Our observations show that phosphangulene introduces these topological problems in its complexes with metals. As a result, the complexes are effective agents for producing cocrystals, particularly with fullerenes and other partners that have complementary convex electron-poor surfaces. As demonstrated by the structure of $[Ag(O_3SCF_3)(toluene)(Phang)_2]_2 \bullet 2\ C_{60} \bullet 3$ toluene, phosphangulene has a remarkable ability to orchestrate the one-step assembly of ordered solids that integrate both metals and fullerenes.

4.2.5 Experimental Section

All reagents and solvents were obtained from commercial sources and used without further purification unless otherwise indicated. Phosphangulene was prepared by a published procedure.[11] Silver salts and their complexes are typically sensitive to light, so they were handled in the dark, and phosphangulene must be stored and handled under inter atmospheres to prevent its conversion into oxide **2**.

$[Ag(Phang)_4]^+$ BF_4^-. Under dry N_2, a mixture of $AgBF_4$ (14.0 mg, 71.9 μmol) and phosphangulene (86.1 mg, 283 μmol) in CH_2Cl_2 (3 mL) was stirred at 25 °C for 1 h. The addition of hexane (15 mL) caused precipitation of a colorless solid. The supernatant was removed by syringe, and the solid was washed with hexane (5 mL) and dried under N_2 to give $[Ag(Phang)_4]^+$ BF_4^- as a colorless crystalline solid (58.9 mg, 41.7 μmol, 59%): mp 250 °C (dec); FTIR (ATR) 3091, 1604, 1581, 1458, 1421, 1227, 1213, 1057, 1029, 972, 809, 782, 753, 727, 539, 458, 416 cm^{-1}; HRMS (ESI-TOF) *m/z* $[M]^-$ calcd for BF_4 87.00376, found 87.00347; HRMS (ESI-TOF) *m/z* $[M - 2\ Phang]^+$ calcd for $C_{36}H_{18}AgO_6P_2$ 714.96296, found 714.96201. Anal. Calcd for $C_{72}H_{36}AgBF_4O_{12}P_4$: C, 61.26; H, 2.57. Found: C, 61.02; H, 2.39.

Single crystals suitable for analysis by X-ray diffraction could be obtained by partial evaporation of a solution in CH_2Cl_2. Analysis by powder X-ray diffraction confirmed that the crude product was uniformly crystalline and identical in structure to single crystals grown from CH_2Cl_2.[52]

$[Cu(Phang)_4]^+$ BF_4^-. Under dry N_2, a mixture of $[Cu(MeCN)_4]^+$ BF_4^- (4.10 mg, 13.0 μmol) and phosphangulene (15.2 mg, 50.0 μmol) in CH_2Cl_2 (1.5 mL) and MeCN (0.5 mL) was stirred at 25 °C for 12 h. Solvent was allowed to evaporate under a flow of dry N_2, and the solid residue was triturated with hot anhydrous ethanol (2–3 mL). The mixture was filtered, and crystals of $[Cu(Phang)_4]^+$ BF_4^- appeared as the filtrate cooled.

$[Cu(Phang)_4]^+$ PF_6^- • 3 MeOH. An analogous procedure, starting from $[Cu(MeCN)_4]^+$ PF_6^- (4.65 mg, 12.5 μmol) and phosphangulene (15.2 mg, 50.0 μmol) in a mixture of CH_2Cl_2 (1.0 mL) and MeCN (1.0 mL), followed by crystallization from hot MeOH, yielded crystals of $[Cu(Phang)_4]^+$ PF_6^- • 3 MeOH.

$Cu_2Cl_2(Phang)_4$ and $Cu_2Cl_2(Phang)_3$. Under dry N_2, a mixture of CuCl (1.25 mg, 12.6 μmol) and phosphangulene (15.2 mg, 50.0 μmol) in CH_2Cl_2 (1.5 mL) and anhydrous EtOH (0.5 mL) was stirred at 25 °C for 12 h. Solvent was removed from the precipitated solid by syringe, and the residue was triturated with hot anhydrous EtOH (1–2 mL). Cooling the filtered extracts led to the formation of crystals of $Cu_2Cl_2(Phang)_4$ and $Cu_2Cl_2(Phang)_3$.

Crystallizations of Other Complexes. Stock solutions (2.4 μM) of metallic salts in dry degassed EtOH or MeCN were prepared, and aliquots (1.0 mL) were placed in 1-dram vials. A stock solution (9.6 μM) of phosphangulene in dry degassed toluene was also prepared, and

aliquots (1.0 mL, 4.0 equiv) were added to the vials. Additional toluene (2.0 mL) was added to fill the vials, which were then closed with punctured septa, sonicated if necessary to ensure dissolution, and placed in a glovebag under dry N_2 to allow slow evaporation. Crystals of the following complexes were grown in this manner, using the indicated amounts of reagents.

$[Cu_2I_2(Phang)_4]$ • 1 toluene. CuI (0.45 mg, 2.4 μmol) in EtOH (1.0 mL), combined with phosphangulene (2.9 mg, 9.5 μmol) in toluene (1.0 mL), followed by the addition of toluene (2.0 mL).

$[Ag(O_3SCF_3)(H_2O)(Phang)]_2$ and $[Ag(O_3SCF_3)(toluene)(Phang)]_2$. AgO_3SCF_3 (0.61 mg, 2.4 μmol) in EtOH (1.0 mL), combined with phosphangulene (2.9 mg, 9.5 μmol) in toluene (1.0 mL), followed by the addition of toluene (2.0 mL).

$[Ag(ClO_4)(toluene)(Phang)]_2$ and $[Ag(ClO_4)(MeCN)_2(Phang)]_2$. $AgClO_4 • H_2O$ (0.49 mg, 2.2 μmol) in MeCN (1.0 mL), combined with phosphangulene (2.9 mg, 9.5 μmol) in toluene (1.0 mL), followed by the addition of toluene (2.0 mL).

$[Ag(O_3SCF_3)(toluene)(Phang)_2]$ • 1 C_{60}. AgO_3SCF_3 (0.61 mg, 2.4 μmol) in EtOH (1.0 mL), combined with phosphangulene (2.9 mg, 9.5 μmol) in toluene (1.0 mL), C_{60} (6.8 mg, 9.4 μmol) in toluene (1.0 mL), and additional toluene (1.0 mL).

Supporting Information Available: Additional experimental information and crystallographic details, including descriptions of selected structures, ORTEP drawings, and tables of structural data in CIF format. This material is available free of charge via the Internet at http://pubs.acs.org.

Acknowledgments. We are grateful to the Natural Sciences and Engineering Research Council of Canada, the Ministère de l'Éducation du Québec, the Canada Foundation for Innovation, the Canada Research Chairs Program, and Université de Montréal for financial support. In addition, we thank reviewers for insightful comments.

Notes. The authors declare no competing financial interest.

4.2.6 References

1. Krebs, F. C.; Larsen, P. S.; Larsen, J.; Jacobsen, C. S.; Boutton, C.; Thorup, N. Synthesis, Structure, and Properties of 4,8,12-Trioxa-12c-phospha-4,8,12,12c-tetrahydrodibenzo[*cd*,*mn*]pyrene, a Molecular Pyroelectric. *J. Am. Chem. Soc.* **1997**, *119*, 1208–1216.
2. Madsen, G. K. H.; Krebs, F. C.; Lebech, B.; Larsen, F. K. Evaluation of the Solid State Dipole Moment and Pyroelectric Coefficient of Phosphangulene by Multipolar Modeling of X-ray Structure Factors. *Chem. Eur. J.* **2000**, *6*, 1797–1804.
3. Faldt, A.; Krebs, F. C.; Thorup, N. Synthesis, Structure and Properties of Various Molecules Based on the 4,8,12-Trioxa-4,8,12,12c-tetrahydrodibenzo[*cd*,*mn*]pyrene System with an Evaluation of the Effect Differing Molecular Substitution Patterns has on the Space Group Symmetry. *J. Chem. Soc., Perkin Trans 2* **1997**, 2219–2227.
4. Hirai, M.; Tanaka, N.; Sakai, M.; Yamaguchi, S. Structurally Constrained Boron-, Nitrogen-, Silicon-, and Phosphorus-Centered Polycyclic π-Conjugated Systems. *Chem. Rev.* **2019**, *119*, 8291–8331.

5. Yamamura, M.; Hasegawa, T.; Nabeshima, T. Synthesis of Phosphorus-Centered and Chalcogen-Bridged Concave Molecules: Modulation of Bowl Geometries and Packing Structures by Changing Bridging Atoms. *Org. Lett.* **2016,** *18*, 816–819.

6. Yamamura, M.; Nabeshima, T. Relationship between the Bowl-Shaped Geometry of Phosphangulene and an Axial Group on the Phosphorus Atom. *Bull. Chem. Soc. Jpn.* **2016,** *89*, 42–49.

7. Yamamura, M.; Hongo, D.; Nabeshima, T. Twofold Fused Concave Hosts Containing Two Phosphorus Atoms: Modules for the Sandwich-Type Encapsulation of Fullerenes in Variable Cavities. *Chem. Sci.* **2015**, *6*, 6373–6378.

8. Yamamura, M.; Sukegawa, K.; Nabeshima, T. Tuning the Depth of Bowl-Shaped Phosphine Hosts: Capsule and Pseudo-Cage Architectures in Host–Guest Complexes with C_{60} Fullerene. *Chem. Commun*. **2015**, *51*, 12080–12083.

9. Yamamura, M.; Saito, T.; Nabeshima, T. Phosphorus-Containing Chiral Molecule for Fullerene Recognition Based on Concave/Convex Interaction. *J. Am. Chem. Soc.* **2014**, *136*, 14299–14306.

10. Heskia, A.; Maris, T.; Wuest, J. D. Putting Fullerenes in Their Place: Cocrystallizing C_{60} and C_{70} with Phosphangulene Chalcogenides. *Cryst. Growth Des*. **2019**, *19*, 5418-5428.

11. Heskia, A.; Maris, T.; Wuest, J. D. Foiling Normal Patterns of Crystallization by Design. Polymorphism of Phosphangulene Chalcogenides. *Cryst. Growth Des*. **2019**, *19*, 5390-5406.

12. Lee, H.; Park, C.; Sin, D. H.; Park, J. H.; Cho, K. Recent Advances in Morphology Optimization for Organic Photovoltaics. *Adv. Mater.* **2018**, *30*, 1800453.

13. Lai, Y.-Y.; Cheng, Y.-J.; Hsu, C.-S. Applications of Functional Fullerene Materials in Polymer Solar Cells, *Energy Environ. Sci.* **2014**, *7*, 1866–1883.

14. Dang, M. T.; Hirsch, L.; Wantz, G.; Wuest, J. D. Controlling the Morphology and Performance of Bulk Heterojunctions in Solar Cells. Lessons Learned from the Benchmark Poly(3-hexylthiophene):[6,6]-Phenyl-C_{61}-butyric Acid Methyl Ester System. *Chem. Rev.* **2013**, *113*, 3734–3765.

15. Ganin, A. Y.; Takabayashi, Y.; Jeglič, P.; Arčon, D.; Potočnik, A.; Baker, P. J.; Ohishi, Y.; McDonald, M. T.; Tzirakis, M. D.; McLennan, A.; Darling, G. R.; Takata, M.; Rosseinsky, M. J.; Prassides, K. Polymorphism Control of Superconductivity and Magnetism in Cs_3C_{60} Close to the Mott Transition. *Nature* **2010**, *466*, 221–225.

16. Schiros, T.; Kladnik, G.; Prezzi, D.; Ferretti, A.; Olivieri, G.; Cossaro, A.; Floreano, L.; Verdini, A.; Schenck, C.; Cox, M.; Gorodetsky, A. A.; Plunkett, K.; Delongchamp, D.; Nuckolls, C.; Morgante, A.; Cvetko, D.; Kymissis, I. Donor-Acceptor Shape Matching Drives Performance in Photovoltaics. *Adv. Energy Mater*. **2013**, *3*, 894−902.

17. Kraft, A.; Roger, C.; Schmidt, D.; Stangl, J.; Müller-Buschbaum, K.; Beuerle, F. Metal-Based Diversity for Crystalline Metal-Fullerene Frameworks. *Chem. Eur. J.* **2017**, *23*, 15864−15868.

18. Rice, A. M.; Dolgopolova, E. A.; Shustova, N. B. Fulleretic Materials: Buckyball- and Buckybowl-Based Crystalline Frameworks. *Chem. Mater*. **2017**, *29*, 7054−7061.

19. Balch, A. L.; Winkler, K. Two-Component Polymeric Materials of Fullerenes and the Transition Metal Complexes: A Bridge between Metal−Organic Frameworks and Conducting Polymers. *Chem. Rev*. **2016**, *116*, 3812−3882.

20. Selmani, S.; Schipper, D. J. π-Concave Hosts for Curved Carbon Nanomaterials. *Chem. Eur. J.* **2019**, *25*, 6673–6692.

21. Sygula, A. Corannulene-Adorned Molecular Receptors for Fullerenes Utilizing the π–π Stacking of Curved-Surface Conjugated Carbon Networks. Design, Synthesis and Testing. *Synlett* **2016**, *27*, 2070–2080.

22. Kooijman, H.; Spek, A. L.; van Bommel, K. J. C.; Verboom, W.; Reinhoudt, D. N. A Triclinic Modification of Triphenylphosphine. *Acta Crystallogr., Sect. C: Struct. Chem.* **1998**, *54*, 1695–1698.

23. Livant, P.; Sun, Y. J.; Webb, T. R. Structure of Tris(2,6-dimethoxyphenyl)phosphine. *Acta Crystallogr., Sect. C: Struct. Chem.* **1991**, *47*, 1003–1005.

24. Cotton, F. A.; Goodgame, D. M. L. Tetrakis(triphenylphosphine)-silver(I) and -copper(I) Complexes. *J. Chem. Soc.* **1960**, 5267–5269.

25. Wada, M.; Higashizaki, S. A Highly Basic Triphenylphosphine, [2,4,6-$(MeO)_3C_6H_2]_3P$. *J. Chem. Soc., Chem. Commun.* **1984**, 482–483.

26. Yamashoji, Y.; Matsushita, T.; Tanaka, M.; Shono, T.; Wada, M. Ion-Pair Extraction of the Gallium(III) Ion from Hydrochloric Acid with Various Methoxy-Substituted Triarylphosphines. *Polyhedron* **1989**, *8*, 1053–1059.

27. Streuli, C. A. Determination of Basicity of Substituted Phosphines by Nonaqueous Titrimetry. *Anal. Chem*. **1960**, *32*, 985–987.

28. Wada, M.; Hayase, S.; Fujiwara, M.; Kawaguchi, T.; Iwasaki, T.; Uo, A.; Erabi, T. Crystal Structure and Chemical Properties of Tris(2,6-dimethoxyphenyl)phosphine Selenide. *Bull. Chem. Soc. Jpn.* **1996**, *69*, 655–664.

29. Follet, E.; Mayer, P.; Stephenson, D. S.; Ofial, A. R.; Berionni, G. Reactivity-Tuning in Frustrated Lewis Pairs: Nucleophilicity and Lewis Basicity of Sterically Hindered Phosphines. *Chem. Eur. J.* **2017**, *23*, 7422–7427.

30. Yasui, S.; Itoh, K.; Ohno, A. Kinetic Study on Debromination of *vic*-Dibromides with Trivalent Phosphorus Compounds. *Heteroatom Chem.* **2001**, *12*, 217–222.

31. Meijboom, R.; Bowen, R. J.; Berners-Price, S. J. Coordination Complexes of Silver(I) with Tertiary Phosphine and Related Ligands. *Coord. Chem. Rev.* **2009**, *253*, 325–342.

32. Ng, S. W. Tetrakis(triphenylphosphane-*κP*)silver(I) Trifluoroacetate Ethanol Monosolvate. *Acta Crystallogr., Sect. E: Crystallogr. Commun.* **2012**, *68*, m1536.

33. Huang, X.; Qiu, Q.-M.; Wang, X.; Jin, Q.-H.; Zhang, C.-L. Tetrakis(triphenylphosphane-*κP*)silver(I) Tetrafluoridoborate. *Acta Crystallogr., Sect. E: Crystallogr. Commun.* **2012**, *68*, m706.

34. Jiang, Y.-H.; Cui, L.-N.; Huang, X.; Jin, Q.-H.; Zhang, C.-L. Tetrakis(triphenylphosphane-*κP*)silver(I) Trifluoromethanesulfonate Dichloromethane Monosolvate. *Acta Crystallogr., Sect. E: Crystallogr. Commun.* **2011**, *67*, m1499.

35. Wen, J.; Jiang, Y.-H.; Wu, M.-H.; Jin, Q.-H.; Gong, H.-L. Crystal Structure of Tetrakis(triphenylphospine-*κP*)silver(I) Trifluoromethanesulfonate, $[Ag(P(C_6H_5)_3)_4][SO_3CF_3]$. *Z. Kristallogr.* **2011**, *226*, 269–270.

36. Altaf, M.; Stoeckli-Evans, H. Silver(I) Tertiary Phosphine Complexes: Influence of the Anion on the Structural and Spectroscopic Properties. *Polyhedron* **2010**, *29*, 710–708.

37. Ma, Z.; Lin, Y.; Chen, Z. Syntheses and Crystal Structures of Two Silver(I) Complexes Isolated by the Reaction of $[Ag(PPh_3)_2(MeCN)](SbF_6)$ with a N6 Ligand. *Chin. J. Struct. Chem.* **2004**, *23*, 1277–1281.

38. Ellis, D. D.; Spek, A. L. Tetrakis(triphenylphosphine)silver(I) Tetraphenylborate Acetonitrile Solvate. *Acta Crystallogr., Sect. C: Struct. Chem.* **2000**, *56*, e547–e548.

39. Cotton, F. A.; Luck, R. L. Structure of $[Ag(PPh_3)_4]PF_6$. *Acta Crystallogr., Sect. C: Struct. Chem.* **1989**, *45*, 1222–1224.

40. Engelhardt, L. M.; Pakawatchai, C.; White, A. H.; Healy, P. C. Lewis-Base Adducts of Group 1B Metal(I) Compounds. Part 13. Crystal Structure Determinations of Tetrakis(triphenylphosphine)copper(I) and -silver(I) Perchlorates, Bis(pyridine)bis(tripheny1phosphine)copper(I) Perchlorate, (2,2'-Bipyridyl)bis(triphenylphosphine)copper(I) Perchlorate, and Tetrahydroboratobis(triphenylphosphine)copper(I)-Pyridine (1/0.5). *J. Chem. Soc., Dalton Trans.* **1985**, 125–133.

41. Pelizzi, C.; Pelizzi, G.; Tarasconi, P. Synthesis and Crystal and Molecular Structure of a Silver Tin Complex Salt, $[Ag(PPh_3)_4][SnPh_2(NO_3)_2(Cl,NO_3)]$. *J. Organomet. Chem.* **1984**, *277*, 29–35.

42. Dance, I.; Scudder, M. Molecules Embracing in Crystals. *CrystEngComm* **2009**, *11*, 2233–2247.

43. Scudder, M.; Dance, I. Sixfold Phenyl Embraces with Substituted Phenyl in PPh_3. *J. Chem. Soc., Dalton Trans.* **2000**, 2909–2915.

44. Dance, I.; Scudder, M. Crystal Supramolecularity: Sixfold Phenyl Embraces Between PPh_3 Ligands, Forming Extended Nets in One-, Two-, and Three-Dimensions. *J. Chem. Soc., Dalton Trans.* **2000**, 1587–1594.

45. Dance, I.; Scudder, M. Intramolecular and Supramolecular Geometry of Coordinated PPh_3. *J. Chem. Soc., Dalton Trans.* **2000**, 1579–1585.

46. Hirshfeld surfaces and two-dimensional fingerprint plots were generated by using CrystalExplorer17. Turner, M. J.; McKinnon, J. J.; Wolff, S. K.; Grimwood, D. J.; Spackman, P. R.; Jayatilaka, D.; Spackman, M. A. *CrystalExplorer17*; University of Western Australia, 2017.

47. McKinnon, J. J.; Spackman, M. A.; Mitchell, A. S. Novel Tools for Visualizing and Exploring Intermolecular Interactions in Molecular Crystals. *Acta Crystallogr., Sect. B: Struct. Sci.* **2004**, *60*, 627–668.

48. Maly, K. E.; Gagnon, E.; Wuest, J. D. Engineering Molecular Crystals with Abnormally Weak Cohesion. *Chem. Commun.* **2011**, 5163−5165.

49. Gagnon, E.; Halperin, S. D.; Métivaud, V.; Maly, K. E.; Wuest, J. D. Tampering with Molecular Cohesion in Crystals of Hexaphenylbenzenes. *J. Org. Chem.* **2010**, *75*, 399−406.

50. Zhou, H.; Dang, H.; Yi, J.-H.; Nanci, A.; Rochefort, A.; Wuest, J. D. Frustrated 2D Molecular Crystallization. *J. Am. Chem. Soc.* **2007**, *129*, 13774−13775.

51. Lebel, O.; Maris, T.; Perron, M.-È.; Demers, E.; Wuest, J. D. The Dark Side of Crystal Engineering: Creating Glasses from Small Symmetric Molecules that Form Multiple Hydrogen Bonds. *J. Am. Chem. Soc.* **2006**, *128*, 10372−10373.

52. See the Supporting Information for details.

53. Alyea, E. C.; Malito, J.; Nelson, J. H. Identification by Stopped-Exchange Solution ^{31}P NMR Spectroscopy of the Stepwise Formation of $[AgL_n]PF_6$ (n = 1-4). Comparison of Metal-Phosphorus Coupling Constants for Triphenylphosphine and 5-Phenyldibenzophosphole. *Inorg. Chem.* **1987**, *26*, 4294−4296.

54. Socol, S. M.; Verkade, J. G. Ligation of Phosphorus Ligands to Silver(I). 2. Electronic and Steric Effects in the Coordination of One to Four $P(OR)_3$ and PR_3 Ligands. *Inorg. Chem.* **1984**, *23*, 3487−3493.

55. Maini, L.; Braga, D.; Mazzeo, P. P.; Ventura, B. Polymorph and Isomer Conversion of Complexes Based on CuI and PPh_3 Easily Observed *via* Luminescence. *Dalton Trans.* **2012**, *41*, 531−539.

56. Lazarou, K.; Bednarz, B.; Kubicki, M.; Verginadis, I. I.; Charalabopoulos, K.; Kourkoumelis, N.; Hadjikakou, S. K. Structural, Photolysis and Biological Studies of the Bis(μ_2-chloro)-tris(triphenylphosphine)-di-copper(I) and Chloro-tris(triphenylphosphine)-copper (I) Complexes. Study of Cu(I)–Cu(I) Interactions. *Inorg. Chim. Acta* **2010**, *363*, 763–772.

57. Kräuter, T.; Neumüller, B. Triphenylphosphane Complexes of Copper(I): Structural and ^{31}P NMR Investigations. *Polyhedron* **1996**, *15*, 2851−2857.

58. Darensbourg, D. J.; Holtcamp, M. W.; Klausmeyer, K. K.; Reibenspies, J. H. Crystal Structure of Di-μ-chloro-tris(triphenylphosphine)dicopper(I)−Dichloromethane, $C_{55}H_{47}Cl_4Cu_2P_3$. *Z. Kristallogr.* **1995**, *210*, 615–616.

59. Gill, J. T.; Mayerle, J. J.; Welcker, P. S.; Lewis, D. F.; Ucko, D. A.; Barton, D. J.; Stowens, D.; Lippard, S. J. Structural Determinations of Four Mono- and Binuclear Tertiary Phosphine and Arsine Complexes of Copper(I) Chloride. *Inorg. Chem.* **1976**, 15, 1155−1168.

60. Albano, V. G.; Bellon, P. L.; Ciani, G.; Manassero, M. Crystal and Molecular Structure of Di-μ-chloro-tris(triphenylphosphine)dicopper(I), $Cu_2Cl_2(PPh_3)_3$. *J. Chem. Soc., Dalton Trans.* **1972**, 171–175.

61. Lewis, D. F.; Lippard, S. J.; Weicker, P. S. Structure of Dichlorotris(triphenylphosphine)dicopper(I)−Benzene, a Chloride-Bridged Dimer Containing Both Three- and Four-Coordinate Copper. *J. Am. Chem. Soc.* **1970**, *92*, 3805–3807.

62. Dyason, J. C.; Engelhardt, L. M.; Pakawatchai, C.; Healy, P. C.; White, A. H. Lewis-Base Adducts of Group 1B Metal(I) Compounds. XXI. The Crystal and Molecular Structures of the Unsolvated Forms of Dibromotris(triphenylphosphine)dicopper(I) and 'Step' Tetrabromotetrakis(triphenylphosphine)tetracopper(I). *Aust. J. Chem.* **1985**, *38*, 1243–1250.

63. Negita, H.; Hiura, M.; Kushi, Y.; Kuramoto, M.; Okuda, T. The Crystal Structure of Di-μ-bromo-tris(triphenylphosphine)dicopper(II). *Bull. Chem. Soc. Jpn.* **1981**, 54, 1247–1248.

64. Eller, P. G.; Kubas, G. J.; Ryan, R. R. Synthesis and Properties of Sulfur Dioxide Adducts of Organophosphinecopper(I) Iodides. Structures of the Dinuclear Compounds Tetrakis(methyldiphenylphosphine)di-μ-iodo-dicopper(I)−Sulfur Dioxide and Tris(triphenylphosphine)di-μ-iodo-dicopper(I). *Inorg. Chem.* **1977**, *16*, 2454−2462.

65. Fife, D. J.; Moore, W. M.; Morse, K. W. Solution Equilibria of Tertiary Phosphine Complexes of Copper(I) Halides. *Inorg. Chem.* **1984**, *23*, 1684–1691.

66. Lawrance, G. A. Coordinated Trifluoromethanesulfonate and Fluorosulfate. *Chem. Rev.* **1986**, *86*, 17–33.

67. Lettko, L.; Wood, J. S.; Rausch, M. D. Synthesis of (Phosphine)silver(I) Trifluoromethanesulfonate Complexes and the Molecular Structure of Di-μ-

trifluoromethanesulfonate-(tetrakis-triphenylphosphine)disilver(I). *Inorg. Chim. Acta* **2000**, *308*, 37–44.

68. Bardají, M.; Crespo, O.; Laguna, A.; Fischer, A. K. Structural Characterization of Silver(I) Complexes $[Ag(O_3SCF_3)(L)]$ (L = PPh_3, PPh_2Me, SC_4H_8) and $[AgL_n](CF_3SO_3)$ (*n* = 2–4), (L = PPh_3, PPh_2Me). *Inorg. Chim. Acta* **2000**, *304*, 7–16.

69. Mulliken, R. S. Molecular Compounds and their Spectra. II. *J. Am. Chem. Soc.* **1952**, *74*, 811–824.

70. Cui, L.-N.; Jin, Q.-H.; Hu, K.-Y.; Zhang, C.-L. (Methanol-*κO*)(perchlorato-*κO*)bis(triphenylphosphine-*κP*)silver(I). *Acta Crystallogr., Sect. E: Struct. Rep*. **2010**, *66*, m969.

71. Cui, L.-N.; Hu, K.-Y.; Jin, Q.-H.; Zhang, C.-L. (Perchlorato-*κO*)tris(triphenylphosphine-*κP*)silver(I). *Acta Crystallogr., Sect. E: Struct. Rep*. **2010**, *66*, m871.

72. Effendy; Marchetti, F.; Pettinari, C.; Skelton, B. W.; White, A. H. Synthesis and Structural Characterization of Adducts of Silver(I) Perchlorate with PR_3 (R = Ph, cy, *o*-tolyl) and Oligodentate Aromatic Bases Derivative of 2,2'-Bipyridyl, L, $AgClO_4$:PR_3:L (1:1:1). *Inorg. Chem. Acta* **2007**, *360*, 1414–1432.

73. Zhang, Z.-X.; Li, Y.; Li, K.-C.; Song, W.-D.; Li, Q.-S.; Xiong, H.-P.; Xu, J.-Q.; Pan, L.-Y. Synthesis, Crystal Structure and Third-Order Nonlinear Optical Properties of Heterometallic Cluster $[WM_2S_4(PPh_3)_3] \cdot DMF$ (M_2 = 1.25Ag+0.75Cu). *J. Mol. Struct.* **2006**, *791*, 117–121.

74. Edwards, D. A.; Harker, R. M.; Mahon, M. F.; Molloy, K. C. Crystallographic Analysis of an Intramolecularly Stabilised Organosilver Tetramer,

[$Ag(C_6H_4CH_2NMe_2\text{-}2)]_4$, and the First Structurally Characterised Silver Siloxide, {[$Ag(PPh_3)]_2(\mu\text{-}OMe_2SiOSiMe_2O)\}_2$. *J. Chem. Soc., Dalton Trans.* **1997**, 3509–3513.

75. Schmidbaur, H.; Schier, A. Argentophilic Interactions. *Angew. Chem. Int. Ed.* **2015**, *54*, 746–784.

76. Xia, C.-K.; Min, Y.-Y.; Yang, K.; Sun, W.; Jiang, D.-L.; Chen, M. Syntheses, Crystal Structures, and Properties of Three Novel Silver–Organic Frameworks Assembled from 1,2,3,5-Benzenetetracarboxylic Acid Based on Argentophilic Interactions. *Cryst. Growth Des.* **2018**, *18*, 1978–1986.

77. Soliman, S. M.; Elsilk, S. E. Synthesis, X-Ray Structure, DFT and Antimicrobial Studies of Ag(I) Complexes with Nicotinic Acid Derivatives. *J. Photochem. Photobiol. B* **2018**, *187*, 48–53.

78. Lamming, G.; Kolokotroni, J.; Harrison, T.; Penfold, T. J.; Clegg, W.; Waddell, P. G.; Probert, M. R.; Houlton, A. Structural Diversity and Argentophilic Interactions in One-Dimensional Silver-Based Coordination Polymers. *Cryst. Growth. Des*. **2017**, *17*, 5753–5763.

79. Johnson, R. D.; Bethune, D. S.; Yannoni, C. S. Fullerene Structure and Dynamics: A Magnetic Resonance Potpourri. *Acc. Chem. Res*. **1992**, *25*, 169−175.

80. Langis-Barsetti, S.; Maris, T.; Wuest, J. D. Molecular Organization of 2,1,3-Benzothiadiazoles in the Solid State. *J. Org. Chem.* **2017**, *82*, 5034−5045.

4.2.7 Table of Contents Graphic

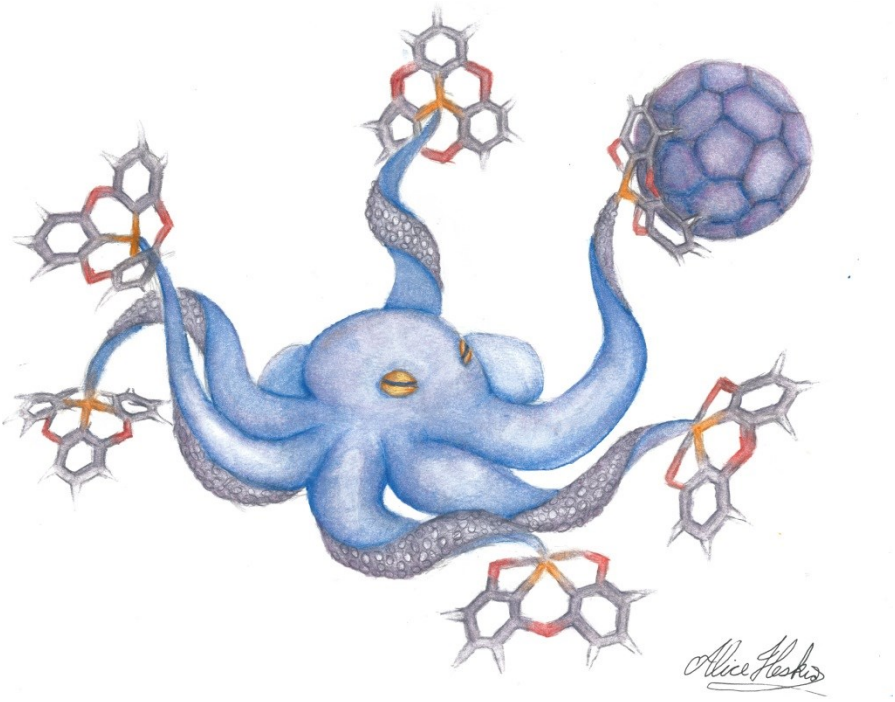

4.3 Conclusions

Nous avons réussi à synthétiser une série de complexes métalliques de phosphangulène analogues à ceux de la triphénylphosphine. Nous avons été en mesure de juger de la qualité en tant que ligand du phosphangulène en le comparant avec la triphénylphosphine. Il semblerait qu'un effet stérique plutôt qu'un effet électronique soit à l'origine de la force de ligand du phosphangulène.

Nous avons réussi à obtenir une structure incluant des fullerènes disposés dans les cavités de phosphangulène d'un complexe avec Ag(I). Ceci démontre la faisabilité du concept selon lequel il est possible de construire un réseau constitué d'un centre autour duquel de nombreuses surfaces concaves de phosphangulène sont disposées de façon à permettre des molécules de fullerène à venir se loger.

Chapitre 5 :
Sels de bis(phosphangulène)iminium

5.1 Introduction

Comme expliqué dans le chapitre précédent, nous voulions produire des composés présentant de nombreux sites concaves pouvant interagir avec des fullerènes. À l'instar de la stratégie du chapitre dernier, consistant à s'inspirer des précédents basés sur l'analogie avec la triphénylphosphine, nous nous sommes intéressés au cation μ-nitrido-bis(triphénylphosphine) et à la possibilité de synthétiser une structure similaire dérivée du phosphangulène. Ici, plutôt que d'employer un métal de transition pour lier plusieurs unités phosphines, on se sert d'un atome d'azote. Le résultat est une espèce cationique dans laquelle deux phosphines sont pontées par un atome d'azote. Ce qui rend ce cation encore plus intéressant est qu'il est connu pour stabiliser des anions complexes et instables. Il n'est donc pas difficile d'imaginer notre intérêt pour la synthèse de l'analogue phosphangulène dans l'optique de former des sels stables avec des fullerènes anioniques.

5.1.1 Cation μ-nitrido-bis(triphénylphosphine)

L'isolation et la cristallisation de certains anions complexes peuvent être facilitées par l'emploi de cations massifs et organiques permettant d'obtenir des sels solubles dans des solvants organiques polaires. Les sels de ce genre de cations sont souvent plus stables que si l'anion avait été pairé avec un cation plus simple. À titre d'appui, on peut citer les travaux de Ruff *et al.*,[8] qui démontrent qu'il est possible d'isoler ainsi des sels de complexes anioniques comportant des ligands labiles de carbonyles, $[M_m(CO)_n]^{x-}$ (M = Cr, Mn, W, Mo, V), qui sont autrement instables.

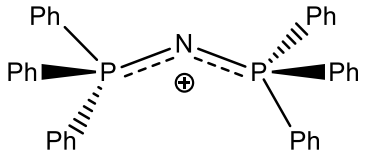

PPN^+

Cation μ-nitrido-bis(triphénylphosphine)
Bis(triphénylphosphine)iminium
Bis(triphénylphosphoranylidène)iminium
Bis(triphénylphosphoranylidène)ammonium
Hexaphényldiphosphazènium

Plus tard, lorsque l'engouement pour les anions de fullerènes comme supraconducteurs naquit, Reed,[9] Moriyama[10] et leurs collaborateurs intéressèrent à ce cation et présentèrent des travaux montrant que le bis(triphénylphosphine)iminium peut cocristalliser avec des anions de C_{60} permettant de donner des structures suffisamment stables et de qualité pour l'étude de l'électronique du fullerure. L'application du PPN^+ pour stabiliser et organiser

[8] Ruff, J. K.; Schlientz, W. J. *Inorg. Synth.* **1974**, *15*, 84–90.
[9] Bhyrappa, P.; Paul, P.; Stinchcombe, J.; Boyd, P. D. W.; Reed, C. A. *J. Am. Chem. Soc.* **1993,** *115* (23), 11004-11005.
[10] Moriyama, H.; Kobayashi, H.; Kobayashi, A.; Watanabe, T. *J. Am. Chem. Soc.* **1993,** *115* (3), 1185-1187.

les fullerures rejoignant exactement nos objectifs de recherche, la synthèse de l'analogue de phosphangulène est d'autant plus pertinente.

De plus, la simplicité de synthèse du PPN^+ pourrait en principe rendre la cible analogue de phosphangulène facilement accessible. Ruff et Schlientz[8] avaient également développé une procédure simplifiée pour synthétiser le PPN^+, qui originellement se faisait en quatre étapes.[11] Le cation est maintenant obtenu sous forme de sel de chlorure en une seule étape par la procédure suivante : la triphénylphosphine est d'abord traitée au Cl_2, suivi de l'addition *in situ* de l'hydroxylamine pour y introduire l'azote. Lalor *et al.*[12] démontrèrent qu'il est possible et même encore plus simple d'employer du Br_2 pour l'étape initiale, résultant au sel de bromure.

[11] Appel, R.; Hauss, A. *Z. Anorg. Allg. Chem.* **1961,** *311* (5-6), 290-301.
[12] Lalor, F. J.; Chaona, S., *J. Organomet. Chem.* **1988,** *344* (2), 163-165.

5.1.2 Objectifs

Les travaux décrits dans le présent chapitre ont eu pour buts dans un premier temps de synthétiser le cation de bis(phosphangulène)iminium, analogue au bis(triphénylphosphine)iminium, sous forme de sels avec des contre-ions variés. À partir de là, nous avons visé à produire des structures cocristallines des différents sels de bis(phosphangulène)iminium avec des fullerènes, afin d'en étudier la structure cristalline et les interactions intermoléculaires. Le niveau supérieur de ce projet, constituant ainsi le but ultime des travaux présentés ici, a été de cocristalliser notre cation avec un fullerure sans aucun autre contre-ion, afin d'obtenir une structure du genre $[PPN]_n^+[C_{60}]^{n-}$.

5.2 Article 4

Manuscrit soumis à

Cryst. Growth Des.

Bis(phosphangulene)iminium Salts.

Holding on to Fullerenes with Phangs

Alice Heskia, Thierry Maris, and James D. Wuest*

Département de Chimie, Université de Montréal, Montréal, Québec H3C 3J7 Canada

*Author to whom correspondence may be addressed.

E-mail: *james.d.wuest@umontreal.ca*

5.2.1 Abstract

Phosphangulene ("Phang") is an analogue of triphenylphosphine with a conical shape and electron-rich aromatic surface that complements the electron-poor surface of fullerenes, both geometrically and electronically. Large molecular surfaces with multiple areas of concavity can be made by grafting units of Phang onto selected cores, using the ability of phosphorus to form covalent bonds with many other elements. Incorporating multiple conical subunits of Phang creates molecules that are awkwardly shaped, unable to pack efficiently, and predisposed to form cocrystals. To demonstrate the potential of this approach, we made salts of the bis(phosphangulene)iminium cation ($[(Phang)_2N]^+$), in which the phosphorus atoms of two Phang groups are bonded to a single atom of nitrogen. Analysis of the structures of various salts shows that $[(Phang)_2N]^+$ has a unique ability to stabilize unusual anions, including those incorporating fullerenes.

5.2.2 Introduction

Phosphangulene (**1**), a hexacyclic triarylphosphine first reported by Krebs and coworkers in 1997,[1] continues to attract attention.[2–12] A feature of particular interest is the distinctive conical topology of phosphangulene and its derivatives. The shape of phosphangulene favors molecular stacking (Figure 5.1a), which leads to the formation of *R*3*m* crystals that are polar and pyroelectric.[1,2] Converting phosphangulene into the corresponding oxide **2** or other chalcogenides adds only one atom but creates awkwardly-shaped molecules that can no longer be stacked efficiently and are forced to crystallize in less favorable ways, typically by forming offset clamshell pairs held together by mutual C-H···π interactions (Figure 5.1b).[6,11] Evidence that the crystallization of oxide **2** and related compounds is inherently problematic is provided by the observation that they are highly polymorphic and yield crystals with large numbers of molecules in the unit cell and asymmetric unit, and form solid solutions, solvates, and cocrystals.[11]

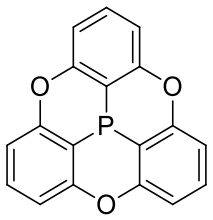

1

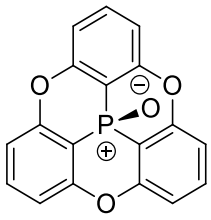

2

a b

Figure 5.1 : Comparison of molecular organization in crystals of phosphangulene (**1**) and oxide **2**. (a) Stacking of molecules of phosphangulene in crystals grown from ethyl acetate.[1] (b) Offset clamshell pair formed by molecules of oxide **2** in crystals of a representative polymorphic form. Atoms of carbon appear in gray, hydrogen in white, oxygen in red, and phosphorus in yellow-orange.

Phosphangulene offers a concave electron-rich aromatic surface that is geometrically and electronically complementary to the convex electron-poor surface of C_{60} and other fullerenes. As a result, suitable derivatives of phosphangulene can bind fullerenes in solution or can form cocrystals in which fullerenes are positioned in various ways.[7–10] Finding effective ways to arrange fullerenes is a prerequisite for exploiting their utility, such as their ability to serve as electron acceptors in the active layers of molecule-based optoelectronic devices, including solar cells. If properly positioned with respect to other components,[13–15] fullerenes and related compounds can accept electrons from the excited states of neighboring chromophores and then allow the electrons to be conducted to the cathode through chains of fullerene-fullerene

contacts. Properly positioned fulleride anions can also give rise to high-temperature superconductivity, as demonstrated by the behavior of crystals of Cs_3C_{60} in both face-centered and body-centered cubic forms.[16] These examples provide strong motivation to learn how to organize fullerenes by exploiting their affinity for derivatives of phosphangulene and other suitably designed small molecules, based on concave-convex complementarity and other phenomena.[17-21]

Phosphangulene is an effective ligand (abbreviated as Phang), and its coordination to metals permits the simple one-step synthesis of complexes in which multiple Phang ligands are held in well-defined positions.[12] The surfaces of these complexes have multiple concave patches with a strong affinity for fullerenes. Moreover, like simpler *P*-substituted derivatives of phosphangulene, the complexes have an awkward shape and cannot be packed efficiently without complementary partners. As a result, the complexes are promising agents for producing cocrystals, including those that incorporate fullerenes, hold them in predetermined arrangements, and place them in proximity to metals.

We recognized that another simple way to make large molecular surfaces with multiple regions of concavity is to graft units of Phang onto suitable cores, by using the ability of phosphorus to form strong covalent bonds with many other elements. To test the feasibility of this strategy, we selected a small but intriguing target in which the phosphorus atoms of two Phang groups are bonded to a single atom of nitrogen to create the bis(phosphangulene)iminium cation ($[(Phang)_2N]^+$). Salts of the analogous bis(triphenylphosphine)iminium cation ($[(Ph_3P)_2N]^+$) were first reported in 1961,[22] and over 1000 structures have since been described.[23,24] Salts of $[(Ph_3P)_2N]^+$ have special properties

attributed to the large globular shape and aromatic surface of the cation.[23-29] These features help make the $[(Ph_3P)_2N]^+$ ion weakly coordinating and enhance the solubility of its salts in organic solvents, facilitate crystallization, and stabilize reactive anions. We expected the corresponding $[(Phang)_2N]^+$ ion to have unique properties of its own and to be able to form unusual salts, such as those including fullerenes or their anionic reduced forms, which are normally species of high reactivity.[30,31]

5.2.3 Results and Discussion

Synthesis and Crystallization of Salts of $[(Phang)_2N]^+$. Phosphangulene was made by modifying the original method of Krebs and coworkers.[1,11] $[(Phang)_2N]^+ Br^-$ was prepared in 82% yield by treating phosphangulene with Br_2 and NH_2OH under conditions similar to those used to make $[(Ph_3P)_2N]^+ Br^-$.[23] Other salts of $[(Phang)_2N]^+$ were typically made by simple metathesis.

$[(Phang)_2N]^+ BF_4^-$. Crystals of $[(Phang)_2N]^+ BF_4^-$ were grown by allowing solvent to evaporate slowly from solutions in CS_2. Crystallographic data are provided in Table 5.1, and views of the structure are shown in Figure 5.2. The structures of many salts of $[(Ph_3P)_2N]^+$ have been described, but very few have included small anions; however, two structures of the BF_4^- salt have been reported.[32,33] In $[(Phang)_2N]^+ BF_4^-$, the average P-N bond length (1.571 Å) is closely similar to the average (1.58 Å) calculated for all $[(Ph_3P)_2N]^+$ structures deposited in the Cambridge Structural Database (CSD).[23,24] Closely similar average values (1.582 Å) are found in both structures of $[(Ph_3P)_2N]^+ BF_4^-$.[26,27] The average P-N-P bond angle for all salts of $[(Ph_3P)_2N]^+$ is 142.6°, based again on data in the CSD, but individual values vary widely, and the angle observed in $[(Phang)_2N]^+ BF_4^-$ lies at the lower end of the range (136.4°). Similar

values (137.7° and 138.5°) are observed in the structures of $[(Ph_3P)_2N]^+ BF_4^-$.[32,33] Bonding to nitrogen flattens the conical shape of Phang slightly, and the average C-P-C angle in $[(Phang)_2N]^+ BF_4^-$ is 100.2°, whereas the value is 93.0° in phosphangulene itself

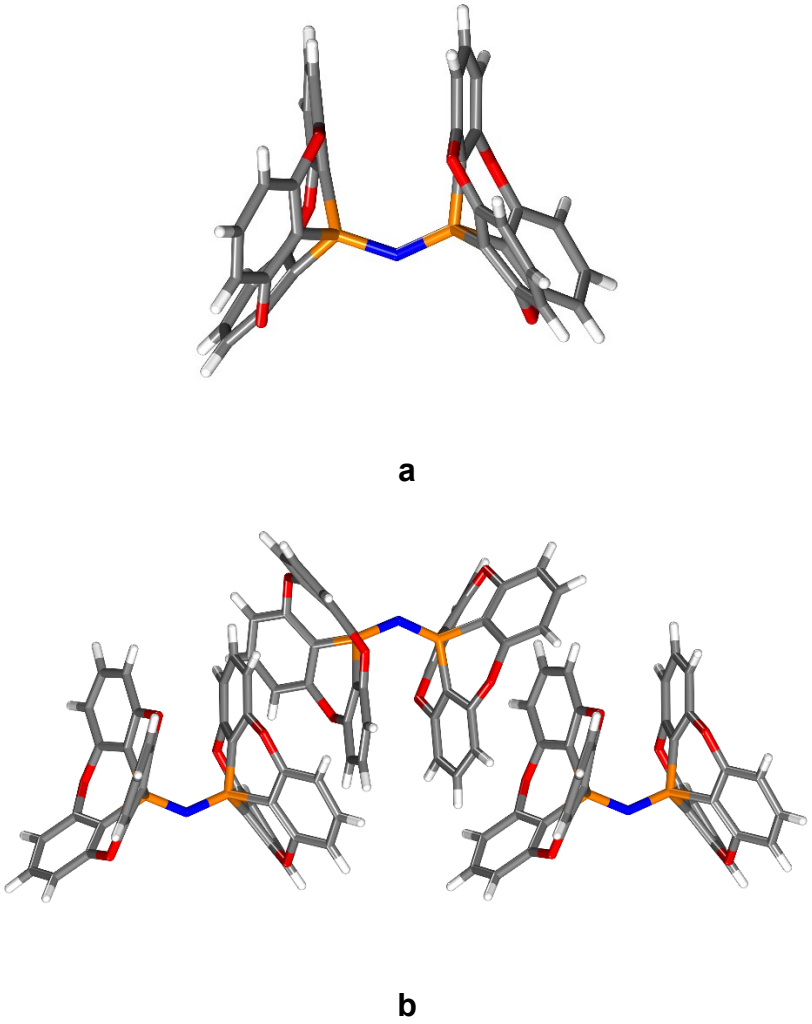

a

b

Figure 5.2 : Representations of the structure of crystals of $[(Phang)_2N]^+ BF_4^-$ grown from CS_2. (a) View showing an individual cation. (b) Image showing undulating chains of cations linked by offset clamshell pairing of Phang groups. Atoms of carbon appear in gray, hydrogen in white, nitrogen in blue, oxygen in red, and phosphorus in yellow-orange. BF_4^- counterions are omitted for clarity.

Table 5.1 : Crystallographic Data for Salts of $[(Phang)_2N]^+$

Compound	$[(Phang)_2N]^+$ BF_4^-	$[(Phang)_2N]^+$ $CF_3SO_3^-$	$[(Phang)_2N]^+$ I^-	$[(Phang)_2N]_4^+$ $[Ag_4Br_8]^{-4}$ • 2 PhCl • 1 H_2O	$[(Phang)_2N]^+$ $[Ag_7F_{24}O_{24}S_8]^-$ • 1 C_{60} • 3 Mes • 2 H_2O
crystallization medium	CS_2	CS_2/CH_2Cl_2	CH_2Cl_2/ acetone	PhCl	mesitylene
formula	$C_{36}H_{18}BF_4NO_6P_2$	$C_{37}H_{18}F_3NO_9P_2S$	$C_{36}H_{18}INO_6P_2$	$C_{156}H_{84}Ag_4Br_8Cl_2N_4O_{25}P_8$	$C_{131}H_{62}Ag_7F_{24}NO_{34}P_2S_8$
crystal system	monoclinic	monoclinic	monoclinic	monoclinic	monoclinic
space group	$P2_1/n$	$P2_1/n$	$C2/c$	$P2_1/n$	$P2_1/m$
a (Å)	13.0119(4)	13.6251(6)	21.7542(11)	15.9625(5)	13.8832(6)
b (Å)	15.6210(5)	15.5532(6)	21.1692(11)	16.9936(5)	35.9157(17)
c (Å)	14.9019(5)	15.1460(6)	14.5338(8)	25.4614(8)	14.1516(6)
α (°)	90	90	90	90	90
β (°)	97.364(2)	98.224(1)	97.072(3)	97.837(2)	119.080(2)
γ (°)	90	90	90	90	90
V (Å^3)	3003.96(17)	3176.6(2)	6642.2(6)	6842.2(4)	6166.8(5)
Z	4	4	8	2	2
Z'	1	1	1	0.5	0.5
F(000)	1440	1568	2976*	3740	3224*
T (K)	150	150	100	150	150
ρ_{calc} (g cm^{-3})	1.568	1.613	1.499*	1.846	1.792*
λ (Å)	1.34179	1.34139	1.54178	1.34139	1.34139
μ (mm^{-1})	3.583	1.677	8.877*	6.142	7.588*
measured reflections	39003	45190	57899	100896	89811
independent reflections	6844	7304	6461	15154	14410
R_{int}	0.0572	0.0340	0.0456	0.0674	0.0602
R_σ	0.0400	0.0216	0.0236	0.0322	0.0360
observed reflections	5369	6932	5817	12256	11791
R_1, $I > 2\sigma(I)$	0.0590	0.0395	0.0508	0.0638	0.0624
R_1, all data	0.0785	0.0408	0.0552	0.0796	0.0723
wR_2, $I > 2\sigma(I)$	0.1457	0.1016	0.1300	0.1701	0.1678
wR_2, all data	0.1571	0.1030	0.1340	0.1867	0.1745
GoF	1.167	1.082	1.068	1.021	1.050
max/min (e Å^{-3})	0.841/-0992	0.421/-0.663	0.848/-0.624	1.295/-1.554	1.571/-1.476

*Calculated without the contribution of disordered molecules of included solvent

Ph_3P groups and structural analogues such as trityl (Ph_3C) can engage in multiple C-H···π interactions, including characteristic patterns known as phenyl embraces.[34,35] A classic sixfold embrace results when two Ph_3P groups or analogues adopt propeller-shaped conformations of opposite configuration and interdigitate to form a cyclic array of six phenyl rings. Each ring of each Ph_3P group or analogue can then take part simultaneously in edge-to-face C-H···π interactions with two rings contributed by the other group. Ph_3P groups and analogues can also participate in related but less extensive fourfold embraces, simple edge-to-face pairing, and other standard aromatic interactions. The surface of $[(Ph_3P)_2N]^+$ has a particularly rich array of phenyl groups, and the participation of the cation in embraces has been examined in detail.[23]

In contrast, the rigid conical shape of phosphangulene prevents derivatives such as $[(Phang)_2N]^+$ ions from taking part in similar interdigitated phenyl embraces. Instead, cations in the BF_4^- salt form undulating chains that are aligned with the *b*-axis and are linked by Phang groups, which form offset clamshell pairs held together by mutual C-H···π interactions involving only the concave surfaces (Figure 5.2b). Each cationic chain is surrounded by six others, which participate in various inter-chain C-H···π interactions. Space between the chains accommodates BF_4^- counterions.

Closely related offset clamshell pairing is observed in the structure of phosphangulene oxide (**2**), as shown in Figure 5.1b, and in the structures of many other *P*-substituted derivatives of phosphangulene.[10–12] The similarity of the pairing can be highlighted by comparing Hirshfeld surfaces of molecules in crystals of oxide **2** and $[(Phang)_2N]^+ BF_4^-$.[36,37] As normally portrayed, Hirshfeld surfaces define where the calculated electron density derived from a molecule in a crystal is equal to the total density contributed by all other atoms in the structure. The concave

surface of a molecule of phosphangulene oxide (**2**) in a representative polymorphic form is shown in Figure 5.3a. The color at each point on the surface corresponds to the local value of d_e, which is the distance to the nearest atom in another molecule, and the colors vary from hot (red) to blue (cool) as d_e increases. The conspicuous red spots on the concave face of oxide **2** denote multiple C-H···π interactions (Figure 5.3a), and a nearly identical pattern appears on the corresponding surface of $[(Phang)_2N]^+$ ions (Figure 5.3b). As a result, the pairing of Phang groups defines an associative motif that is strong enough to overcome cation-cation repulsion.

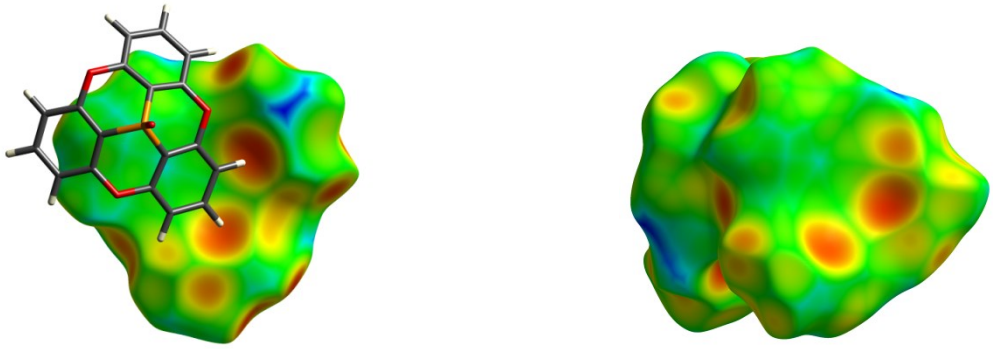

a **b**

Figure 5.3 : Comparison of molecular organization in crystals of phosphangulene oxide (**2**) and $[(Phang)_2N]^+ BF_4^-$. (a) Hirshfeld surface corresponding to a representative concave face in paired molecules of oxide **2**. (b) Corresponding Hirshfeld surface of the concave face of a $[(Phang)_2N]^+$ ion. Colors of the Hirshfeld surfaces range from hot (red) to cool (blue) as d_e increases.

$[(Phang)_2N]^+ CF_3SO_3^-$. Crystals of $[(Phang)_2N]^+ CF_3SO_3^-$ were grown by slow evaporation of solvent from a solution in CS_2/CH_2Cl_2. X-ray diffraction established that the $CF_3SO_3^-$ and BF_4^-

salts are isostructural, and Table 5.1 summarizes additional crystallographic data. The average P-N bond lengths in the $CF_3SO_3^-$ and BF_4^- salts are closely similar (1.575 Å and 1.571 Å, respectively), as are the average P-N-P bond angles (136.5° and 136.4°). The fact that changing anions does not alter the structure substantially confirms that offset clamshell pairing of Phang groups can serve as a reliable director of molecular organization.

$[(Phang)_2N]^+ I^-$. Crystals of $[(Phang)_2N]^+ I^-$ were grown by slow evaporation of solvent from a solution in CH_2Cl_2/acetone, and crystallographic data are compiled in Table 5.1. The crystals were found to include disordered molecules of solvent and to have an approximate composition of $[(Phang)_2N]^+ I^- \bullet 4\ CH_2Cl_2 \bullet 4$ acetone. The geometric parameters of the cation are similar to those observed in the corresponding BF_4^- and $CF_3SO_3^-$ salts; in particular, the average P-N bond length is normal (1.582 Å), as is the P-N-P bond angle (130.0°). Molecular organization in the three salts is related but not identical. In $[(Phang)_2N]^+ I^-$, the cations are paired by standard clamshell interactions of Phang, but the pairs are not further linked to form chains as they are in the BF_4^- and $CF_3SO_3^-$ salts (Figure 5.2b). Instead, Phang groups not involved in clamshell pairing take part in other C-H···π interactions, possibly to accommodate the inclusion of guests.

$[(Phang)_2N]_4^+ [Ag_4Br_8]^{-4} \bullet 2$ PhCl $\bullet 1\ H_2O$. The product formed by mixing $[(Phang)_2N]^+ Br^-$ and Ag(I) tetrafluoroborate in $MeCN/CH_2Cl_2$ was crystallized from PhCl. Unexpectedly, the resulting crystals to be composed of the salt $[(Phang)_2N]_4^+ [Ag_4Br_8]^{-4}$. Table 5.1 summarizes crystallographic data, and Figure 4 provides views of the structure. The average P-N bond length in the cation (1.572 Å) and the average P-N-P bond angle (138.5°) are similar to the values observed in the other three $[(Phang)_2N]^+$ salts examined. However, the cations are not

joined in the usual way by paired Phang groups to form chains, but are instead packed in sheets that have the thickness of a single cation and are bounded by Phang groups (Figure 5.4a). Each cation in the sheets is surrounded by eight others to form an array held together by C-H···π interactions, π-stacking, and short C-H···O interactions involving the oxygen atoms of Phang groups. The cationic sheets are separated by thin anionic layers composed of tetranuclear $[Ag_4Br_8]^{-4}$ ions, partially disordered molecules of PhCl, and molecules of H_2O (Figure 5.4b).

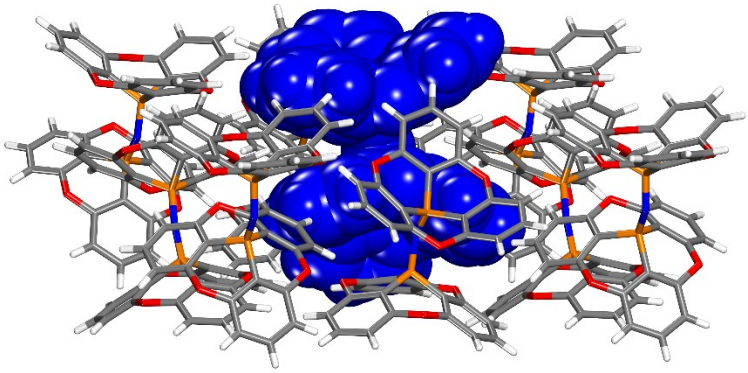

a

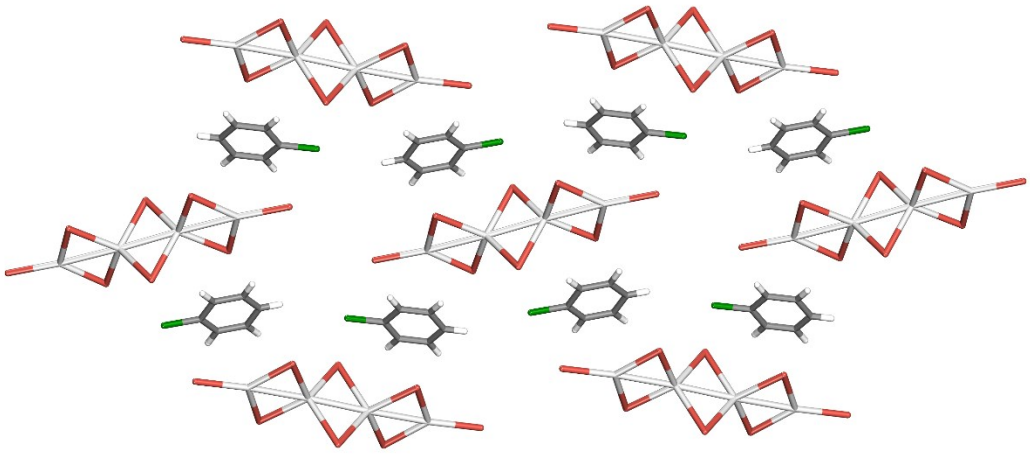

b

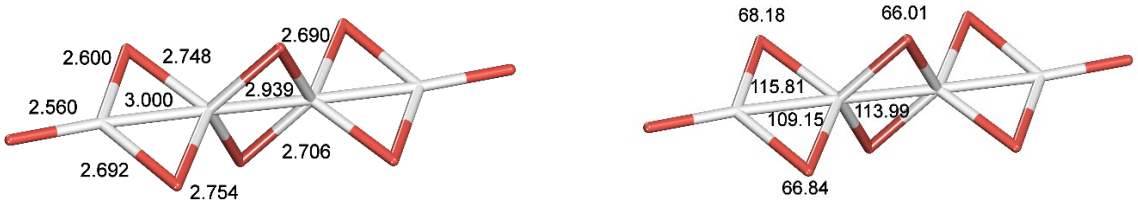

Figure 5.4 : Representations of the structure of crystals of $[(Phang)_2N]_4^+$ $[Ag_4Br_8]^{-4}$ grown from PhCl. (a) Side view of part of a single sheet, showing a central $[(Phang)_2N]^+$ ion (blue) surrounded by eight neighbors. (b) Top view showing part of an anionic sheet consisting of $[Ag_4Br_8]^{-4}$ ions and partly disordered molecules of PhCl. (c) Detailed view of the S_2-symmetric structure of $[Ag_4Br_8]^{-4}$, showing bond distances in Å. (d) Bond angles (°) in $[Ag_4Br_8]^{-4}$ ions. Unless indicated otherwise, atoms of carbon appear in dark gray, hydrogen in white, nitrogen in blue, oxygen in red, phosphorus in yellow-orange, chlorine in green, bromine in brown, and silver in light gray. Molecules of H_2O are omitted to simplify the images.

Typically, crystalline haloargentates are polymeric anionic species in which Ag(I) is 4-coordinated, and discrete haloargentates are uncommon.[38] In particular, tetranuclear bromoargentate ions have been observed in only three previously reported structures.[39-41] In crystals of $[(Phang)_2N]_4^+$ $[Ag_4Br_8]^{-4}$, the anion is S_2-symmetric, with two terminal 3-coordinated atoms of Ag(I) and two internal 4-coordinated atoms of Ag(I), as shown in Figures 4c–d. As found in other structures,[40,41] the lengths of the terminal Ag-Br bonds (2.560 Å) are shorter than the average for the bridging Ag-Br bonds (2.698 Å). However, other reported structures of $[Ag_4Br_8]^{-4}$ show large bridging Ag-Br-Ag angles (>83°) and long Ag···Ag separations (>3.5 Å), whereas Ag-Br-Ag angles in the $[(Phang)_2N]^+$ salt are much

smaller (<67°), and contiguous atoms of Ag(I) are much closer (average Ag···Ag separation = 2.970 Å), thereby increasing Ag-Ag bonding significantly. These observations underscore the potential of $[(Phang)_2N]^+$ ions to induce the formation of salts that incorporate unusual anions and allow them to adopt abnormal geometries.

$[(Phang)_2N]^+$ $[Ag_7F_{24}O_{24}S_8]^-$ • 1 C_{60} • 3 Mes • 2 H_2O. Further evidence of the ability of $[(Phang)_2N]^+$ ions to give rise to noteworthy new salts came from analyzing crystals formed by adding C_{60} to the product of the reaction of $[(Phang)_2N]^+$ Br^- with Ag(I) trifluoromethanesulfonate,. Crystallographic data are compiled in Table 5.1, and views of the structure appear in Figure 5. The structure consists of anionic layers that include molecules of C_{60}, separated by cationic layers of $[(Phang)_2N]^+$ ions. In the anionic layers, isolated molecules of C_{60} are embedded in a complex continuous network derived from Ag(I) trifluoromethanesulfonate (Figure 5a). Each molecule of C_{60} is bonded to four ordered atoms of Ag(I) positioned symmetrically around its equator. Two of these atoms are coordinated in η^1 fashion, with an Ag-C distance of 2.452 Å, and the two others are bonded in unsymmetrical η^2 fashion, with Ag-C distances of 2.300 Å and 2.464 Å. Atoms of Ag(I) in the network that are not coordinated by C_{60} are partly disordered.

The equatorial arrangement of bound atoms of Ag(I) leaves the poles of each molecule of C_{60} free to be capped by the Phang groups of $[(Phang)_2N]^+$ ions (Figure 5.5b), which pack loosely to form cationic layers. In the cations, normal values are found for the P-N bond lengths (1.561 Å) and P-N-P bond angle (147.0°). The radius of C_{60} can be considered to be 3.55 Å, and the separation of layers in graphite is 3.35 Å,[42,43] so the distance between the centroid of C_{60} and an atom of carbon in van der Waals contact is 6.90 Å. In crystals of $[(Phang)_2N]^+$

$[C_8H_4Ag_7F_{24}O_{26}S_8]^-$ • 1 C_{60} • 3 Mes • 2 H_2O, the centroid-centroid distances between C_{60} and the capping aromatic rings of $[(Phang)_2N]^+$ ions are all significantly shorter (6.583–6.678 Å), suggesting that the interaction of $[(Phang)_2N]^+$ ions with C_{60} is favored by topological and electronic complementarity. Similarly short distances have been observed in cocrystals of fullerenes with other derivatives of phosphangulene.[10,12]

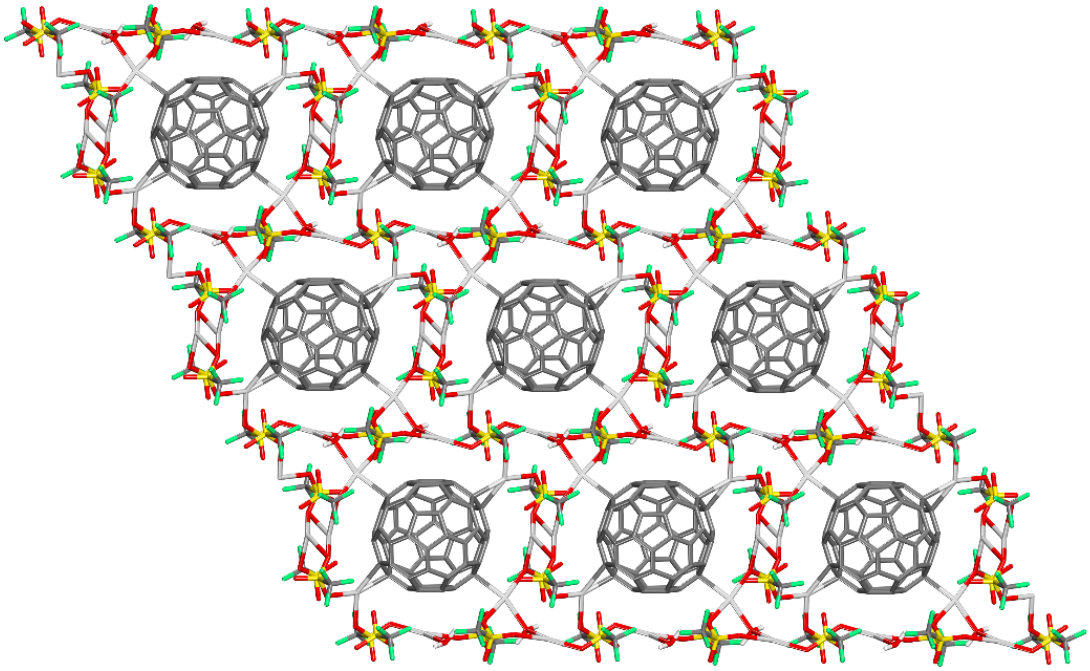

a

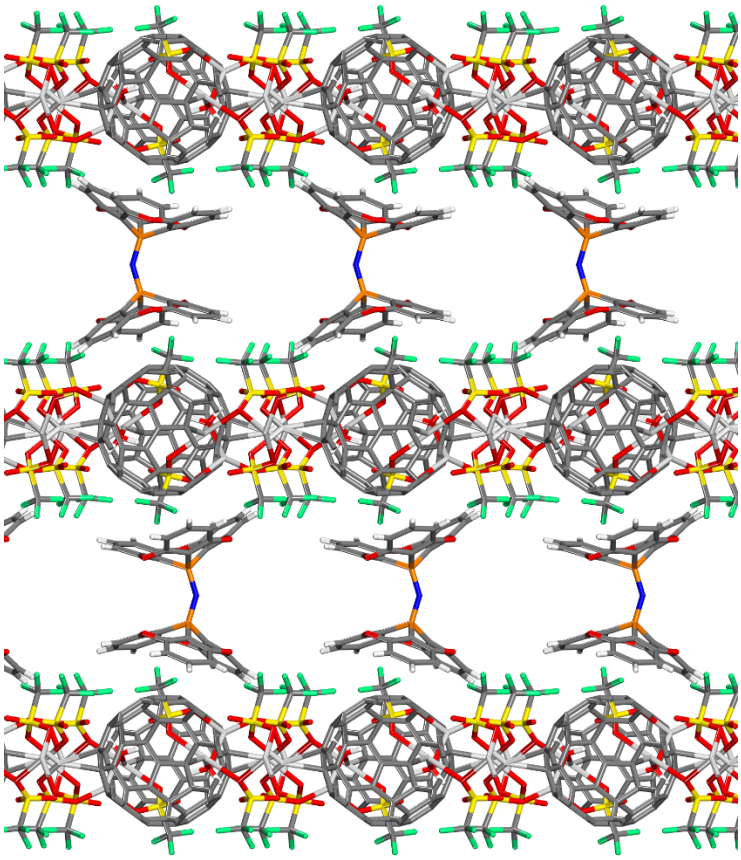

b

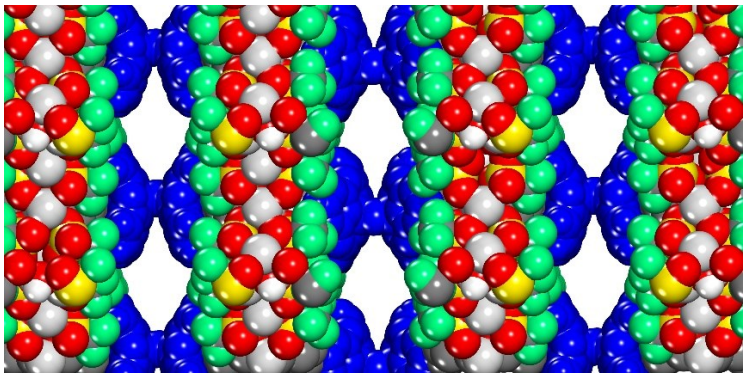

c

Figure 5.5 : Representations of the structure of crystals of $[(Phang)_2N]^+ [C_8H_4Ag_7F_{24}O_{26}S_8]^-$ • 1 C_{60} 3 Mes • 2 H_2O grown from mesitylene. (a) Top view of part of an anionic sheet, showing molecules of C_{60} embedded in a continuous network derived from Ag(I) trifluoromethanesulfonate. (b) Side view showing alternating ionic layers, with molecules of C_{60} doubly capped by $[(Phang)_2N]^+$ ions. (c) Space-filling view along the *b*-axis with $[(Phang)_2N]^+$ ions in blue, showing solvent-accessible volume in the cationic layers. Unless indicated otherwise, atoms of carbon appear in dark gray, hydrogen in white, nitrogen in blue, oxygen in red, fluorine in pale green, phosphorus in yellow-orange, sulfur in yellow, and silver in light gray. Guest molecules of mesitylene and H_2O are not shown.

Direct bonding of Ag(I) to fullerenes has few precedents. Coordination to C_{60} itself has been reported only once, in a remarkable structure described by Olmstead, Maitra, and Balch in 1999.[44] By combining C_{60} and Ag(I) nitrate under suitable conditions, they obtained crystals in which individual molecules of fullerene are encapsulated in a neutral three-dimensional open network constructed from nitrate-bridged atoms of Ag(I). Four atoms of Ag(I) are η^1- or η^2-coordinated by each molecule of C_{60}. Only two related structures have been described subsequently,[45,46] and in both cases the coordination does not involve C_{60} itself, but rather covalently-modified derivatives with additional sites for binding that bring Ag(I) into closer proximity.

In the observed structure, $[(Phang)_2N]^+$ ions again demonstrate a special ability to form salts of unusual anions. This behavior can be attributed in part to the large globular shape and

extended aromatic surface of the cation, as in the case of analogous $[(Ph_3P)_2N]^+$ ions. Both cations have dumbbell-shaped wheel-and-axle topologies and therefore belong to a family of molecular structures that cannot normally be packed with high efficiency.[47] As a result, both cations are disposed to form relatively open structures with sub-optimal intermolecular interactions and ample volumes for including counterions.

The inherent difficulty of packing $[(Ph_3P)_2N]^+$ ions is made even greater in the case of $[(Phang)_2N]^+$ ions by the peculiar topological features of Phang groups, which cannot form efficiently interdigitated structures held together by multiple C-H···π interactions. For this reason, $[(Phang)_2N]^+$ ions show behavior without parallels in the chemistry of $[(Ph_3P)_2N]^+$ ions. An example of important differences is provided by the structure of the cationic layers formed by $[(Phang)_2N]^+$ $[C_8H_4Ag_7F_{24}O_{26}S_8]^-$ • 1 C_{60} • 3 Mes • 2 H_2O. The layers are conspicuously open, with large channels containing disordered molecules of solvent aligned with the *b*-axis (Figure 5.5c). Approximately 29% of the structure is accessible to guests.[48–50] This observation suggests that $[(Phang)_2N]^+$ ions will be effective for engineering other porous or permeable solids that incorporate anions with unusual structures and chemical reactivity. Moreover, the cations are ideal for inducing fullerenes to join ionic structures.

5.2.4 Conclusions

Our work provides a straightforward way to convert phosphangulene into salts of the bis(phosphangulene)iminium cation ($[(Phang)_2N]^+$. The cation has an awkward topology that results from incorporating two conical Phang groups and connecting them to form a dumbbell-shaped ion. These features appear to facilitate the formation of salts with anions that have little or no precedent in the literature of chemistry. Like other derivatives of phosphangulene, $[(Phang)_2N]^+$ ions have a conical electron-rich aromatic surface that underlies special affinity for the convex electron-poor surface of fullerenes. The remarkable structure of $[(Phang)_2N]^+$ $[C_8H_4Ag_7F_{24}O_{26}S_8]^-$ • 1 C_{60} • 3 Mes • 2 H_2O confirms that the cation can facilitate the integration of fullerenes in ionic solids and control how they are positioned with respect to other components. As a result, $[(Phang)_2N]^+$ ions appear to be particularly well suited for producing salts in which fulleride anions are arranged in desirable ways, including those designed to favor conductivity.

5.2.5 Experimental Section

All common reagents and solvents were obtained from commercial sources and used without further purification unless otherwise indicated. Phosphangulene was prepared by a published procedure.[11]

$[(Phang)_2N]^+$ Br^-. A stirred suspension of phosphangulene (**1**; 1.21 g, 3.98 mmol) in dry 1,1,2,2-tetrachloroethane (5.5 mL) was sparged with N_2 for 30 min, cooled to 0 °C, and treated dropwise with bromine (133 μL, 2.60 mmol) during 3 min. During the addition, the suspended solid began to dissolve, and the mixture was transformed from a yellow-green suspension into a yellow-orange solution. The solution was stirred at 25 °C for 2 h, and then hydroxylamine hydrochloride (0.0917 g, 1.32 mmol) was added. The resulting mixture was heated at reflux for 20 h, cooled to 25 °C, and poured into ethyl acetate (100 mL). The beige precipitate was separated by filtration, washed with ethyl acetate (100 mL), and dried under vacuum to give $[(Phang)_2N]^+$ Br^- as a beige solid (0.760 g, 1.08 mmol, 82%). Further purification can be achieved if desired by dissolving the solid in boiling H_2O (50-60 mL), filtering off any insoluble material (phosphangulene oxide), cooling the filtrate, and allowing crystallization of $[(Phang)_2N]^+$ Br^- to occur. Alternatively, the product can be purified by gradient column chromatography on silica gel using an eluent consisting of CH_2Cl_2 containing MeOH in an amount rising from 0% to 5-10%: mp 255 °C (dec); R_f 0.28 (5% MeOH/CH_2Cl_2); FTIR (ATR) 3058, 1588, 1576, 1459, 1421, 1264, 1233, 1212, 1164, 968, 840, 790, 757, 726, 524, 506, 469, 405 cm^{-1}; ^1H NMR (400 MHz, $CDCl_3$) δ 7.67 (t, ^3J = 8.4 Hz, 6H), 7.26 (dd, ^3J = 8.4 Hz, ^4J (^{31}P, ^1H) = 5.6 Hz, 12H); ^{31}P NMR (162 MHz, $CDCl_3$) δ -54.70; ^{13}C (100 MHz, $CDCl_3$) δ 159.6, 136.8, 116.6 (m), 103.3 (dd, ^1J (^{13}C, ^{31}P) = 109 Hz, ^3J (^{13}C, ^{31}P) = 2.9 Hz); HRMS

(ESI-TOF) *m/z* $[M]^+$ calcd for $C_{36}H_{18}NO_6P_2$ 622.06039, found 622.05811; HRMS (ESI-TOF) *m/z* $[M]^-$ calcd for Br 78.91857, found 78.91587.

Formation of Other Salts $[(Phang)_2N]^+$ Y^- by Metathesis: General Procedure. $[(Phang)_2N]^+$ Br^- (702 mg, 1.00 mmol) was dissolved in a hot 2:3 mixture of MeOH and H_2O (30.0 mL) to give a solution with a concentration of 33.3 mM. Aliquots (7.50 mL, 0.250 mmol) were added to solutions of Na^+ Y^- (0.500 mmol) in H_2O (3.0 mL), causing $[(Phang)_2N]^+$ Y^- to precipitate. The resulting solids were separated by filtration, washed with H_2O (10-15 mL), and dried under vacuum at 60 °C for 12 h.

$[(Phang)_2N]^+$ BF_4^-. Using $NaBF_4$ in the general procedure afforded $[(Phang)_2N]^+$ BF_4^- as a beige solid (159 mg, 0.224 mmol, 89%). Crystals could be grown by allowing solvent to evaporate slowly from solutions in CS_2: FTIR (ATR) 3081, 1590, 1577, 1460, 1423, 1236, 1215, 1168, 970, 841, 802, 758, 726, 655, 525, 507, 471, 408 cm^{-1}; ^1H NMR (400 MHz, $CDCl_3$) δ 7.68 (t, ^3J = 8.4 Hz, 6 H), 7.27 (dd, ^3J = 8.4 Hz, ^4J (^{31}P, ^1H) = 5.6 Hz, 12 H); ^{31}P NMR (162 MHz, $CDCl_3$) δ -54.63; HRMS (ESI-TOF) *m/z* $[M]^+$ calcd for $C_{36}H_{18}NO_6P_2$ 622.06039, found 622.06214; MS (ESI-TOF) *m/z* $[M]^-$ calcd for $^{11}BF_4$ 87.00347, found 87.00379.

$[(Phang)_2N]^+$ $CF_3SO_3^-$. Using sodium trifluoromethanesulfonate in the general procedure afforded $[(Phang)_2N]^+$ $CF_3SO_3^-$ as a beige solid (150 mg, 0.194 mmol, 78%). Crystals could be grown by slow evaporation of solvent from a solution in CS_2/CH_2Cl_2: FTIR (ATR) 3079, 1590, 1577, 1460, 1423, 1267, 1235, 1233, 1213, 1161, 1031, 970, 839, 791, 757, 725, 654, 572, 525, 509, 470, 409 cm^{-1}; ^1H NMR (400 MHz, $CDCl_3$) δ 7.68 (t, ^3J = 8.4 Hz, 6 H), 7.28 (dd, ^3J = 8.4 Hz, ^4J (^{31}P, ^1H) = 5.6 Hz, 12 H); ^{31}P NMR (162 MHz, $CDCl_3$) δ -54.66; HRMS

(ESI-TOF) *m/z* $[M]^+$ calcd for $C_{36}H_{18}NO_6P_2$ 622.06039, found 622.06221; HRMS (ESI-TOF) *m/z* $[M]^-$ calcd for CF_3O_3S 148.95257, found 148.95258.

$[(Phang)_2N]^+$ PF_6^-. Using $NaPF_6$ in the general procedure afforded $[(Phang)_2N]^+$ PF_6^- as a beige solid (153 mg, 0.199 mmol, 80%): FTIR (ATR) 3089, 1591, 1578, 1461, 1424, 1292, 1237, 1216, 1169, 1046, 971, 835, 802, 758, 726, 655, 525, 507, 471, 409 cm^{-1}; ^1H NMR (400 MHz, $CDCl_3$) δ 7.67 (t, ^3J = 8.4 Hz, 6 H), 7.26 (dd, ^3J = 8.4 Hz, ^4J (^{31}P, ^1H) = 5.6 Hz, 12 H); ^{31}P NMR (162 MHz, $CDCl_3$) δ -55.02 (s), -144.16 (septuplet, ^1J (^{31}P, ^{19}F) = 720 Hz); HRMS (ESI-TOF) *m/z* $[M]^+$ calcd for $C_{36}H_{18}NO_6P_2$ 622.06039, found 622.06281; HRMS (ESI-TOF) *m/z* $[M]^-$ calcd for PF_6 144.96473, found 144.96471.

$[(Phang)_2N]^+$ BPh_4^-. Using $NaBPh_4$ in the general procedure afforded $[(Phang)_2N]^+$ BPh_4^- as a beige solid (186 mg, 0.198 mmol, 79%): FTIR (ATR) 3056, 1591, 1578, 1460, 1264, 1237, 1215, 1167, 971, 787, 732, 703, 524, 471, 408 cm^{-1}; ^1H NMR (300 MHz, DMSO-d_6) δ 7.78 (t, ^3J = 8.4 Hz, 6 H), 7.44 (dd, ^3J = 8.4 Hz, ^4J (^{31}P, ^1H) = 5.0 Hz, 12 H), 7.21-7.12 (m, 8 H), 6.92 (t, ^3J = 7.0 Hz, 8 H), 6.78 (t, ^3J = 7.0 Hz, 4 H); ^{31}P NMR (162 MHz, $CDCl_3$) δ -54.73; HRMS (ESI-TOF) *m/z* $[M]^+$ calcd for $C_{36}H_{18}NO_6P_2$ 622.06039, found 622.06235; HRMS (ESI-TOF) *m/z* $[M]^-$ calcd for $C_{24}H_{20}{}^{11}B$ 319.16581, found 319.16718.

$[(Phang)_2N]^+$ I^-. Using NaI in a metathesis similar to the one described in the general procedure but on a smaller scale (15.1 mg = 0.0215 mmol of the bromide) gave $[(Phang)_2N]^+$ I^- as an orange solid (12.4 mg, 0.0165 mmol, 77%). Crystals suitable for structural analysis by X-ray diffraction could be grown by slow evaporation of solvent from a solution in CH_2Cl_2/acetone: FTIR (ATR) 3000, 1590, 1577, 1459, 1266, 1234, 1214, 1166, 970, 789, 728, 656, 524, 471 cm^{-1}; ^1H NMR (400 MHz, $CDCl_3$) δ 7.70 (t, ^3J = 8.4 Hz, 6 H), 7.28 (dd, ^3J = 8.4 Hz, ^4J (^{31}P, ^1H) = 5.6 Hz, 12 H); ^{31}P NMR (162 MHz, $CDCl_3$) δ -55.28; HRMS (ESI-TOF)

m/z $[M]^+$ calcd for $C_{36}H_{18}NO_6P_2$ 622.06039, found 622.06114; HRMS (ESI-TOF) *m/z* $[M]^-$ calcd for I 126.90502, found 126.90455.

$[(Phang)_2N]_4^+$ $[Ag_4Br_8]^{-4}$ • 2 PhCl • 1 H_2O. A solution of $[(Phang)_2N]^+$ Br^- (5.0 mg, 7.1 μmol) in MeCN (1.0 mL) was mixed with a saturated solution of $AgBF_4$ in MeCN (1.0 mL). CH_2Cl_2 (3.0 mL) was added, and the mixture was filtered. Volatiles were removed from the filtrate by evaporation under reduced pressure, the residue was triturated with PhCl (4.0 mL), and the resulting mixture was filtered. Slow evaporation of solvent from the filtrate yielded crystals of $[(Phang)_2N]_4^+$ $[Ag_4Br_8]^{-4}$ • 2 PhCl • 1 H_2O suitable for structural analysis by X-ray diffraction. The amount of crystalline material obtained was insufficient for analysis by other methods.

$[(Phang)_2N]^+$ $[C_8H_4Ag_7F_{24}O_{26}S_8]^-$ • 1 C_{60} • 3 Mes • 2 H_2O. A solution of $[(Phang)_2N]^+$ Br^- (5.0 mg, 7.1 μmol) in MeCN (1.0 mL) was mixed with a saturated solution of Ag(I) trifluoromethanesulfonate in MeCN (1.0 mL). CH_2Cl_2 (3.0 mL) was added, and the mixture was filtered. Volatiles were removed from the filtrate by evaporation under reduced pressure, a solution of C_{60} (5.1 mg, 7.1 μmol) in mesitylene (4.0 mL) was added, and the mixture was filtered. Slow evaporation of solvent from the filtrate yielded crystals of $[(Phang)_2N]^+$ $[C_8H_4Ag_7F_{24}O_{26}S_8]^-$ • 1 C_{60} • 3 Mes • 2 H_2O suitable for structural analysis by X-ray diffraction. The amount of crystalline material obtained was insufficient for analysis by other methods.

Supporting Information Available: NMR spectra of $[(Phang)_2N]^+$ Br^- and additional crystallographic details, including ORTEP drawings. Deposition Numbers 1948970-1948974 contain supplementary crystallographic data for this paper. These data are provided free of

charge by the joint Cambridge Crystallographic Data Centre and Fachinformationszentrum Karlsruhe Access Structures service www.ccdc.cam.ac.uk/structures.

Acknowledgments. We are grateful to the Natural Sciences and Engineering Research Council of Canada, the Ministère de l'Éducation du Québec, the Canada Foundation for Innovation, the Canada Research Chairs Program, and Université de Montréal for financial support.

Notes. The authors declare no competing financial interest.

5.2.6 References

1. Krebs, F. C.; Larsen, P. S.; Larsen, J.; Jacobsen, C. S.; Boutton, C.; Thorup, N. Synthesis, Structure, and Properties of 4,8,12-Trioxa-12c-phospha-4,8,12,12c-tetrahydrodibenzo[*cd*,*mn*]pyrene, a Molecular Pyroelectric. *J. Am. Chem. Soc.* **1997**, *119*, 1208–1216.
2. Madsen, G. K. H.; Krebs, F. C.; Lebech, B.; Larsen, F. K. Evaluation of the Solid State Dipole Moment and Pyroelectric Coefficient of Phosphangulene by Multipolar Modeling of X-ray Structure Factors. *Chem. Eur. J.* **2000**, *6*, 1797–1804.
3. Faldt, A.; Krebs, F. C.; Thorup, N. Synthesis, Structure and Properties of Various Molecules Based on the 4,8,12-Trioxa-4,8,12,12c-tetrahydrodibenzo[*cd*,*mn*]pyrene System with an Evaluation of the Effect Differing Molecular Substitution Patterns has on the Space Group Symmetry. *J. Chem. Soc., Perkin Trans 2* **1997**, 2219–2227.
4. Hirai, M.; Tanaka, N.; Sakai, M.; Yamaguchi, S. Structurally Constrained Boron-, Nitrogen-, Silicon-, and Phosphorus-Centered Polycyclic π-Conjugated Systems. *Chem. Rev.* **2019**, *119*, 8291–8331.

5. Yamamura, M.; Hasegawa, T.; Nabeshima, T. Synthesis of Phosphorus-Centered and Chalcogen-Bridged Concave Molecules: Modulation of Bowl Geometries and Packing Structures by Changing Bridging Atoms. *Org. Lett.* **2016,** *18*, 816–819.

6. Yamamura, M.; Nabeshima, T. Relationship between the Bowl-Shaped Geometry of Phosphangulene and an Axial Group on the Phosphorus Atom. *Bull. Chem. Soc. Jpn.* **2016,** *89*, 42–49.

7. Yamamura, M.; Hongo, D.; Nabeshima, T. Twofold Fused Concave Hosts Containing Two Phosphorus Atoms: Modules for the Sandwich-Type Encapsulation of Fullerenes in Variable Cavities. *Chem. Sci.* **2015**, *6*, 6373–6378.

8. Yamamura, M.; Sukegawa, K.; Nabeshima, T. Tuning the Depth of Bowl-Shaped Phosphine Hosts: Capsule and Pseudo-Cage Architectures in Host–Guest Complexes with C_{60} Fullerene. *Chem. Commun*. **2015**, *51*, 12080–12083.

9. Yamamura, M.; Saito, T.; Nabeshima, T. Phosphorus-Containing Chiral Molecule for Fullerene Recognition Based on Concave/Convex Interaction. *J. Am. Chem. Soc.* **2014**, *136*, 14299–14306.

10. Heskia, A.; Maris, T.; Wuest, J. D. Putting Fullerenes in Their Place: Cocrystallizing C_{60} and C_{70} with Phosphangulene Chalcogenides. *Cryst. Growth Des.* **2019**, *19*, 5418-5428.

11. Heskia, A.; Maris, T.; Wuest, J. D. Foiling Normal Patterns of Crystallization by Design. Polymorphism of Phosphangulene Chalcogenides. *Cryst. Growth Des.* **2019**, *19*, 5390-5406.

12. Heskia, A.; Maris, T.; Aguiar, P. M.; Wuest, J. D., Building Large Structures with Curved Aromatic Surfaces by Complexing Metals with Phosphangulene. *J. Am. Chem. Soc.* **2019,** *141*, 18740-18753.

13. Lee, H.; Park, C.; Sin, D. H.; Park, J. H.; Cho, K. Recent Advances in Morphology Optimization for Organic Photovoltaics. *Adv. Mater.* **2018**, *30*, 1800453.

14. Lai, Y.-Y.; Cheng, Y.-J.; Hsu, C.-S. Applications of Functional Fullerene Materials in Polymer Solar Cells, *Energy Environ. Sci.* **2014**, *7*, 1866–1883.

15. Dang, M. T.; Hirsch, L.; Wantz, G.; Wuest, J. D. Controlling the Morphology and Performance of Bulk Heterojunctions in Solar Cells. Lessons Learned from the Benchmark Poly(3-hexylthiophene):[6,6]-Phenyl-C_{61}-butyric Acid Methyl Ester System. *Chem. Rev.* **2013**, *113*, 3734–3765.

16. Ganin, A. Y.; Takabayashi, Y.; Jeglič, P.; Arčon, D.; Potočnik, A.; Baker, P. J.; Ohishi, Y.; McDonald, M. T.; Tzirakis, M. D.; McLennan, A.; Darling, G. R.; Takata, M.; Rosseinsky, M. J.; Prassides, K. Polymorphism Control of Superconductivity and Magnetism in Cs_3C_{60} Close to the Mott Transition. *Nature* **2010**, *466*, 221–225.

17. Selmani, S.; Schipper, D. J. π-Concave Hosts for Curved Carbon Nanomaterials. *Chem. Eur. J.* **2019**, *25*, 6673–6692.

18. Xu, Y.; Kaur, R.; Wang, B.; Minameyer, M. B.; Gsanger, S.; Meyer, B.; Drewello, T.; Guldi, D. M.; von Delius, M. Concave−Convex $\pi-\pi$ Template Approach Enables the Synthesis of [10]Cycloparaphenylene−Fullerene [2]Rotaxanes. *J. Am. Chem. Soc.* **2018**, *140*, 13413−13420.

19. Saito, M.; Shinokubo, H.; Sakurai, H. Figuration of Bowl-Shaped π-Conjugated Molecules: Properties and Functions. *Mater. Chem. Front.* **2018**, 2, 635−661.

20. Gallego, M.; Calbo, J.; Krick Calderon, R. M.; Pla, P.; Hsieh, Y.-C.; Pérez, E. M.; Wu, Y.-T.; Ortí, E.; Guldi, D. M.; Martín, N. Complexation and Electronic Communication between Corannulene-Based Buckybowls and a Curved Truxene-TTF Donor. *Chem. Eur. J.* **2017**, *23*, 3666–3673.

21. Sygula, A. Corannulene-Adorned Molecular Receptors for Fullerenes Utilizing the π–π Stacking of Curved-Surface Conjugated Carbon Networks. Design, Synthesis and Testing. *Synlett* **2016**, *27*, 2070–2080.

22. Appel, R.; Hauss, A. Über einige Reaktionen des Triphenylphosphinimins und des Triphenylphosphin-bromimins. *Z. Anorg. Allg. Chem*. **1961**, *311*, 290–301.

23. Lewis, G. R.; Dance, I. Crystal Supramolecularity. Multiple Phenyl Embraces by $[PPN]^+$ Cations. *J. Chem. Soc., Dalton. Trans.* **2000**, 299–306.

24. Bauzá, A.; Frontera, A.; Mooibroek, T. J.; Reedijk, J. The N-Atom in $[N(PR_3)_2]^+$ Cations (R = Ph, Me) Can Act as Electron Donor for (Pseudo) Anti-Electrostatic Interactions. *CrystEngComm* **2015**, *17*, 3768–3771.

25. Boeré, R. T.; Roemmele, T. L.; Krall, M. K. A Variable Temperature X-Ray Diffraction Investigation of $[PPN^+][S_4N_5^-]$: Supramolecular Interactions Governing an Order/Disorder Transformation and the First High Resolution X-Ray Structure of the Anion. *Molecules* **2014**, *19*, 1956–1975.

26. Bolli, C.; Gellhaar, J.; Jenne, C.; Keßler, M.; Scherer, H.; Seeger, H.; Uzun, R. Bis(triphenyl-λ^5-phosphanylidene)ammonium Fluoride: A Reactive Fluoride Source to Access the Hypervalent Silicates $[Me_nSiF_{5-n}]^-$ (n = 0–3). *Dalton Trans*. **2014**, *43*, 4326–4334.

27. Martinsen, A.; Songstad, J. Preparation and Properties of Some Bis(triphenylphosphine)iminium Salts, $[(Ph_3P)_2N]X$. *Acta Chem. Scand*. **1977**, *A31*, 645–650.

28. Ruff, J. K.; Schlientz, W. J. μ-Nitrido-bis(triphenylphosphorus)(1+) ("PPN") Salts with Metal Carbonyl Anions. *Inorg. Synth.* **1974**, *15*, 84–90.

29. Lalor, F. J.; Chaona, S. An Economical Small-Scale Synthesis of the μ-Nitridobis(triphenylphosphonium) Cation, $[PPN]^+$. *J. Organomet. Chem.* **1988**, *344*, 163–165.

30. Boyd, P. D. W.; Bhyrappa, P.; Paul, P.; Stinchcombe, J.; Bolskar, R. D.; Sun, Y.; Reed, C. A. The C_{60}^{2-} Fulleride Ion. *J. Am. Chem. Soc*. **1995**, *117*, 2907–2914.

31. Moriyama, H.; Kobayashi, H.; Kobayashi, A.; Watanabe, T. Electrocrystallization and ESR Spectra of the Single Crystal $[N(P(C_6H_5)_3)_2]C_{60}$. *J. Am. Chem. Soc*. **1993**, *115*, 1185–1187.

32. Bertocco, P.; Bolli, C.; Correia Bicho, B. A.; Erken, B.; Jenne, C.; Laitenen, R. S.; Seeger, H. A.; Takaluoma, T. T. A Theoretical and Synthetic Study on the Existence, Structures, and Bonding of the Halide-Bridged $[B_2X_7]^-$ (X = F, Cl, Br, I) Anions. Inorg. Chem. **2016**, *55*, 3599–3604.

33. Liau, R.-Y.; Ehlich, H.; Schier, A.; Schmidbaur, H. Bis(triphenylphosphoranylidene)ammonium Dicyanoaurate(I). *Z. Naturforsch. B Chem. Sci.* **2002**, *57*, 1085–1089.

34. Dance, I.; Scudder, M. Molecules Embracing in Crystals. *CrystEngComm* **2009**, *11*, 2233–2247.

35. Dance, I.; Scudder, M. Crystal Supramolecularity: Sixfold Phenyl Embraces Between PPh_3 Ligands, Forming Extended Nets in One-, Two-, and Three-Dimensions. *J. Chem. Soc., Dalton Trans.* **2000**, 1579–1585.

36. Hirshfeld surfaces and two-dimensional fingerprint plots were generated by using CrystalExplorer17. Turner, M. J.; McKinnon, J. J.; Wolff, S. K.; Grimwood, D. J.; Spackman, P. R.; Jayatilaka, D.; Spackman, M. A. *CrystalExplorer17*; University of Western Australia, 2017.

37. McKinnon, J. J.; Spackman, M. A.; Mitchell, A. S. Novel Tools for Visualizing and Exploring Intermolecular Interactions in Molecular Crystals. *Acta Crystallogr., Sect. B: Struct. Sci.* **2004**, *60*, 627–668.

38. Jagner, S.; Helgesson, G. On the Coordination Number of the Metal in Crystalline Halogenocuprates(I) and Halogenoargentates(I). *Adv. Inorg. Chem*. **1991**, *37*, 1−45.

39. Liu, Q.-X.; Hu, Z.-L.; Yu, S.-C.; Zhao, Z.-X.; Wei, D.-C.; Li, H.-L. NHC Pd(II) and Ag(I) Complexes: Synthesis, Structure, and Catalytic Activity in Three Types of C−C Coupling Reactions. *ACS Omega* **2018**, *3*, 4035−4047.

40. Chen, S.-C.; Hsueh, H.-H.; Chen, C.-H.; Lee, C. S.; Liu, F.-C.; Lin, I. J. B.; Lee, G.-H.; Peng, S.-M. Synthesis and Structures of Polymeric Silver and Mercury Complexes with Amido-Functionalized N-Heterocyclic Carbenes. *Inorg. Chim. Acta* **2009**, *362*, 3343−3350.

41. Helgesson, G.; Jagner, S. Haloargentates(I) with Unusual Coordination Geometries. Synthesis and Structure of Potassium−Crypt Salts of Chloro-, Bromo-, and Iodoargentates(I), Including the First Example of a Two-Coordinated Chloroargentate(I) in the Solid State. *Inorg. Chem.* **1991**, *30*, 2574−2577.

42. Johnson, R. D.; Bethune, D. S.; Yannoni, C. S. Fullerene Structure and Dynamics: A Magnetic Resonance Potpourri. *Acc. Chem. Res*. **1992**, *25*, 169−175.

43. Langis-Barsetti, S.; Maris, T.; Wuest, J. D. Molecular Organization of 2,1,3-Benzothiadiazoles in the Solid State. *J. Org. Chem.* **2017**, *82*, 5034−5045.

44. Olmstead, M. M.; Maitra, K.; Balch, A. L. Formation of a Curved Silver Nitrate Network That Conforms to the Shape of C_{60} and Encapsulates the Fullerene—Structural Characterization of $C_{60}\{Ag(NO_3)\}_5$. *Angew. Chem. Int. Ed.* **1999**, *38*, 231−233.

45. Peng, P.; Li, F.-F.; Bowles, F. L.; Neti, V. S. P. K.; Metta-Magana, A. J.; Olmstead, M. M.; Balch, A. L.; Echegoyen, L. High Yield Synthesis of a New Fullerene Linker and its Use in the Formation of a Linear Coordination Polymer by Silver Complexation. *Chem. Commun*. **2013**, *49*, 3209−3211.

46. Chancellor, C. J.; Olmstead, M. M.; Balch, A. L. Formation of Crystalline Polymers from the Reaction of Amine-Functionalized C_{60} with Silver Salts. *Inorg. Chem*. **2009**, *48*, 1339−1345.

47. Toda, F. In *Comprehensive Supramolecular Chemistry*; MacNicol, D. D., Toda, F., Bishop, R., Eds.; Elsevier: London, 1996; Vol. *6*, pp 465−516.

48. The percentage of volume accessible to guests was estimated by the PLATON program (References 49 and 50). PLATON calculates the accessible volume by allowing a spherical probe of variable radius to roll over the van der Waals surface of the network. PLATON uses a default value of 1.20 Å for the radius of the probe, which is an appropriate model for small guests such as water. The van der Waals radii (in Å) used to define surfaces for these calculations are Ag: 1.72, C: 1.70, H: 1.09, I: 1.98, N: 1.55,

O: 1.52, P: 1.80, and S: 1.80. The percentage of accessible volume is given by $100V_g/V$, where V is the volume of the unit cell and V_g is the guest-accessible volume as calculated by PLATON.

49. Spek, A. L. *PLATON, A Multipurpose Crystallographic Tool*; Utrecht University: Utrecht, The Netherlands, 2001.

50. van der Sluis, P.; Spek, A. L. BYPASS: an Effective Method for the Refinement of Crystal Structures Containing Disordered Solvent Regions. *Acta Crystallogr.* **1990**, *A46*, 194–201

5.2.7 Table of Contents Graphic

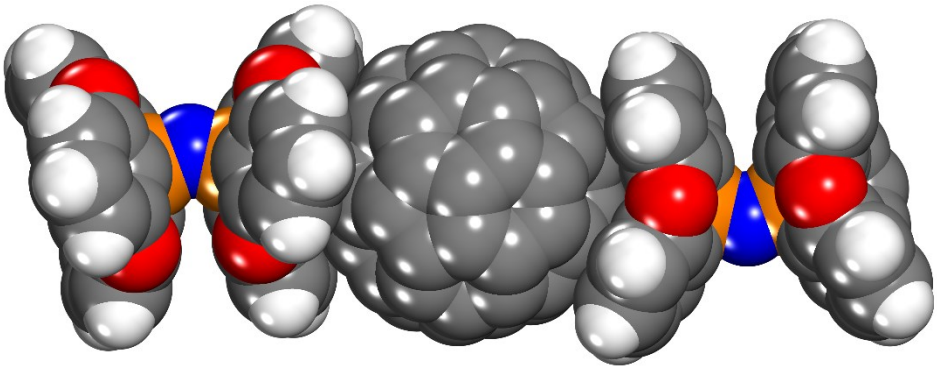

The new cation $[(Phang)_2N]^+$, which is constructed from two conical subunits of phosphangulene ("Phang") bonded to a central atom of nitrogen, has an awkward shape that facilitates the formation of unusual salts, including those incorporating anions derived from C_{60}.

Keywords

Phosphangulene, Cocrystals, Bis(phosphangulene)iminium Salts, Fullerenes

5.3 Conclusions

En résumé, nous avons réussi à synthétiser le bis(phosphangulène)iminium sous forme de bromure dans un premier temps, puis avec d'autres contre-ions par métathèse avec les sels de sodium correspondants. Quelques structures ont été élucidées par des études cristallographiques, permettant ainsi d'étudier la structure du cation PPN^+ dérivé du phosphangulène. Nous sommes également parvenus à produire et à caractériser un cocristal avec un fullerène, incluant des ions triflate comme contre-ions. À ce jour, nous ne sommes malheureusement pas encore arrivés à cocristalliser un fullerure avec notre cation. Néanmoins, nous ne fermons pas encore la porte à cette partie du projet et nous prévoyons faire d'autres tentatives.

Chapitre 6 :
Conclusions et perspectives

6.1 Résumé et retour sur les objectifs

Le but ultime du projet résumé dans cette thèse était de concevoir et de synthétiser des composés pouvant contrôler l'organisation des fullerènes, surtout dans le but de favoriser une morphologie productive de la couche active des cellules photovoltaïques de type organique. Pour atteindre cet objectif, nous avons choisi le phosphangulène, qui offre un squelette de base susceptible de cocristalliser avec les fullerènes et facilement fonctionnalisable. Nos objectifs étaient d'abord de synthétiser de nouveaux composés dérivés du phosphangulène, puis de les cocristalliser avec des fullerènes afin d'en étudier la structure, pour ultimement trouver des applications en photovoltaïque ou en électronique.

Ainsi, le premier et plus basique objectif était d'établir des procédures de synthèse de nouveaux dérivés du phosphangulène. Nous avons amélioré la synthèse du phosphangulène publiée par Krebs et collaborateurs et nous avons modifié les préparations des chalcogénures correspondants. Nous avons également découvert un grand nombre de nouvelles formes polymorphiques des chalcogénures. De plus, nos études synthétiques ont généré une nouvelle famille importante de complexes métalliques du phosphangulène, ainsi que des solides dans lesquels des fullerènes et des dérivés du phosphangulène sont intégrés. Finalement, nous avons réussi la première synthèse du cation bis(phosphangulène)iminium.

L'impact principal de notre premier manuscrit (chapitre 2), décrivant de nouveaux polymorphes des dérivés chalcogénures, est une validation de principes de base sur le polymorphisme. Nous avons démontré, dans un système rigide avec l'ajout d'un seul atome, que la forme et l'efficacité d'empilement sont reliées au polymorphisme et éventuellement à la tendance à cocristalliser avec d'autres composés.

En effet, le polymorphisme des dérivés chalcogénures est une indication de leur potentiel à cocristalliser avec d'autres composés, tel que démontré dans le deuxième manuscrit (chapitre 3) sur la cocristallisation avec des fullerènes. Au cours de cette exploration, nous avions l'opportunité d'étudier pour la première fois les interactions concave-convexe chez nos molécules. Nos observations dans ces deux premiers articles soutiennent la thèse que la frustration de forme favorise le génération de nombreux polymorphes, dont certains avec des paramètres *Z'* élevés, et est à l'origine de la tendance à cocristalliser comme stratégie pour régler les frustrations de cristallisation.[1]

Dans le troisième manuscrit (chapitre 4), nous avons résumé les travaux ayant mené à la formation de complexes de coordination du phosphangulène, permettant ainsi d'obtenir des composés présentant plusieurs cavités aptes à accueillir des invités convexes tels que les buckyballes. Effectivement, une structure où le C_{60} vient se loger dans une cavité de phosphangulène retenu dans un complexe de triflate d'argent, $Ag[Phang]_2OTf$, a été caractérisée par une étude cristallographique et présentée dans ce manuscrit.

Dans le dernier manuscript soumis, présenté au chapitre 5, nous avons décrit la synthèse et les propriétés des sels du cation bis(phosphangulène)iminium. Nous avons également obtenu des cocristaux avec le C_{60}, permettant d'en étudier les interactions. Le cation est très intéressant car en principe il permettrait de stabiliser des fullerènes anioniques lors de leur auto-assemblage.

6.2 Perspectives

6.2.1 Caractérisation en photovoltaïque

Le point de départ du projet de cette thèse était la problématique de l'intégration des fullerènes avec d'autres substances pour créer des matériaux multi-composantes ayant une organisation prédéterminée. Un objectif particulièrement important est de réussir à contrôler la morphologie de la couche active dans les cellules solaires organiques avec une architecture d'hétérojonction de masse, dans lesquelles les fullerènes sont souvent présents comme accepteurs d'électrons. Nous avons complété les études préliminaires dans ce but en étudiant les interactions à l'état cristallin entre les dérivés du phosphangulène et les buckyballes. Les résultats obtenus dans nos travaux ouvrent la porte pour des études appliquées d'incorporation de nos dérivés dans des substrats photovoltaïques. Quelques résultats préliminaires en ce sens ont été obtenus avec la participation de Dr. Minh-Trung Dang, expert dans la fabrication et caractérisation des cellules photovoltaïques organiques. Ces résultats suggèrent qu'employé comme additif, le phosphangulène permet de maintenir le rendement de conversion d'énergie au travers des cycles et donc d'améliorer la longévité de la cellule.

6.2.2 Autres dérivés du phosphangulène

D'autres molécules cibles intéressantes ont été identifiées durant ce doctorat, mais leurs synthèses n'ont cependant pas été menées à terme ou n'ont pas été entreprises du tout.

6.2.2.1 Fonctionnalisation sur le squelette carboné

Parmi ces cibles sont des composés où les cycles aromatiques sont fonctionnalisés en position para. Partant du phosphangulène, nous avons tenté sans succès d'y installer trois groupements

pinacolborane en suivant les procédures de borylation de pyrène employées par Conventry *et al.*[2] et Crawford *et al.*[3] (Schéma 6.1). Supposant la cause de l'échec comme étant la coordination compétitive de la phosphine sur le catalyseur d'iridium employé, nous avons tenté la synthèse à partir de l'oxyde du phosphangulène afin de priver le substrat de son doublet libre d'électrons. Malgré ce contournement de problème, le produit désiré n'a pas été obtenu. Nous attribuons l'échec à la diminution de densité électronique dans le réseau aromatique découlant du groupement faiblement électron-attracteur P^+-O^-. Yamamura *et al.*[4] ont rapporté la synthèse d'un dérivé de phosphangulène dont les anneaux aromatiques sont substitués en position méta en incorporant les groupements avant l'étape de fermeture de cycles. Cette stratégie résultait en un mélange d'isomères ayant ainsi chacun des rendements faibles. Cette perspective nous a semblé peu attirante. Il reste qu'un dérivé substitué aux positions para serait intéressant et mériterait plus d'investigation.

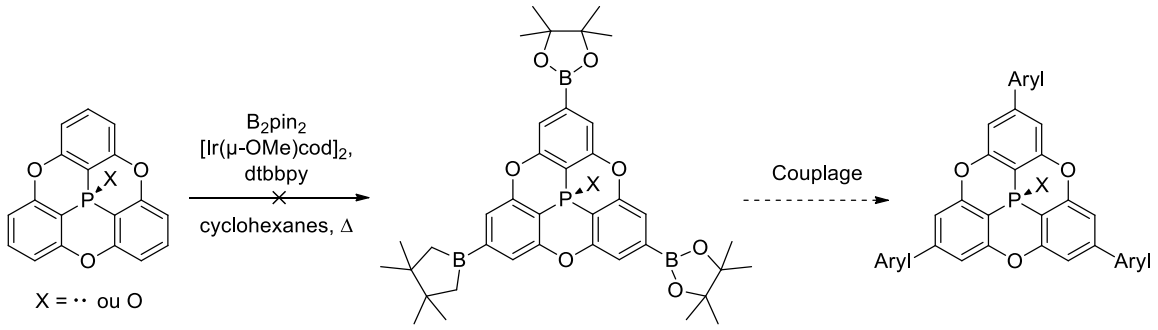

Schéma 6.1 : Fonctionnalisation du squelette carboné.

6.2.2.2 Connecteurs benzyliques et sels organiques

Aux cours de nos études, nous avons tenté de former des structures bis(phosphangulène) dans lesquelles les phosphines sont reliées par un connecteur xylyle de par leurs atomes de

phosphore. En principe, ces composés pourraient être obtenus en faisant réagir des dérivés α-bromo de xylènes avec le phosphangulène en espérant une double substitution nucléophile (Schéma 6.2). La version monosubstituée était obtenue en chauffant le phosphangulène avec le bromure de benzyle, qui sert de solvant et est présent en grand excès. Cette réaction est beaucoup plus lente que la substitution analogue avec la triphénylphosphine. La différence est attribuable au caractère s prononcé du doublet libre du phosphangulène, tel que discuté dans le chapitre 4 sur les complexes métalliques. Le chauffage nécessaire pour effectuer une substitution avec le phosphangulène est problématique puisqu'elle nécessite en général une température élevée se rapprochant de la température de dégradation du composé. Nous avons exploré la voie de la méchano-chimie au travers d'expériences préliminaires. Les moulins réactionnels n'employant aucun solvant permettraient un mélange homogène à basse température (environ 70 °C) sous atmosphère inerte. Une faible quantité du composé désiré semble avoir été produite après mouture et vieillissement à 80 °C pendant 10 jours. Le rendement préliminaire est bas (autour de 5%), mais semble pouvoir être amélioré avec des optimisations appropriées.

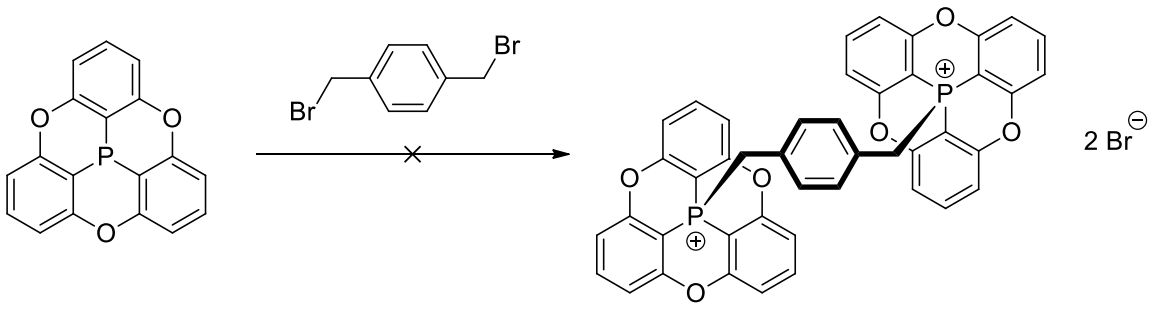

Schéma 6.2 : Mise en place ratée d'un connecteur benzylique.

6.2.2.3 Carbone pontant : allène de bis(phosphangulène)

Il serait intéressant de synthétiser un composé du type « PCP » analogue au μ-nitrido-bis(phosphangulène) mais ayant un atome de carbone plutôt que d'azote au centre. Contrairement à la version azotée qui est courbée, le dérivé PCP serait linéaire et offrirait un pontage différent entre les fullerènes. Le chemin synthétique pour l'obtention de cette cible n'est pas encore très clair et mérite plus amples investigations dans la littérature à ce sujet.

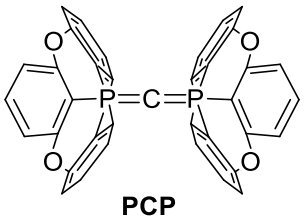

PCP

6.2.2.4 Cage de phosphangulène

À l'instar des cycloparaphénylènes, il serait intéressant de réussir à synthétiser une cage de phosphangulènes reliés par des paraphénylènes en position para des phosphines. Pour ce faire, il faudrait réussir à fonctionnaliser le phosphangulène à ces positions. Tel qu'expliqué, nous avons tenté de placer des pinacolboranes à ces positions, mais sans succès. Toutefois, un tel composé constituerait un hôte pour fullerènes intéressant du point de vue de la chimie supramoléculaire.

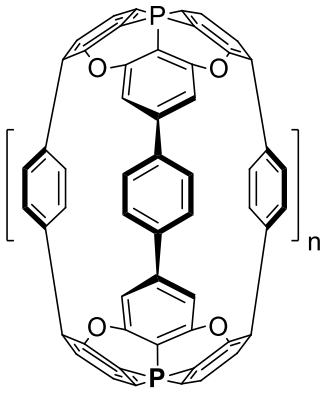

Cage de phosphangulènes

6.3 Conclusions

En somme, les objectifs posés dans cette thèse ont été remplis. Nous avons étudié le sujet du phosphangulène assez longuement et en profondeur, mais malgré cela, il reste encore beaucoup d'aspects et de dérivés potentiels à explorer.

6.4 Références

1. Steed, K. M.; Steed, J. W. *Chem. Rev.* **2015,** *115* (8), 2895-2933.
2. Coventry, D. N.; Batsanov, A. S.; Goeta, A. E.; Howard, J. A. K.; Marder, T. B.; Perutz, R. N. *Chem. Commun.* **2005,** (16), 2172-2174.
3. Crawford, A. G.; Liu, Z.; Mkhalid, I. A. I.; Thibault, M.-H.; Schwarz, N.; Alcaraz, G.; Steffen, A.; Collings, J. C.; Batsanov, A. S.; Howard, J. A. K.; Marder, T. B. *Chem. Eur. J.* **2012,** *18* (16), 5022-5035.
4. Yamamura, M.; Saito, T.; Nabeshima, T. *J. Am. Chem. Soc.* **2014,** *136* (40), 14299-14306.

Chapitre 7:
Annexes

7.1 Informations supplémentaires de l'article 1

Supporting Information

Foiling Normal Patterns of Crystallization by Design.

Polymorphism of Phosphangulene Chalcogenides

Alice Heskia, Thierry Maris, and James D. Wuest*

Département de Chimie, Université de Montréal, Montréal, Québec H3C 3J7 Canada

*Author to whom correspondence may be addressed.

E-mail: *james.d.wuest@umontreal.ca*

7.1.1 Phosphangulene oxide (2a)

Table 7.1 : Crystal structure data for polymorph A of phosphangulene oxide (**2a**) crystallized from EtOH.

crystallization medium	EtOH
formula	$C_{18}H_9O_4P$
Mr	320.22
crystal system	monoclinic
space group	$P2_1/n$
a (Å)	10.0282(6)
b (Å)	25.0624(16)
c (Å)	10.6559(7)
α (°)	90
β (°)	94.416(2)
γ (°)	90
V (Å^3)	2670.2(3)
Z	8
Z'	2
F(000)	1312
T (K)	150
ρ_{calc} (g cm^{-3})	1.593
λ (Å)	1.34139
μ (mm^{-1})	1.309
measured reflections	36387
independent reflections	6142
R_{int}	0.0274
R_σ	0.0186
observed reflections	5815
R_1, $I > 2\sigma(I)$ (all)	0.0369
R_1, all data	0.0383
wR_2, $I > 2\sigma(I)$ (all)	0.0929
wR_2, all data	0.0946
GoF	1.063
Max/Min (e Å^{-3})	0.389 / -0.449
Flack Parameter	N/A

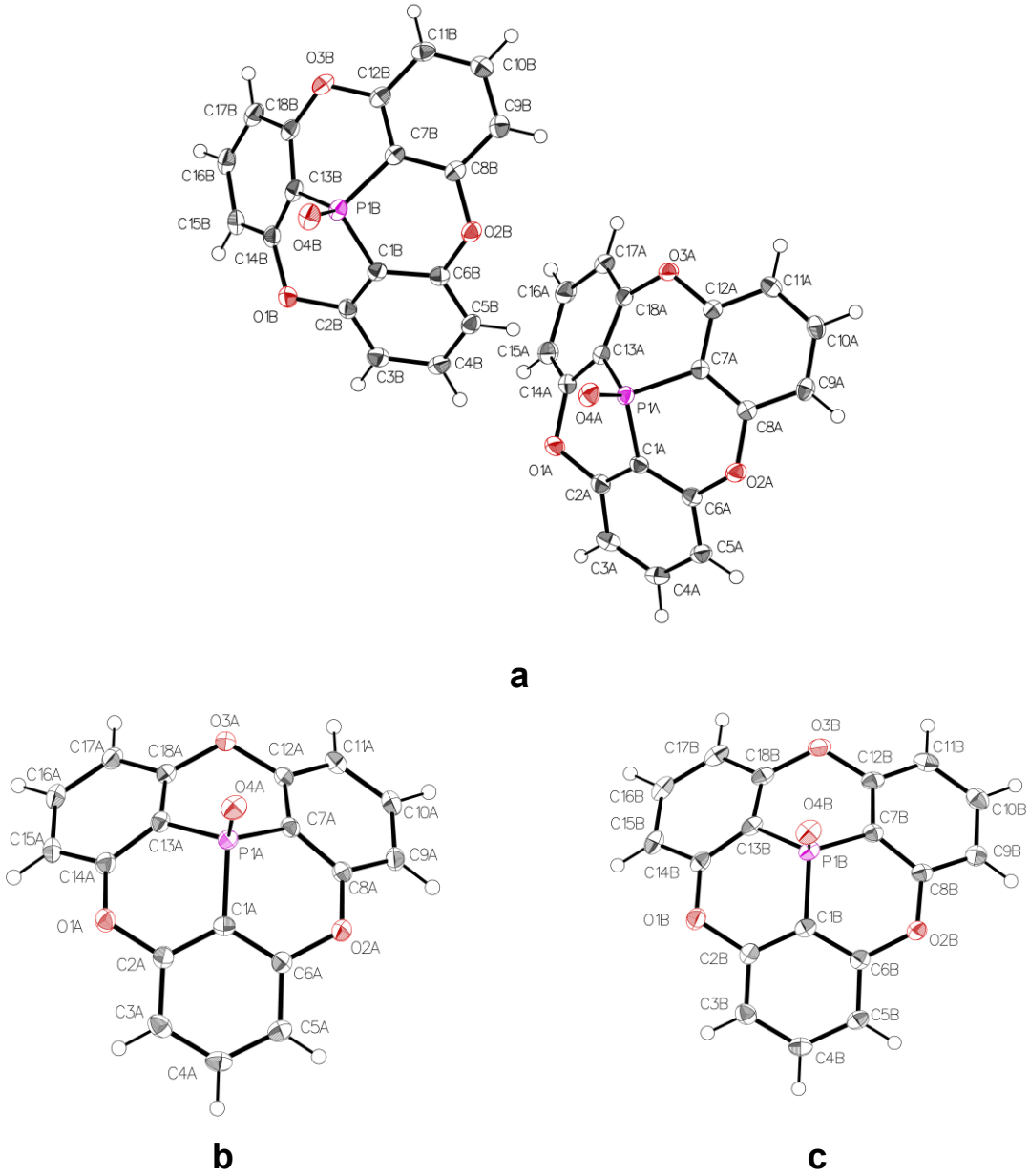

Figure 7.1 : Thermal atomic displacement ellipsoid plot of the structure of crystals of polymorph A of phosphangulene oxide (**2a**) grown from EtOH and measured at 150 K. The ellipsoids of non-hydrogen atoms are drawn at the 50% probability level, and hydrogen atoms are represented by a sphere of arbitrary size. (a) View of the asymmetric unit. (b), (c) Individual views of the two molecules in the asymmetric unit.

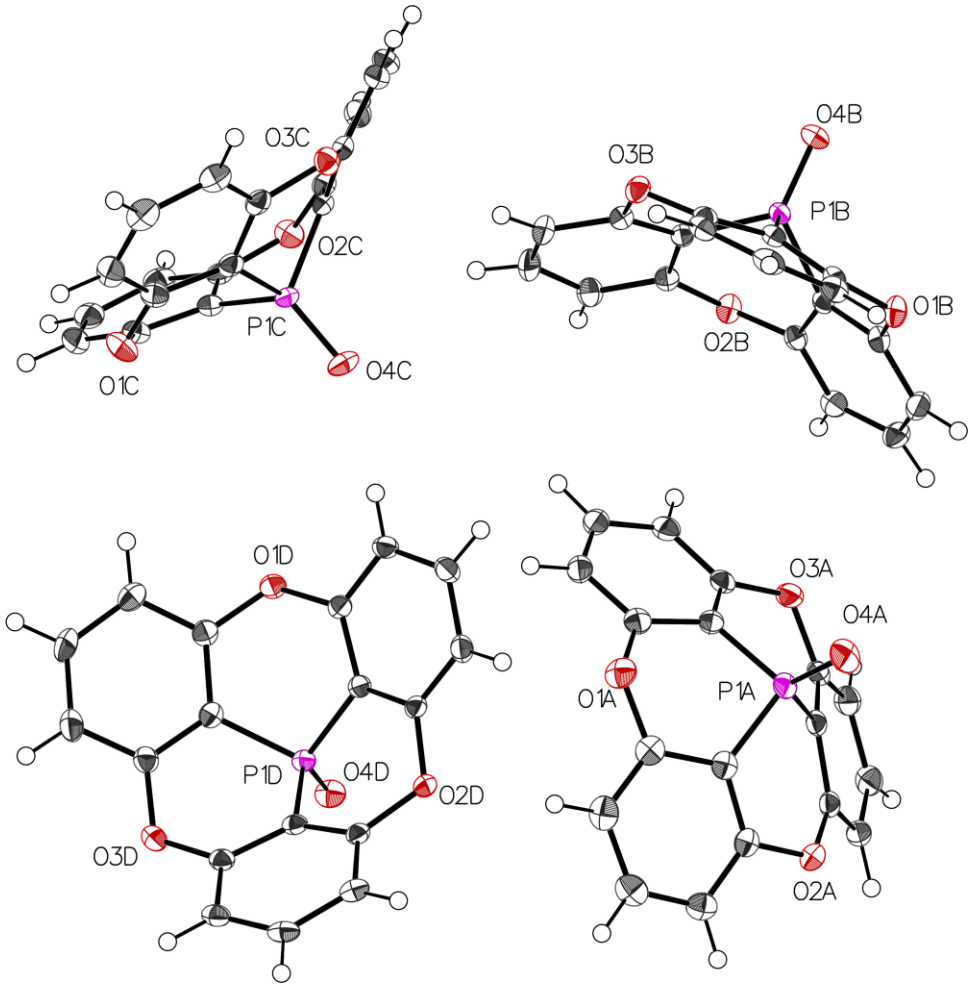

Figure 7.2 : Thermal atomic displacement ellipsoid plot of the structure of crystals of polymorph B of phosphangulene oxide (**2a**) grown from EtOH and measured at 150 K. The ellipsoids of non-hydrogen atoms are drawn at the 50% probability level, and hydrogen atoms are represented by a sphere of arbitrary size. View of the asymmetric unit with labeled heteroatoms.

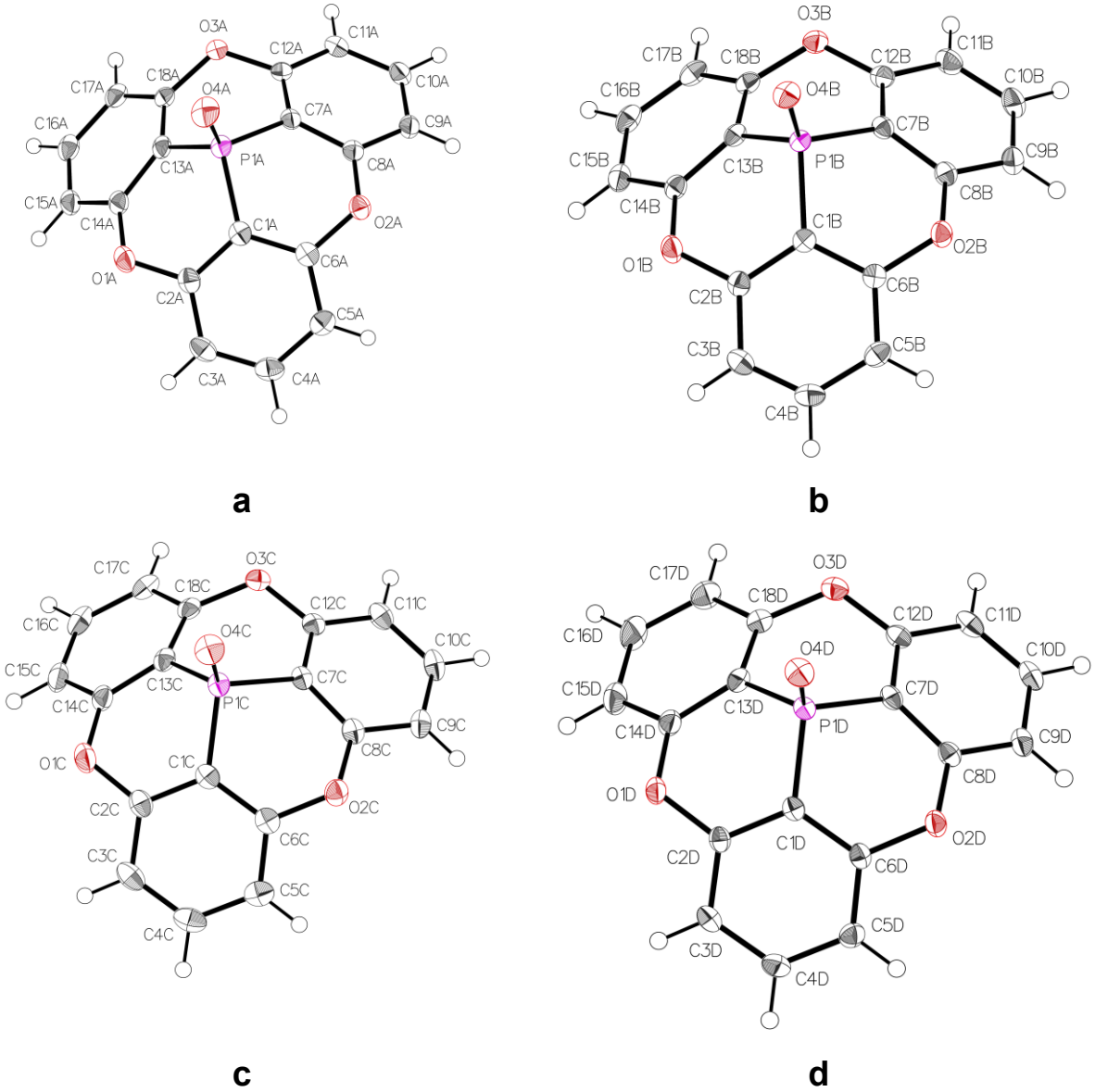

Figure 7.3 : Thermal atomic displacement ellipsoid plot of the structure of crystals of polymorph B of phosphangulene oxide (**2a**) grown from EtOH and measured at 150 K. The ellipsoids of non-hydrogen atoms are drawn at the 50% probability level, and hydrogen atoms are represented by a sphere of arbitrary size. (a), (b), (c), (d) Individual views of the four molecules in the asymmetric unit with all atoms labeled.

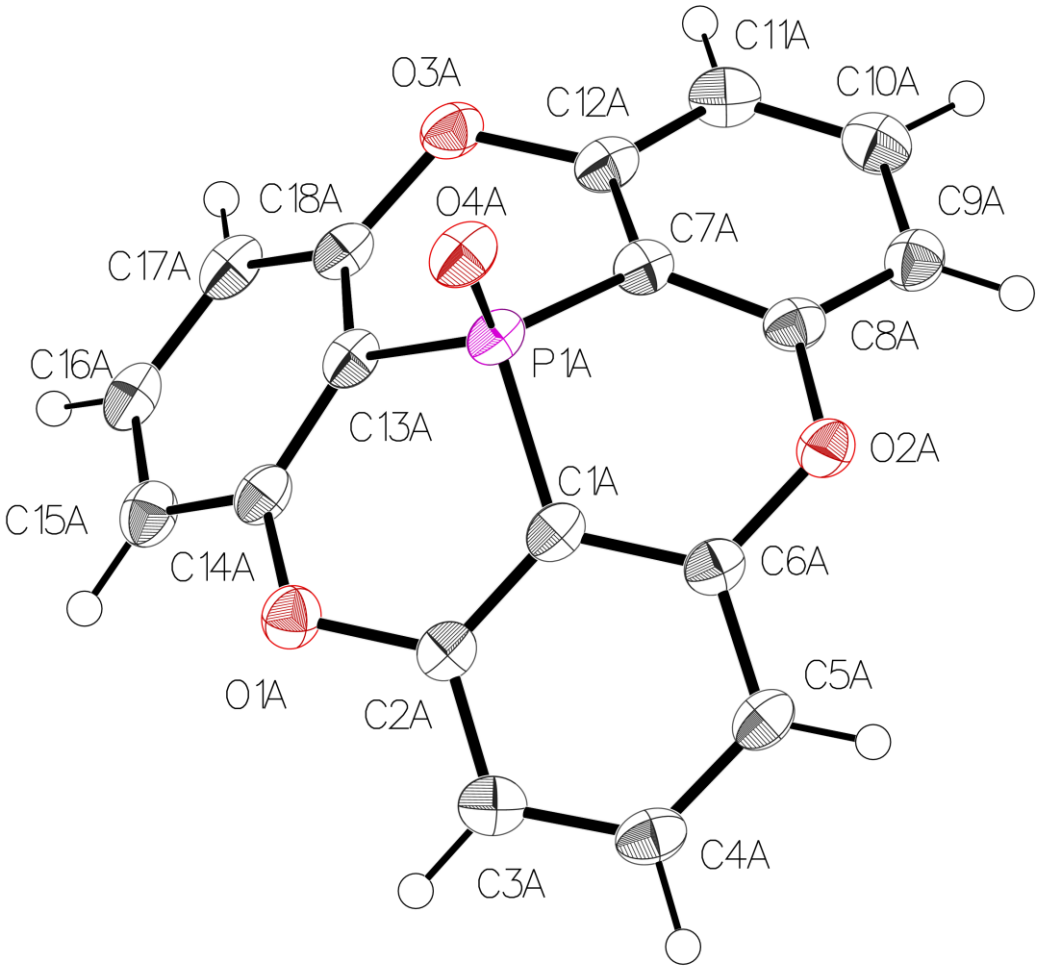

Figure 7.4 : Thermal atomic displacement ellipsoid plot of the structure of crystals of polymorph C of phosphangulene oxide (**2a**) grown from EtOH and measured at 150 K. The ellipsoids of non-hydrogen atoms are drawn at the 50% probability level, and hydrogen atoms are represented by a sphere of arbitrary size.

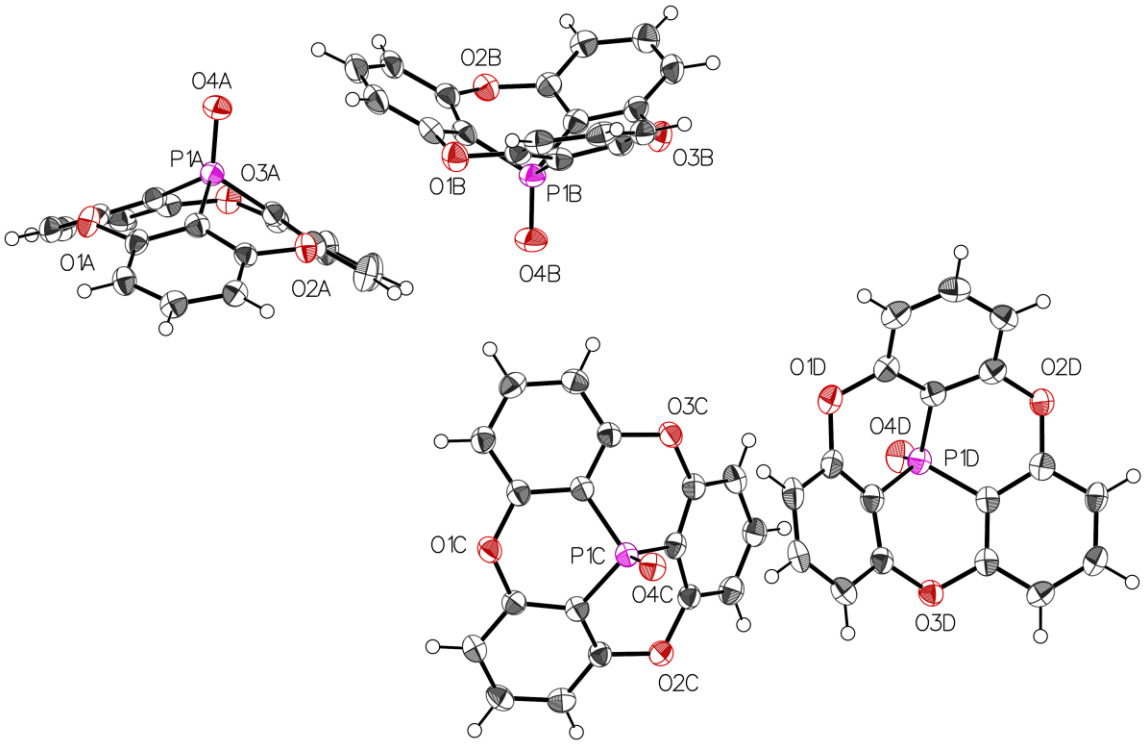

Figure 7.5 : Thermal atomic displacement ellipsoid plot of the structure of crystals of polymorph D of phosphangulene oxide (**2a**) grown from EtOH and measured at 150 K. The ellipsoids of non-hydrogen atoms are drawn at the 50% probability level, and hydrogen atoms are represented by a sphere of arbitrary size. View of the asymmetric unit with labeled heteroatoms.

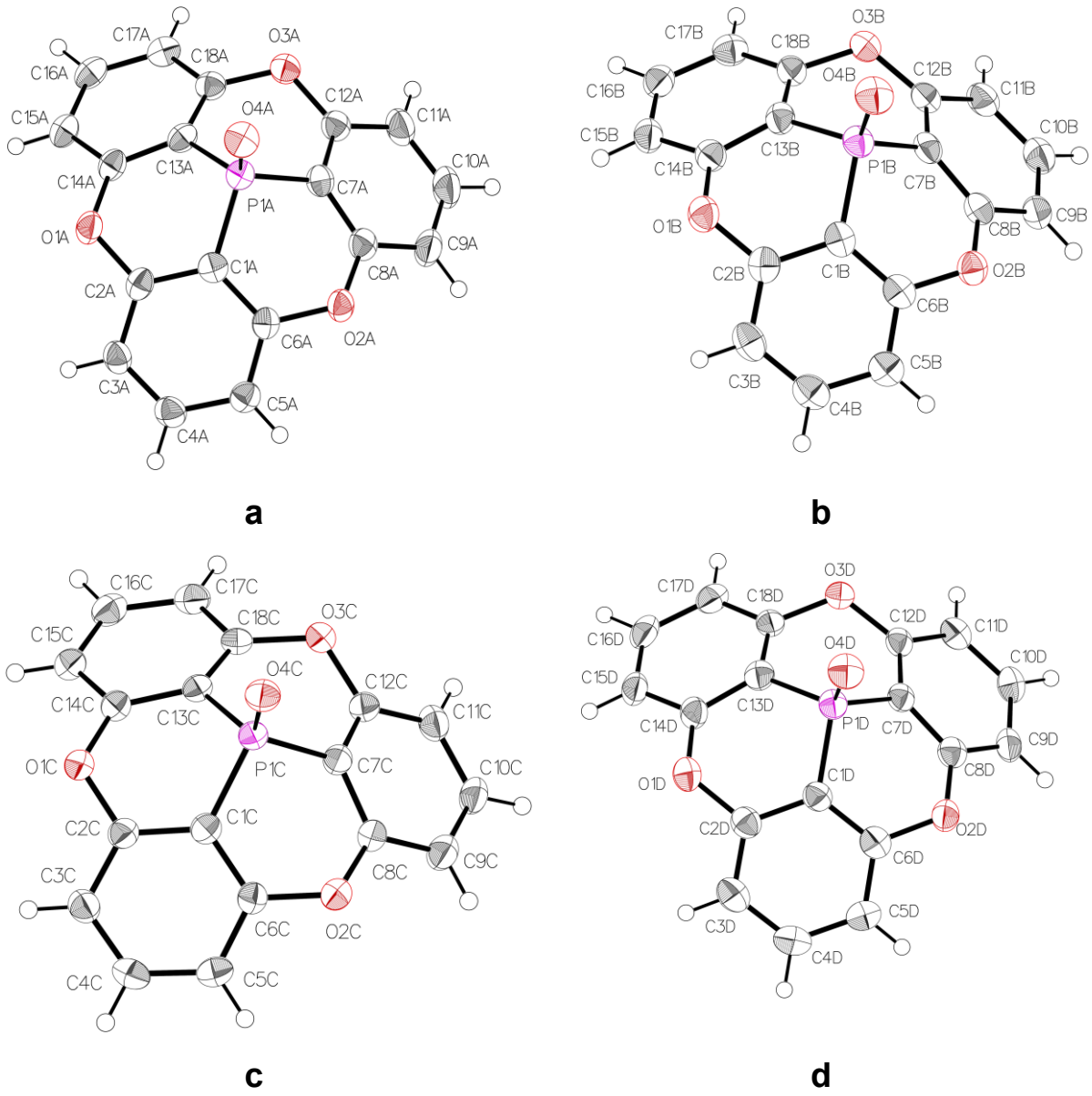

Figure 7.6 : Thermal atomic displacement ellipsoid plot of the structure of crystals of polymorph D of phosphangulene oxide (**2a**) grown from EtOH and measured at 150 K. The ellipsoids of non-hydrogen atoms are drawn at the 50% probability level, and hydrogen atoms are represented by a sphere of arbitrary size. (a), (b), (c), (d) Individual views of the four molecules in the asymmetric unit with all atoms labeled.

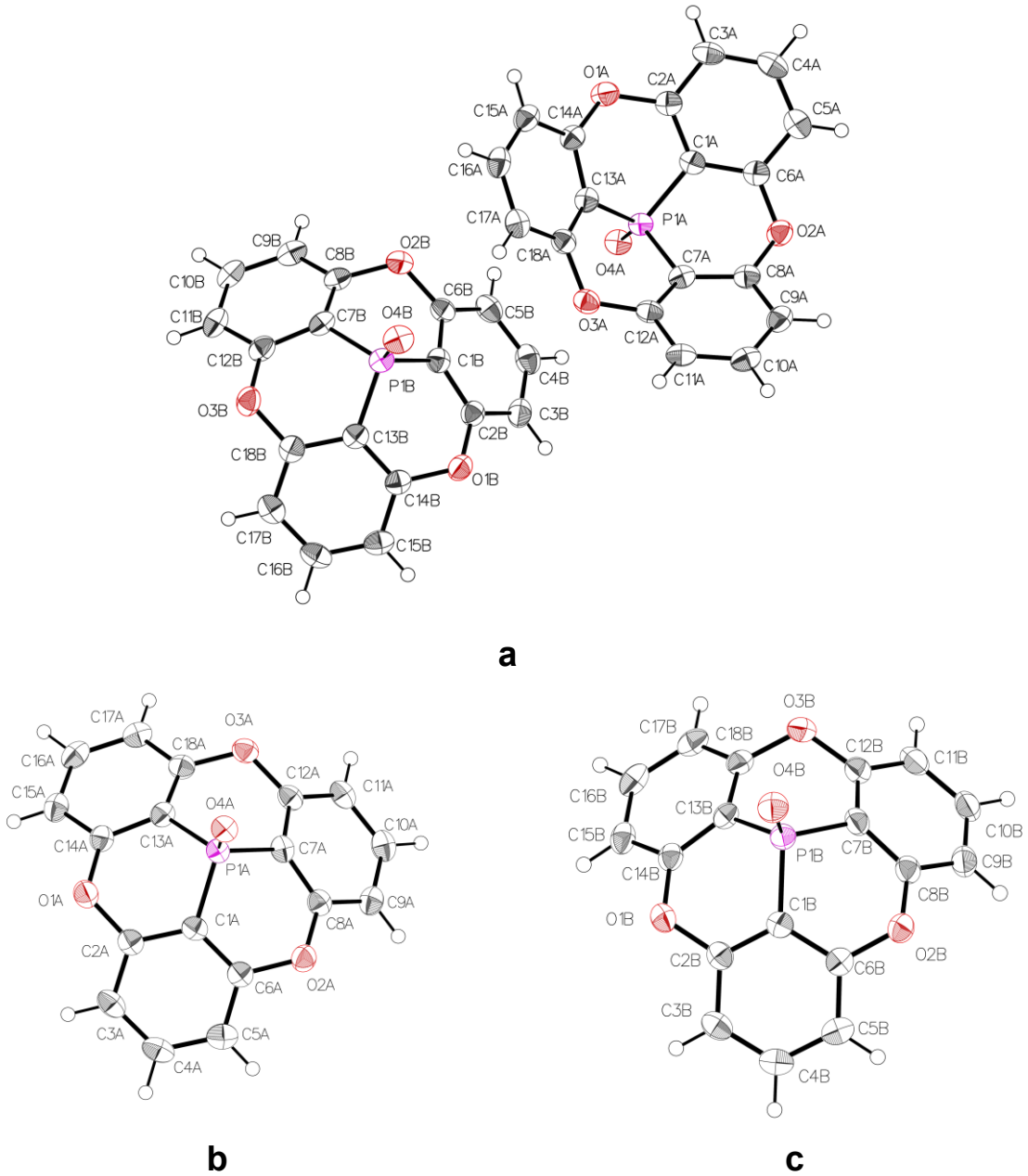

Figure 7.7 : Thermal atomic displacement ellipsoid plot of the structure of crystals of polymorph E of phosphangulene oxide (**2a**) grown from EtOH and measured at 150 K. The ellipsoids of non-hydrogen atoms are drawn at the 50% probability level, and hydrogen atoms are represented by a sphere of arbitrary size. (a) View of the asymmetric unit. (b), (c) Individual views of the two molecules in the asymmetric unit.

Comparison of crystal packing in the polymorphs of phosphangulene oxide (2a) and discussion of the similarity of polymorphs B and D.

To assess the similarity of crystal packing in the five polymorphs of phosphangulene oxide (**2a**), we analyzed the structures and compared them using CrystalCMP software.[1] Packing similarity was evaluated by overlapping a cluster of molecules (one central molecule and 10 neighbors) in the structures, by matching a selected fragment of the molecule (here the central phosphorus atom and its four connected atoms), and then calculating a similarity matrix shown as a dendrogram tree.

This comparison, performed for the five polymorphs (Figure S8), shows that the packings of polymorphs are distinctly different, except in the cases of polymorphs B and D, where the asymmetric units are identical and a cluster of several molecules overlaps almost perfectly (Figure S9). These two polymorphs have different crystal lattice symmetry (centrosymmetric monoclinic $P2_1/c$ *vs* non-centrosymmetric polar orthorhombic $Pca2_1$) but similar unit-cell lattice parameters for the cell lengths. As a result, the polymorphs differ only in the value of the β angle (99° *vs* 90°). This similarity is also visible when the Hirschfeld plots for each of the four independent molecules are compared (Figure S10). A packing analysis comparison can also be performed using the Materials Module wizard of CCDC Mercury.[2] This gives a comparable result, as Mercury is able to overlay 48 molecules out of a generated cluster of 50 molecules. Differentiation between the two polymorphs occurs only when the translation symmetry is applied and the packing generated with more than one unit cell is considered (Figure S11). The difference in the crystal packing can also be seen in the calculated X-ray powder diffraction patterns, as shown by a view in a restricted 2θ angular range in Figure S12.

	0	1	2	3	4
0	0.0000	45.7401	35.2784	49.3662	54.6179
1	45.7401	0.0000	42.4817	0.0406	48.3142
2	35.2784	42.4817	0.0000	43.7755	52.0513
3	49.3662	0.0406	43.7755	0.0000	47.3841
4	54.6179	48.3142	52.0513	47.3841	0.0000

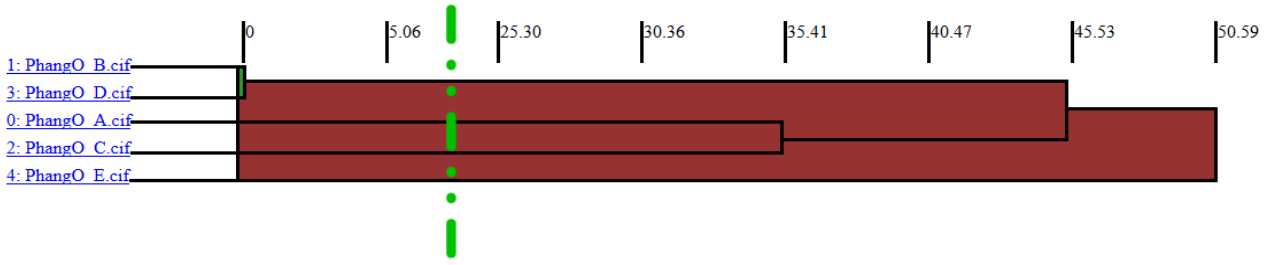

Figure 7.8 : Packing similarity matrix (top) and associated tree diagram (bottom) for the five polymorphs of phosphangulene oxide (**2a**). Part of the tree diagram between 5 and 25 (indicated by the dotted green line) was removed to make the figure shorter and the diagram more readable.

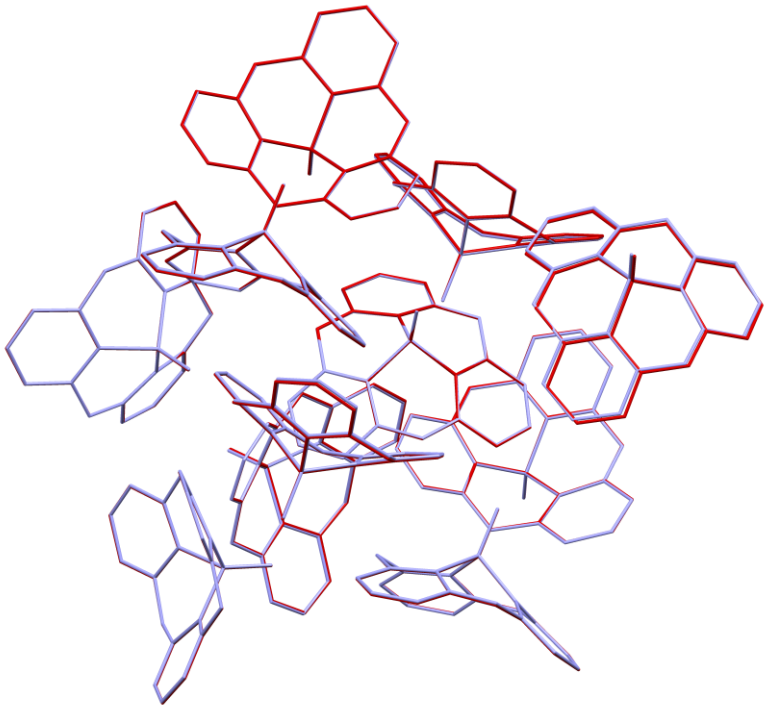

Figure 7.9 : Molecular overlay calculated by CrystalCMP showing clusters of ten molecules from the structures of polymorphs B and D of phosphangulene oxide (**2a**).

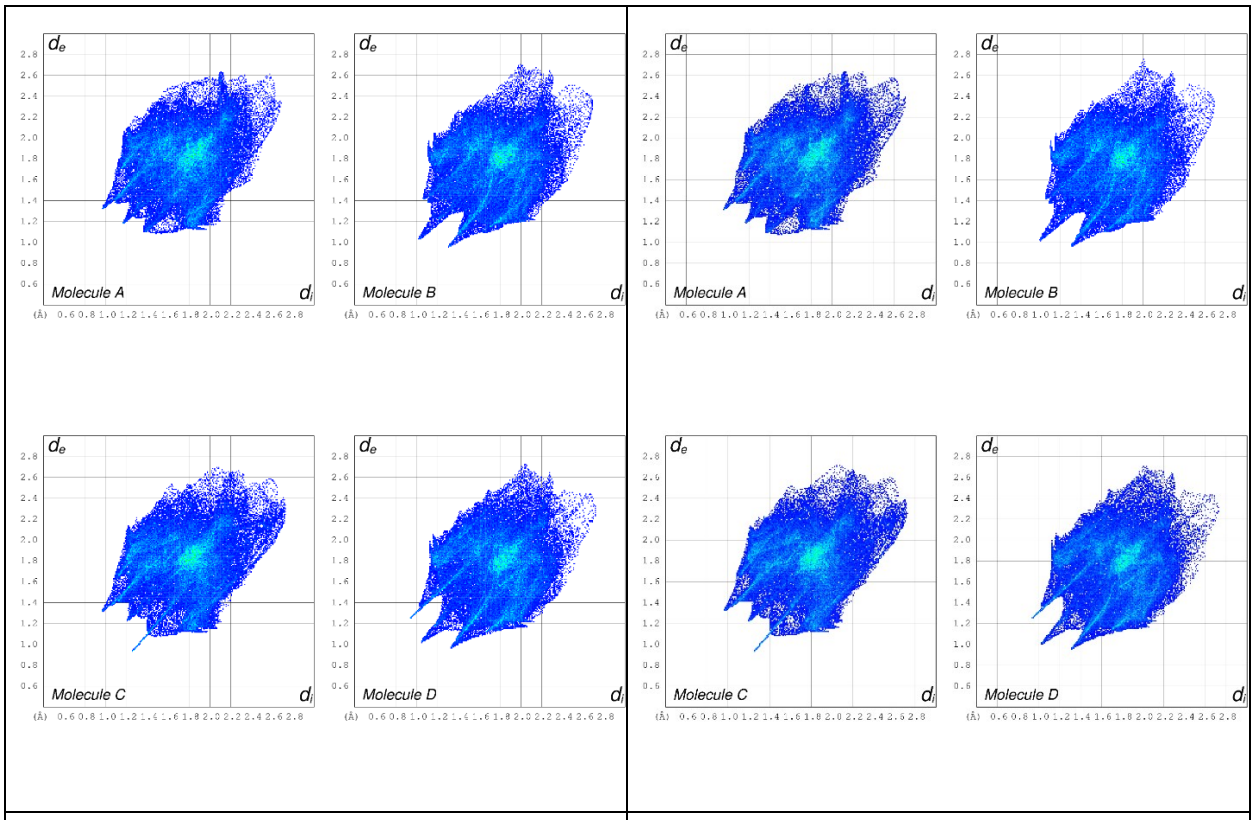

Figure 7.10 : Fingerprint plots of Hirshfeld surfaces for the four symmetry-inequivalent molecules of phosphangulene oxide (**2a**) in polymorphs D (left) and B (right).

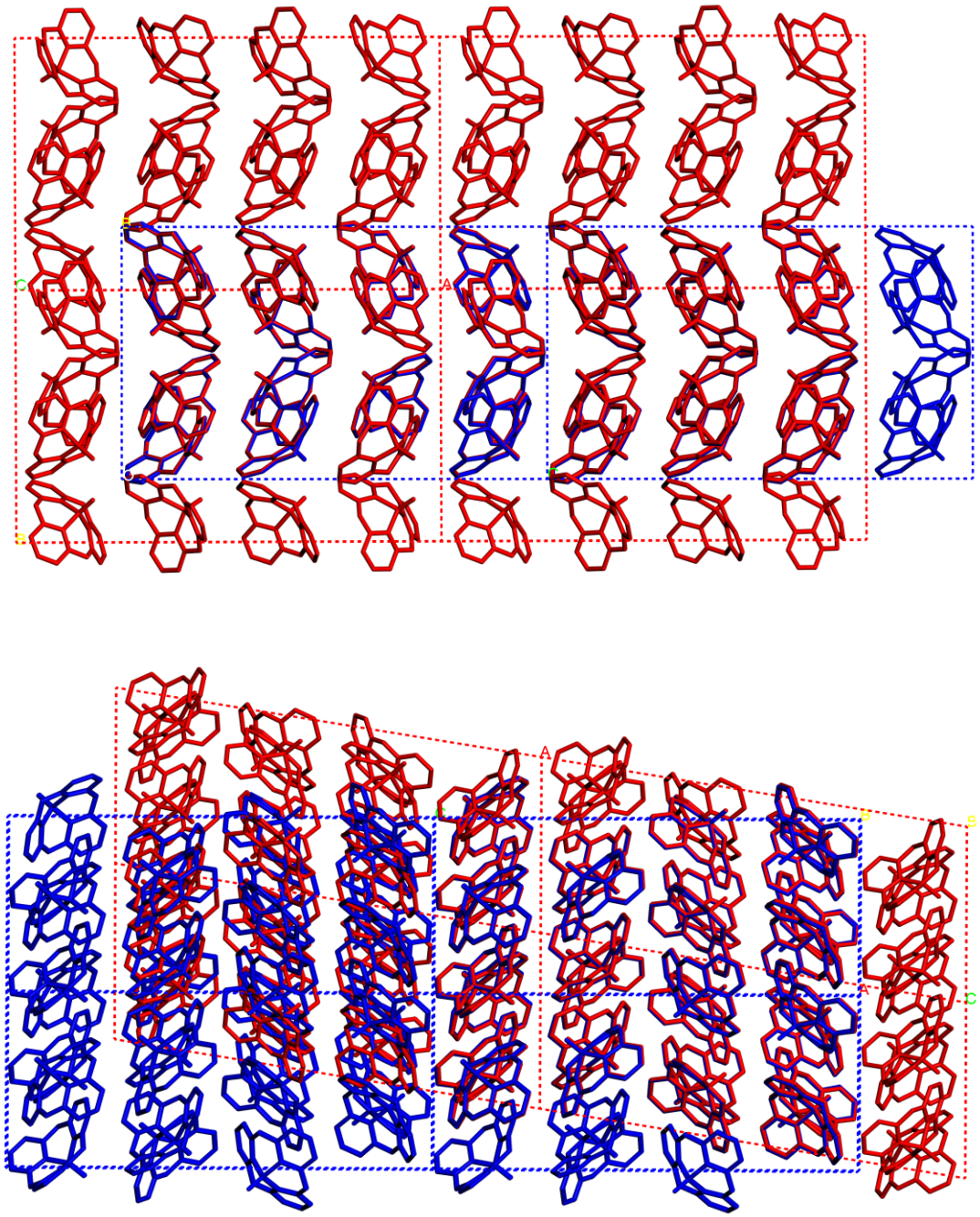

Figure 7.11 : Views of the superposition of the structures of polymorphs B (red) and D (blue) (2 × 2 × 2 arrays of unit cells) of phosphangulene oxide (**2a**). The structures are viewed along two perpendicular directions to show to what extent the molecules overlap.

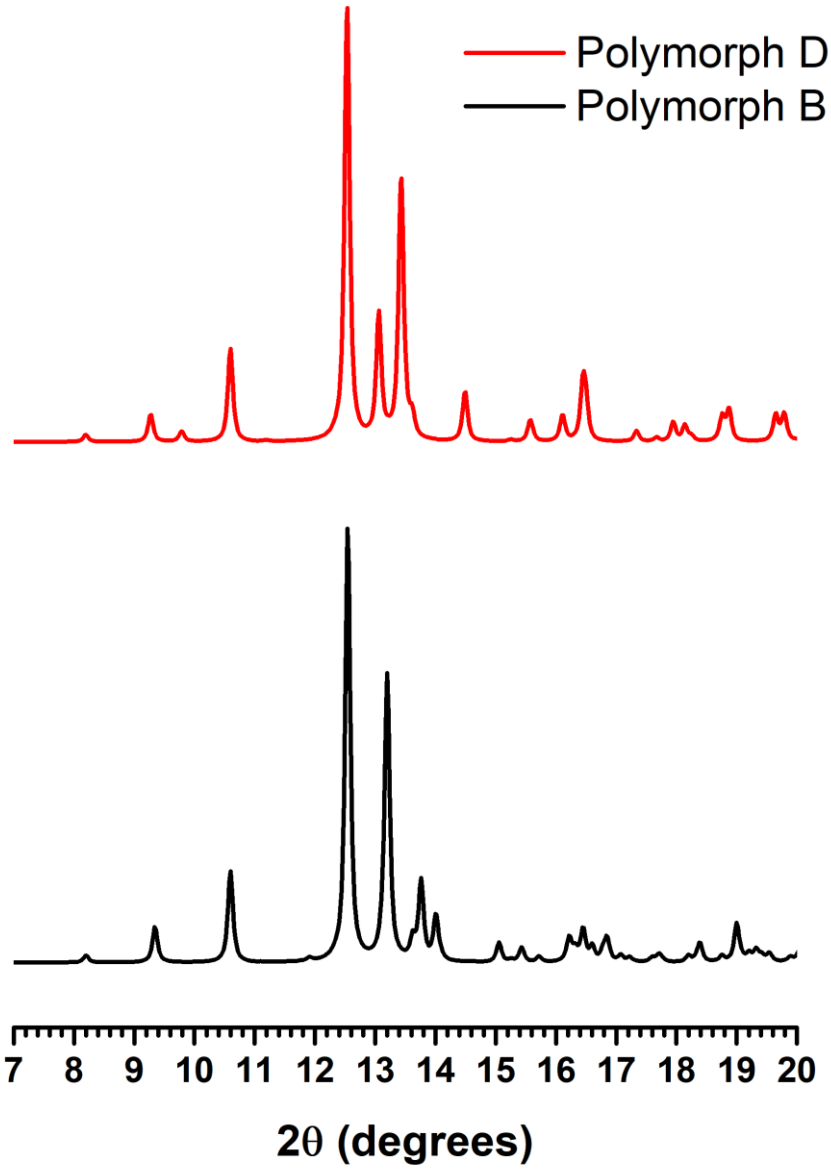

Figure 7.12 : Simulated XRD powder patterns for polymorphs B and D of phosphangulene oxide (**2a**).

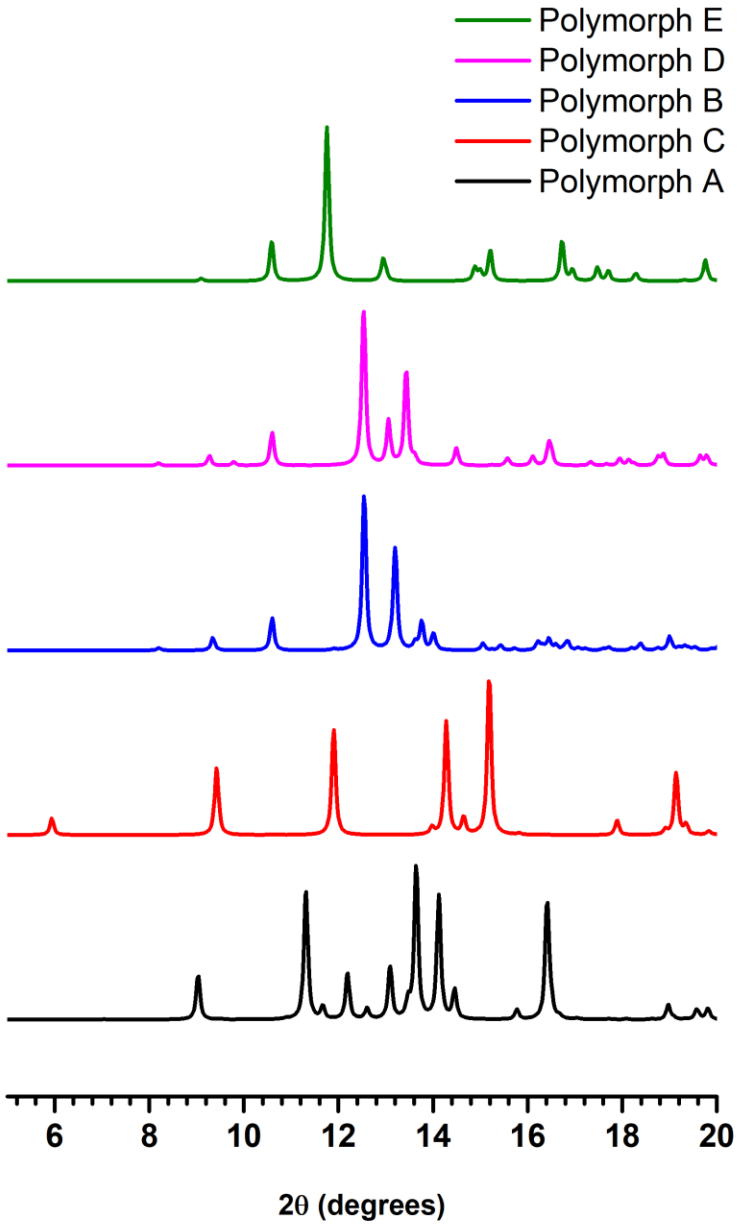

Figure 7.13 : Simulated XRD patterns for the five polymorphs of phosphangulene oxide (**2a**).

7.1.2 Phosphangulene sulfide (2b)

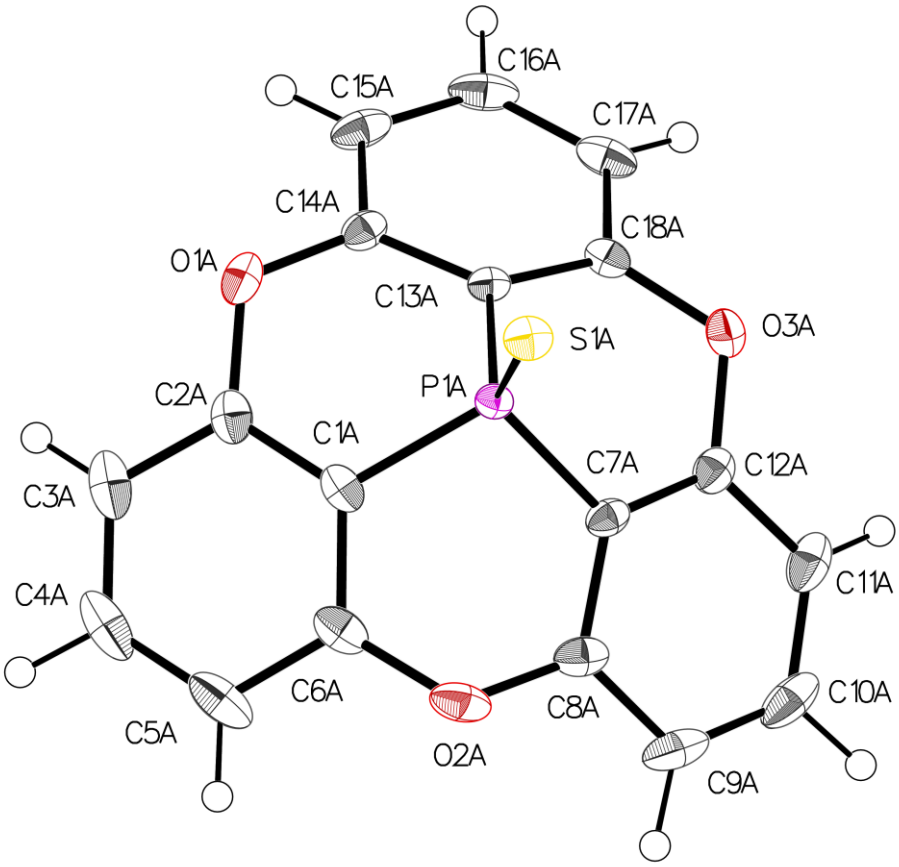

Figure 7.14 : Thermal atomic displacement ellipsoid plot of the structure of crystals of polymorph B of phosphangulene sulfide (**2b**) grown from EtOH and measured at 150 K. The ellipsoids of non-hydrogen atoms are drawn at the 50% probability level, and hydrogen atoms are represented by a sphere of arbitrary size.

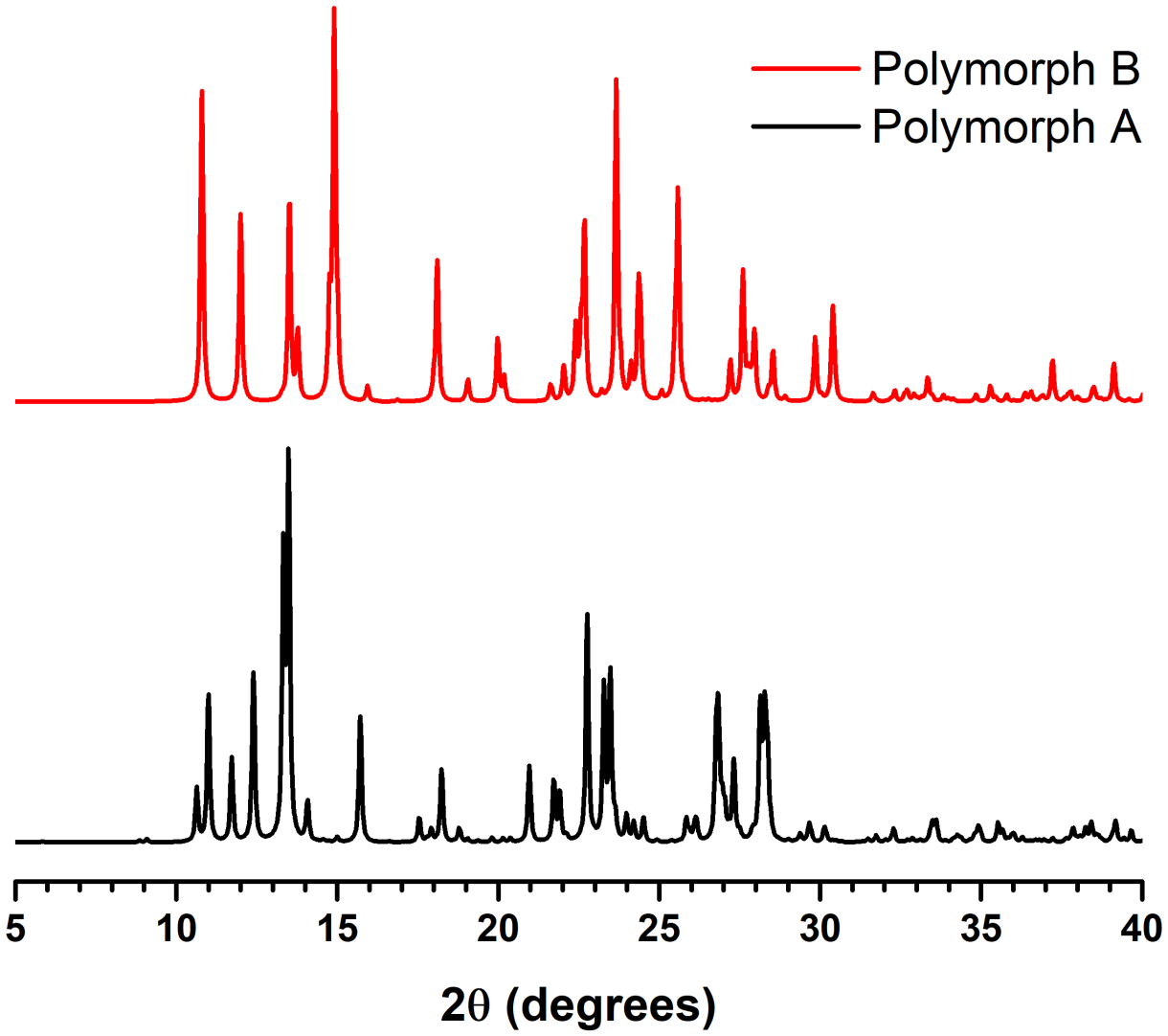

Figure 7.15 : Simulated XRD patterns for the two polymorphs of phosphangulene sulfide (**2b**).

7.1.3 Phosphangulene selenide (2c)

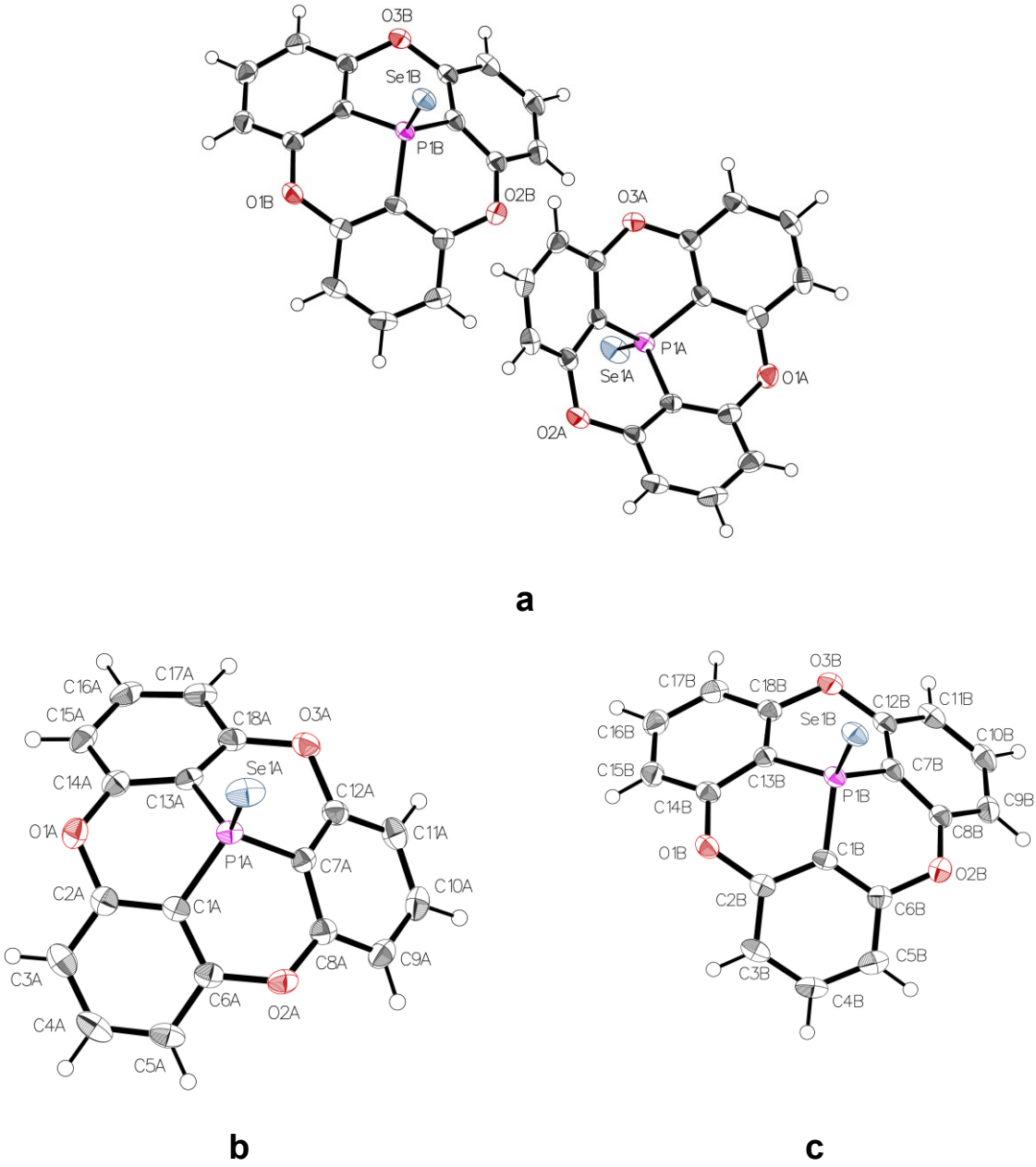

Figure 7.16 : Thermal atomic displacement ellipsoid plot of the structure of crystals of polymorph B of phosphangulene selenide (**2c**) grown from CS_2 and measured at 150 K. The ellipsoids of non-hydrogen atoms are drawn at the 50% probability level, and hydrogen atoms are represented by a sphere of arbitrary size. (a) View of the asymmetric unit with heteroatoms

labeled. (b), (c) Individual views of the two molecules in the asymmetric unit with all atoms labeled.

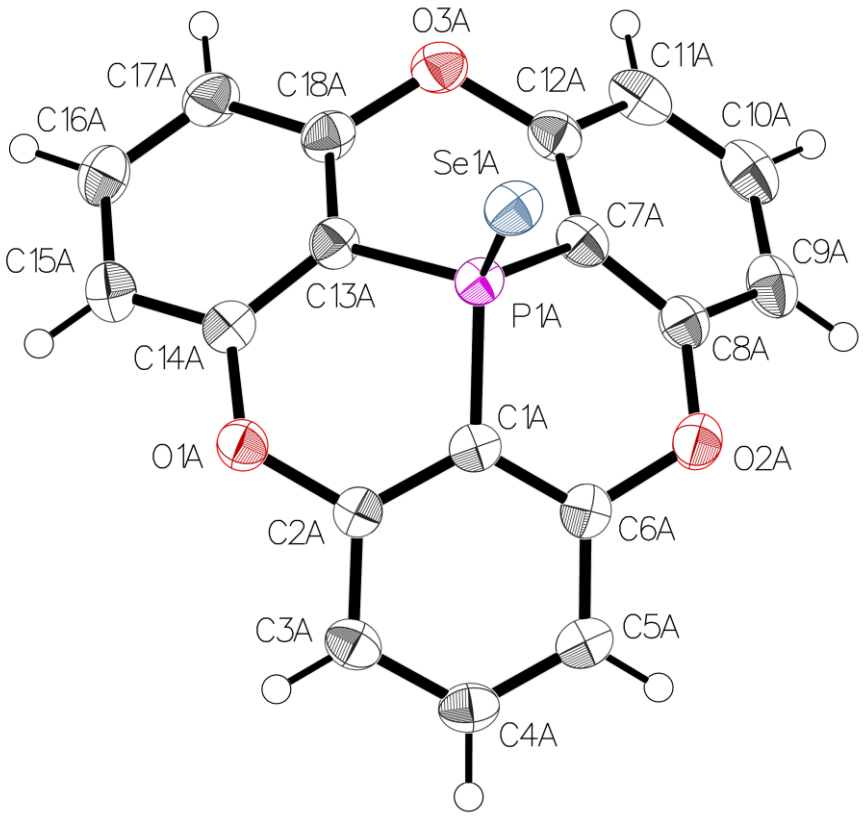

Figure 7.17 : Thermal atomic displacement ellipsoid plot of the structure of crystals of polymorph C of phosphangulene selenide (**2c**) grown from CS_2 and measured at 150 K. The ellipsoids of non-hydrogen atoms are drawn at the 50% probability level, and hydrogen atoms are represented by a sphere of arbitrary size.

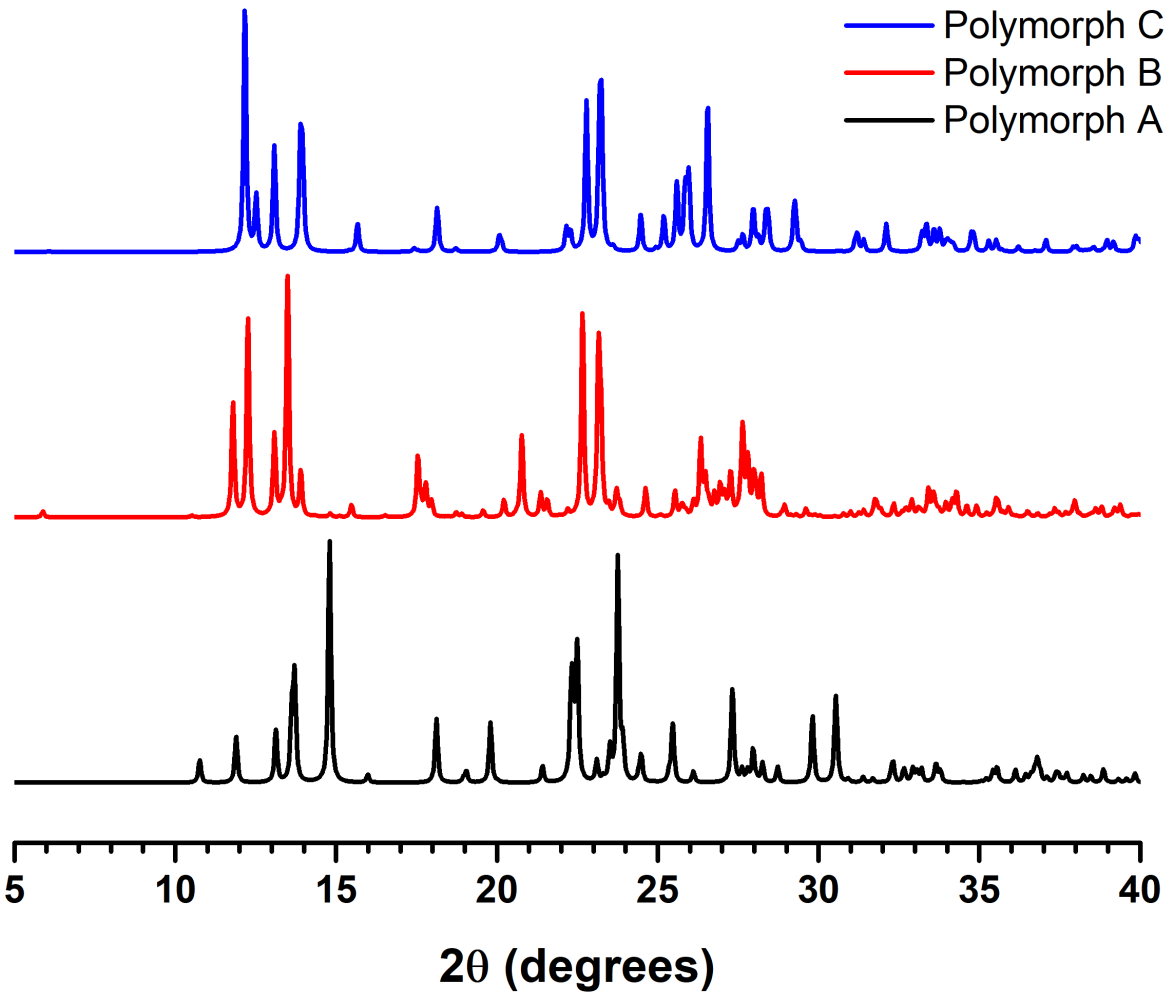

Figure 7.18 : Simulated XRD patterns for the three polymorphs of phosphangulene selenide (**2c**).

7.1.4 Mixed crystals

Table 7.2 : Crystal structure data for mixed crystals of phosphangulene (**1**) and phosphangulene oxide (**2a**) crystallized from EtOAc.

Crystal sample	1	2	3
crystallization medium	EtOAc	EtOAc	EtOAc
formula	$C_{18}H_9O_{3.85}P$	$C_{18}H_9O_{3.70}P$	$C_{18}H_9O_{3.50}P$
Mr	317.90	315.48	312.28
crystal system	orthorhombic	orthorhombic	orthorhombic
space group	*Pbca*	*Pbca*	*Pbca*
a (Å)	12.0696(5)	12.0473(4)	12.0382(8)
b (Å)	7.4375(3)	7.4364(3)	7.4286(5)
c (Å)	29.7131(2)	29.7151(10)	29.694(2)
α (°)	90	90	90
β (°)	90	90	90
γ (°)	90	90	90
V (Å^3)	2667.28(19)	2662.13(17)	2655.4(3)
Z	8	8	8
Z'	1	1	1
F(000)	1303	1293	1280
T (K)	150	150	150
ρ_{calc} (g cm^{-3})	1.583	1.574	1.562
λ (Å)	1.34139	1.34139	1.34139
μ (mm^{-1})	1.302	1.295	1.287
measured reflections	19132	38341	26465
independent reflections	2473	2538	2505
R_{int}	0.0439	0.0591	0.0605
R_σ	0.0255	0.0221	0.0285
observed reflections	2130	2375	2388
R_1, $I > 2\sigma(I)$ (all)	0.0376	0.0466	0.0624
R_1, all data	0.0476	0.0493	0.0646
wR_2, $I > 2\sigma(I)$ (all)	0.0851	0.1205	0.1620
wR_2, all data	0.0907	0.1225	0.1636
GoF	1.060	1.114	1.152
Max/Min (e Å^{-3})	0.361 / -0.343	0.388 / -0.529	0.422 / -0.455

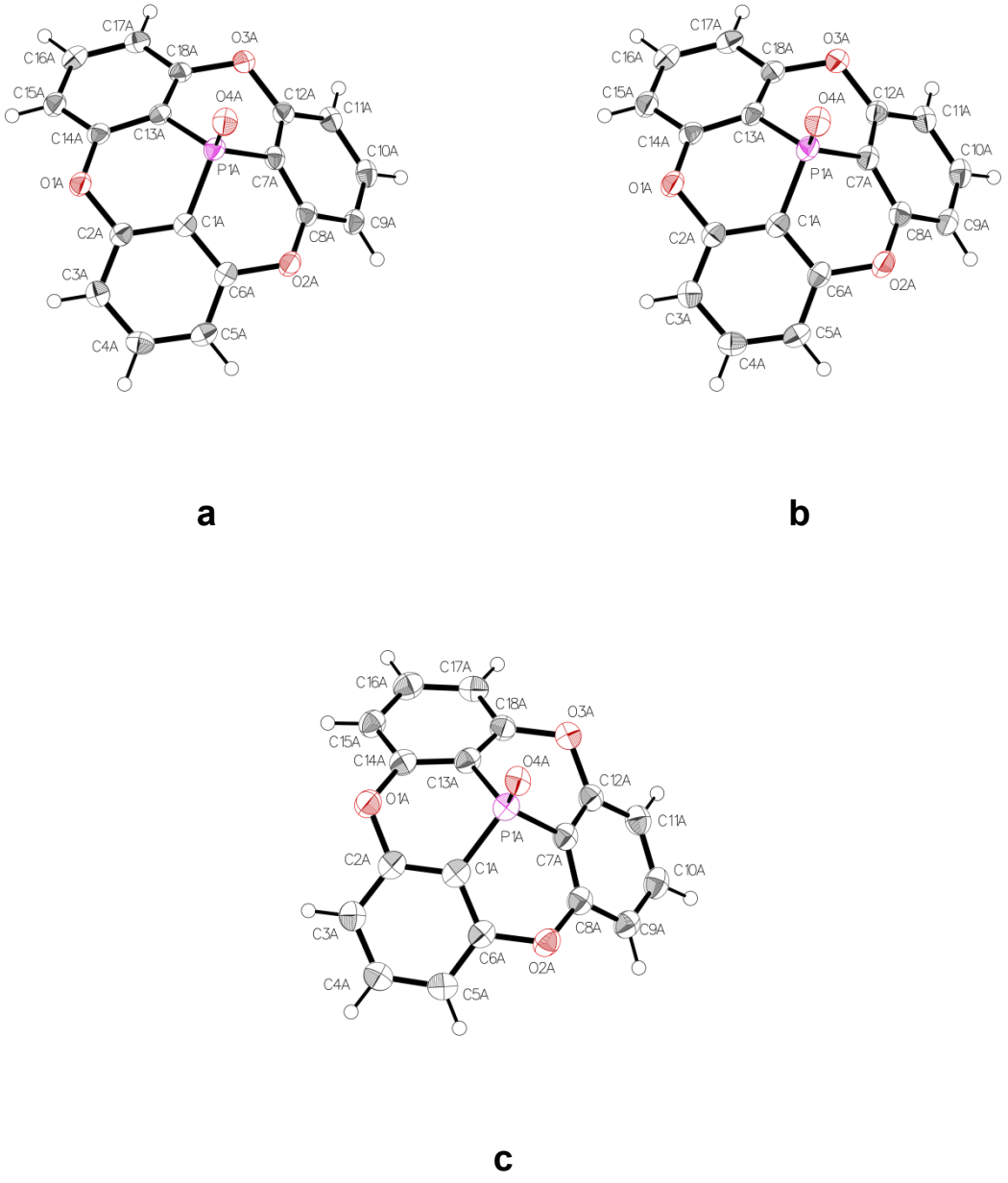

Figure 7.19 : Thermal atomic displacement ellipsoid plot of the structure of mixed crystals of phosphangulene (**1**) and phosphangulene oxide (**2a**) grown from EtOAc and measured at 150 K. The ellipsoids of non-hydrogen atoms are drawn at the 50% probability level, and hydrogen atoms are represented by a sphere of arbitrary size. (a) $C_{18}H_9O_{3.85}P$. (b) $C_{18}H_9O_{3.70}P$. (c) $C_{18}H_9O_{3.5}P$.

Table 7.3 : Crystal structure data for mixed crystals of phosphangulene oxide (**2a**) and phosphangulene sulfide (**2b**) crystallized from CH_2Cl_2/hexane.

Crystal	1	2	3	4
crystallization medium	CH_2Cl_2/hexane	CH_2Cl_2/hexane	CH_2Cl_2/hexane	CH_2Cl_2/hexane
formula	$C_{18}H_9O_{3.71}PS_{0.29}$	$C_{18}H_9O_{3.72}PS_{0.28}$	$C_{18}H_9O_{3.65}PS_{0.35}$	$C_{18}H_9O_{3.63}PS_{0.37}$
Mr	324.92	324.64	325.88	326.20
crystal system	monoclinic	monoclinic	monoclinic	monoclinic
space group	$P2_1/n$	$P2_1/c$	$P2_1/c$	$P2_1/c$
a (Å)	10.1281(8)	14.4805(5)	14.5033(5)	14.5020(4)
b (Å)	25.426(2)	16.6226(6)	16.6611(6)	16.6652(5)
c (Å)	10.6714(8)	11.7323(4)	11.7398(4)	11.7455(4)
α (°)	90	90	90	90
β (°)	93.978(4)	101.205(2)	101.117(1)	101.037(1)
γ (°)	90	90	90	90
V (Å^3)	2741.5(4)	2770.18(17)	2783.58(17)	2786.13(15)
Z	8	8	8	8
Z'	2	2	2	2
F(000)	1331	1330	1335	1336
T (K)	150	150	150	150
ρ_{calc} (g cm^{-3})	1.574	1.557	1.555	1.555
λ (Å)	1.34139	1.34139	1.34139	1.34139
μ (mm^{-1})	1.539	1.508	1.569	1.586
measured reflections	359672	46622	23378	23463
independent reflections	6310	6332	5139	5167
R_{int}	0.0642	0.0332	0.0318	0.0242
R_σ	0.0447	0.0220	0.0241	0.0181
observed reflections	5529	5536	4784	4989
Parameters	424	424	424	424
R_1, $I > 2\sigma(I)$ (all)	0.0746	0.0405	0.0350	0.0339
R_1, all data	0.0822	0.0487	0.0381	0.0350
wR_2, $I > 2\sigma(I)$ (all)	0.1650	0.0992	0.0855	0.0846
wR_2, all data	0.1694	0.1038	0.0877	0.0856
GoF	1.079	1.074	1.070	1.121
Max/Min (e Å^{-3})	0.495 / -0.518	0.363 / -0.382	0.272/-0.356	0.247 / -0.403

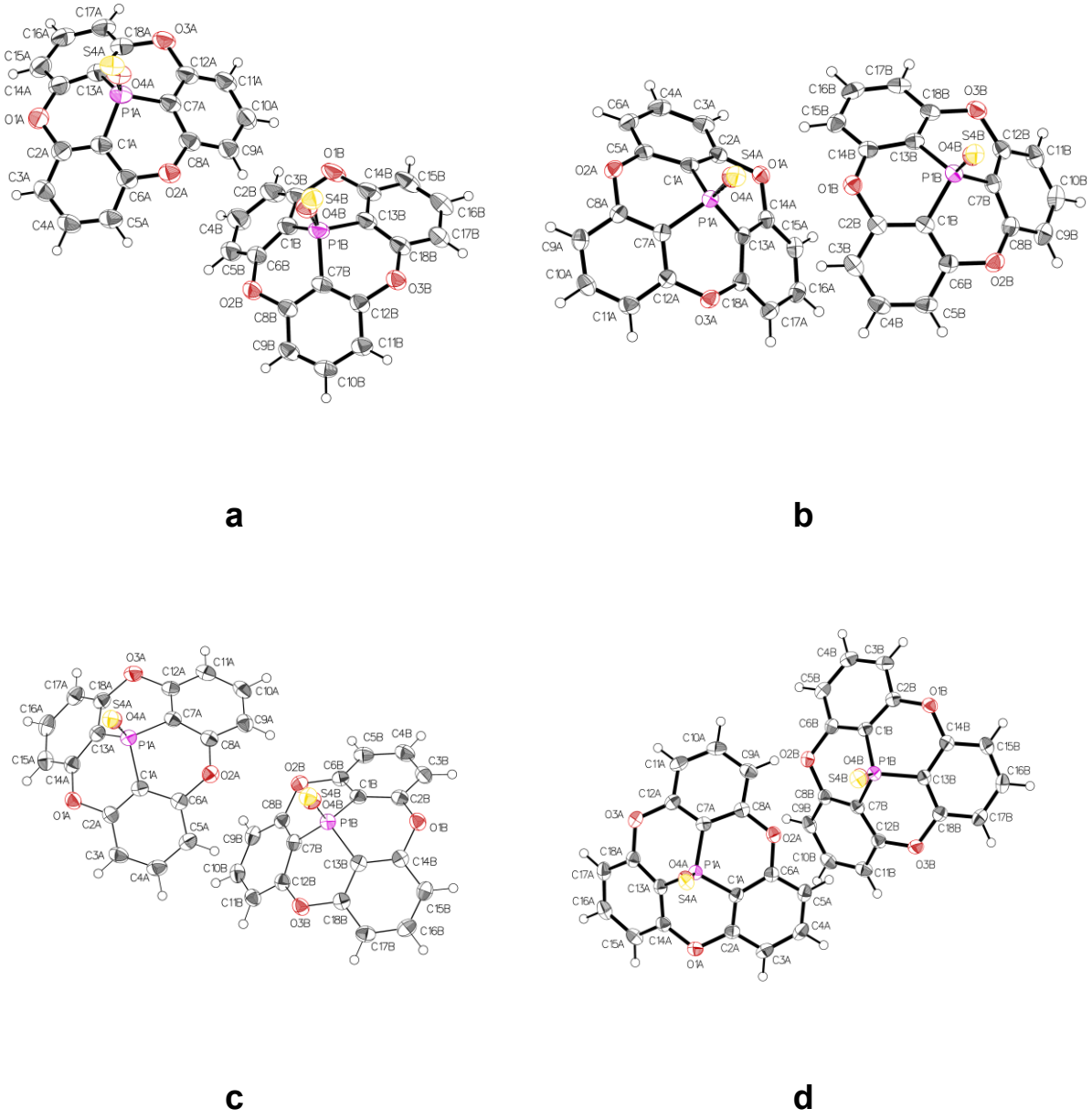

Figure 7.20 : Thermal atomic displacement ellipsoid plot of the structure of mixed crystals of phosphangulene oxide (**2a**) and phosphangulene sulfide (**2b**) grown from CH_2Cl_2/hexane and measured at 150 K. The ellipsoids of non-hydrogen atoms are drawn at the 50% probability level, and hydrogen atoms are represented by a sphere of arbitrary size. (a) $C_{18}H_9O_{3.71}PS_{0.29}$. (b) $C_{18}H_9O_{3.72}PS_{0.28}$. (c) $C_{18}H_9O_{3.65}PS_{0.35}$. (d) $C_{18}H_9O_{3.63}PS_{0.37}$.

7.1.5 References

1 Rohlíček, J.; Skořepová, E.; Babor, M.; Čejka, J. *J Appl. Crystallogr.* **2016**, *49*, 2172–2183.

2 Macrae, C. F.; Bruno, I. J.; Chisholm, J. A.; Edgington, P. R.; McCabe, P.; Pidcock, E.; Rodriguez-Monge, L.; Taylor, R.; van de Streek, J.; Wood, P. A. *J Appl. Crystallogr.* **2008**, *41*, 466–470.

7.2 Informations supplémentaires de l'article 2

Supporting Information

Putting Fullerenes in Their Place:

Cocrystallizing C_{60} and C_{70} with Phosphangulene Chalcogenides

Alice Heskia, Thierry Maris, and James D. Wuest*

Département de Chimie, Université de Montréal, Montréal, Québec H3C 3J7 Canada

*Author to whom correspondence may be addressed.

E-mail: *james.d.wuest@umontreal.ca*

7.2.1 Additional Crystallographic Information

Data were collected on a Bruker Venture Metaljet diffractometer using GaKα radiation (λ = 1.34139 Å). During all experiments, samples were cooled using an Oxford Cryostream liquid-nitrogen device (150 K for 2 **2a** • C_{60} • PhMe and 6 **2a** • 4 C_{60} • MeOH; 105 K for **2a** • C_{60} • PhCl). The cell lattice parameters were determined using reflections taken from three sets of 104 frames measured and harvested within the APEX3 suite of programs.[1] Integration of frames was performed using *SAINT*,[1] and a semiempirical absorption correction was applied with *SADABS* in the case of normal samples or with *TWINABS* for twinned samples.[2] The structures were solved using a dual space and intrinsic phasing approach with *SHELXT*,[3] and the refinement was carried out using *SHELXL*-2018/3.[4]

Crystals of compounds **2a** • C_{60} • PhCl and 2 **2c** • 2 C_{60} • PhCl proved to be two-component twins. The unit cell was checked using *CELL_NOW*, and the integration was performed using the two components to produce an HKLF5-type reflection file. For structures crystallizing in the chiral space group $P2_1$ (**2b** • C_{60} • CS_2, **2b** • C_{70} • CS_2, and **2c** • C_{60} • CS_2), the Flack parameter was estimated as part of the refinement using the TWIN/BASF method.

In the structures of the compounds **2a** • C_{60} • PhCl and 6 **2a** • 4 C_{60} • MeOH, molecules of C_{60} were found to be disordered and were refined as rigid bodies, using a model involving two and three molecules, respectively, for each disordered site.

7.2.2 ORTEP Diagrams

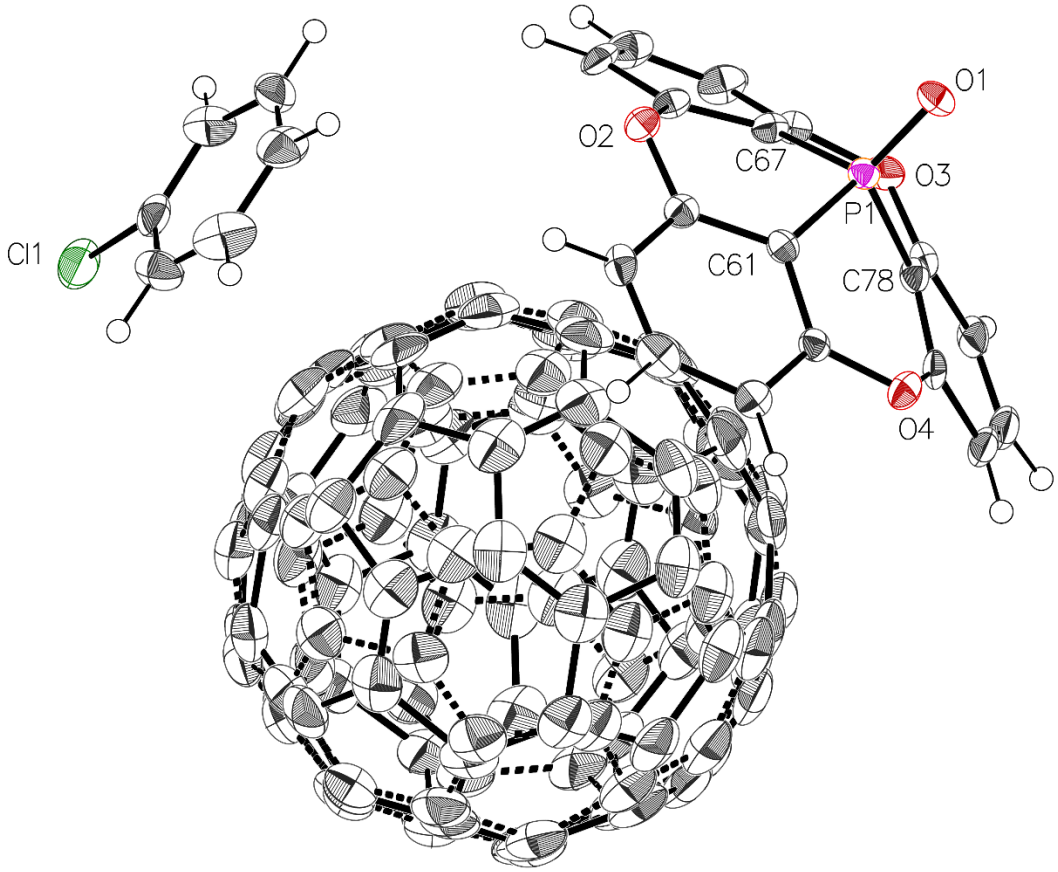

Figure 7.21 : Thermal atomic displacement ellipsoid plot of the structure of 1:1 cocrystals of phosphangulene oxide (**2a**) and C_{60} grown from PhCl. The ellipsoids of non-hydrogen atoms are drawn at the 50% probability level, and hydrogen atoms are represented by a sphere of arbitrary size.

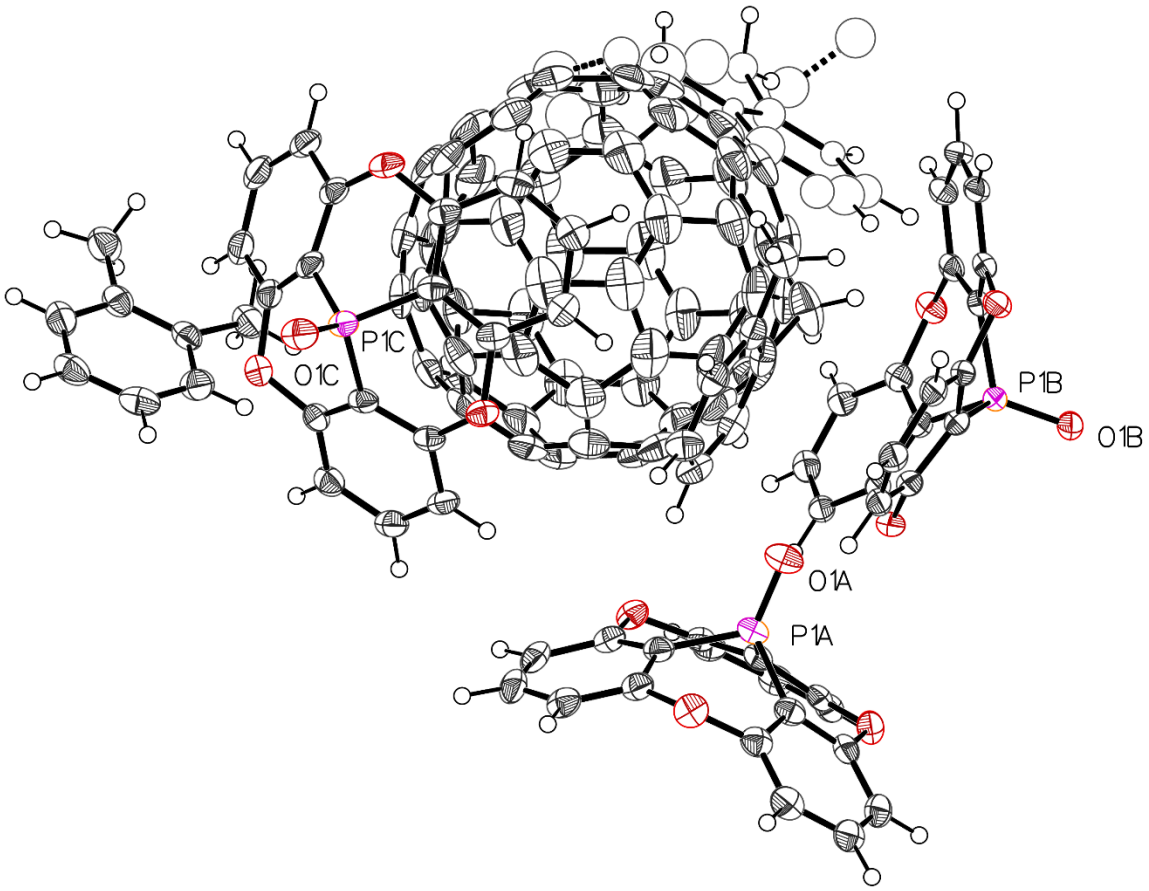

Figure 7.22 : Thermal atomic displacement ellipsoid plot of the structure of 3:1 cocrystals of phosphangulene oxide (**2a**) and C_{60} grown from *o*-xylene. The ellipsoids of non-hydrogen atoms are drawn at the 50% probability level, and hydrogen atoms are represented by a sphere of arbitrary size.

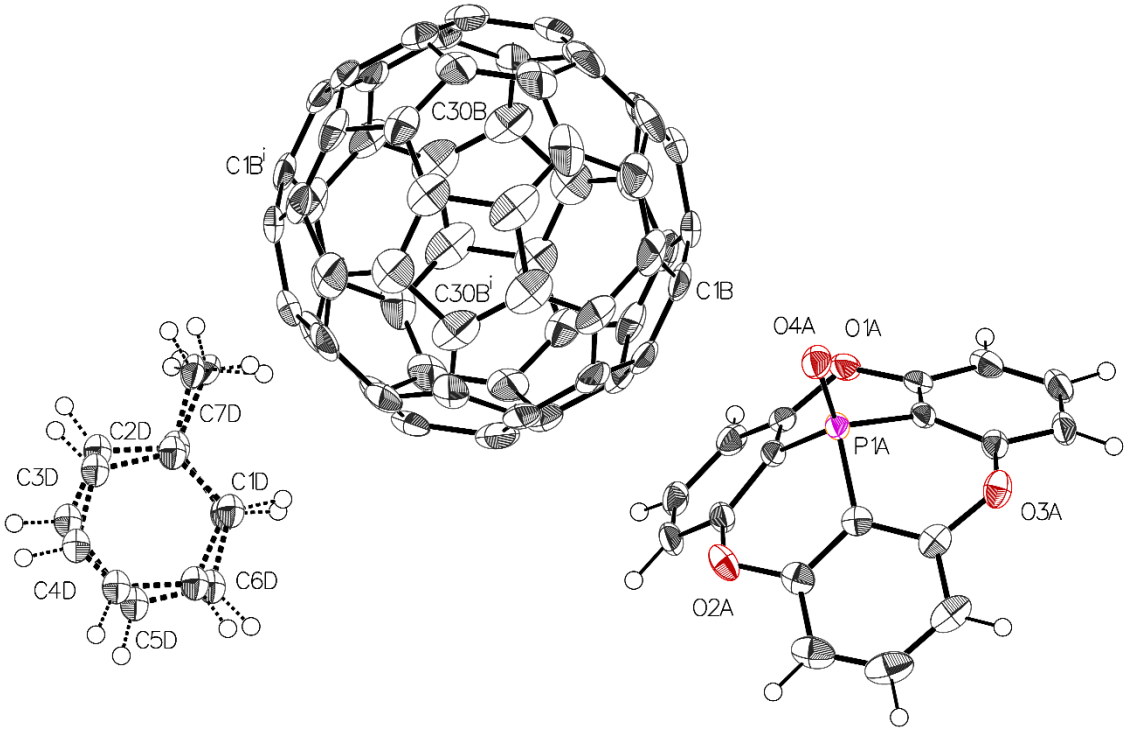

Figure 7.23 : Thermal atomic displacement ellipsoid plot of the structure of 2:1 cocrystals of phosphangulene oxide (**2a**) and C_{60} grown from PhMe. The ellipsoids of non-hydrogen atoms are drawn at the 50% probability level, and hydrogen atoms are represented by a sphere of arbitrary size.

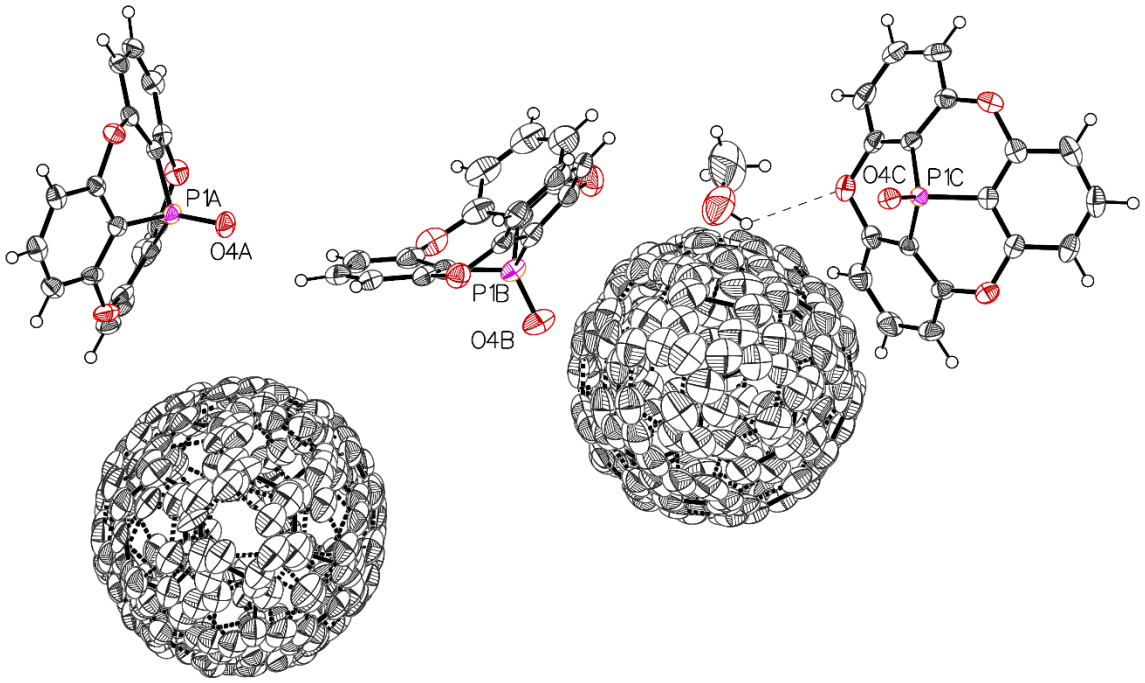

Figure 7.24 : Thermal atomic displacement ellipsoid plot of the structure of 6:4 cocrystals of phosphangulene oxide (**2a**) and C_{60} grown from MeOH. The ellipsoids of non-hydrogen atoms are drawn at the 50% probability level, and hydrogen atoms are represented by a sphere of arbitrary size.

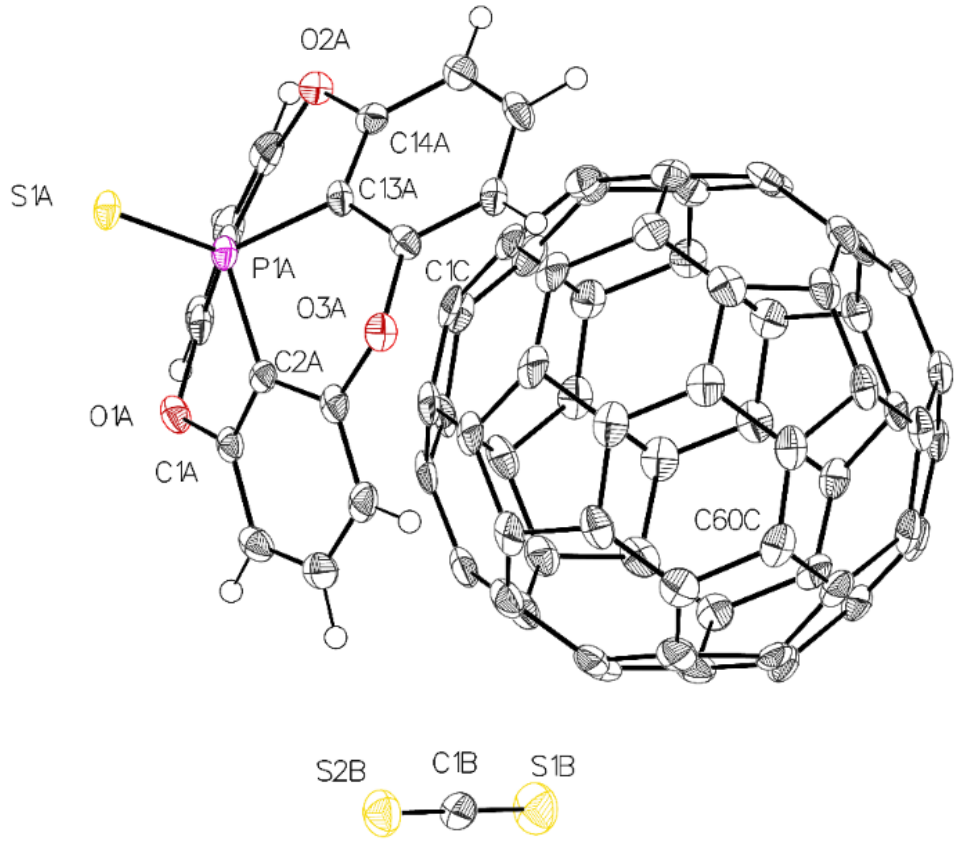

Figure 7.25 : Thermal atomic displacement ellipsoid plot of the structure of 1:1 cocrystals of phosphangulene sulfide (**2b**) and C_{60} grown from CS_2. The ellipsoids of non-hydrogen atoms are drawn at the 50% probability level, and hydrogen atoms are represented by a sphere of arbitrary size.

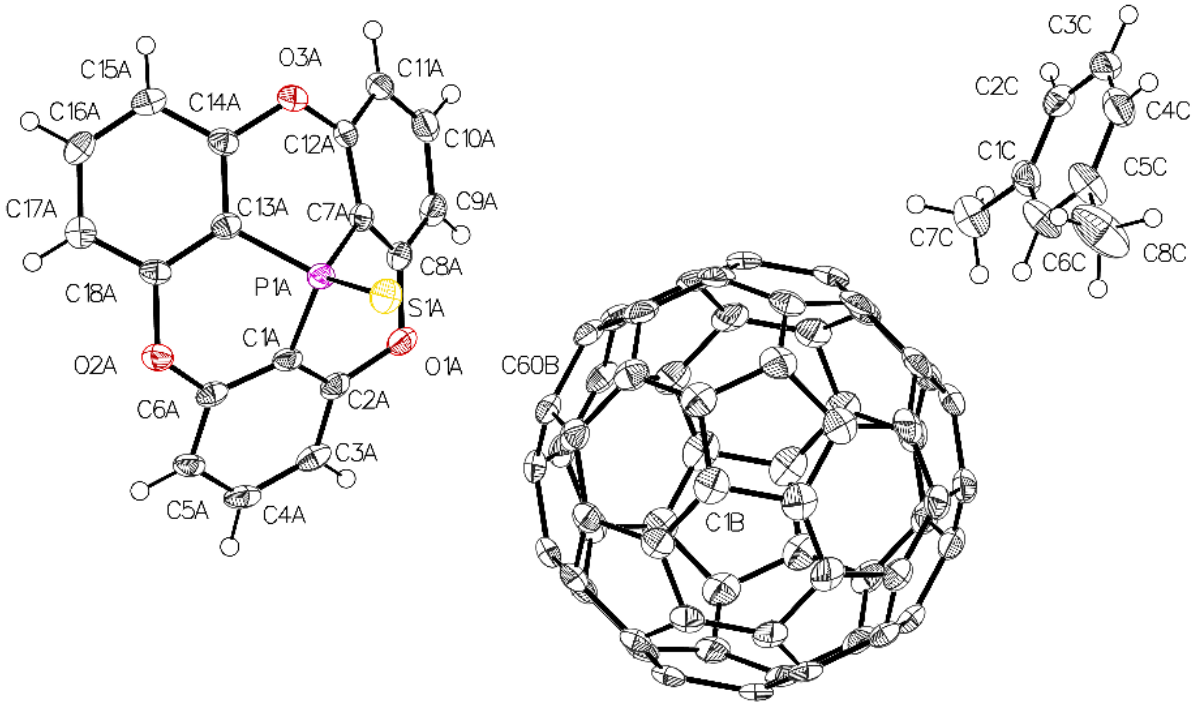

Figure 7.26 : Thermal atomic displacement ellipsoid plot of the structure of 1:1 cocrystals of phosphangulene sulfide (**2b**) and C_{60} grown from *m*-xylene. The ellipsoids of non-hydrogen atoms are drawn at the 50% probability level, and hydrogen atoms are represented by a sphere of arbitrary size.

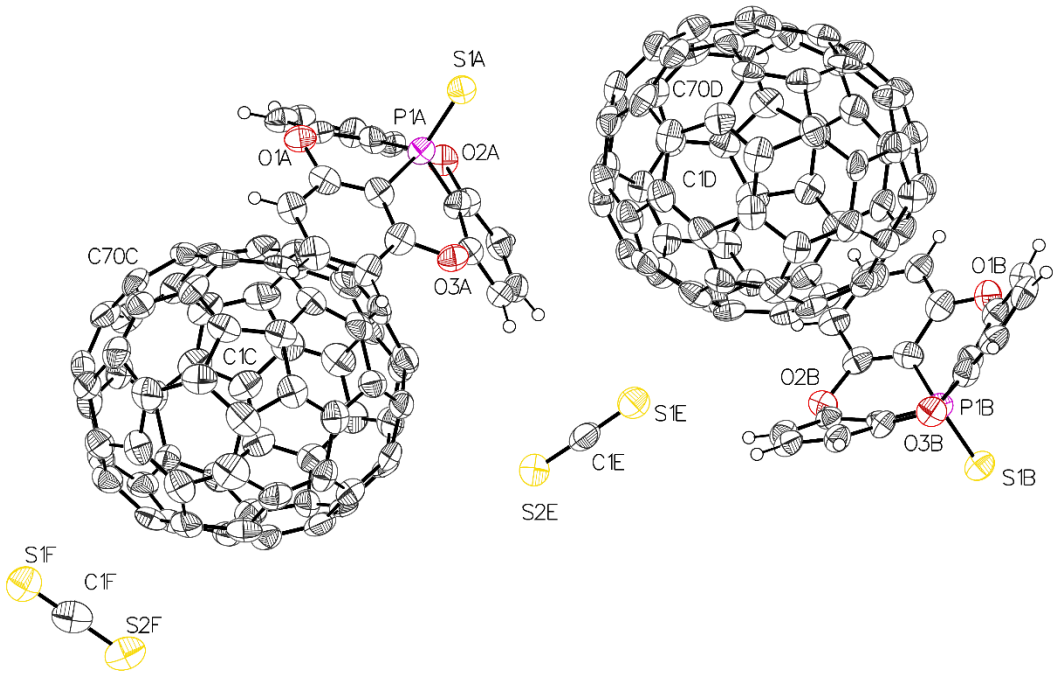

Figure 7.27 : Thermal atomic displacement ellipsoid plot of the structure of 1:1 cocrystals of phosphangulene sulfide (**2b**) and C_{70} grown from CS_2. The ellipsoids of non-hydrogen atoms are drawn at the 50% probability level, and hydrogen atoms are represented by a sphere of arbitrary size.

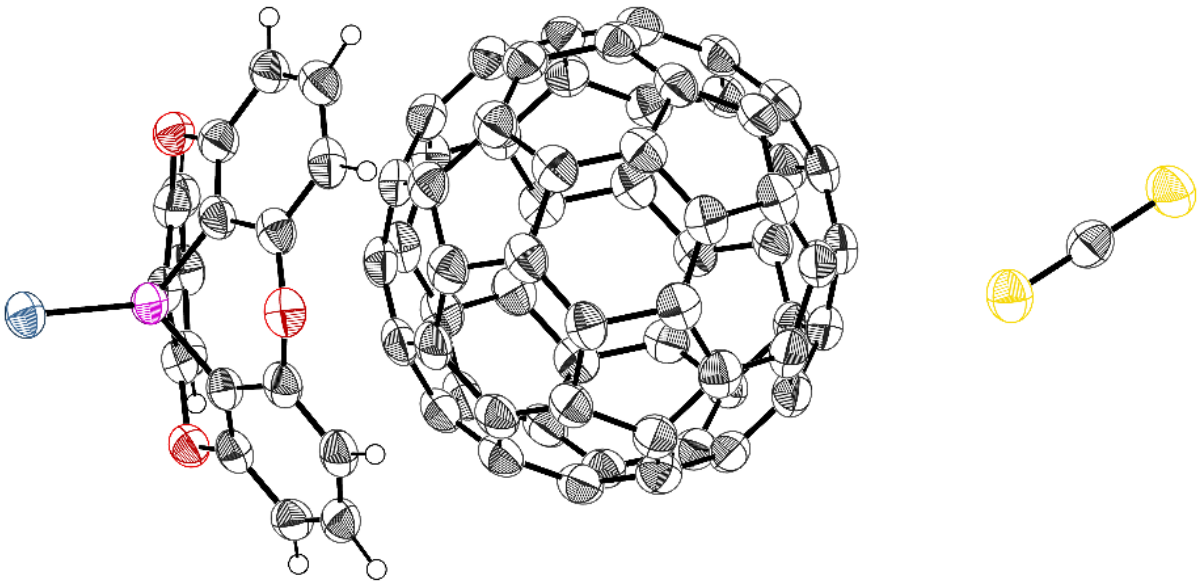

Figure 7.28 : Thermal atomic displacement ellipsoid plot of the structure of 1:1 cocrystals of phosphangulene selenide (**2c**) and C_{60} grown from CS_2. The ellipsoids of non-hydrogen atoms are drawn at the 50% probability level, and hydrogen atoms are represented by a sphere of arbitrary size.

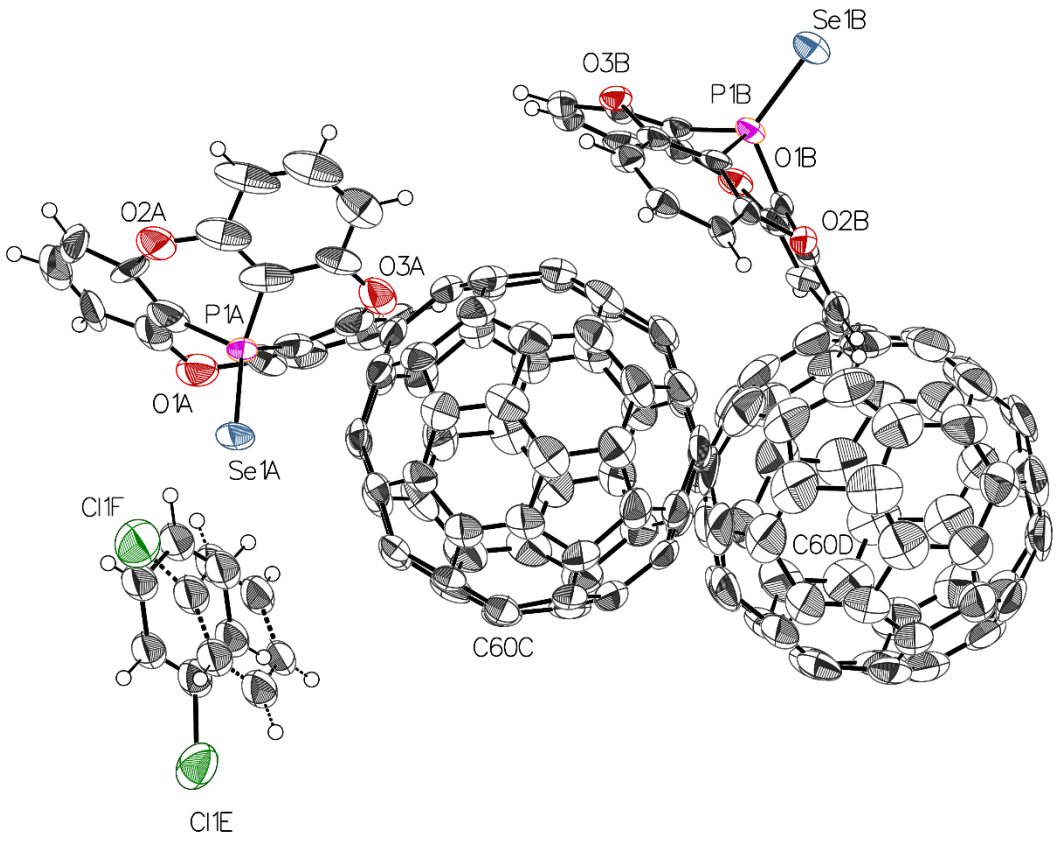

Figure 7.29 : Thermal atomic displacement ellipsoid plot of the structure of 1:1 cocrystals of phosphangulene selenide (**2c**) and C_{60} grown from PhCl. The ellipsoids of non-hydrogen atoms are drawn at the 50% probability level, and hydrogen atoms are represented by a sphere of arbitrary size.

7.2.3 References

1. Bruker (2017). APEX3 and SAINT, Bruker AXS Inc., Madison, Wisconsin, USA.
2. Krause, L.; Herbst-Irmer, R.; Sheldrick, G. M.; Stalke, D. *J. Appl. Cryst.* **2015**, *48*, 3–10.
3. Sheldrick, G. M. *Acta Crystallogr.* **2015**, *A71*, 3–8.
4. Sheldrick, G. M. *Acta Crystallogr.* **2015**, *C71*, 3–8.

7.3 Informations supplémentaires de l'article 3

Supporting Information

Building Large Structures with Curved Aromatic Surfaces by Complexing Metals with Phosphangulene

Alice Heskia, Thierry Maris, Pedro M. Aguiar, and James D. Wuest *

Département de Chimie, Université de Montréal, Montréal, Québec H3C 3J7 Canada

*Author to whom correspondence may be addressed.

E-mail: *james.d.wuest@umontreal.ca.*

7.3.1 Powder X-Ray Diffraction

Bulk solids obtained by mixing phosphangulene with salts of Ag(I) and Cu(I) were routinely analyzed by powder X-ray diffraction. The solids were typically crystalline, although they did not always consist of a single phase or have the same structure as the one determined by analysis of single crystals. Only in the case of $[Ag(Phang)_4]^+ BF_4^-$ did the crude product prove to be uniformly crystalline and to have a structure identical to the one determined by single-crystal X-ray diffraction (Figure 7.30).

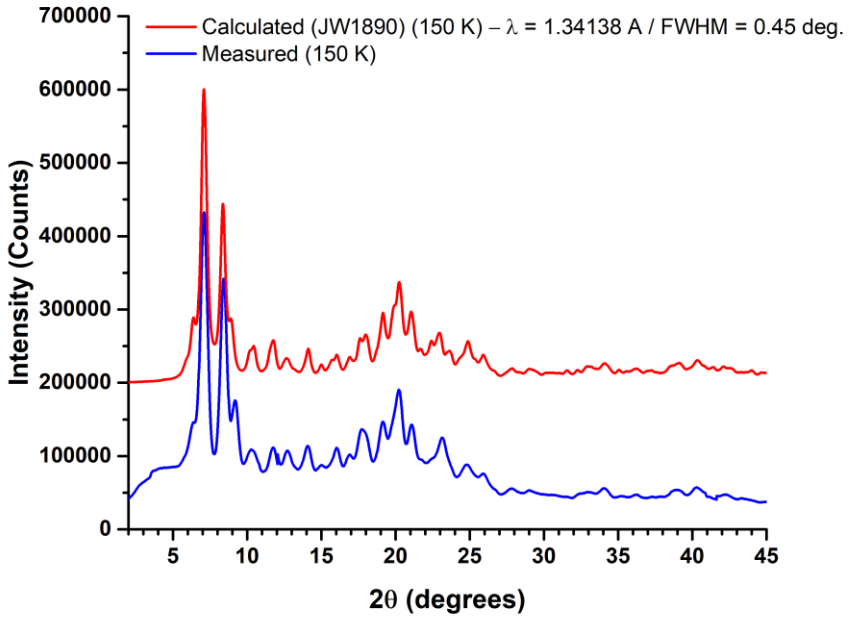

Figure 7.30 : Simulated and observed powder X-ray diffraction patterns for bulk crystalline $[Ag(Phang)_4]^+ BF_4^-$.

7.3.2 Low-Temperature ^{31}P NMR Spectroscopy

Low-temperature (183.2 K) $^{31}P\{^{1}H\}$ NMR spectra were recorded on a Bruker Avance 500 NMR instrument at 202.43 MHz, using a 5 mm Bruker BBO probe. Quantitative single-pulse experiments were carried out, with a 30-degree tip-angle excitation pulse (ν_{rf} = 16 kHz), Waltz-65 ^{1}H inverse-gated decoupling (ν_{rf} = 2.65 kHz), and a recycle delay of 10 s. In total, 32 co-added transients were collected. Chemical shifts are reported relative to 85% aqueous H_3PO_4 and were calibrated by setting the ^{1}H signal from CH_2Cl_2 to δ 5.31 ppm and using the established resonance frequency ratio for ^{31}P (Ξ = 40.480742).[1] When resolution permitted, coupling constants for both isotopomers ($^{107}Ag/^{109}Ag$) were extracted directly from the spectra. When couplings were unresolved, the center of the peaks was used to determine an average value of *J*.

Samples for analysis were prepared from stock solutions of $AgBF_4$ and phosphangulene. $AgBF_4$ (22.0 mg, 113 μmol) was dissolved in a mixture of CH_2Cl_2:diethyl ether (2.5:1.0 by volume, 13.0 mL) to create a solution with a concentration of 8.7 μM. A mixture of CH_2Cl_2 and diethyl ether was used to increase solubility. Phosphangulene (60.2 mg, 198 μmol) was dissolved in CH_2Cl_2 (5.0 mL) to produce a solution with a concentration of 40 μM). In four vials were placed equal amounts of the $AgBF_4$ stock solution (2.3 mL, 20 μmol, 1.0 equiv), and adjusted amounts of the phosphangulene stock solution were then added to each vial (0.50 mL, 20 μmol, 0.99 equiv; 1.0 mL, 40 μmol, 2.0 equiv; 1.5 mL, 59 μmol, 3.0 equiv; 2.0 mL, 79 μmol, 4.0 equiv). The contents of the vials were stirred, and 1 mL of each solution was withdrawn and placed in an NMR tube.

A control experiment was carried out as described above, using triphenylphosphine in place of phosphangulene, to confirm that the results previously reported by of Alyea et al. could be reproduced under our conditions,[2] even though we used CH_2Cl_2/diethyl ether in place of pure CH_2Cl_2 in our experiments, and we substituted $AgBF_4$ for $AgPF_6$. As shown in Figure S2, the results of Alyea et al. could be reproduced, showing that the addition of diethyl ether does not have a significant effect on the results, nor does replacement of $AgPF_6$ by $AgBF_4$.

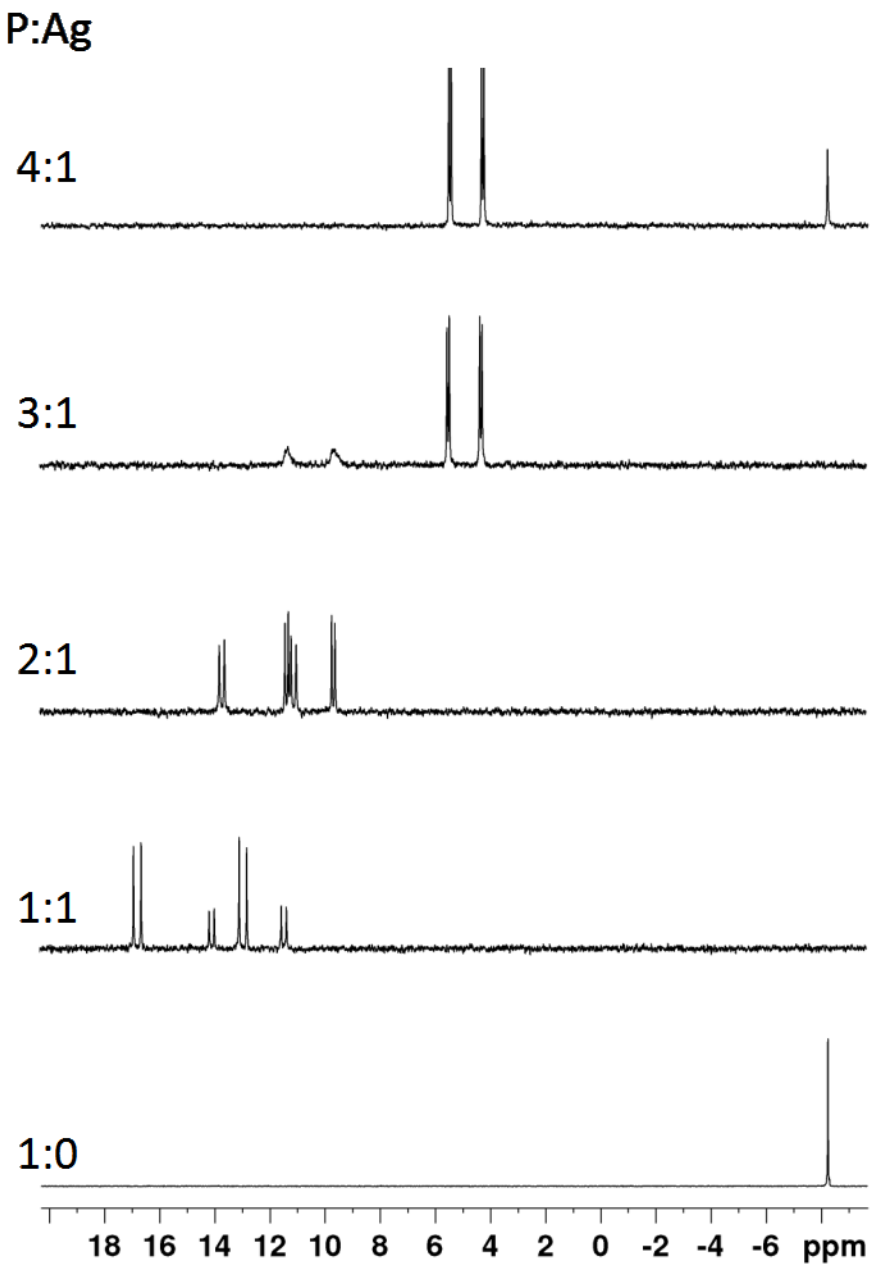

Figure 7.31 : Low-temperature (183 K) ^{31}P NMR spectra of solutions prepared in CH_2Cl_2/diethyl ether by mixing $AgBF_4$ and PPh_3 in four different ratios (1:1, 1:2, 1:3, and 1:4), along with a spectrum of the free ligand in the absence of $AgBF_4$ (1:0).

7.3.3 Solid-State ^{31}P NMR Spectroscopy

$^{31}P\{^{1}H\}$ MAS NMR experiments were performed on a Bruker Avance 600 NMR spectrometer (ν_L = 242.91 MHz), using a Bruker 2.5 mm MAS probe. Quantitative single-pulse experiments were carried out using a sample spinning rate of 24 kHz, with a 30-degree tip-angle excitation pulse (ν_{rf} = 55 kHz), spinal-64 ^{1}H decoupling (ν_{rf} = 83 kHz), and a recycle delay of 60 s. A total of 966 co-added transients were collected. Chemical shifts are reported relative to 85% aqueous H_3PO_4 and were calibrated using ammonium dihydrogen phosphate as a secondary external reference (δ = 0.81 ppm).[3]

MAS spectra were simulated using WSolids (Ver. 1.21.3). Both isotopomers (^{107}Ag/^{109}Ag) were included in the simulation. ^{31}P isotropic shifts were assumed to be identical for both isotopomers, and the ratio of the *J*-couplings was considered to be fixed by the ratio of the magnetogyric ratios of the silver isotopes. Voigt line broadening (50:50, LB:GB) of 320 Hz was added to the simulation.

In our analysis of low-temperature ^{31}P NMR spectra of solutions prepared by mixing phosphangulene and $AgBF_4$ in CH_2Cl_2/diethyl ether (see Figure 5 of the paper), we were confident that the sharp pair of doublets was correctly assigned to $[Ag(Phang)_4]^+$. However, the size of ^{1}J (^{107}Ag, ^{31}P) reflects the number of coordinated phosphines, and we noted that the observed value (^{1}J = 264 Hz) lies between those reported for tetracoordinated $[Ag(PPh_3)_4]^+$ (^{1}J = 224 Hz) and tricoordinated $[Ag(PPh_3)_3]^+$ (^{1}J = 319 Hz).[2] We confirmed our assignment by analyzing the solid-state ^{31}P NMR spectrum of crystalline **[**$Ag(Phang)_4]^+$ BF_4^-, in which Ag(I) is known to be tetracoordinated. In the observed structure, the four Phang ligands are symmetry-inequivalent, so we expected to see four signals A–D in the solid-state spectrum. In

fact, there are three resolved signals in a 1:1:2 ratio (Figure 7.32), and all show coupling with ^{107}Ag and ^{109}Ag. A small amount of free phosphangulene (singlet at δ ^{31}P = -135) can be attributed to decomposition of the complex.

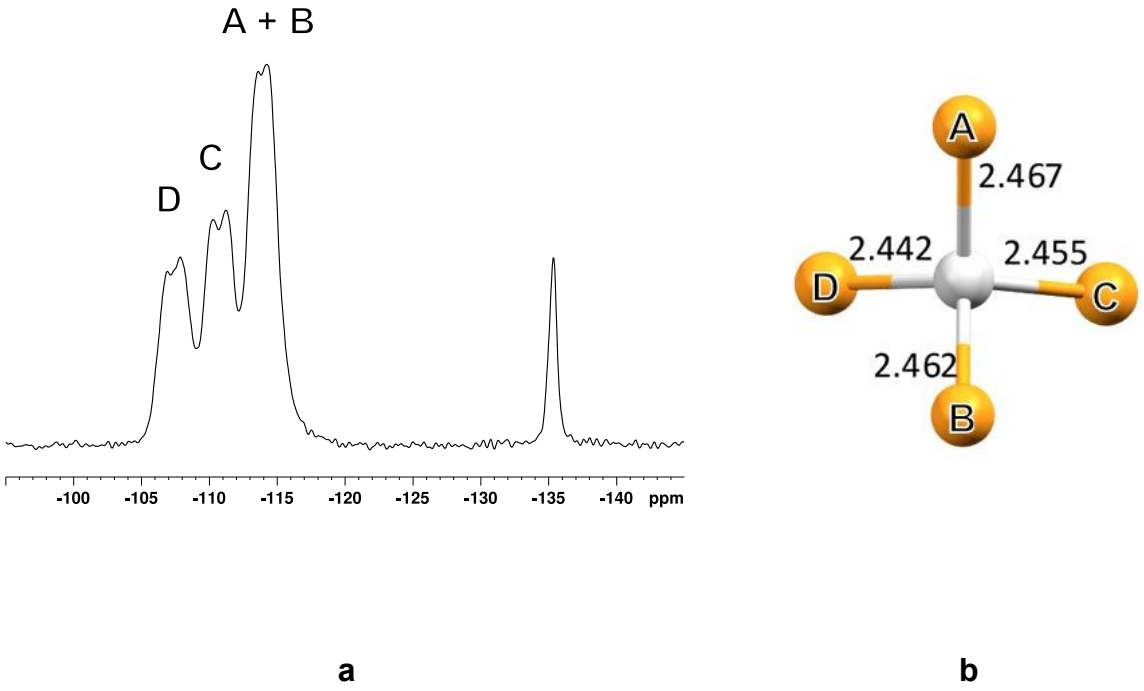

Figure 7.32 : (a) Solid-state ^{31}P NMR spectrum of crystalline $[Ag(Phang)_4]^+$ BF_4^-, showing signals A–D corresponding to four symmetry-inequivalent Phang ligands. A small amount of free phosphangulene (δ ^{31}P = -135) arises from decomposition of the complex. (b) Partial structure of $[Ag(Phang)_4]^+$ BF_4^-, showing the central atom of silver (light gray) and four bonded atoms of phosphorus (yellow-orange), with bond lengths given in Å and assignments based jointly on (1) the typical correlation of shielding and bond length and (2) the smaller value of ^1J ($^{107/109}$Ag, ^{31}P) expected for the most shielded signal.

If the shortest Ag-P distances correspond to the most deshielded signals (largest change in shift relative to the free ligand), then the specific assignments shown in Figure S3 can be made. The magnitude of ^{1}J ($^{107/109}$Ag, ^{31}P) is known to increase as the Ag-P distance decreases.[4,5] The measured value of ^{1}J ($^{107/109}$Ag, ^{31}P) for the most shielded signal (250 ± 10 Hz) is consistent with the hypothesis that it arises from the two atoms of phosphorus that form the longest Ag-P bonds. The average value of ^{1}J ($^{107/109}$Ag,^{31}P) in the solid state is 265 ± 10 Hz, which agrees very well with the value measured in solution (^{1}J = 264 Hz), thereby supporting our interpretation of the low-temperature spectra in solution (see Figure 5 in the paper). The increased magnitude of ^{1}J ($^{107/109}$Ag,^{31}P) for **[**Ag(Phang)$_4$]$^+$ relative to the value reported for [Ag(PPh$_3$)$_4$]$^+$ can be attributed to the smaller cone angle of Phang. Smaller cone angles are also known to be correlated with larger differences in δ ^{31}P resulting from the complexation of phosphines.[6] Inspection of the low-temperature ^{31}P NMR spectrum in Figure 5 in the paper (1:4 ratio) shows that the chemical shift of Phang changes by 24.6 ppm upon complexation, whereas the formation of [Ag(PPh$_3$)$_4$]$^+$ leads to a difference of only 13.1 ppm.

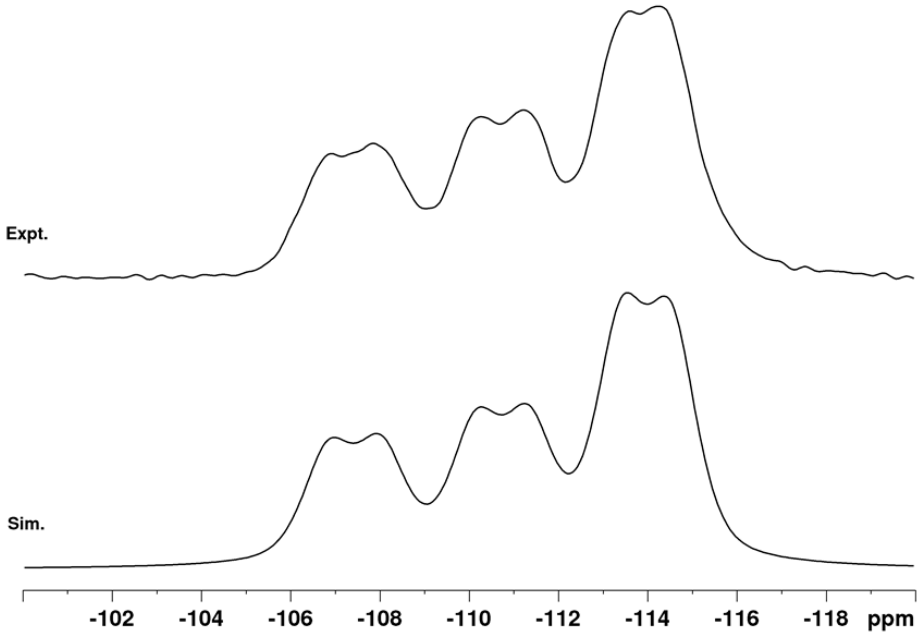

Figure 7.33 : Experimental ^{31}P MAS NMR spectrum of crystalline $[Ag(Phang)_4]^+ BF_4^-$, along with a simulation used to extract isotropic shifts and values of ^1J ($^{107/109}$Ag, ^{31}P).

Table 7.4:. NMR Parameters Extracted by Simulating the ^{31}P MAS NMR Spectrum of $[Ag(Phang)_4]^+ BF_4^-$

Site	δ_{iso}	^1J (^{107}Ag, ^{31}P)	Pop.
1	-107.4 ± 0.2	270± 10	1.0 ± 0.1
2	-110.7 ± 0.2	270 ± 10	1.2 ± 0.1
3	-114.0 ± 0.2	255 ± 10	2.0 ± 0.1

Note: ^1J (^{109}Ag, ^{31}P) was fixed in the simulation to be 1.1496 × ^1J (^{107}Ag, ^{31}P) and δ_{iso} of the two isotopomers was assumed to be identical.

7.3.4 Additional Crystallographic Information

Data collection was carried out on a Bruker Venture Metaljet diffractometer using GaKα radiation (λ = 1.34139 Å). During all experiments, the samples were cooled using an Oxford Cryostream liquid-nitrogen device at 150 K. The cell lattice parameters were determined using reflections taken from three sets of 104 frames measured and harvested within the APEX3 suite of programs.[7] Integration of frames was performed using *SAINT*,[7] and a semiempirical absorption correction was applied with *SADABS* in the case of normal samples or with *TWINABS* for the twinned samples.[8] The structures were solved using a dual space and intrinsic phasing approach with *SHELXT*,[9] and the refinement was carried out using *SHELXL*-2018/3.[10]

Several structures have at least one part disordered. The disordered parts are the following: (1) the BF_4^- anion in $[Ag(Phang)_4]^+$ BF_4^- and $[Cu(Phang)_4]^+$ BF_4^-; (2) the PF_6^- anion in $[Cu(Phang)_4]^+$ PF_6^- • 3 MeOH; (3) one Phang ligand in $Cu_2Cl_2(Phang)_3$; (4) the triflate anion in $[Ag(O_3SCF_3)(toluene)(Phang)]_2$; (5) one Phang ligand and one toluene ligand in $[Ag(ClO_4)(toluene)(Phang)]_2$; and (6) the C_{60} molecule in $[Ag(O_3SCF_3)(toluene)(Phang)_2]_2$ • 2 C_{60} • 3 toluene. In addition, the sample of the latter compound was refined as a two-component twin. Its unit cell was checked using *CELL_NOW*, and the integration was performed using the two components to produce an HKLF5-type reflection file. This file was used for the refinement, which involved treating the disordered C_{60} molecule as a rigid body with two molecules sharing the disordered site.

7.3.5 Descriptions of Additional Structures

$[Cu(Phang)_4]^+ PF_6^- \bullet 3$ MeOH. Mixing $[Cu(MeCN)_4]^+ PF_6^-$ and phosphangulene in a 1:4 ratio in CH_2Cl_2/MeOH yielded a solid that was then crystallized from hot MeOH. The resulting crystals were found to have the composition $[Cu(Phang)_4]^+ PF_6^- \bullet 3$ MeOH. Other crystallographic data are provided elsewhere (see **Table 4.1** of the paper). The coordination of Cu(I) in $[Cu(Phang)_4]^+$ is approximately tetrahedral, and the P-Cu-P bond angles lie in the narrow range 108.2–110.1°, with an average of 109.5°. The average Cu-P bond length in $[Cu(Phang)_4]^+$ is 2.284 Å, which is much shorter than the average distance found in the case of $[Cu(PPh_3)_4]^+ ClO_4^-$ (2.58 Å).[11] The overall structure closely resembles the one formed by $[Cu(Phang)_4]^+ BF_4^-$, except that each cation in the PF_6^- salt is linked to four neighbors by normal clamshell pairing of Phang ligands, whereas one of the four neighbors in the BF_4^- salt is joined by a distorted pair (see Figure 4.1c in the paper). As a result, the arrangement of linked cations in the PF_6^- salt is somewhat less compact than in the BF_4^- salt, thereby creating space for the inclusion of MeOH.

$Cu_2I_2(Phang)_4 \bullet 1$ Toluene. Crystals of $Cu_2I_2(Phang)_4 \bullet 1$ toluene were obtained by slow evaporation of a solution prepared by mixing CuI and phosphangulene in EtOH/toluene. Crystallographic data are presented elsewhere (see Table 4.2 of the paper), and views of the structure appear below (Figure 7.34). The geometry of the coordination of Cu(I) resembles the one observed in $Cu_2Cl_2(Phang)_4$. Specifically, the average Cu-P bond length in the iodide complex is 2.270 Å (versus 2.264 Å in the chloride), and the P-Cu-P bond angle is 110.8° (versus 110.4° in the chloride). However, the transannular Cu···Cu distance in the iodide (2.875 Å) is much shorter than in the chloride (3.138 Å), so metal-metal bonding is more

important. Similar geometric parameters have been observed in the structure of $Cu_2I_2(PPh_3)_3$, where the average Cu-P bond length for the tetracoordinated atom of Cu is 2.263 Å, and the Cu···Cu distance is 3.041 Å.[12] However, the P-Cu-P bond angle in $[Cu_2I_2(PPh_3)_3]$ is opened to 125.2°, presumably because PPh_3 has a larger cone angle. As in the case of $Cu_2Cl_2(Phang)_4$, each molecule of $Cu_2I_2(Phang)_4$ is linked tetragonally to four coplanar neighbors by offset clamshell pairing of Phang ligands (Figure 7.34a). This arrangement leads again to the formation of sheets constructed from cyclic quartets, which surround a cavity that accommodates disordered molecules of toluene (Figure 7.34b).

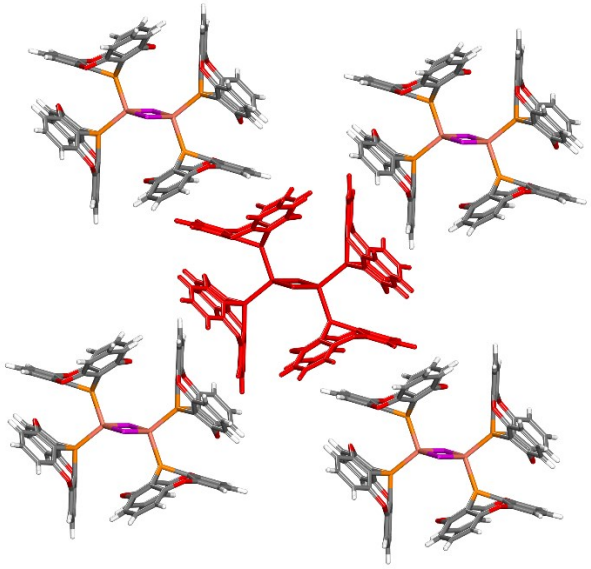

a

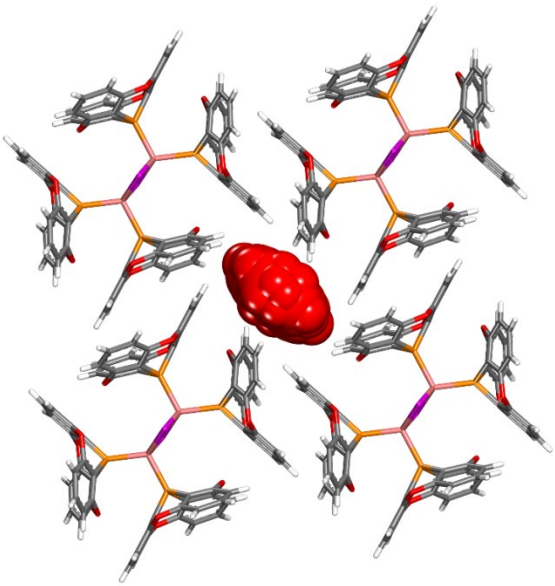

b

Figure 7.34 : Representations of the structure of crystals of $Cu_2I_2(Phang)_4$ grown from EtOH/toluene. (a) Image showing a central complex (in red) linked to four coplanar neighbors by offset clamshell pairing of Phang ligands. (b) View of a cyclic quartet surrounding a disordered molecule of toluene (in red). Unless indicated otherwise, atoms of carbon appear in gray, hydrogen in white, oxygen in red, phosphorus in yellow-orange, copper in orange, and iodine in purple.

$Cu_2Cl_2(Phang)_3$. The reaction of phosphangulene with CuCl produces the unprecedented tetracoordinated complex $Cu_2Cl_2(Phang)_4$, but the same conditions also yield crystals of the tricoordinated complex $Cu_2Cl_2(Phang)_3$, which is analogous to the well-known compound $Cu_2Cl_2(PPh_3)_3$. **Table 4.2** (see paper) summarizes crystallographic data, and Figure S6 provides views of the structure. As in $Cu_2Cl_2(PPh_3)_3$, the atoms of Cu(I) in $Cu_2Cl_2(Phang)_3$ are inequivalent and have approximately trigonal and tetrahedral coordination (Figure 7.36a). Bond lengths in the two complexes are very similar; in particular, the average Cu-P length at the tetrahedral center is 2.235 Å for the Phang complex and 2.240 Å for the monoclinic form of the PPh_3 complex,[13] and the corresponding lengths at the trigonal center are 2.174 Å and 2.183 Å. When two bulky PPh_3 ligands are bound to Cu(I), the P-Cu-P angle in $Cu_2Cl_2(PPh_3)_3$ must increase (131.8°), whereas the corresponding angle in $Cu_2Cl_2(Phang)_3$ is only 114.5°. In both $Cu_2Cl_2(Phang)_3$ and $Cu_2Cl_2(PPh_3)_3$, the Cu···Cu distances are long (3.022 Å and 2.909 Å, respectively), so there are no notable metal-metal interactions. As in the cases of $Cu_2Cl_2(Phang)_4$ and $Cu_2I_2(Phang)_4$, molecules of $Cu_2Cl_2(Phang)_3$ pack to form sheets held together in part by interactions of Phang ligands (Figure S6b). However, normal offset clamshell pairs are not observed, possibly because the geometry of $Cu_2Cl_2(Phang)_3$ creates attractive alternatives with interdigitated Phang ligands.

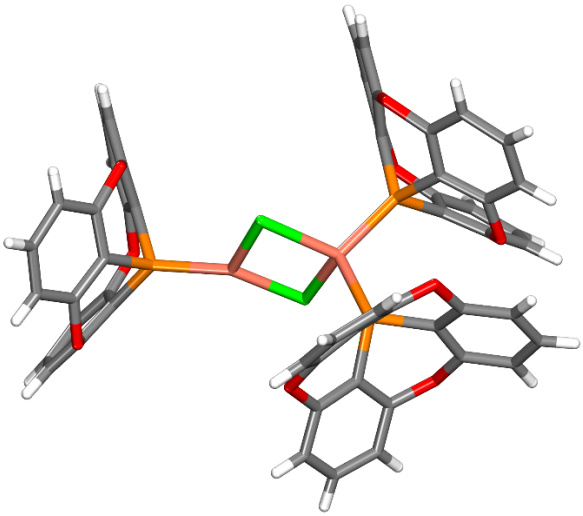

a

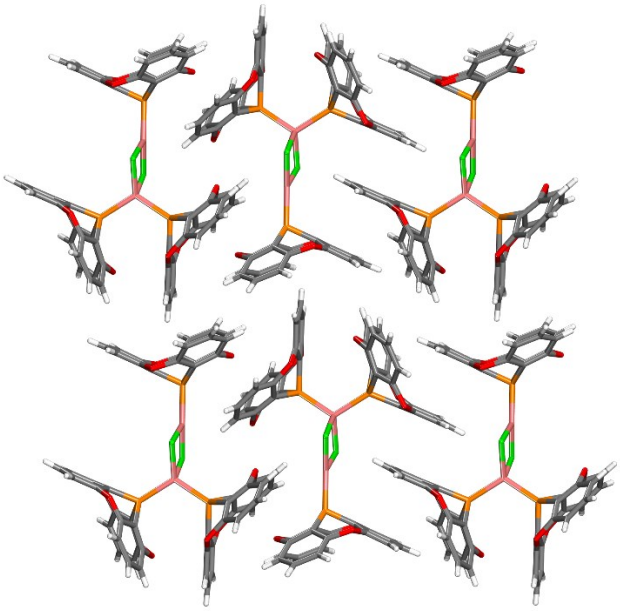

b

Figure 7.35 : Representations of the structure of crystals of $Cu_2Cl_2(Phang)_3$ grown from EtOH. (a) Image showing a single molecule of the complex. (b) View showing how molecules of $Cu_2Cl_2(Phang)_3$ form sheets held together by extensive interdigitation of Phang ligands. Atoms of carbon appear in gray, hydrogen in white, oxygen in red, phosphorus in yellow-orange, copper in orange, and chlorine in green.

$[Ag(O_3SCF_3)(toluene)(Phang)]_2$. The complex $[Ag(O_3SCF_3)(toluene)(Phang)]_2$ crystallized when AgO_3SCF_3 and phosphangulene were combined in EtOH/toluene, followed by slow evaporation of solvent. Table 4.3 (see paper) summarizes crystallographic data, and Figure S7a provides a view of the structure. The two Ag(I) centers are doubly bridged by triflate to form an eight-membered $Ag_2O_4S_2$ ring. The bridging is nearly symmetric, and the Ag-O bond lengths (2.393 Å and 2.397 Å in one of the two inequivalent complexes in the unit cell) are both shorter than those found in $[Ag(O_3SCF_3)(H_2O)(Phang)]_2$ (2.508 Å and 2.720 Å). The average Ag-P bond length in $[Ag(O_3SCF_3)(toluene)(Phang)]_2$ (2.389 Å) is similar to the one observed in $[Ag(O_3SCF_3)(H_2O)(Phang)]_2$ (2.361 Å). In $[Ag(O_3SCF_3)(toluene)(Phang)]_2$, toluene is bound according to Mulliken's model,[14] with Ag(I) positioned directly above one of the carbon atoms in the aromatic ring. The Ag-C bond lengths are 2.560 Å and 2.600 Å, and the average Ag···centroid distance is 2.948 Å. As in the case of $[Ag(O_3SCF_3)(H_2O)(Phang)]_2$, molecules of $[Ag(O_3SCF_3)(toluene)(Phang)]_2$ are joined to form chains by standard clamshell pairing of Phang ligands.

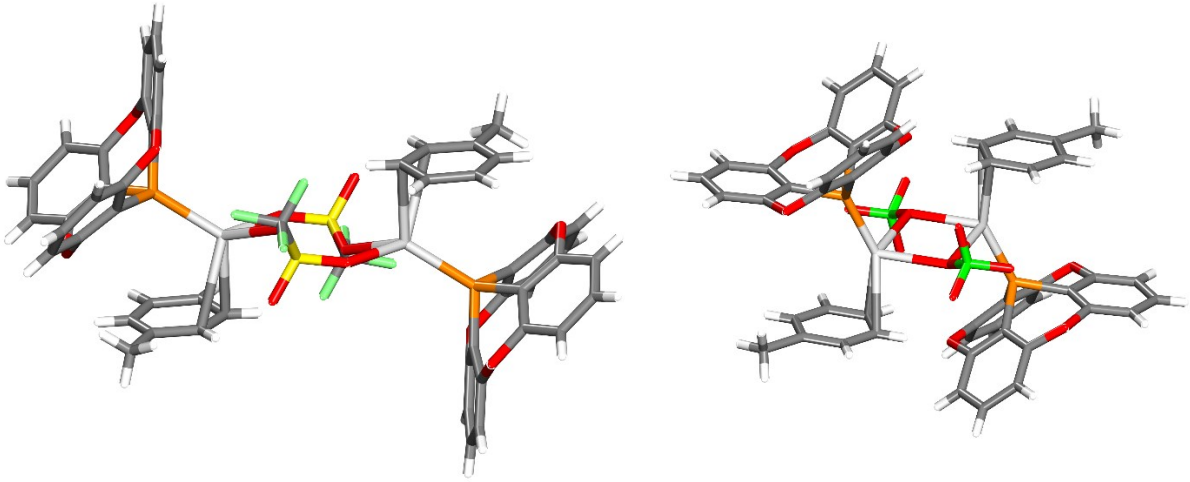

a **b**

Figure 7.36 : (a) Representation of one of the two inequivalent molecules of $[Ag(O_3SCF_3)(toluene)(Phang)]_2$ in the structure of crystals grown from EtOH/toluene. (b) Representation of a molecule of $[Ag(ClO_4)(toluene)(Phang)]_2$ in the structure of crystals grown from MeCN/toluene. Atoms of carbon appear in gray, hydrogen in white, oxygen in red, fluorine in yellow-green, phosphorus in yellow-orange, sulfur in yellow, chlorine in green, and silver in light gray.

$[Ag(ClO_4)(toluene)(Phang)]_2$. Crystals of a perchlorate-bridged analogue of the triflate-bridged complex $[Ag(O_3SCF_3)(toluene)(Phang)]_2$ were formed by slow evaporation of a solution prepared by mixing $AgClO_4$ and phosphangulene in MeCN/toluene. Crystallographic data are compiled in Table 4.3 (see paper), and a view of the structure appears in Figure 7.36b. The two Ag(I) centers are doubly bridged by single atoms of oxygen contributed by perchlorate to form a four-membered Ag_2O_2 ring. Bridging is unsymmetric, and the two Ag-O bond lengths at each metal center are 2.415 Å and 2.569 Å. In addition, the Ag···centroid

distance for the bound molecule of toluene (2.722 Å) is shorter than the one observed in $[Ag(O_3SCF_3)(toluene)(Phang)]_2$ (2.948 Å). As in the cases of $[Ag(O_3SCF_3)(H_2O)(Phang)]_2$ and $[Ag(O_3SCF_3)(toluene)(Phang)]_2$, molecules of $[Ag(ClO_4)(toluene)(Phang)]_2$ are linked into chains by normal clamshell pairing of Phang ligands.

7.3.6 ORTEP Diagrams

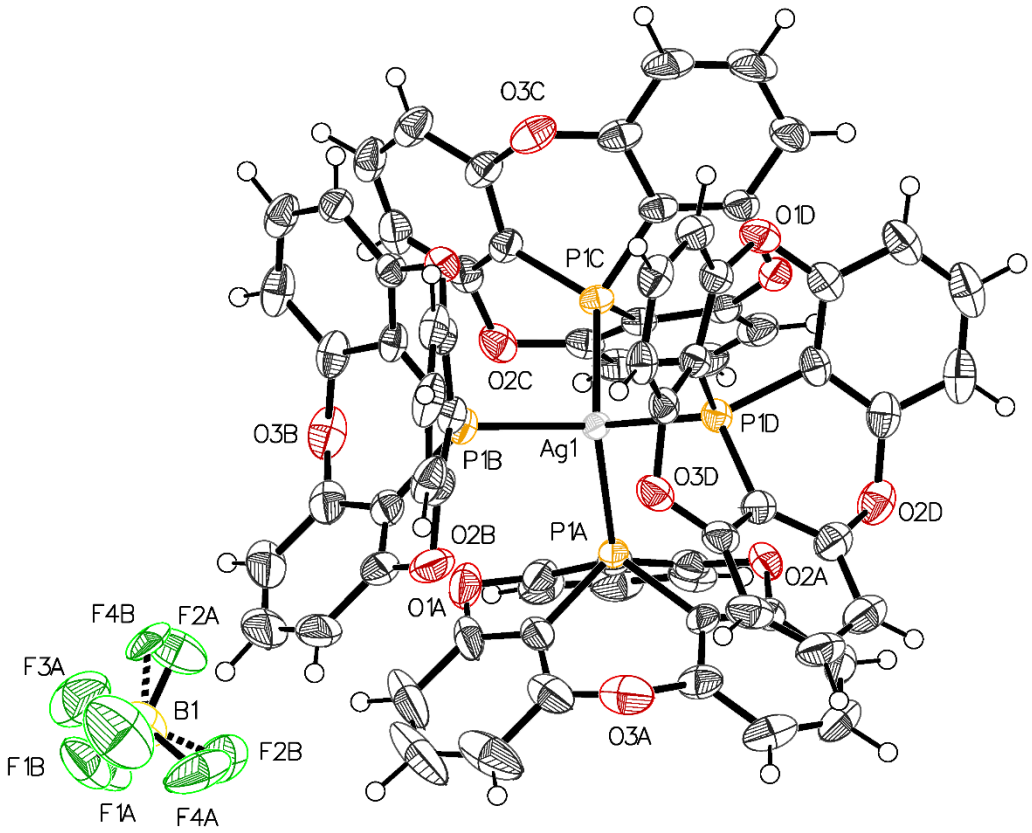

Figure 7.37 : Thermal atomic displacement ellipsoid plot of the structure of crystals of $[Ag(Phang)_4]^+ BF_4^-$ grown from CH_2Cl_2. The ellipsoids of non-hydrogen atoms are drawn at the 50% probability level, and hydrogen atoms are represented by a sphere of arbitrary size.

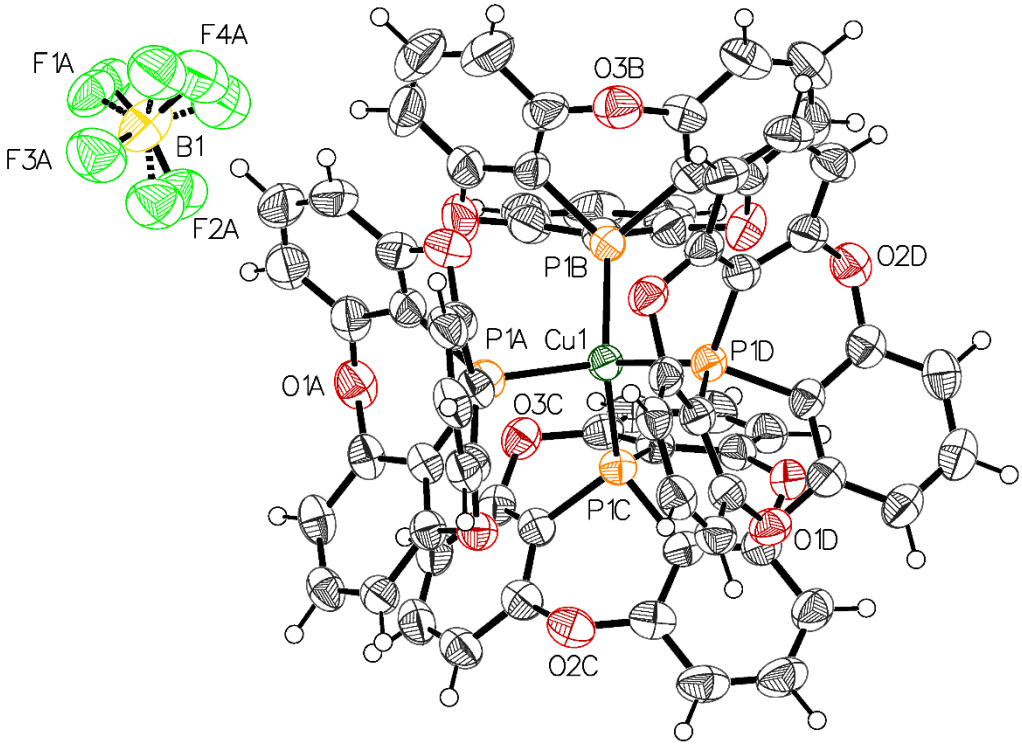

Figure 7.38 : Thermal atomic displacement ellipsoid plot of the structure of crystals of $[Cu(Phang)_4]^+$ BF_4^- grown from EtOH. The ellipsoids of non-hydrogen atoms are drawn at the 50% probability level, and hydrogen atoms are represented by a sphere of arbitrary size.

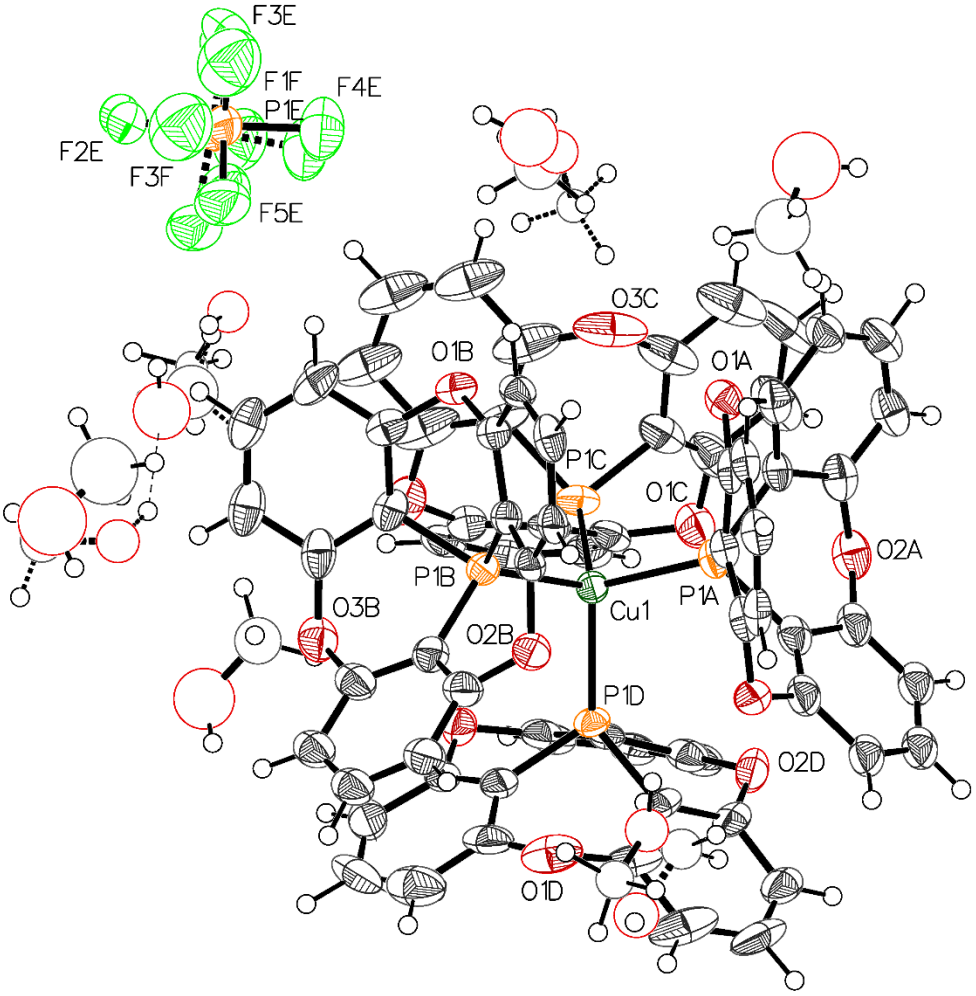

Figure 7.39 : Thermal atomic displacement ellipsoid plot of the structure of crystals of $[Cu(Phang)_4]^+ PF_6^- \bullet 3$ MeOH grown from MeOH. The ellipsoids of non-hydrogen atoms are drawn at the 50% probability level, and hydrogen atoms are represented by a sphere of arbitrary size.

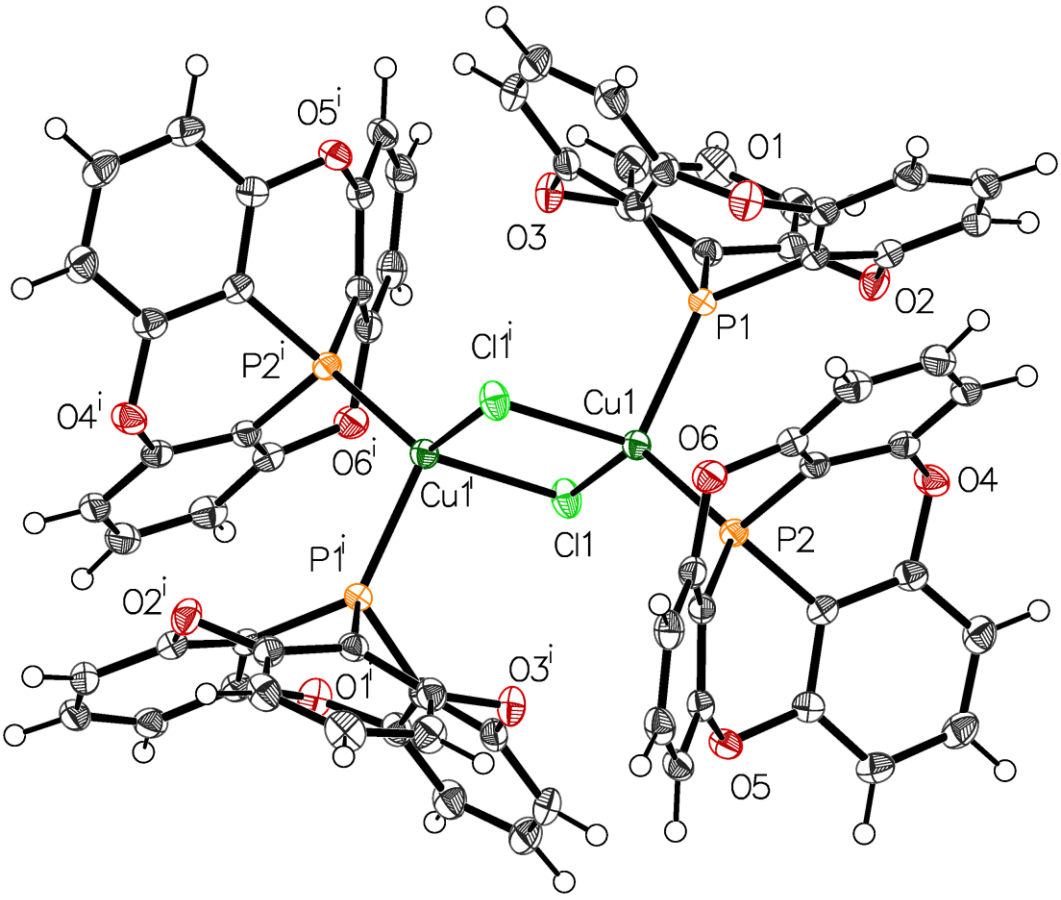

Figure 7.40 : Thermal atomic displacement ellipsoid plot of the structure of crystals of $Cu_2Cl_2(Phang)_4$ grown from EtOH. The ellipsoids of non-hydrogen atoms are drawn at the 50% probability level, and hydrogen atoms are represented by a sphere of arbitrary size. Symmetry code (i): 1-x, 1-y, 1-z

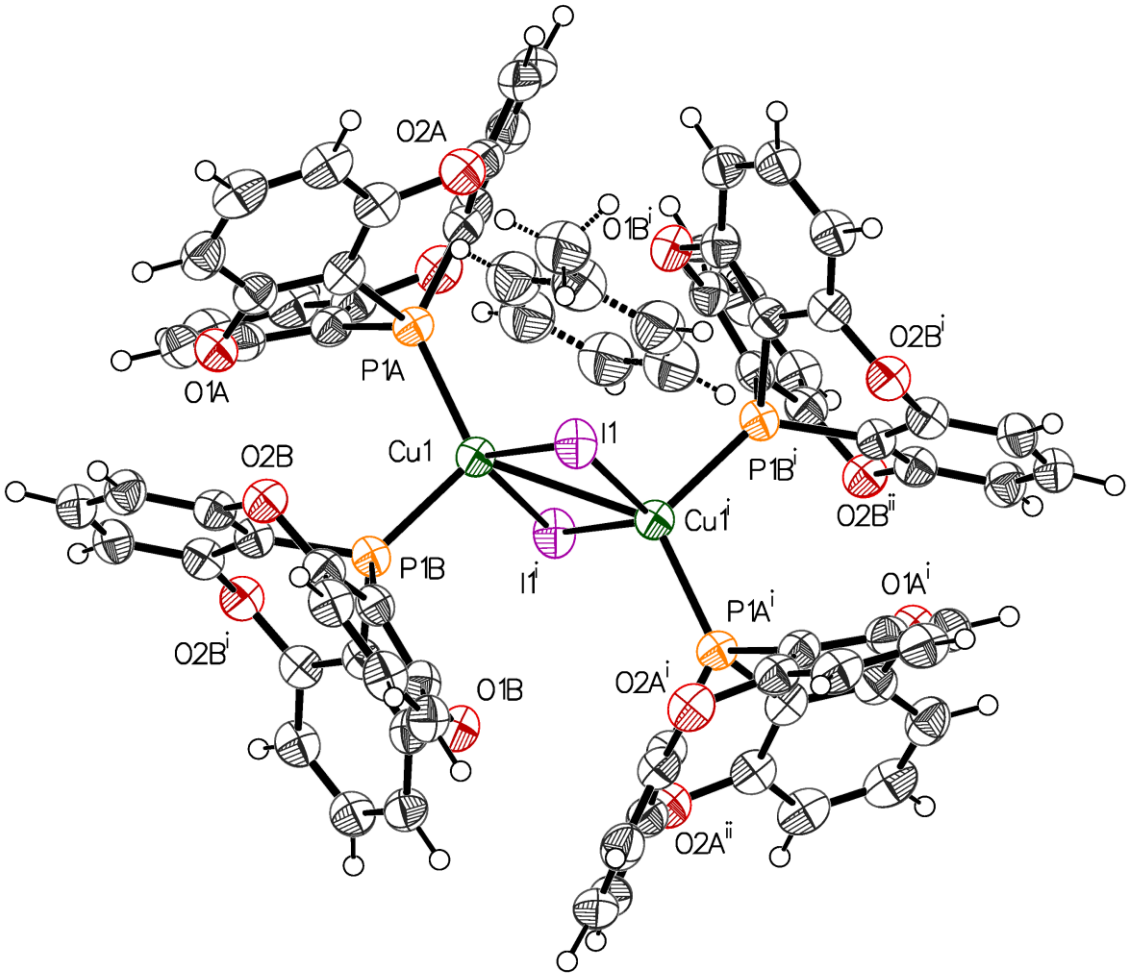

Figure 7.41 : Thermal atomic displacement ellipsoid plot of the structure of crystals of $Cu_2I_2(Phang)_4$ • 1 toluene grown from EtOH/toluene. The ellipsoids of non-hydrogen atoms are drawn at the 50% probability level, and hydrogen atoms are represented by a sphere of arbitrary size. Symmetry code (i): 1-x, 2-y, 1-z; (ii): x, y, 1-z.

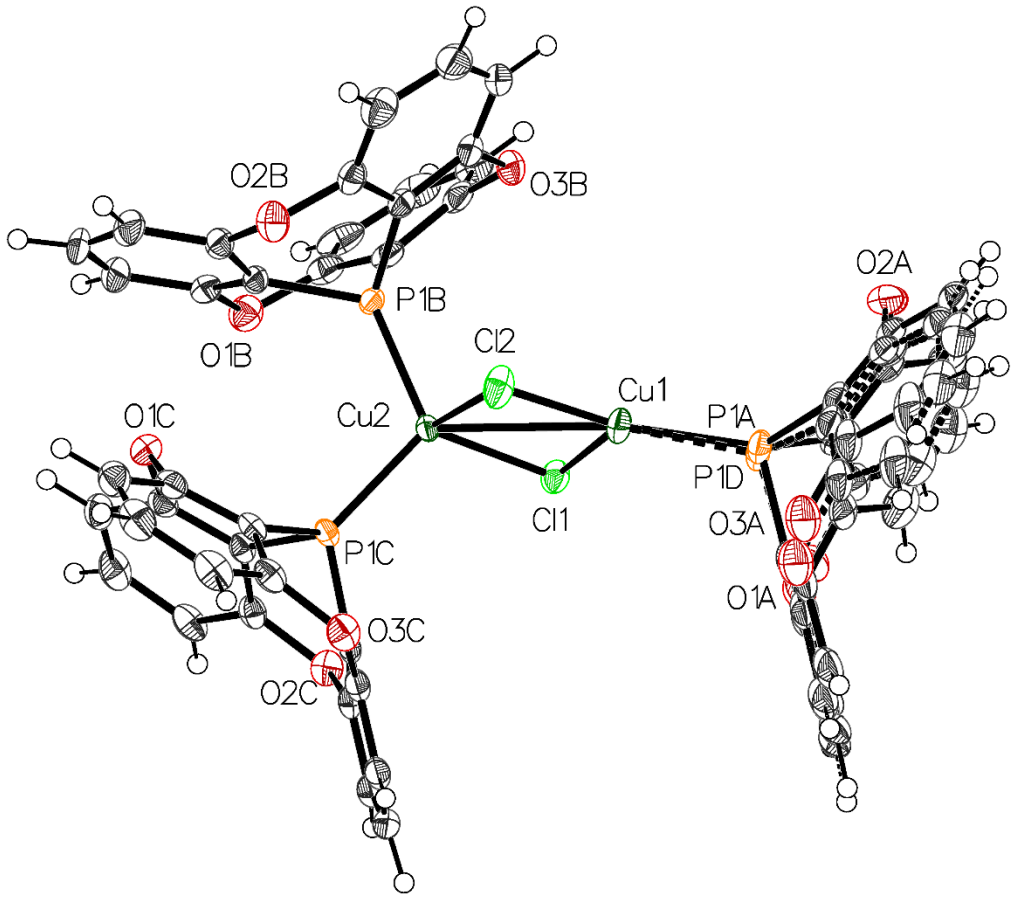

Figure 7.42 : Thermal atomic displacement ellipsoid plot of the structure of crystals of $Cu_2Cl_2(Phang)_3$ grown from EtOH. The ellipsoids of non-hydrogen atoms are drawn at the 50% probability level, and hydrogen atoms are represented by a sphere of arbitrary size.

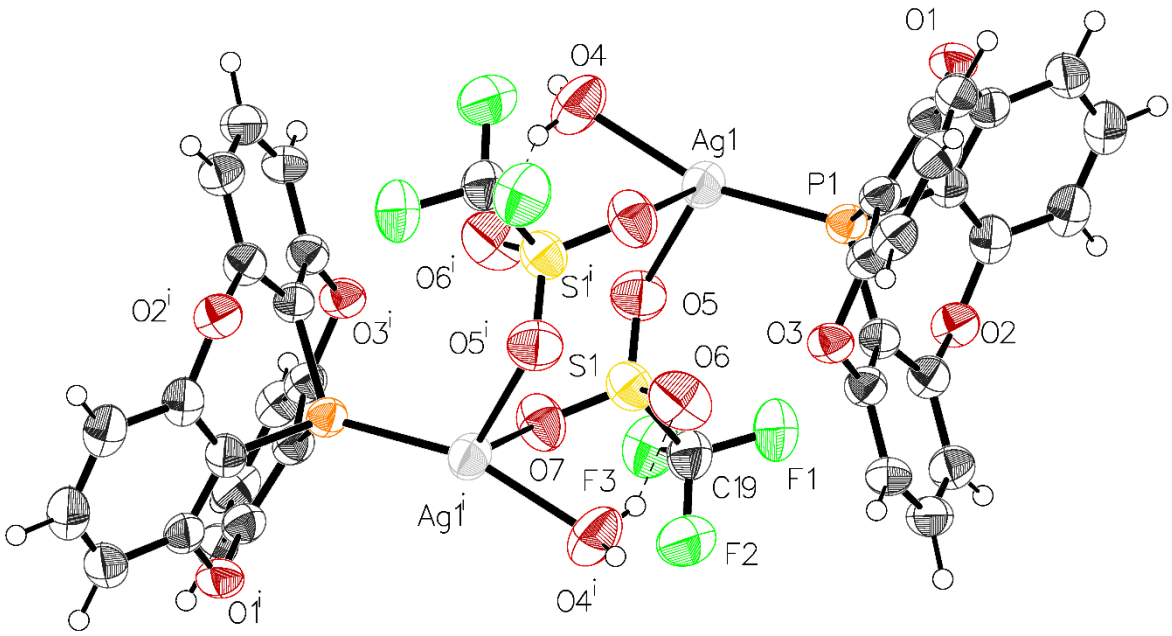

Figure 7.43 : Thermal atomic displacement ellipsoid plot of the structure of crystals of $[Ag(O_3SCF_3)(H_2O)(Phang)]_2$ grown from EtOH/toluene. The ellipsoids of non-hydrogen atoms are drawn at the 50% probability level, and hydrogen atoms are represented by a sphere of arbitrary size. Symmetry code (i): 1-x, 1-y, 1-z.

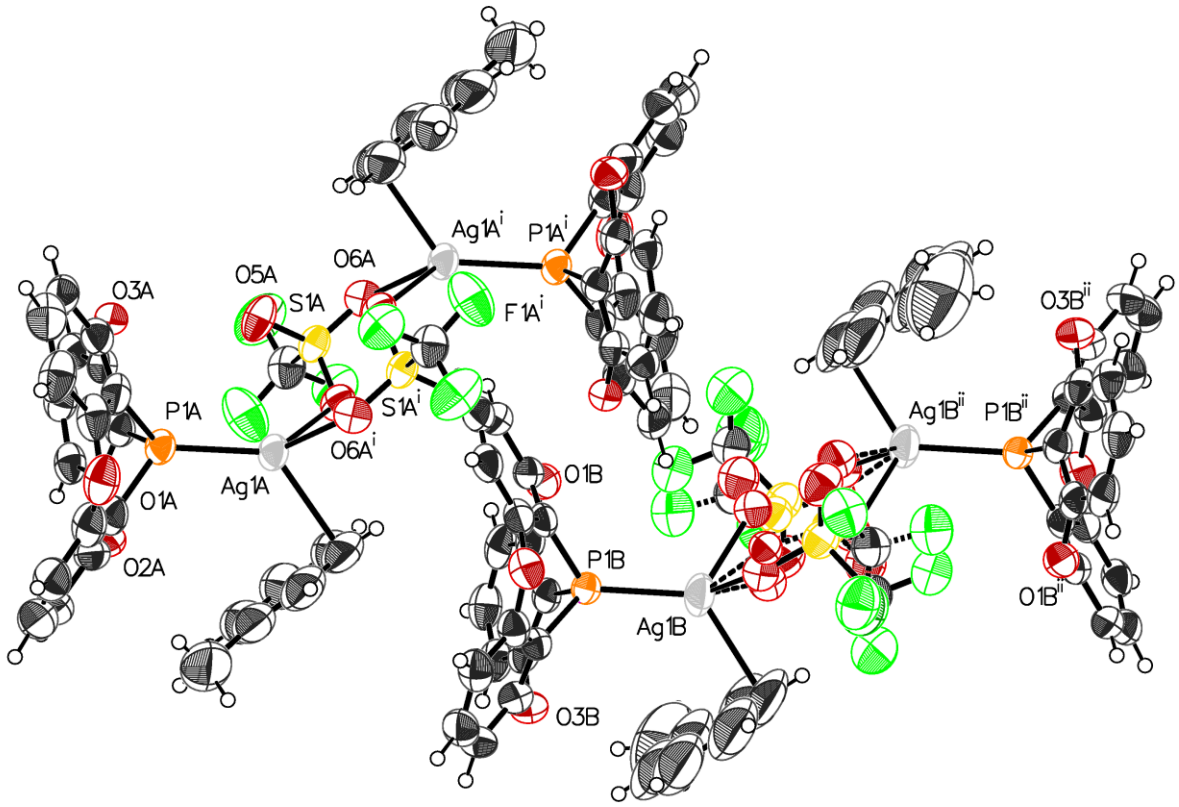

Figure 7.44 : Thermal atomic displacement ellipsoid plot of the structure of crystals of $[Ag(O_3SCF_3)(toluene)(Phang)]_2$ grown from EtOH/toluene. The ellipsoids of non-hydrogen atoms are drawn at the 50% probability level, and hydrogen atoms are represented by a sphere of arbitrary size. Symmetry code (i): 1-x, 1-y, 1-z; (ii): 1-x, 1-y, 2-z.

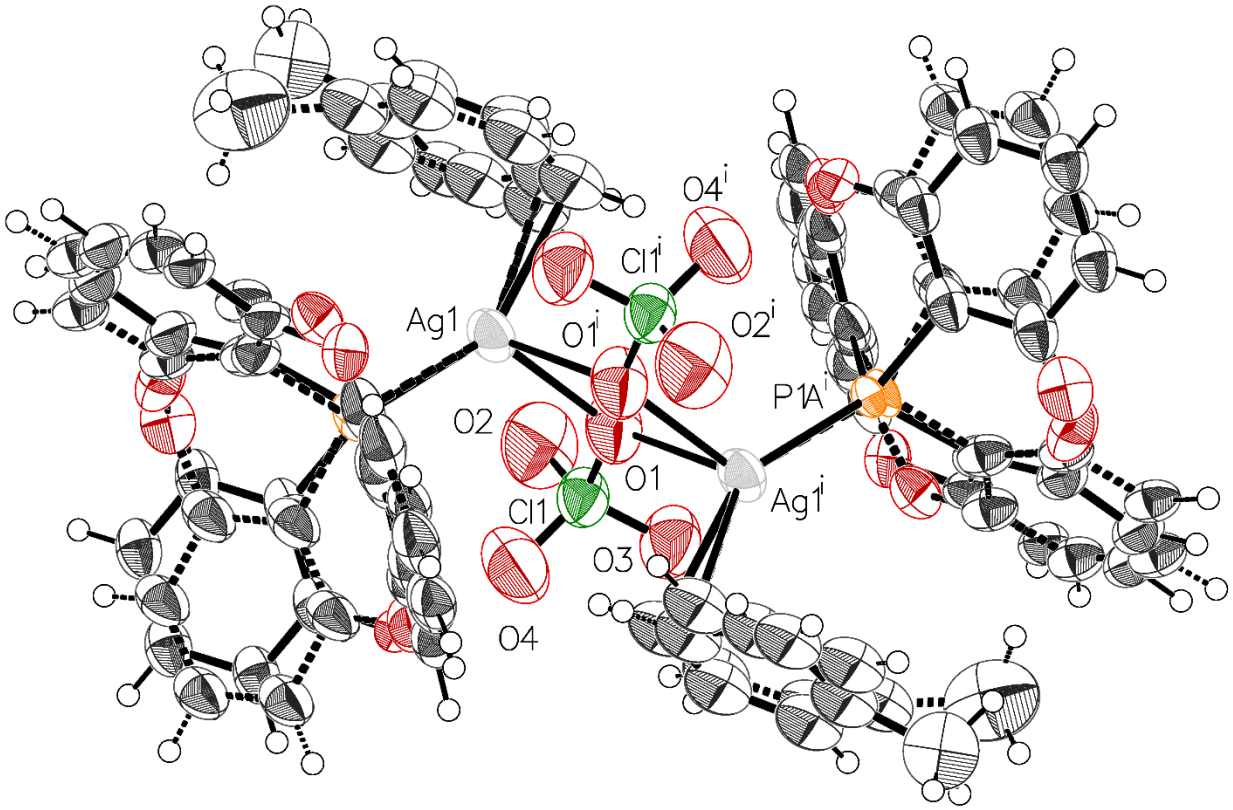

Figure 7.45 : Thermal atomic displacement ellipsoid plot of the structure of crystals of $[Ag(ClO_4)(toluene)(Phang)]_2$ grown from MeCN/toluene. The ellipsoids of non-hydrogen atoms are drawn at the 50% probability level, and hydrogen atoms are represented by a sphere of arbitrary size. Symmetry code (i): 1-x, 1-y, 1-z.

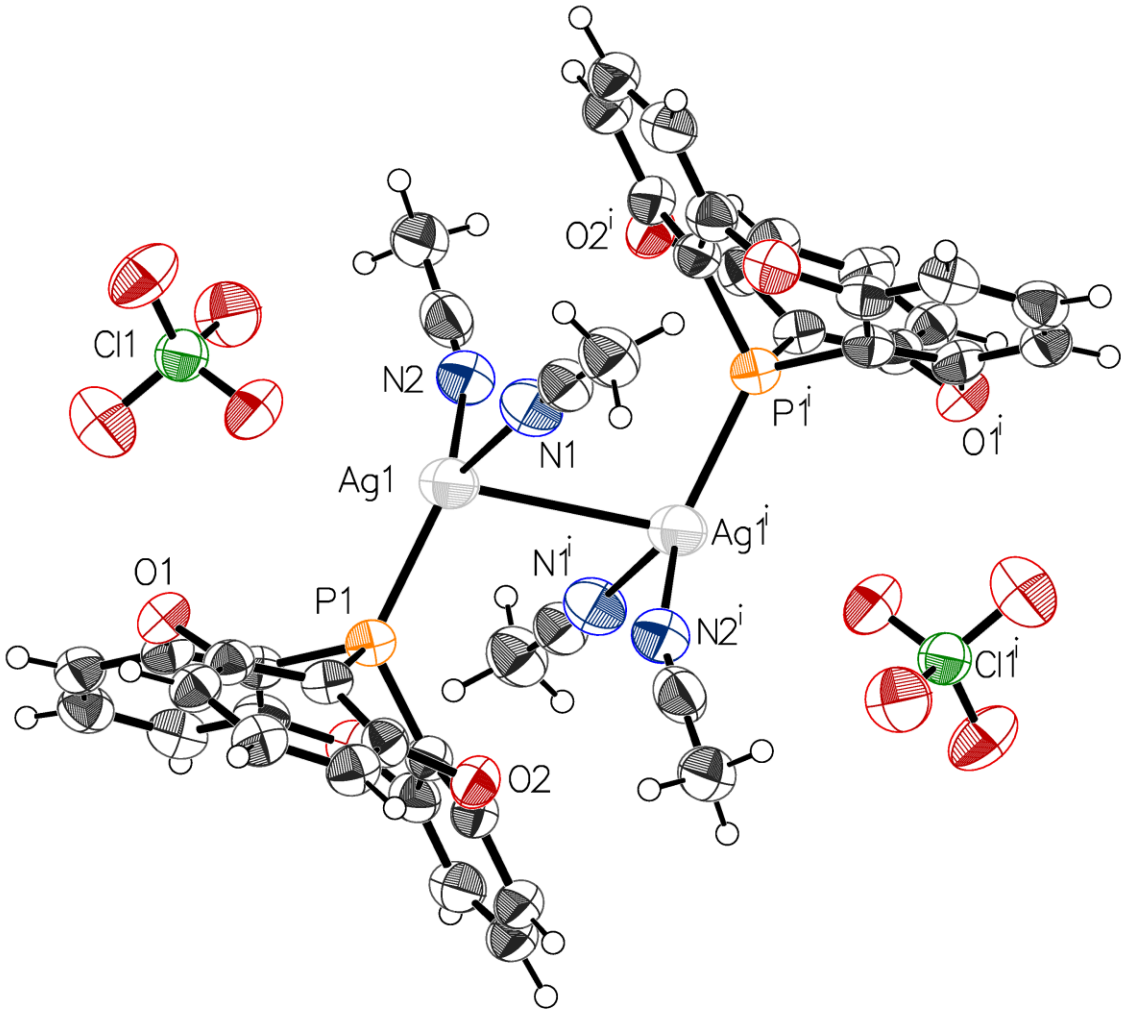

Figure 7.46 : Thermal atomic displacement ellipsoid plot of the structure of crystals of $[Ag(ClO_4)(MeCN)_2(Phang)]_2$ grown from MeCN/toluene. The ellipsoids of non-hydrogen atoms are drawn at the 50% probability level, and hydrogen atoms are represented by a sphere of arbitrary size. Symmetry code (i): 1-x, 1-y, 1-z.

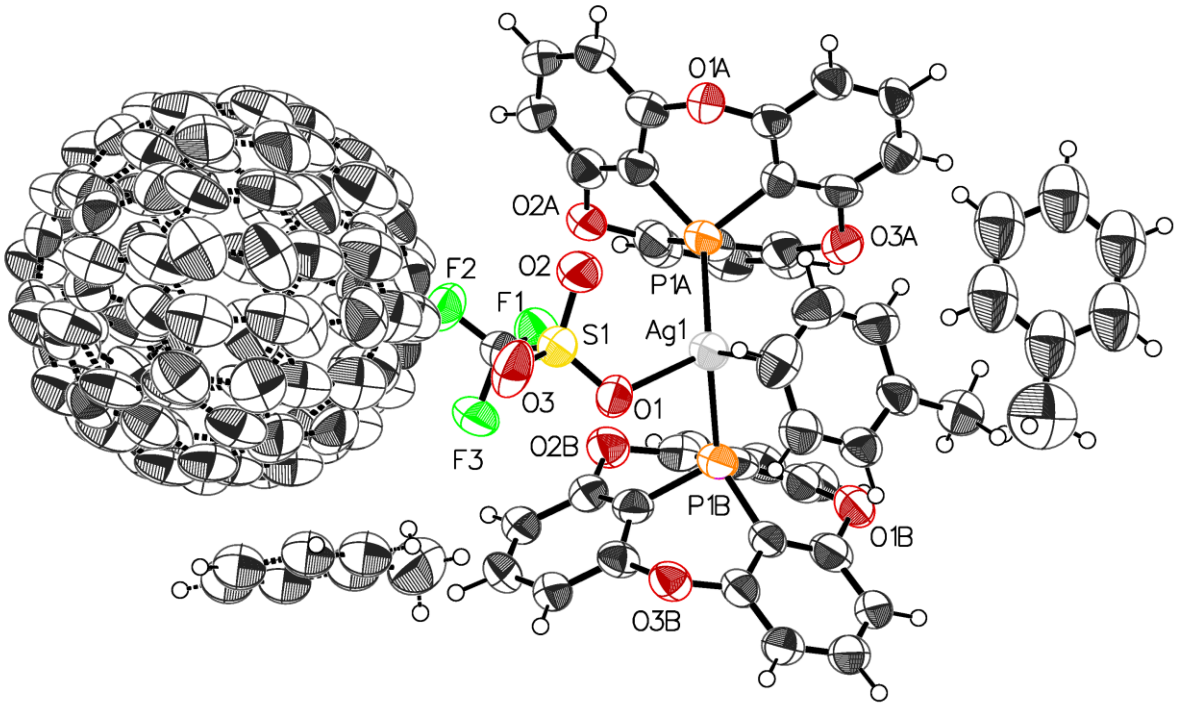

Figure 7.47 : Thermal atomic displacement ellipsoid plot of the structure of crystals of $[Ag(O_3SCF_3)(toluene)(Phang)_2]_2 \bullet 2\ C_{60} \bullet 3$ toluene grown from EtOH/toluene. The ellipsoids of non-hydrogen atoms are drawn at the 50% probability level, and hydrogen atoms are represented by a sphere of arbitrary size. Symmetry code (i): 1-x, 1-y, 1-z.

7.3.7 References

1. Harris, R. K.; Becker, E. D.; Cabral de Menezes, S. M.; Granger, P.; Hoffman, R. E.; Zilm, K. W. Further Conventions for NMR Shielding and Chemical Shifts. *Pure Appl. Chem.* **2008**, *80*, 59–84.

2. Alyea, E. C.; Malito, J.; Nelson, J. H. Identification by Stopped-Exchange Solution ^{31}P NMR Spectroscopy of the Stepwise Formation of [AgL$_n$]PF6 (n = 1-4). Comparison of Metal-Phosphorus Coupling Constants for Triphenylphosphine and 5-Phenyldibenzophosphole. *Inorg. Chem.* **1987**, *26*, 4294−4296.

3. Bryce, D. L.; Bernard, G. M.; Gee, M.; Lumsden, M. D.; Eichele, K.; Wasylishen, R. E. Practical Aspects of Modern Routine Solid-State Multinuclear Magnetic Resonance Spectroscopy: One-Dimensional Experiments. *Can. J. Anal. Sci. Spectrosc.* **2001**, *46*, 46−82.

4. Attar, S.; Alcock, N. W.; Bowmaker, G. A.; Frye, J. S.; Bearden, W. H.; Nelson, J. H. Phosphole Complexes of Silver(I). Investigations of Structure and Bonding by X-ray Crystallography, Infrared Spectroscopy, and CP/MAS and Solution ^{31}P NMR Spectroscopy. *Inorg. Chem.* **1991**, *30*, 4166–4176.

5. Chen, F.; Oh, S.-W.; Wasylishen R. E. *Can. J. Chem*. **2009**, *87*, 1090–1101.

6. Tolman, C. A. Steric Effects of Phosphorus Ligands in Organometallic Chemistry and Homogeneous Catalysis. *Chem. Rev.* **1977**, *77*, 313–348.

7. Bruker (2017). *APEX3* and *SAINT*, Bruker AXS Inc., Madison, Wisconsin, USA.

8. Krause, L.; Herbst-Irmer, R.; Sheldrick, G. M.; Stalke, D. Comparison of Silver and Molybdenum Microfocus X-Ray Sources for Single-Crystal Structure Determination. *J. Appl. Cryst*. **2015**, *48*, 3–10.

9. Sheldrick, G. M. *SHELXT* – Integrated Space-Group and Crystal-Structure Determination. *Acta Crystallogr*. **2015**, *A71*, 3–8.

10. Sheldrick, G. M. Crystal Structure Refinement with *SHELXL*. *Acta Crystallogr*. **2015**, *C71*, 3–8.

11. Engelhardt, L. M.; Pakawatchai, C.; White, A. H.; Healy, P. C. Lewis-Base Adducts of Group 1B Metal(I) Compounds. Part 13. Crystal Structure Determinations of Tetrakis(triphenylphosphine)copper(I) and -silver(I) Perchlorates, Bis(pyridine)bis(tripheny1phosphine)copper(I) Perchlorate, (2,2'-Bipyridyl)bis(triphenylphosphine)copper(I) Perchlorate, and Tetrahydroboratobis(triphenylphosphine)copper(I)-Pyridine (1/0.5). *J. Chem. Soc., Dalton Trans.* **1985**, 125–133.

12. Eller, P. G.; Kubas, G. J.; Ryan, R. R. Synthesis and Properties of Sulfur Dioxide Adducts of Organophosphinecopper(I) Iodides. Structures of the Dinuclear Compounds Tetrakis(methyldiphenylphosphine)di-μ-iodo-dicopper(I)−Sulfur Dioxide and Tris(triphenylphosphine)di-μ-iodo-dicopper(I). *Inorg. Chem.* **1977**, *16*, 2454−2462.

13. Gill, J. T.; Mayerle, J. J.; Welcker, P. S.; Lewis, D. F.; Ucko, D. A.; Barton, D. J.; Stowens, D.; Lippard, S. J. Structural Determinations of Four Mono- and Binuclear Tertiary Phosphine and Arsine Complexes of Copper(I) Chloride. *Inorg. Chem.* **1976**, 15, 1155−1168.

14. Mulliken, R. S. Molecular Compounds and their Spectra. II. *J. Am. Chem. Soc.* **1952**, *74*, 811–824.

7.4 Informations supplémentaires de l'article 4

Supporting Information

Bis(phosphangulene)iminium Salts.

Holding on to Fullerenes with Phangs

Alice Heskia, Thierry Maris, and James D. Wuest*

Département de Chimie, Université de Montréal, Montréal, Québec H3C 3J7 Canada

*Author to whom correspondence may be addressed.

E-mail: *james.d.wuest@umontreal.ca*

7.4.1 Additional Crystallographic Details

Data were collected on a Bruker Venture Metaljet diffractometer using GaKα radiation (λ = 1.34139 Å), except for the case of $[(Phang)_2N]^+ I^-$, where a Bruker Smart APEX II diffractometer equipped with an Incoatec Microfocus Source IμS (λ = 1.54179 Å) was used. During all experiments, the samples were kept at 150 K (100 K for $[(Phang)_2N]^+ I^-$) using an Oxford Cryostream liquid-nitrogen device. The cell lattice parameters values were determined using reflections taken from three sets of 104 frames measured and harvested within the APEX3 suite of programs.[1] Integration of frames was performed using *SAINT*,[1] and a semiempirical absorption correction was applied with *SADABS* for single specimens or with *TWINABS* for twinned samples.[2] The structures were solved using a dual space and intrinsic phasing approach with *SHELXT*,[3] and the refinement was carried out using *SHELXL*-2018/3.[4]

The sample of crystals of $[(Phang)_2N]_4^+ [Ag_4Br_8]^{-4}$• 2 PhCl • 1 H_2O grown from PhCl turned out to be a two-component twin specimen. The unit cell was checked using *CELL_NOW*, and the integration was performed using the two components to produce an HKLF5-type reflection file. For two structures, guest molecules of solvent were found to be highly disordered, and a mask procedure similar to the BYPASS PLATON/SQUEEZE procedure was applied.[5] This was the case for crystals of the salt $[(Phang)_2N]^+ I^-$ grown from CH_2Cl_2/acetone. The solvent-accessible volume was found to be 1099 $Å^3$ (16.5%), filled with a total of 319 electrons. This volume is split into four sites of 93 $Å^3$ with 35 electrons (close to one molecule of acetone with 32 electrons) and two sites of 364 $Å^3$ with 89 electrons (close to two molecules of CH_2Cl_2). Similarly, for crystals of compound $[(Phang)_2N]^+ [C_8H_4Ag_7F_{24}O_{26}S_8]^-$ • 1 C_{60} • 3 mesitylene • 2 H_2O grown from mesitylene, the solvent mask recovered 429 electrons in two

sites of 853 $Å^3$, and the total solvent-accessible volume was 1756 $Å^3$ or 28.5%, including two additional sites of 25 $Å^3$ without electrons. This corresponds roughly to three molecules of mesitylene (198 electrons) and two molecules of H_2O in each of the two larger sites.

7.4.2 ORTEP Diagrams

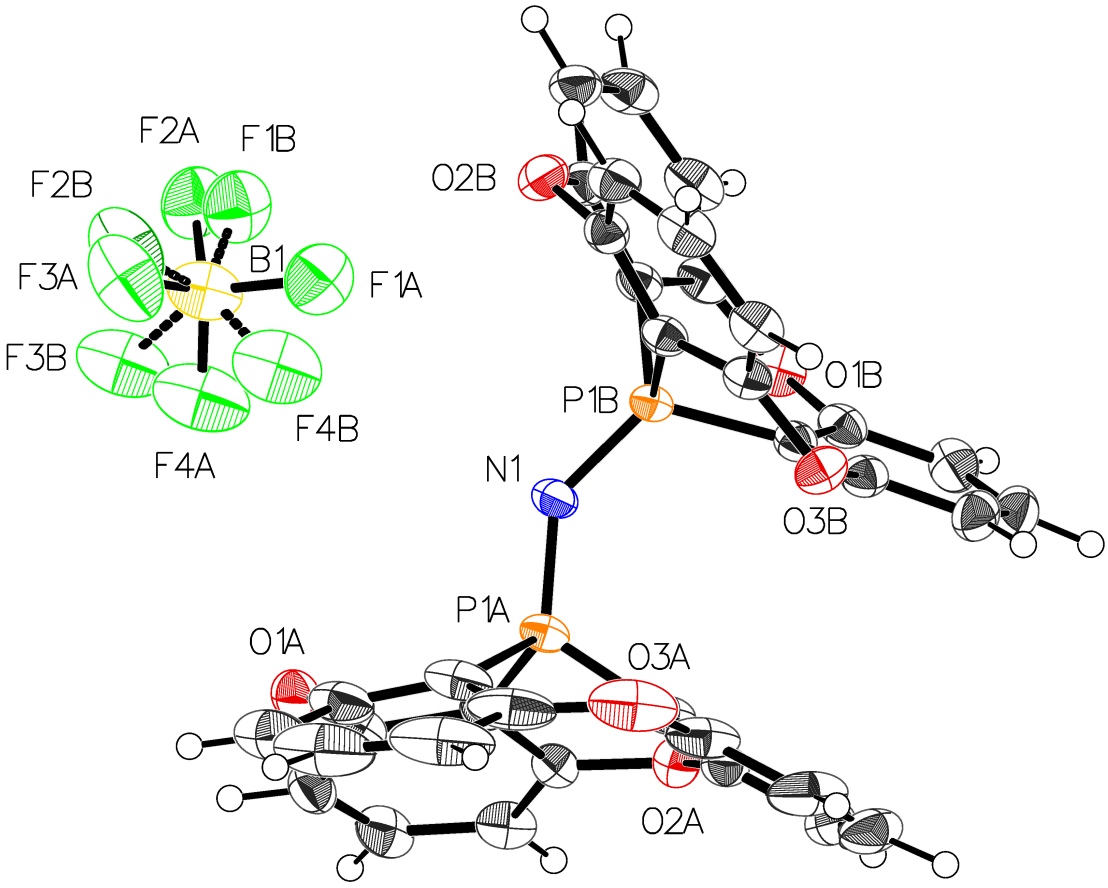

Figure 7.48 : Thermal atomic displacement ellipsoid plot of the structure of crystals of $[(Phang)_2N]^+ BF_4^-$ grown from CS_2. The ellipsoids of non-hydrogen atoms are drawn at the 50% probability level, and hydrogen atoms are represented by a sphere of arbitrary size.

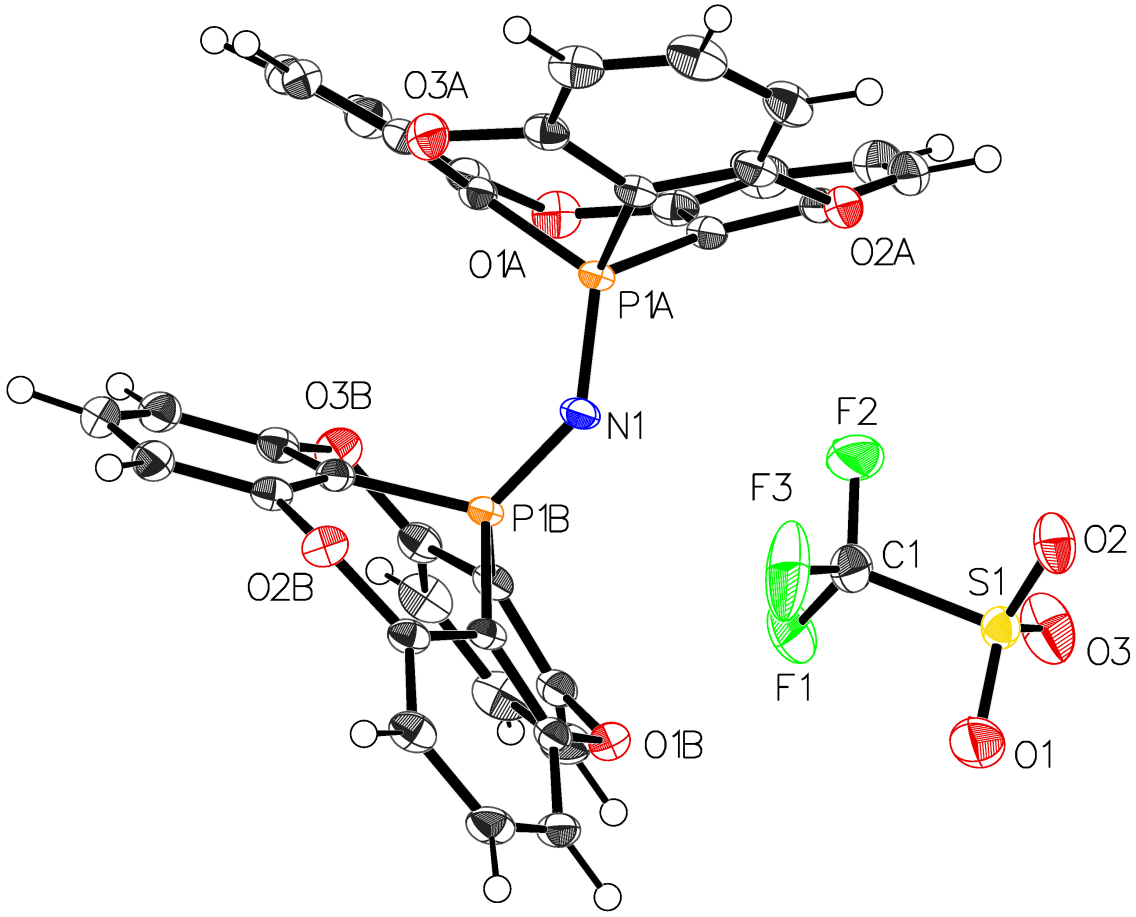

Figure 7.49 : Thermal atomic displacement ellipsoid plot of the structure of crystals of $[(Phang)_2N]^+ CF_3SO_3^-$ grown from CS_2/CH_2Cl_2. The ellipsoids of non-hydrogen atoms are drawn at the 50% probability level, and hydrogen atoms are represented by a sphere of arbitrary size.

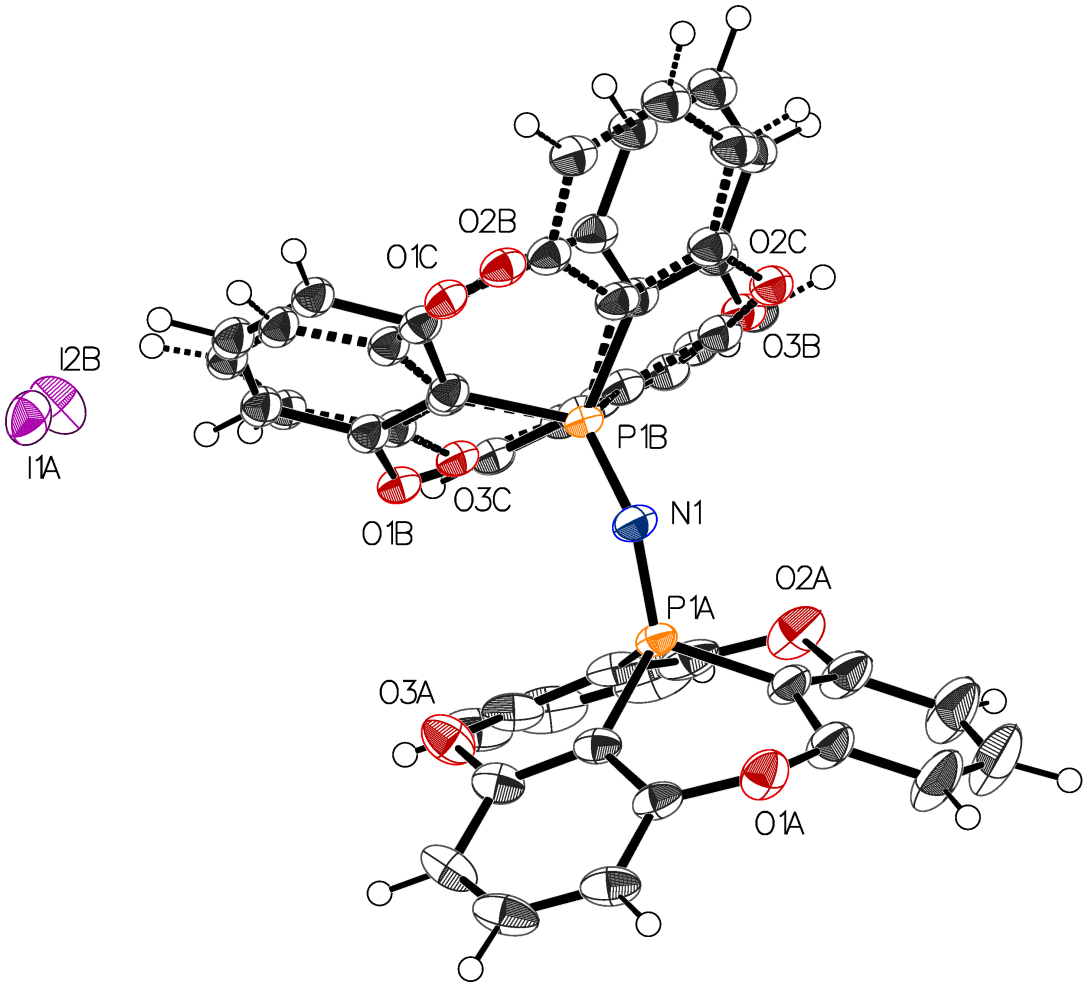

Figure 7.50 : Thermal atomic displacement ellipsoid plot of the structure of crystals of $[(Phang)_2N]^+ I^-$ grown from CH_2Cl_2/acetone. The ellipsoids of non-hydrogen atoms are drawn at the 50% probability level, and hydrogen atoms are represented by a sphere of arbitrary size.

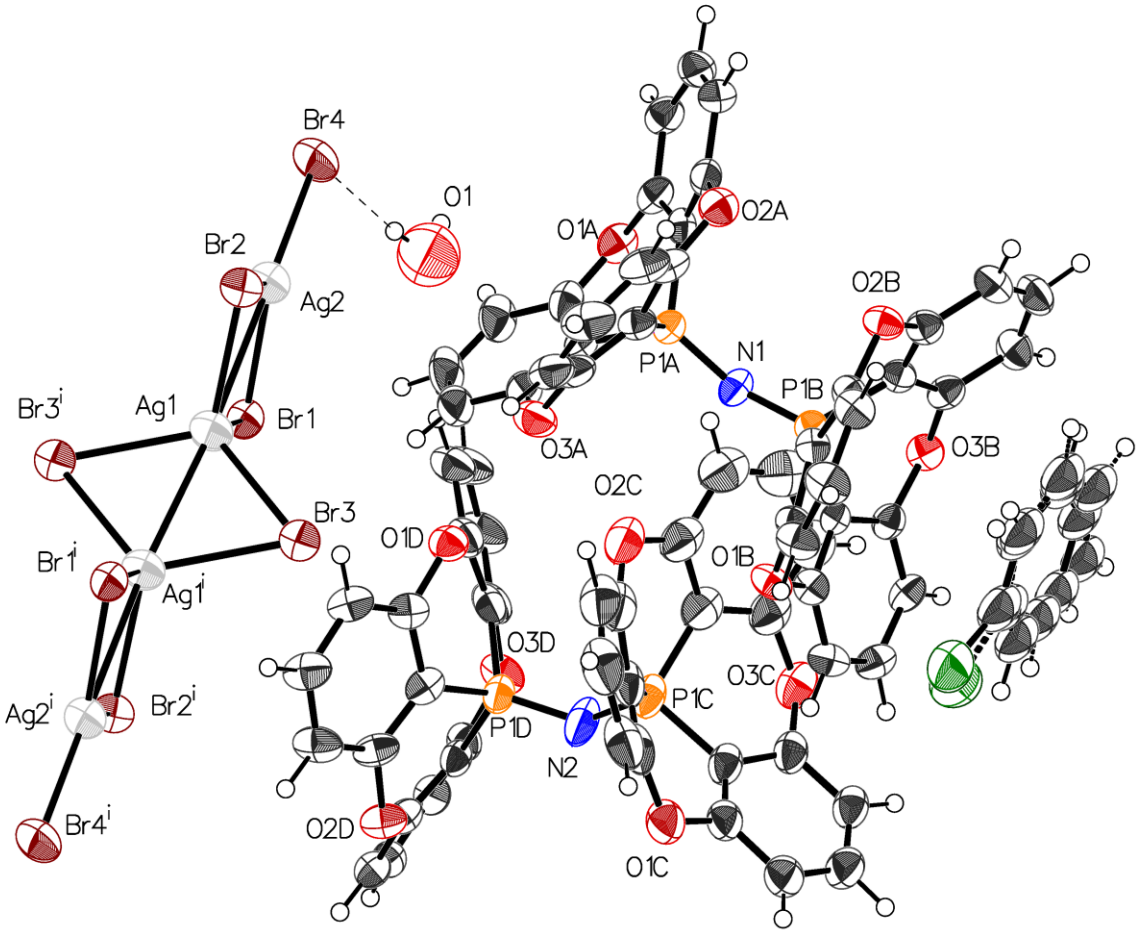

Figure 7.51 : Thermal atomic displacement ellipsoid plot of the structure of crystals of $[(Phang)_2N]_4^+$ $[Ag_4Br_8]^{-4}$ • 2 PhCl • 1 H_2O grown from PhCl. The ellipsoids of non-hydrogen atoms are drawn at the 50% probability level, and hydrogen atoms are represented by a sphere of arbitrary size. Symmetry code (i): -x, 1-y, 1-z.

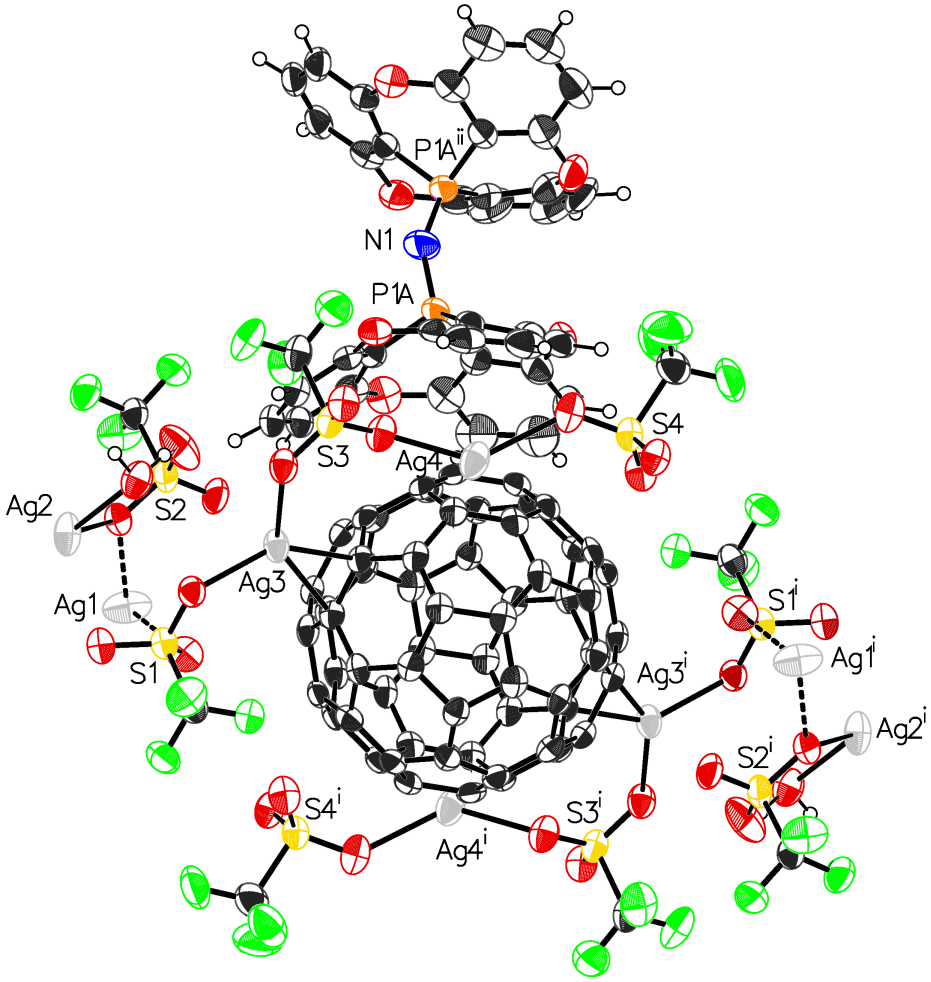

Figure 7.52 : Thermal atomic displacement ellipsoid plot of the structure of crystals of $[(Phang)_2N]^+$ $[C_8H_4Ag_7F_{24}O_{26}S_8]^-$ • 1 C_{60} • 3 mesitylene • 2 grown from mesitylene. The ellipsoids of non-hydrogen atoms are drawn at the 50% probability level, and hydrogen atoms are represented by a sphere of arbitrary size. Symmetry code (i): -x, 1-y, -z; (ii): x, ½-y, z.

7.4.3 References

1. Bruker (2017). *APEX3* and *SAINT*, Bruker AXS Inc., Madison, Wisconsin, USA.
2. Krause, L.; Herbst-Irmer, R.; Sheldrick, G. M.; Stalke, D. Comparison of Silver and Molybdenum Microfocus X-Ray Sources for Single-Crystal Structure Determination. *J. Appl. Cryst.* **2015**, *48*, 3–10.
3. Sheldrick, G. M. *SHELXT* – Integrated Space-Group and Crystal-Structure Determination. *Acta Crystallogr.* **2015**, *A71*, 3–8.
4. Sheldrick, G. M. Crystal Structure Refinement with *SHELXL*. *Acta Crystallogr.* **2015**, *C71*, 3–8.
5. Spek, A. L. *PLATON* SQUEEZE: A Tool for the Calculation of the Disordered Solvent Contribution to the Calculated Structure Factors. *Acta Crystallogr.* **2015**, *C71*, 9-18.